Measurement methods for the determination of powder properties for compaction modelling.

Korachkin, Dzmitry

Measurement Methods for the Determination of Powder Properties for Compaction Modelling

by

Dzmitry Korachkin B.Eng. (Hons.)

Thesis submitted to the University of Wales Swansea
for the degree of Doctor of Philosophy

2006

School of Engineering
University of Wales Swansea

ProQuest LLC.
789 East Eisenhower Parkway
P.O. Box 1346
Ann Arbor, MI 48106 – 1346

Declaration

This work has not previously been accepted in substance for any degree and is not being concurrently submitted in candidature for any degree.

Signed (candidate):

_____

Date: 6.10.2006

_____

Statement 1

This thesis is the result of my own investigations, except where otherwise stated. Other sources are acknowledged by the use of explicit references. A bibliography is appended.

Signed (candidate):

_____

Date: 6.10.2006

_____

Statement 2

I hereby give consent for my thesis, if accepted, to be available for photocopying and for inter-library loan, and for the title and summary to be made available to outside organisations.

Signed (candidate):

_____

Date: 6.10.2006

_____

Acknowledgements

I would like to thank the following people and organisations, who have helped me in the work undertaken in this thesis

Professor D.T. Gethin, my supervisor, for his guidance, encouragement, inexhaustible support and unending optimism

AEA Technology Plc. for financial support of the project, materials and experimental data. (AEA Technology managed the DTI funded project MPMP5.2, the work in this thesis was funded by the project.).

Dr. J. Tweed, Dr. D. Guyoncourt, Dr. S. Burch of AEA Technology Plc., for their help and support

The members of the Industrial Advisory Group[1] for their help and support and particularly H. Hodgson of Dynamic-Ceramic for the ceramic powders and samples

Overseas Research Student Award Scheme for helping to cover the tuition fees

Professor R.W. Lewis for his guidance and support in the writing of this thesis

Dr. P. Mosbah for his help and support

P. Matthews and A. Jolly for their continuous help with the experimental program

Technical staff at the Mechanical Engineering workshop, for making sure my designs were successfully manufactured and for their help throughout this project

M.A. Fox for her immeasurable contribution
My parents for their continuous support and encouragement
My friends and colleagues for their help and support

---

[1] Brico, DTI, Dynamic Ceramic, EPMA, Foseco Steel, GKN Sinter Metals, Johnson Matthey Catalysts, Kanthal, LSM, Magnet Applications, Marshalls Hardmetals, Merck Sharp and Dohme, Morgan Advanced Ceramics, Morgan Group Technology, NPL, SG Magnets, Swift Levick Magnets, Synetix

Summary

In this thesis an experimental investigation into the measurement methods for determination of model parameters for the compaction, unloading and ejection stages and a numerical investigation on the effects of fill density distribution are presented.

The numerical investigation explored the effect of fill density distribution on green density in powder compacts and on tool forces. This was achieved by comparing the results of simulations with uniform and non-uniform fill density distributions. The investigation considered three different powder types (ferrous, hard metal and ceramic), a selection of different geometries and a selection of fill density distributions based on the review of die filling research. Non-uniform fill density was found to result in higher density variation and in increased tool forces.

A novel floating die modification to the shear plate friction measurement apparatus has been proposed. The equipment was used to measure the friction coefficient for a wide range of loading conditions, where the compaction and normal load have been explored independently. For ferrous powders friction was found to reduce with the compaction load and for lower compaction pressures also with normal load. Admixed and die wall lubricant performance was also assessed, with even small quantities providing significant reduction in friction. The compact surface was examined in a bid to explore the friction mechanisms with regards to lubrication.

A review of different experimental techniques for measurement of parameters for the unloading and ejection stages is presented. The instrumented die, the unconstrained compression, the three point bending and the Brazilian disc tests have been explored for a selection of powders. A correction function has been proposed to enable the measurement of radial pressure in the instrumented die during ejection. A novel split die modification to the instrumented die test has been introduced and used to explore the axial recovery during ejection.

Table of Contents

List of Figures

List of Tables

Chapter 1 Introduction

1.1 An Introduction to Powder Compaction Manufacturing (PCM)

The manufacturing of products via powder compaction is a well established industry that is still growing rapidly as more and more new products are developed and new materials are employed. It is one of the most diverse manufacturing approaches among the different metalworking technologies. Its attraction is the ability to economically produce high quality, complex parts with tight tolerances. In some cases PCM is the only way to achieve certain product properties, e.g. parts with controlled porosity. The advantages of the powder compaction process are the energy efficiency, very low material waste and ability to produce final shapes with only minimal machining. PCM is now used to produce parts of increasingly complex shapes.

The European Powder metallurgy market alone has an annual turnover of over Six Billion Euros, with annual worldwide metal powder production of around one million tonnes (EPMA 2004). Powder shipment figures, presented in Figure 1.1 demonstrate the steady growth of the industry in recent years. The hard metal sector is also growing, as seen from Figure 1.2

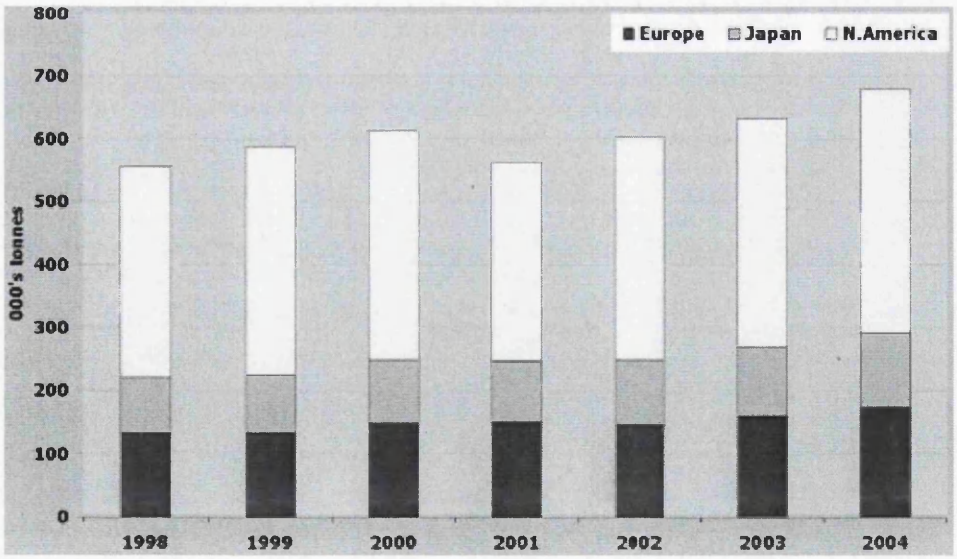

Figure 1.1 Global powder shipments for PM 1998–2004 (Dunkley 2005)

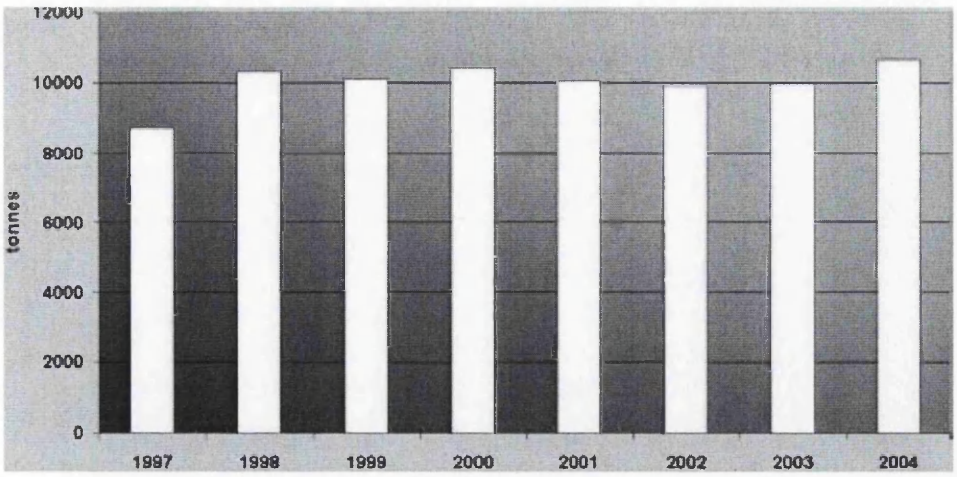

Figure 1.2 Estimated European hardmetal production 1997–2004 (Dunkley 2005)

The growth of the powder manufacturing industry can mainly be attributed to the cost-savings associated with net (or near-net) shape processing compared to casting and forging. In some cases changing from a casting, or wrought process, to powder compaction can produce savings of 40% and higher (EPMA 2004). Powder metallurgy becomes even more attractive when raw material and energy prices are high, as it is a process with very high material utilisation and low energy consumption. The advantages of PCM will be discussed in more detail in Section 1.5.

1.2 History of PCM

Powder compaction manufacturing has been present in various forms for a very long time. For instance, daggers ornamented with gold powder were found in the tomb of the Egyptian Pharaoh Tutankhamen. There is evidence of the Incas making objects by sintering powders of precious metals (these were made by hot forging a sintered powder mass, not through conventional compaction process) (Tsukerman 1965).

The first industrial application of modern powder metallurgy methods was made by the prominent Russian scientist Petr Grigor'evich Sobolevskii in the 1820's. It came about after a new deposit of platinum was discovered in Russia. It was decided to use the platinum for the production of coins. However, the melting point of platinum was too high for industrial production at the time. The

contemporary way of obtaining malleable platinum from ore involved the use of arsenic, which was dangerous to the workforce. Sobolevskii discovered an alternative method, which involved packing purified sponge platinum (obtained by the chemical processing of natural compounds) into a mould and pressing it. Then the compressed product was heated and pressed again. The result of this working was that the metal changed its appearance and solid platinum products were obtained. Similar work was performed in England at approximately the same time. However, this method was later abandoned with the invention of the oxy-hydrogen flame and its use for melting platinum.

The next time powder metallurgy became extensively used was when tungsten filaments for incandescent light bulbs were developed. Powder metallurgy was used to produce the tungsten rods, from which wire for the filaments was drawn. Additionally, the need for hard wearing tools to draw the hard tungsten wire fuelled the search for artificial hard materials to replace the diamond tools, which were too expensive. This search resulted in many new materials, such as hard metal carbides, which are now widely used as cutting tool materials. These tools were also manufactured through powder compaction.

Another of the early PCM products were the self-lubricated bearings, which are typically made of bronze. The compaction process facilitates the inclusion and control of porosity. The porous matrix is then impregnated with oil and the bearing does not require further lubrication throughout the life of the machine in which it is used.

Since the 1940s the range of materials was expanded to include refractory metals and their alloys. Metal used for structural purposes have also experienced a major growth during the same period. The majority of structural powder compaction manufactured parts are ferrous, but a vast number of PCM products tailored for nuclear, aerospace, electrical and magnetic applications were also developed (German 1994).

1.3 PCM Applications

Some of the products currently manufactured through powder compaction are summarised in Table 1 and examples of PCM components are presented in Figure 1.3-Figure 1.5.

Table 1 PCM Applications

Powder type	PCM products	Application	Example
Ferrous	Structural parts	Automotive industry	Gears
Nonferrous	Porous and nonporous bearings	Hand tools	bushings
Ceramics	Cutting tools, other	Machining	Cutting tips
Hard metal	Cutting tools	Machining	Cutting tips
Food and Pharmaceutical	Tablets Sweets, Stock cubes	Medicine Culinary	Aspirin Mints, Stock cubes
Others	Composite friction materials	Automotive industry, heavy machinery	Clutches, brakes, brake linings
	Diamond cutting tools	Machining	Grinding and cutting disks
	magnetic and electrical	Servomotors Consumer Electronics	Pot cores Magnets and electrical contacts

Figure 1.3 PCM Components I

Figure 1.4 Metal Injection Moulding components (MIM is a subset of PCM)

Figure 1.5 Ceramic PCM components (Dynamic-Ceramic)

1.4 PCM Process

In spite of their diversity, for most of the products mentioned above the manufacturing process consists of the common steps outlined below.

1. Prepare the powder, or powders, required for the process. There are a number of different methods of producing powders. The three most common methods are: reduction of a compound (usually the oxide, in the solid state), electro-deposition and the atomisation of molten metal.

2. Mix the powder, or powders, with a suitable lubricant or binder (may not be required in some cases).

3. Load the powder mixture into a die. This may be followed by a transfer stage, where the die geometry changes at constant volume and no compaction takes place. The pressure is then applied and compaction takes place. Once the desired density is reached the compact is unloaded and finally ejected. This produces a compact which is often only sufficiently strong to be handled safely and transferred to the next stage. Such compacts are called "green", meaning unsintered. From this the terms green density and green strength originate.

4. Sinter the green compact – sintering is normally performed in a controlled atmosphere and at temperatures of typically 65-75% of the melting point of the major constituent.

5. Perform finishing operations – such as sizing, machining and surface densification.

These basic steps may be modified and expanded on for some applications. For example not all powders require lubricants and some compacts do not undergo sintering.

1.5 Characteristics of the PCM

Previously, powder-based components were selected for their low cost. However, now they are more frequently chosen for their high or even superior quality, homogeneity, or properties as well as the traditional advantages of cost and productivity. The advantage of the PCM may be seen in Figure 1.6 which shows a comparison with other manufacturing processes. Typically, PCM (shown as sintering in the Figure) achieves high dimensional tolerances and has the highest material utilisation level at 95% and the lowest energy requirement at 29MJ/kg in this example. This, together with avoiding expensive machining operations, can add up to savings of 40% or higher.

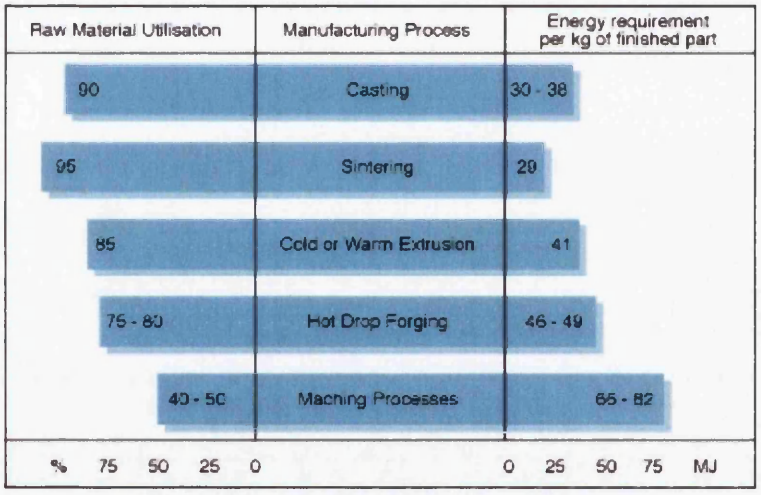

Figure 1.6 Comparison of PCM to other processes (EPMA 2004)

Additionally, PCM can be employed to produce parts out of metals with very high melting points, such as tungsten with a melting point of 3400°C. Such materials are very difficult to produce through casting as the furnace lining will either melt or react with the material being produced (Tsukerman 1965).

Alloyed parts can be fabricated without segregation, often a problem in casting, by using prealloyed powders and sintering at temperatures lower than the melting

point. Moreover, metals insoluble in each other can be alloyed through powder metallurgy (e.g. metals with melting points which are very different, such as tungsten and copper (3400°C and 1083°C respectively), iron and lead (1535°C and 327°C)). PCM can also be used to produce parts with layers of different metals, or with metals and non-metals, and is a convenient method for producing parts with controlled porosity – this is impossible to achieve through casting.

Some of the disadvantages of PCM are the high initial capital investment required and the restriction that is imposed on part geometry. Also, sometimes there may be difficulties with the manufacturing of crack free components, achieving homogenous density and high geometrical accuracy. These problems may be time consuming and expensive to solve, as often they can only be eradicated through trial and error.

The performance characteristics of powder parts, in comparison with parts made by other processes, are not widely publicised. This has led to a low level of awareness at the design stage and so application of the process has been more limited. This deficiency is being addressed through the collation of a global database (EPMA 2004), that includes information on structural performance and fatigue behaviour as this is established and documented.

1.6 Motivation and Approach

While PCM is a highly advanced industry with a wide range of high quality products, it is still evolving with new products, techniques and applications being adopted on a regular basis. These place demands on achieving an improved understanding of the process. This sets new targets and challenges that need to be overcome through research and development.

Numerical modelling is a tool which is becoming widely used both within the research institutions, where it helps to improve the understanding of the compaction process, and in industry where it is employed at the design stage and as a tool for problem solving. The accuracy of a numerical simulation depends on the numerical model used to represent the simulated phenomena and on the quality of input data. The latter is addressed in this thesis through exploring the

measurement methods for determination of powder properties for compaction modelling.

The input data for the numerical simulation of powder compaction consists of a variety of parameters. These include the information about initial conditions in the die, i.e. the powder density and its distribution; the parameters which describe the behaviour of powder during compaction, such as its yield properties and the way it interacts with the tooling, i.e. the friction coefficient. The elastic properties of the material are important during unloading and ejection stages, where the elastic recovery of the compact takes place.

Until recently many simulations assumed uniform fill density conditions. However, the research on die filling has been able to demonstrate that frequently the fill density is far from uniform, particularly in die geometries which include features with high aspect ratios. The sensitivity of green density to the fill density distribution will be explored in Chapter 3 of this thesis through numerical modelling of compaction for cases with uniform and non uniform fill density distributions. Three types of materials will be considered to ensure that any principles apply to a variety of materials. The powder types considered will be ferrous, hard metal and ceramic. Three geometries will be explored – a hollow cylinder and two flanged components, with external and internal flanges. A variety of possible fill density variations based on die filling research will be simulated and compared to the equivalent compacts with uniform fill. The green density and the tool forces will be compared to assess the impact of fill density distribution.

Also the research will focus on the measurement of the friction coefficient, a parameter which is known to evolve throughout the compaction process. Previously, friction has been explored for a variety of die materials and finishes, but there is still a need for a better understanding of friction behaviour for the wide variety of loading conditions that exist during the compaction process. A novel floating die modification to the shear plate friction measurement apparatus will be introduced in Chapter 4. The modification enables full transmission of axial pressure to the bottom of the compact and hence the target surface. It is also

possible to control the normal force during the sliding test independently from the compaction load. Thus, the friction coefficient can be explored for a wider range of loading conditions. The repeatability of the new equipment will be tested and subsequently validated against the instrumented die apparatus.

The floating die shear plate will then be used to explore the evolution of the friction coefficient with changes in compaction loads and independently with normal loads. Simultaneously, the friction coefficient will be explored with regards to the performance of different quantities of admixed lubricant, which is often added to powder to reduce powder-die and inter-particle friction. The friction mechanisms will also be explored with regards to lubrication through analysis of the sliding surfaces of the compacts using an energy dispersive x-ray scanning electron microscope and a white light interferometer. Die wall lubrication will also be considered briefly, in order to assess the applicability of the new friction measurement test equipment.

Next, the measurement methods for the determination of parameters relevant to the unloading and ejection processes will be explored. The instrumented die, the uniaxial compression and the three point bending tests will be evaluated with regards to the measurement of the elastic parameters. Whereas the Brazilian disc test will be used to obtain cohesion data for the ejection stage. The tests will be performed for ferrous and ceramic powders, with such variables as the amount of admixed lubricant and the use of isostatic pressing also being considered.

Finally, the ejection process will be examined with the main considerations being the measurement of the radial stress during ejection and the axial recovery of the compact. A correction procedure for radial stress measurement has been suggested in Chapter 7 in order to make the calibration function used to interpret data from the instrumented die strain gauges applicable to the ejection stage. The axial recovery of the compacts during the ejection stage will be assessed through the application of a novel split die adaptation to the instrumented die equipment.

1.7 Thesis layout

Following this chapter the thesis has the following layout:

Chapter 2 – Literature review

This contains a review of work in the areas of die filling, compaction modelling, friction measurements and ejection.

Chapter 3 – An exploration of the effect of fill density variation on the compaction of ferrous, ceramic and hard metal powder systems

This chapter introduces the investigation into the effects of fill density distribution on green density and tooling loads through numerical simulation of compaction.

Chapter 4 – Friction measurement

In this chapter the new floating die modification to the shear plate apparatus is introduced. The repeatability of the new equipment is tested and the comparisons with previous results and with the instrumented die technique are made.

Chapter 5 – Exploration of admixed and die wall lubrication

In this chapter the floating die shear plate equipment presented in Chapter 4 is put to use in a case study of the effect of varying quantities of admixed lubricants. Simultaneously the friction mechanisms are studied from the perspective of separating normal and compaction loads. The study is supplemented by the use of the white light interferometer to analyse the sliding surface of the compacts. Die wall lubrication is also briefly explored.

Chapter 6 – Ejection and unloading - elastic parameters

In this chapter the measurement methods for determining elastic and cohesive properties of powder compacts at different stages of densification are considered. The methods used include instrumented die, unconstrained compression, three point bending and the Brazilian disc test.

Chapter 7 - Ejection

This chapter introduces the new split die equipment and contains experimental investigations into the ejection process

Chapter 8 – Conclusions and Recommendations

This chapter is a conclusion of the work presented here and also contains recommendations for future work in the area.

Chapter 2 Literature Review

2.1 Introduction

Before proceeding to the work in this thesis it is appropriate to review the relevant literature. The results of research in the area of die filling lead to the input data for the numerical models. These are used in Chapter 3 to analyse the impact of fill density distribution on final density. Friction is another factor that may affect green density distribution. The friction mechanisms and the effect of some of the process parameters on friction are not yet fully understood. Accurate friction data is also a vital component of compaction simulations. However, for modelling the unloading and ejection stages an understanding of the elastic behaviour of powder compacts is equally as important as accurate friction data.

Therefore, the literature review investigates the state of the art in the following areas:

- Die filling
- Compaction Modelling
- Friction Measurements
- Measurements for unloading and ejection

2.2 Die Filling

While at first glance the filling of the die may appear simple, in reality it is a process with a multitude of complications. Previously, a lot of attention has been given to the problem of filling the die completely. This included a large quantity of work on measuring and improving powder flow, both from the feed shoe into the die and inside the hopper. The Hall flowmeter (Peterson and Small 1994) is typically used to measure the flow rate of metal powders and mixtures, but other methods have been suggested. One such measurement apparatus introduced recently is the variable aperture flowmeter. The device comprises a cup with an iris at its base, allowing for a greater range of openings to be considered in testing and for flowability of poor flowing powders to be explored (Guyoncourt and Tweed 2003).

Another method quantifies powders by their ability to fill dies of different apertures. It involves the movement of the feed shoe over a series of die openings of different diameter – the smallest diameter that is filled completely then provides a measure of the flowability. However, if the movement is facilitated manually the test becomes dependent on the operator and comparison between results from different laboratories is difficult.

Other methods for quantifying the poor and non-free-flowing powders were also developed in industries that deal with such powders, such as the chemical, food and pharmaceutical sectors. These were reviewed in (Ullrich 1998). This work identified the key parameters of rate of die fill, its uniformity and reproducibility.

However, it is not only the flowability of powder that is important, but also the way in which process parameters affect die filling. These include die shape, size and orientation, feed shoe speed and kinematics, the type of feed process used and even ambient conditions. The effects of these process parameters go beyond just the capacity of the powder to fill the given die but also impact on the fill density distribution within the die.

A number of investigations on the effect of the process parameters on die filling have been reported in the literature. Demetry, S.Souto et al. (1998) proposed a tactile sensing device to study fill density uniformity. The sensors, protected by two rubber sheets, were placed at the bottom of the die and the density gradients were evaluated from the pressure transmitted from the top punch to the sensors. The authors have suggested that filling powder from directly above the die, rather than from a shoe that slides across the die, would result in a more uniform distribution. Other suggestions for improving fill uniformity included the use of spreading tools: a rake like device and a levelling blade, which would improve the distribution but would not completely remove non-homogeneity.

E. Hjortsberg and B. Bergquist (2002) investigated the effect of fill process parameters on fill density variations in ring shaped compacts. The study looked at four sections of the ring shaped die and compared their densities after filling under a range of varying fill parameters. Those included settling time, feed shoe

speed, number of feed shoe passages and shoe powder level. They also discussed the mechanisms influencing the fill density and highlighted gravity, air resistance, shoe speed and the shear forces from the powder in the shoe as the main influencing factors.

A.C.F. Cocks and C.-Y. Wu et al., in (Cocks, Dihoru et al. 2001) and (Wu, Dihoru et al. 2003), introduced a novel die filling test rig, which consisted of a transparent die and a filling shoe. The transparent design allowed for high speed video cameras to record and study the filling process. Both the quantitative and qualitative assessments of the effect of powder characteristics and shoe motion on powder flow into a constrained cavity were undertaken. These authors then presented measurements of filling rate and ratio for different configurations of die and shoe. The impact of air on die filling was explored through additional tests in vacuum with both positive and negative contributions being reported. The concepts of nose and bulk flow were introduced. In (Wu, Dihoru et al. 2003), the authors also introduced the concept of critical shoe velocity as a method of characterising the flowability of powders. The critical velocity is the maximum shoe velocity at which the die is filled completely and can be used for both powder characterization and to assist process design.

The issue of a critical velocity was also considered by L. Schneider et al. (2005), who used the filling test rig from (Cocks, Dihoru et al. 2001) on four different powders, representative of typical industrial powders of different morphologies. The authors presented both qualitative and quantitative studies of the filling process. The effect of feed shoe speed and powder height on the flow mechanism was described. Critical velocities were measured for the four powders and formulae for critical velocity calculations, fitting with experimental data, were derived.

The same die fill equipment was used again in (Wu and Cocks 2004), where the mechanisms of the flow process were described, with concepts of nose and bulk flow being further explored. While previous work focused on the ability to fill the die, in this case the packing of powder inside the die was also studied with the effects of feed shoe powder height, number of passes, filling intensity, die

geometry and orientation being the factors considered. A localised increase in density induced by shear forces between powder in the shoe and the die was observed in tests with repeated feed shoe passes, confirming the previous findings in other literature. Unlike (Hjortsberg and Bergquist 2002), where only the global density variations in quadrants of the die were considered, in this work the authors looked at a more complex stepped geometry and how features in die cross-section affected the filling process and the density distribution throughout the cross-section. This work also reviewed other techniques available for describing the flowability of the powders. Additionally, the authors addressed the influence of air on the filling process, both as an inhibiting factor when trapped or escaping from the die and as a fluidizing medium, thus increasing the flowability of poor flowing powders.

Wu et al. in (Wu, Cocks et al. 2003) and (Wu, Cocks et al. 2003b) extended their work to include the transfer stage. The authors presented a numerical and experimental study of the transfer process. They employed a transparent stepped die, in conjunction with a high speed video system, to observe the transfer process, which was then simulated via a numerical discrete element method (DEM) model. The authors demonstrated the capability of the discrete element method code to model the filling and transfer processes. In both numerical simulations and experimental tests the die was filled from a feed shoe, resulting in a non-uniform fill density distribution, where the density was lower in the deep narrow sections than in the bulk of the body. The density distribution was then altered as a result of the transfer stage. The authors report that the density in the narrow columns became more uniform as a result of the powder motion during transfer. The powder became denser due to settling as the powder blocks sheared. This resulted in the creation of a dip at the top of the die. Additionally, at the interface of the powder blocks dilation occurred due to shear and a narrow region of lower density was formed. All of this resulted in the density distribution, before compaction, being significantly different from the uniform conditions. The authors stressed the importance of considering the non-uniform powder density in the die after fill and transfer.

While some authors were able to determine bulk density in vertical sections of the compact, more detailed measurements proved more difficult. The sintering of loose powder after fill allows for the density of smaller sections to be determined by conventional methods. However, handling of the die and even sintering itself can affect the density distribution.

A convenient way of determining the fill density distribution is through the use of X-Ray Computerised Tomography (CT), as explored in (Haskins and Jandeska 1998) and later in (Burch, Tweed et al. 2004). Detailed information on compact density distribution can be obtained using the technique. S.F. Burch et al. obtained CT images of compacted tablets and of filled dies, containing loose powder. CT images of pharmaceutical tablets showed in detail the density distribution in a compacted part. For the filled dies they showed a localised increase in density near the top of the die in tests with multiple passes of the feed shoe over the die, confirming the findings of C.-Y. Wu et al. (2004)

Both the fundamental research on die filling and the results of specific case studies, including the CT scans of filled dies, were used to define credible fill density distributions considered in Chapter 3. The aim of the investigation is to assess the effect of different density distributions at fill on the final green density distribution.

2.3 Compaction Modelling

Many numerical models simulating different phases of the compaction process have been reported in the literature. Models exist for all the different stages, including die filling, transfer, compaction, unloading and ejection. The most mature are those concerned with the compaction stage. Fill and transfer stages and unloading and ejection stages have been studied to a lesser extent. In this work a model of the compaction stage was used and thus this review will focus on work in the area of compaction modelling.

Essentially there are two approaches to compaction modelling:

(i) Continuum Modelling, also known as macro-mechanical.

(ii) Discrete modelling or micro-mechanical.

2.3.1 Continuum models

In a continuum model the powder is considered as a continuum, i.e. as a whole rather than a collection of individual particles. Such models predict the macroscopic behaviour of the powder, such as its density, stress state, displacement and final shape of the compact.

The main elements of a continuum model are:

Part geometry – the initial and final shape and size of the modelled compact.

Material properties – the parameters which define the way a material responds to loading and deformation and the way it interacts with other objects (e.g. friction between powder and tooling).

Tool kinematics – i.e. the motion of the tools required to achieve the final geometry, including the velocities and displacements of the tools and the sequence in which they move.

The above elements are also present in discrete models, however these also require data on the size, shape and position of the discrete particles representing powder. This will be expanded further below.

2.3.1.1 Empirical models

The precursors of modern numerical modelling techniques were the empirically derived equations, of which some of the most commonly used today are those by Heckel (1961) and Kawakita and Lüdde (1971). Those equations were derived from experimental results to represent the relationship between the compaction load and the compact's porosity or density. While suitable for a range of powders and loads, these equations are not always accurate and rely on parameters that can not always be tied to physical phenomena. Kawakita's equation performs well for light and fluffy powders, such as found in the pharmaceutical industry. Heckel, however, performed his experiments with metal powders and they are

the ones his equation is most suitable for. A good comparative review of the two equations can be found in (Denny 2002).

Some of the more recent equations include that proposed by Shapiro (1995), who after evaluating many of the previously proposed equations developed a General Compaction Equation. The author found it to be an improvement on those proposed previously, but remarked that further experiments were needed to provide coefficients at higher pressures.

Another of the more recent analytical equations for the interpretation of powder compaction was proposed by Lordi, Cocolas et al. (1997). The equation fitted the criteria of material independence and of physical significance of the calculated parameters, but failed to provide sufficient accuracy at pressures lower than 10MPa, where particle rearrangement is the dominant mode of compaction. The proposed equation was an attractive alternative to the Heckel equation as it did not rely on limiting density values for analysing compaction data.

Panelli and Filho (2001) proposed a new phenomenological equation describing the compaction process. The equation used two parameters: A, related to densification of the compact through plastic deformation, and B related to the initial density. The comparison of this new equation to those of Balshin (Niesz 1996), Heckel (1961), Kawakita (1971) and Ge (1991) showed that it allowed for an improved evaluation of compaction characteristics compared to the other equations. However, it was found that the rearrangement phase of the compaction could impact negatively on the accuracy of the results.

The analytical equations reviewed above are limited, as they cannot be used to predict local densities, particularly for compacts of more complex shapes (i.e. they are restricted to cylinders or discs). They typically cover a limited range of materials and loading conditions.

These limitations and the continuing progress of computer technology led to greater focus being given to finite element models, which are capable of considering more complex geometries and can predict localised variations of

stress and density. Another benefit is the capability of taking the results of die fill simulations as input conditions, although this is not yet widely practised.

2.3.1.2 Finite element models

In order to obtain a quantitative description of physical phenomena a system of differential equations applied to a certain region or domain is typically used. However, only the simplest of equations applied to trivial geometrical boundaries can be readily solved. An approximate solution can be obtained if the domain is discretized into small elements, thus allowing for the equations to be recast in a simpler form (Zienkiewicz and Morgan 1983). Different forms of discretisation exist, but the numerical simulations presented in this review employed the finite element method.

This section of the review will mention briefly some of the work on developing finite element models of the compaction process but will primarily focus on the practical applications of the method. Different compaction models require different input parameters, but these can be grouped into those describing elastic properties, yielding behaviour and friction. Work presented further in this thesis includes the determination of elastic parameters through a variety of experimental techniques. These are particularly important during the unloading and ejection stages. The determination of the yield characteristics is demonstrated in Appendix 1 for the Cam Clay model. The determination of the friction coefficient for the variety of loading conditions which are encountered during the compaction and ejection stages is explored in Chapters 4 and 5.

One of the early models was developed by Tran et al. (1993) who modified the existing soil mechanics models (Mohr-Coulomb, cap and the critical state models) to allow large displacements and stresses. The Coulomb friction law was implemented through the use of frictional interface elements to model the frictional interaction between the powder and the tools. The model was applicable to both metal and ceramic powders and also allowed for the elastic rebound, or springback effect, to be evaluated. The model predictions agreed well with experimental results for simple cases, and an adaptive remeshing

technique was recommended for more complex geometries. The input parameters for the yield model could readily be obtained from standard experimental tests.

Mosbah and Bouvard (1996) implemented an elasto-plastic yield model with elliptical yield surfaces in a finite element code. The model parameters for the iron powder simulated were obtained from instrumented die compaction and simple compression tests. An advanced powder-die friction model was implemented – the friction coefficient was a function of radial stress and the data for it was obtained from a "pin on disc" friction experiment. As well as the compaction stage the paper considered the unloading and ejection stages, which was an improvement on the previous models. The ability to predict the residual stresses after ejection was of value as input data for the modelling of the sintering process. The surface stresses on the tools obtained during the simulation were compared to experimental results and reasonable agreement was observed.

Ariffin, Gethin et al. (1998) presented a numerical simulation of powder compaction, relaxation and ejection and validated it against experimental data obtained in both laboratory and factory conditions. The powder was taken to be a rate independent elastoplastic material. An elliptical cap yield model was used to represent the densification of the powder. A friction model, based on a plasticity analogy, was required for simulation of the ejection process. The numerical simulation was validated for two different compact configurations and was found to have good agreement with the experimental results.

Sun and Kim (1997; 1998) reviewed a range of yield functions and reported that the Cam-clay model produced better agreement when modelling compaction than the Fleck (1992) and Shima and Oyane (1976) models. Of which the model based on the Fleck function provided the better result. In the latter paper the authors also investigated the effect of single ended and double ended compaction kinematics. The compaction was simulated for relative densities of up to 0.75. Good agreement was observed for the model based on the Fleck yield function when a friction coefficient of 0.16 was used.

C.-H. Park et al. (1999) proposed a phenomenological yield criterion for continuum mechanics based modelling of the uniaxial compaction of various ceramic powders. They proposed three parameters that could be obtained from a uniaxial compaction experiment and which characterise the geometric hardening of the compact and the strength of the base material. The model agreed well with experimental results for the three ceramic powders used in the study. The data was only validated for relative densities below 0.6 however that is typically sufficient for ceramic materials.

The PM Modnet Computer Modelling Group (1999) presented a benchmark study on computational models of powder compaction. Models with different representations of yield and friction behaviour were used to simulate the compaction of a two level synchroniser hub. Some of the participants of the study have reported sensitivity of the simulations to fill density distribution, which is a subject that will be examined in more detail in Chapter 3. They have also assessed the impact of different friction models on the simulation. This highlighted the requirement for friction data that is accurate throughout the complete range of densities encountered during the simulation. This will be addressed in Chapters 4 and 5 of this thesis. Overall, encouraging levels of accuracy, both when looking at compact density and tool forces, were achieved with computational demands low enough for simulation to be used as a practical tool in the powder compaction industry.

Another application of compaction modelling simulations is to model cracking. O. Coube and H. Riedel (2000) improved a Drucker-Prager cap model and used it to predict possible crack formation during powder transfer, compaction, relaxation and ejection processes. Two models were developed with the first predicting cracks for a limited number of special conditions. The second model was capable of predicting cracks when they were known to occur in practice, but required that additional parameters were obtained, experimental procedures for which have not been developed at the time.

Although many numerical codes only simulate the compaction stage of the process there are some which attempt to integrate multiple stages. T. Kraft and

H. Riedel (2002) implemented user defined routines for compaction and sintering processes into the general purpose finite element method software ABAQUS and applied it to modelling the compaction and sintering of a complex three dimensional part. The authors were able to suggest improvements to the compaction kinematics, which would reduce undesirable warpage of the sintered part. They also predicted increased tool wear in some of the punches.

Another work linking the compaction and the sintering stages was undertaken by R.M. German (2004), who investigated the effects of green body density distribution on sintered tolerances. The author reports on the need for homogeneous density distribution in order to achieve the required dimensions in sintered parts. One of the parameters highlighted as affecting green density distribution was the die filling process, the effect of which will be addressed in Chapter 3. The author also expressed concern about the quality of input data available for compaction modelling, highlighting the lack of accurate friction information, something which will be addressed with the use of the improved shear plate apparatus presented in Chapter 4.

Work on linking the filling and compaction stages was undertaken by O. Coube et al. (2005). They performed an experimental and numerical study of the effect of die filling and powder transfer on the subsequent compaction of Distaloy AE powder. The authors have validated their discrete element filling and transfer code with experimental results and have used the density distribution data from the simulation as initial conditions for compaction simulations. The authors report that the effect of density variations from powder filling and transfer had a small effect on compaction, compared to that of a depression caused by the lowering of the top inner punch.

An example of the successful application of finite element analysis to the solution of an industrial problem involving powder compaction was presented by Zahlan, Knight et al. (2001). A modified Drucker-Prager constitutive model was applied to simulate the manufacture of a pyrotechnic device containing compressed powder. The simulation was used to predict the pressure distribution

in pressed powder and to predict the compaction loads required to maintain the integrity of the powder throughout the manufacturing process.

Another example of the use of the Drucker-Prager constitutive model can be found in (Michrafy, Ringenbacher et al. 2002). A continuum based finite element analysis was used to simulate the compaction of a pharmaceutical tablet as an alternative to using Heckel or hardness equations. The material parameters used in the simulation were obtained through an experimental calibration procedure. The results of the simulation proved to agree with previous data. The authors planned to further confirm the results with more experimental measurements and to apply the method to other powders.

Sinka, Cunningham et al. (2003) also employed the Drucker-Prager model and validated it for use in modelling the compaction of powders with low apparent fill density, such as some pharmaceutical powders. The model was used to explore the impact of die wall friction on density distribution and the results were compared to those obtained from indentation testing. The authors highlighted the need for accurate friction and initial density data, as well as other process parameters, as their impact on the final compact is significant. In conclusion, the use of finite element modelling as an important tool in the design and manufacturing process was acknowledged.

Michrafy, Dodds et al. (2004) studied the effect of friction on density distribution by modelling the compaction of a pharmaceutical tablet using a Drucker-Prager cap model. The authors reported on the suitability of the modelling method for the simulation of the problem, but stated that measurement of some of the parameters was required. The four point bending technique was used to obtain Young's modulus at different densities, while friction data was gathered from closed die compaction tests.

2.3.2 Discrete models

In discrete modelling the system is described as a collection of individual particles. These can be either considered as being rigid or deformable. A core requirement is the capability to identify new and breaking contacts automatically.

Early models assumed rigid particles and interaction captured through simple contact models. More recent developments use plasticity models to capture the interaction and the most recent combined discrete and finite element simulations effectively capturing all that deformation in the particle. An example of a discrete element model with deformable particles is presented in (Ransing, Gethin et al. 2000). These authors reported good agreement with established models. The discrete method presented also allows consideration of mixtures accounting directly for the influence of combining various powders. This was illustrated for mixtures comprising ductile and brittle particles.

For future applications the attraction of discrete modelling of the powder compaction process is the possibility to link the output data of discrete die filling simulations, such as in (Wu, Cocks et al. 2003) and (Wu, Cocks et al. 2003b), to input conditions of the compaction model. It also provides the opportunity to explore the influence of particle interaction on global material response.

2.4 Friction measurement

For a numerical simulation of the powder compaction process to be successful then accurate input parameters are required. One such parameter is the friction coefficient between the powder and the die. Its significant impact on the simulations has been reported in the literature, (PM Modnet Computer Modelling Group 1999) and (Sinka, Cunningham et al. 2003), and a study focusing on the effect that friction has on green density was performed in (Michrafy, Dodds et al. 2004). Thus, there is a great need for both accurate friction data for specific powders and for a better overall understanding of the friction mechanisms during powder compaction.

The aim of this section is to introduce modern techniques which are used to measure the friction between the powder and tooling and to review the applications of these techniques to improving the understanding of friction mechanisms. There is no single universally accepted technique for measuring powder-die friction, but essentially two approaches are followed: direct and indirect.

The direct measurement techniques involve the measurement of the shear force during the sliding of a compact against a target surface which represents the tooling. The ratio of the shear and normal forces then gives the friction coefficient. The equipment used for direct friction measurement includes the shear plate apparatus and the pin-on-disc machine.

In the indirect approach the friction coefficient value is calculated from a die compaction experiment, where the equipment is instrumented so that the top and bottom axial stresses and also the radial stresses are known. The friction, which prevents a complete transmission of load from the top punch to the bottom punch, can then be quantified. The instrumented die test equipment is an example of an indirect friction measurement apparatus.

Two examples of direct and indirect measurement equipments were compared by the PM Modnet Research Group, who obtained friction data from a number of research groups (PM Modnet Methods and Measurements Group 2000) and (PM Modnet Research Group 2002). The results from each group showed good agreement between the shear plate apparatus but a much larger spread in data when using the instrumented dies. This may be due to variations in the design of the instrumented dies, such as the instrumentation for measuring radial stress and die rigidity. The algorithms that were used to analyse the data from the instrumented die experiments could also be a factor. While the instrumented die can be used to fully characterise powders, the more specialised design of the shear plate apparatus makes it better suited for characterising powder friction.

2.4.1 Shear plate and other direct measurement equipment

The shear plate (also known as sliding piece) apparatus has been used successfully to measure the effect of various process parameters on the friction coefficient.

P. Doremus et al (2001) used a shear plate apparatus ("sliding piece device") to investigate the friction between iron powder and a tungsten carbide tool wall. Density, normal stress, sliding velocity, temperature, and displacement were considered as parameters in the friction process and their effects were evaluated.

The authors concluded that density and normal stress reduced the friction, sliding velocity increased it, and temperature had no significant effect. The amplitude of the displacement was found to greatly affect friction and the amount of damage to green parts.

I.M. Cameron et al (2002) also explored the use of a shear plate apparatus to measure friction between a compacted powder and a target surface which represented the tooling. The authors determined that the variability in experimental data was a physical characteristic of the powder being tested. They then proceeded to confirm the major impact of surface hardness, roughness, and roughness orientation on the friction coefficient. The hardest surface resulted in the minimum values of static and dynamic friction. Smoother surfaces resulted in lower static friction, however, minimum levels of dynamic friction did not always correspond to the smoothest surface.

V. Bonnefoy et al (2003) used a sliding piece device to test a range of tool treatments and coatings when used with poorly lubricated powder mixes. They found that for low quantities of lubricant and certain tool surfaces the experiments could not be completed as the damage to the compact was too high. Even for the lowest friction surfaces some lubrication was required in order to produce a damage free compact. The authors found that the sliding velocity had no effect apart from accelerating the damage of the piece surface. No stick-slip behaviour was encountered during the tests, although the speeds used were up to forty times higher than those used in other laboratories.

Among other direct friction measurement equipment is the novel apparatus introduced by N. Solimanjad (2003). The friction was measured between the top punch and the top of the ringed powder compact, which rotated together with the die. The author explored the effects on friction of the compaction mechanisms and of the roughness of the compact surface at different densities. The relationships between the normal load and the friction coefficient, and the compact density and the friction coefficient were also explored. The friction coefficient was found to decrease for higher densities and normal loads.

2.4.2 Instrumented die

The advantage of using an instrumented die apparatus is that it is possible to include friction measurements into the general powder characterisation tests, which are required in order to obtain material parameters for numerical simulation. The disadvantage is that there is little scope to explore the effect of surface properties, since it implies a need to manufacture a new die for each case under consideration.

Experimental techniques for analysis of the compaction and ejection of metal powder were described by P. Mosbah et al. (1997). The derivation of the friction coefficient from the instrumented die test was included in the analysis. Two types of instrumented dies were described, with information provided on how to interpret the instrumentation readings into a true representation of the radial stress. Both types of instrumented dies produced similar results. The compaction, relaxation and ejection processes were then analysed. Additionally, data collected, together with data from simple compression tests, was used to identify the constitutive equations needed for the numerical simulation of the compaction process.

An alternative way of deriving the friction coefficient was presented by S. Turenne et al (1999). The authors used an instrumented die to evaluate powder-die friction via an empirical parameter called the slide coefficient, which was obtained from the applied pressure/transmitted pressure ratio. In order to obtain the friction coefficient a procedure based on the evaluation of the ratio of radial to axial stress was employed. The friction coefficient for an admixed zinc stearate added iron powder, with and without die wall lubrication, was determined. Die wall lubrication was found to improve the uniformity of the compact and lower the ejection energy per unit volume of the compact.

Later, S. Turenne et al (2000) went on to use the slide coefficient to determine friction in a study of the effect of temperature on the behaviour of lubricants during powder compaction. The motivation for this work was to investigate if lubricant properties were affected by the higher temperatures experienced in

warm compaction. They also highlighted the different roles of admixed lubricants during the initial rearrangement and final compression stages of the compaction process and also during ejection.

2.4.3 Lubrication

The issue of lubrication in PCM is a complex one. While successful compaction is often possible without the addition of a lubricant, the ejection of the compact without causing damage may be more difficult. Thus, the problem is to select the most desirable amount and kind of lubricant so that the benefits of improved green density, or reduced ejection pressure, can be achieved without a negative impact on the apparent density, flowability, and the green or sintered strength (Hirschhorn 1969).

As well as investigating the friction mechanisms and obtaining modelling data, friction tests are extensively used to assess lubricants for the powder compaction process. Two types of lubrication can be identified – admixed lubrication, where a lubricant powder is added to the base powder, and die wall lubrication, where the tooling is coated with a layer of lubricant. Both types of lubrication reduce powder-die friction and help achieve higher densities as well as better density homogeneity in compacts. They also reduce the load and wear on the tool surfaces thus helping to avoid damaging the compacts on ejection.

Admixed lubrication is very common as is very easy to implement, but there are some drawbacks associated with its use. The main disadvantage being that the light lubricant may negatively affect the fill density of the powder and therefore the final density of the compact (as a small quantity by weight results in a large percentage by volume). It is also necessary to remove the lubricant from the compact – this is achieved by burning it off during the sintering stage. Die wall lubrication helps to avoid these problems, but it can be difficult to apply and may require expensive additional equipment.

Research on both the effectiveness of lubrication in powder compaction and methods of applying it is reviewed next. One of the early comparisons of die-wall and admixed lubrication was conducted by Leopold and Nelson (1965). The

authors found that only a small amount of either admixed or die wall lubricant were necessary for a high proportion of the applied force to be transmitted. Increasing the amount of admixed lubricants had little effect. Higher quantities of die wall lubricant, however, resulted in still denser compacts.

Strijbos (1977) evaluated a die wall lubricant during a study of machining groove orientation in the die. Beneficial effects of die wall lubrication were reported. Ward and Billington (1979) studied the behaviour of a zinc stearate lubricant during mixing with iron powder by monitoring the apparent density. Further comparisons were made with powder prepared by depositing a zinc stearate solution onto the iron particles. The powders were then compacted and the friction forces during the compaction and ejection phases were studied. Die wall lubrication was used to determine the relative significance of interparticle friction and powder-die friction.

A comparison between the admixed and die wall lubrication techniques for compaction of aluminium powders was performed by Kehl, Bugajska et al. (1983). Admixed lubrication was found to decrease the true green density and also the green strength of the compacts. The compacts were weakened during dewaxing with dimensional changes also being introduced. The die-wall lubrication technique was found to yield better compacts.

Li, Liu et al. (1996) studied wall friction and lubrication during the compaction of coal logs. The authors found that die wall lubrication reduced the friction coefficient significantly but also promoted an increase in the radial stresses, which may have resulted in increased friction forces and shear deformations. Ejection forces were found to decrease with the use of die wall lubrication.

Briscoe and Ozkan (1997) reported higher densities and reduced friction when using die wall lubrication in their study of the compaction behaviour of agglomerated alumina powders. Other parameters considered in the study were binder type, binder content, moisture level and agglomerate size.

Turenne, Gode're et al. (1999) evaluated the friction conditions in powder compacts when both admixed and die wall lubrication were applied. The friction was found to be significantly lower when a die wall lubricant was used. Additionally, the trend of reduction in friction was observed for higher relative densities.

Li, Ngai et al. (2002) studied the effect of die wall lubrication on warm compaction. The authors concluded that for the range of powder mixtures considered, the results differed with the amount of admixed lubricant. The highest green density values and lowest ejection forces were observed for the compacts pressed with die wall lubrication being used.

Simchi (2003) compared the effects of the admixed and die-wall lubrication approaches for a range of compaction pressures and sintering temperatures. The admixed lubrication was reported to aid densification at lower pressures but was found to limit it at higher pressures. Die wall lubrication was found to be beneficial for a wider range of process parameters, with better densification and green strength being observed.

There are a number of methods of applying die wall lubrication, these range from application by brushing of lubricants dissolved in solvents (Li, Ngai et al. 2002) to spray deposition of electro-statically charged lubricant particles (Ball, Hibner et al. 1997) (Yang, Gui et al. 2006). An automatic system was proposed by (Haeckl 1968), where dissolved lubricant was drawn into the die by capillary action induced by the motion of the die and punches during ejection.

2.5 Unloading and ejection

The research on the unloading and the ejection stages has focused primarily on obtaining elastic data for the unloading stage, analysis of springback during unloading and ejection and evaluation of friction during ejection. To date a number of different tests for gathering the elastic parameters in powder compacts have been used. Among these were the free standing axial compression tests, tensile tests, three and four point bending tests and die tests performed in instrumented dies. A comparison of some of these tests for the determination of

elastic parameters is presented in Chapter 6. Additionally, the new floating die shear plate equipment presented in Chapters 4 and 5 of this thesis can be used for measurement of the friction coefficient under the loading conditions particular to the ejection stage. A review of recent research focusing on the issues relevant to the ejection stage now follows.

Malamataris, Hatjichristos et al. (1996) measured the "apparent" Young's modulus in cylindrical pharmaceutical binary mixture tablets. The Young's modulus was obtained by measuring the compact deformation during compressive axial loading. Radial deformations were not accounted for in the test, thus the "apparent" rather than the precise value of Young's modulus was obtained. The resulting Young's modulus was compared with the tensile strength isotropy, which is expressed as being the ratio of axial to radial tensile strength.

Recently, Kachrimanis and Malamataris (2004) employed the same testing methods to explore the dependence of "apparent" Young's modulus on particle size for pharmaceutical powders. The authors also attempted to correlate values of the percentage of elastic radial recovery to the Young's modulus data.

Poquillon, Baco-Carles et al. (2002) used three point bending tests to evaluate the relationship between powder morphology and mechanical properties of powder compacts. The tests were used to obtain the fracture strength and elastic properties of pressed powder slabs comprising two different iron powders through single action compaction. The maximum loads obtained during the test were used to calculate the transverse green strength. The Young's modulus was also calculated, although it was found to be far lower than that of a polycrystalline iron material. The authors noted that the material behaviour may not be homogenous throughout the thickness of the compact.

Nam, Li et al. (2003) used laser dilatometry and X-ray computer tomography to study the relationship between springback on ejection and the density distribution in the compact. They found unexpectedly, that the expansion of the lower density zone of the compact was greater than that of the higher density zone. The authors also reported the negative impact of binder on final

dimensional tolerances and differential springback. They also reported sinusoidal dimensional variations caused by the differential release of residual stresses during ejection.

Briscoe and Rough (1998) assessed the effect of wall friction on the ejection of ceramic compacts. One of the parameters considered was the die wall lubrication, which was found to significantly reduce the forces required to eject the compact. Compacts pressed in a non lubricated die were found to show stick-slip behaviour during ejection, with the magnitude of fluctuations depending on the frictional forces. Other parameters considered were the aspect ratio, the compaction forces and the ejection speed. The ejection force was found to increase with an increase in aspect ratio and compaction force. The stick-slip fluctuations were found to increase with increases in aspect ratio and compaction stress and with a decrease in the ejection speed.

F.Sanchez et al. (2001) studied the effect of tool kinematics and ejection on the axial density distribution of green compacts. They used a range of kinematics for the uniaxial pressing of a high slenderness bushing. The results showed the significant influence of the compaction process sequence on the final density and highlighted the need to optimize the pressing process for each specific design of a compacted part in order to obtain a satisfactory density distribution.

2.6 Closure

The compaction of powder is affected by numerous process parameters, among which die filling and powder-die friction were identified as some of the most prominent. While the effect of friction on compaction is quite well documented there are still gaps in our understanding of the full impact of fill conditions. From the review of filling research it may be concluded that the die filling stage is affected by a vast array of process conditions, resulting in non uniform fill density distribution. The work in Chapter 3 of this thesis attempts to fill this gap in understanding by using the die filling research as a basis for the initial conditions to be considered in a numerical study of the effect of die filling. The tool forces and green density in simulated compacts pressed from different initial

conditions will be compared. The study will consider a selection of compact shapes and powder materials.

The review of work on compaction modelling showed that accurate friction data is vital if realistic compaction simulations are to be achieved. Recently, a great deal of research was conducted in the area of friction measurement and such factors as compact density, surface finish, hardness and orientation of the target surface and the sliding velocities and distances have been explored. There is however a lack of understanding of friction mechanisms under different load conditions, as many types of test equipment do not allow completely independent control of compaction and normal loads. This is particularly relevant when measuring friction during ejection, as the normal forces present during that stage are much lower than those reached during the compaction process. This is addressed in chapters 4 and 5 through experiments using the new floating die shear plate apparatus. These also explore the friction mechanisms with regards to admixed lubrication. The new equipment is also assessed with respect to its suitability in evaluating die wall lubrication.

The modelling of the unloading and ejection phases is not as comprehensively developed as that of compaction modelling. There is a need for accurate test methods for the measurement of elastic parameters and cohesion. The instrumented die, the unconstrained uniaxial compression, the three point bending and the Brazilian disc experiments will be assessed as methods of determining parameters for ferrous and ceramic powders in Chapter 6. The ejection process will also be considered in Chapter 7, where the problem of radial pressure measurement during the ejection phase will be addressed. Additionally, the axial recovery of the compact during ejection will be explored through the use of a split die, which allows extraction of compacts at any stage before or during ejection.

Chapter 3 An exploration of the effect of fill density variation on the compaction of ferrous, ceramic and hard metal powder systems

3.1 Introduction

This chapter introduces a study of the effect of fill density distribution on the pressed density. The motivation behind this was to assess the significance of fill density distribution on compact pressed density. To achieve this, a series of case studies involving different powders, part geometries and density distributions was performed. These focused on a simulation of the compaction process, starting from different initial fill density, from which its impact on final compact density, stresses and tool forces could be explored. These studies excluded any friction variation effects since these will be explored fully in other chapters within this thesis. This chapter will address the reasons behind fill density variations and their types, and the effect of these variations on pressed density for simple and complex geometries and for powders of different type.

3.2 The Study

Three powders representative of three different powder types were considered in the case study:

- Hard Metal – Tungsten Carbide, supplied by Eurotungstene, composition: 10% Co, 2% PEG, WC balance
- Ferrous – Distaloy AE, supplied by Höganäs, composition: C-UF4 - 0.5%, Kenolube - 0.6%, base powder – 4% Ni, 1.5% Cu, 0.5% Mo, balance Fe.
- Ceramic – Zirconia (ZrO_2) with organic binders, supplied by Dynamic-Ceramic

These powders were chosen since they differ in particle size, shape, roughness, strength and ductility.

Tungsten carbide powder used in this work is granular, with spherical granules of 200-500μm.

Distaloy AE powder used consisted of particles ranging between 25μm and 75μm in size and of rough and irregular shape, see Figure 3.1. These factors are likely to promote particle interlocking and bridging, which together with the ductility of the material will result in particle deformation at lower loads than found when compressing hardmetals. This phenomenon is particularly likely to occur at inter-particle contact points, and will result in a reduced rearrangement phase. The bridges vary in strength and collapse at increasing force levels, resulting in a phase where both particle deformation and rearrangement (during the collapse of the bridges) are present at the same time.

Zirconia powder was agglomerated to a granule size of between 30 and 80 microns, see Figure 3.1. The granules can be broken apart with relative ease. The individual particles are brittle and are much weaker than the ferrous and tungsten carbide particles. Therefore, much lower forces are required for the compaction of Zirconia powder.

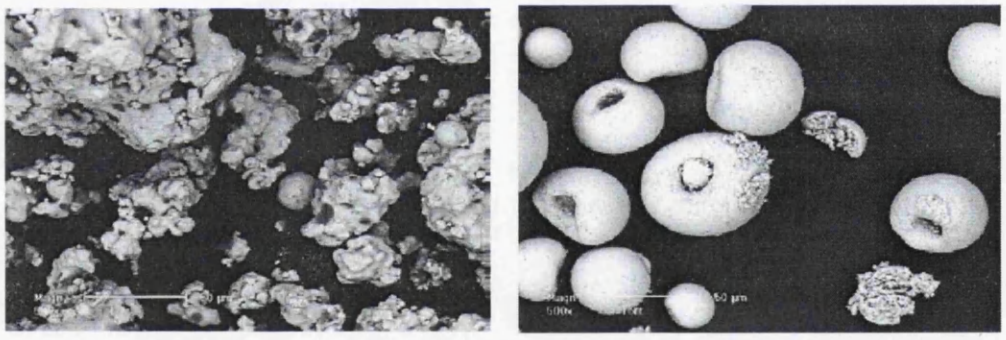

Figure 3.1 SEM micrographs of Distalloy and Zirconia powders (Cocks 2005)

The differences in particle morphology and material properties for the three powders result in different proportional representation of the two compaction modes. This may result in differing sensitivity to fill density variations. Whether this is indeed the case will be explored further in this chapter.

In order to implement these materials into the numerical simulation of compaction, a powder characterisation process needed to be carried out in which

material parameters for the Cam-Clay compaction model were derived from experimental data sets. This was not an easy task as the powder characterization process was complicated by the variations in the amount and format of the experimental data provided. While comprehensive data was available for the tungsten carbide powder, Distaloy AE data was very brief. Data for the Zirconia powder had to be taken from a number of sources, with experiments having been performed under different conditions. The experimental data for the three powders was supplied by Doremus (2002). Additional data for the Zirconia powder was obtained from (Schneider, Thomson et al. 2003). The process of powder characterisation and the derivation of material parameters for the Cam-Clay model are explained in Appendix 1. The material parameters obtained for each powder are also presented in the Appendix. However, prior to exploring fill sensitivity effects it is essential that the compaction models are validated.

3.2.1 Validation of numerical code and material parameters

The numerical code used was validated against other codes and experimental data in a benchmarking study performed by the Modnet group (1999). Five research centres took part in the study, applying codes with different yield and friction models to simulating the compaction of a two level synchroniser hub part. The numerical results were then compared with experimental data for the part. The simulations proved to be sufficiently accurate in both the predicted tool forces and the density distribution.

However, before the code could be used in the study the material parameters obtained during the characterisation process, as shown in Appendix 1, also needed to be validated. This was achieved by reproducing numerically the experiment from which the characterisation data was derived.

The process of validation was time consuming for the hardmetal powder. This was because a compaction simulation of powders which show extensive deformation at low loads, such as tungsten carbide, was computationally demanding. This was caused by the very small size of the initial yield surface in which the hydrostatic and deviatoric stress levels are very small. This required

that the time steps in the simulations were reduced dramatically in order to achieve convergence.

As a step to solving this problem a feature was implemented into the code, which allowed for the size of the initial yield surface to be set manually. This dramatically reduced the computational time required to complete a simulation, but had no effect on the final result. Additionally, a version of the code was compiled to run on a Unix server equipped with four ~1GHz DEC Alpha CPU's and over 9Gb of RAM, which enabled running of a number of simulations simultaneously and on a faster computer.

Another important issue was the density range for which the experimental data was available. In each case the minimum density for which the experimental data was recorded has been significantly higher than the fill density. This meant that it was harder to obtain model parameters which would be appropriate for the whole duration of compaction, as it was impossible to evaluate their accuracy at lower densities.

The simulations in the following section were carried out to validate the material model for each powder. In each case, the top punch force evolution was chosen as the validation parameter. It was previously found (PM Modnet Computer Modelling Group 1999) that the tool forces are harder to predict than the final densities and is therefore a more sensitive parameter for simulation validation.
In each case the geometry used in the simulation was that of a cylinder, see Figure 3.2. Dimensions varied for each case in order to accurately represent those used during characterisation experiments for each powder. As the numerical code used was axisymmetric only one half of the cylinder section was modelled. Three tool boundaries were used: the first representing the top punch, the second representing the die wall and the final tool in place of the bottom punch. A final boundary, with symmetry conditions passing through the middle of the simulated compact, enclosed the domain. The boundary conditions on the tool faces allow for sliding motion, with a constant friction coefficient for the hard metal and ceramic powders and a variable value for the ferrous Distaloy powder.

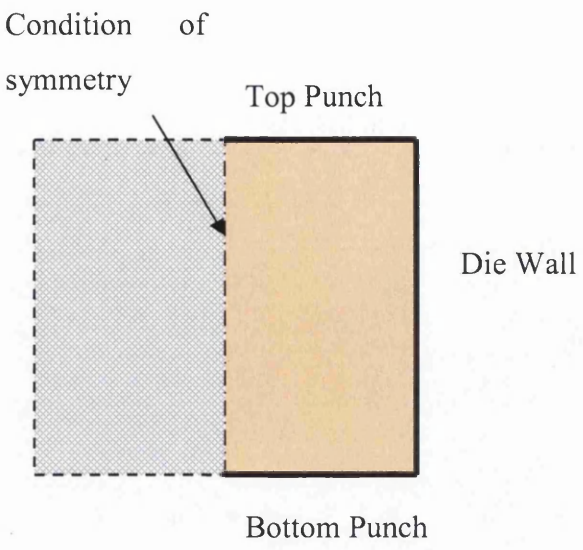

Figure 3.2 Geometry of the validation simulations

3.2.1.1 Material Parameter Validation – Tungsten Carbide

The hard metal powder used was tungsten carbide from Eurotungstene (2006).

The procedure for obtaining the Cam-Clay material model parameters Q_{max}, K_1, K_2 and K_3 and their values are available in Appendix 1. Here the die compaction simulation used to validate the model parameters is presented. The die compaction experiment that provided data for the material parameters was recreated numerically. A uniform fill density distribution was assumed for the simulations with simple single ended compaction kinematics. The predicted top punch forces were compared with those recorded during the experiment. Good agreement can be observed, as seen in Figure 3.3.

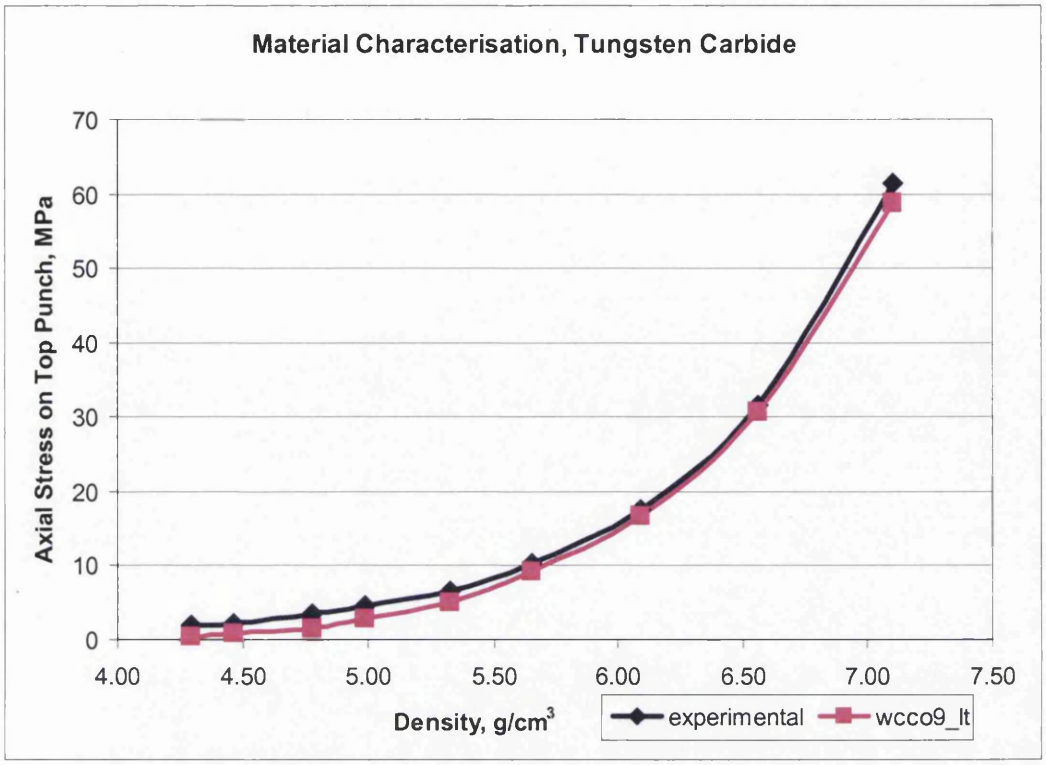

Figure 3.3 Material Characterisation, Tungsten Carbide

3.2.1.2 Material Parameter Validation – Distaloy AE

Material parameter validation for this ferrous powder was performed in the same manner as for the tungsten carbide powder. The plot of top punch loads from experiment and simulation is shown in Figure 3.4. There is good agreement between the model and the experiment.

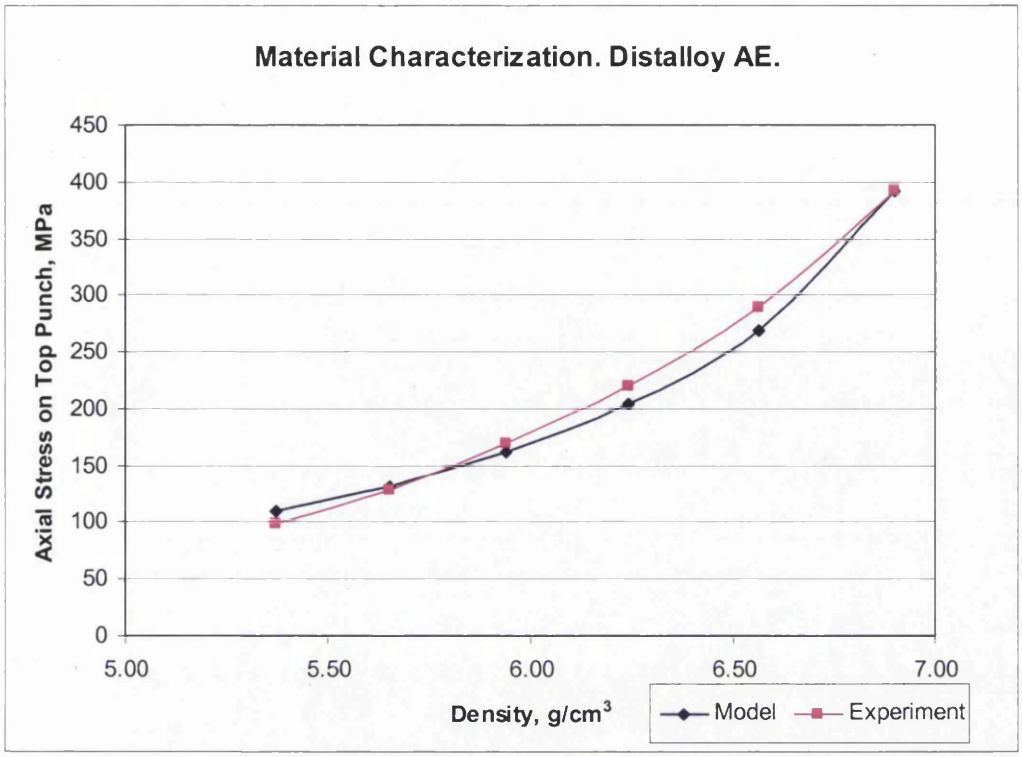

Figure 3.4 Material Characterisation, Distaloy AE.

3.2.1.3 Material Parameter Validation – Zirconia

The plot of predicted and actual top punch forces is shown in Figure 3.4. It was impossible to achieve good agreement throughout the range of densities and accuracy at lower levels of density was sacrificed for good agreement at the end of compaction. This was due to the previously mentioned lack of data for the lower densities.

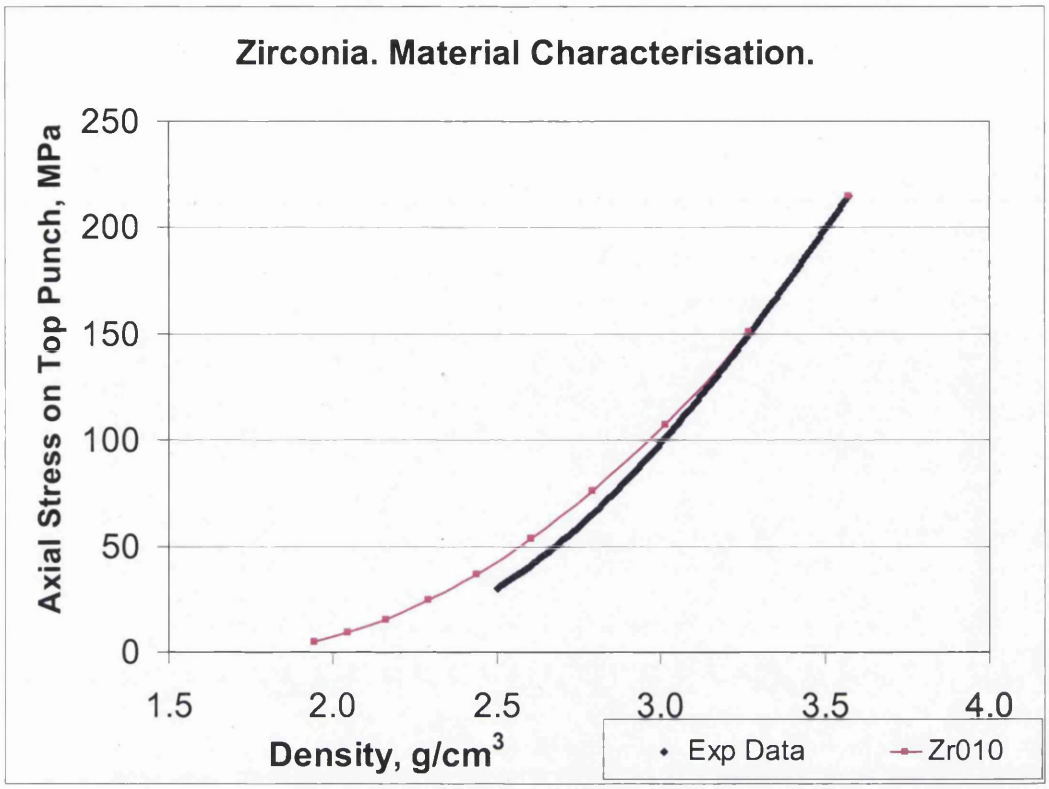

Figure 3.5 Material Characterisation, Zirconia.

Overall, good agreement between the numerical and experimental results was observed for all powders. The material model parameters could now be used to simulate compaction in the study of the effect of initial fill density distribution.

3.2.2 Fill Density Distribution

Fill density distribution can be affected by a number of parameters – flowability of the powder, shape and orientation of the die and filling shoe (how wide or narrow is the die, presence of steps in the die), method of filling used (gravity fed or vacuum assisted fill, the height of powder in the hopper), use of shakes and number of passes of the fill shoe, etc (Schneider, Cocks et al. 2005). This study attempts to assess the impact of fill density distribution, affected by the above process parameters, on the compact pressed density. To that effect a comparison was made between simulated compacts where fill density was uniform and where it was not.

It was appropriate to start the study with a simple geometry. If simple compacts were significantly affected by the fill density distribution then it would very likely have an effect on more complex geometries.

A hollow cylindrical geometry was considered as the first shape for the study. Hollow cylindrical components are a common product of the powder metallurgy industry. The presence of a core rod in the geometry restricts powder movement both via its physical presence and through friction between the rod and the powder. The internal and outer diameters of the selected hollow cylinder geometry were common with the lower section dimensions of the Dienet geometry (Doremus 2002). The dimensions are shown in Table 3.1:

Table 3.1 Hollow cylinder ferrous geometry

Nominal geometry	
H, mm	30
Inner diameter, mm	25.8
Outer diameter, mm	47.8
H, fill height, mm	60
Assumed fill density, g/cm3	3.3
Compaction ratio	2

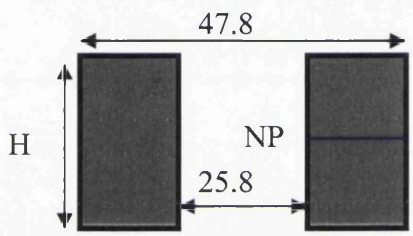

Wu and Cocks (2004) have identified that in their work on die filling for geometries with high aspect ratio there was a risk of air entrapment and bridging. This would most likely occur for powders with irregular shapes and high surface roughness as such particles would be most likely to interlock, promoting the formation of bridges. This kind of geometry may also be difficult to fill completely in a given time for lower density materials, as light particles would be prevented from entering the die by the extruded air. However, in this study the focus was on the variation of fill density in the die, rather than on whether the die could be filled completely. With that in mind the irregular Distaloy AE powder was considered for this geometry.

Another common subset of geometries consists of flanged components with either an external or an internal flange. A component with an external flange was considered in a Dienet group study (Brewin and Federzoni 2006). One example

of an internal flange components was the synchroniser hub considered by the Modnet group in the benchmarking study of compaction modelling computational codes (PM Modnet Computer Modelling Group 1999). Both geometries were considered in this study.

Originally the Dienet range of geometries had common diameters, with fill heights and compression ratios varying for each of the powders considered. However, in this work common values for fill heights were used for all powders. The desired compaction ratio was achieved by adjusting the displacement during the compaction stroke. An example of the Dienet geometry with dimensions for the ferrous powder case can be seen in Figure 3.6

Nominal geometry	
H1, mm	11.36
H2, mm	22.72
Target press density	7.1
Fill density	3.09
Comp ratio	2.2
Part internal radius, mm	1.0
Fill geometry	
H1, filling, mm	25
H2, filling, mm	50

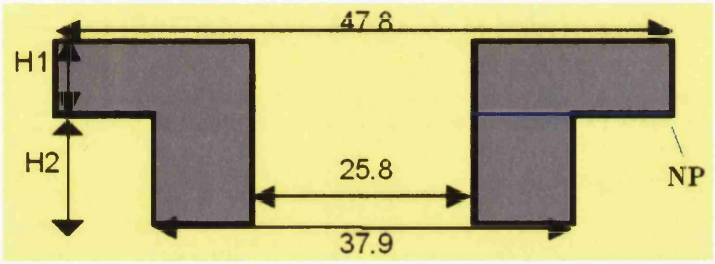

Figure 3.6 Dienet ferrous geometry

The final Modnet geometry is shown in Table 3.2

Nominal geometry	
H1, fill height, mm	32
H2, fill height, mm	26
Inner diameter, mm	29
Mid. diameter, mm	68
Outer diameter, mm	78
Assumed fill density, g/cm3	3.3
Compaction ratio	2

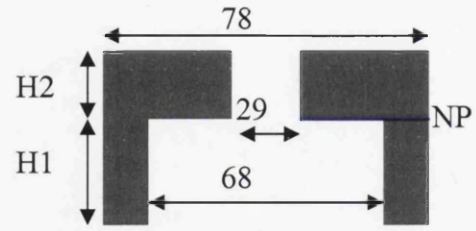

Table 3.2 Modnet part ferrous geometry

Both flanged geometries consisted of a wider top part and a narrow lower part. Burch (2004) has identified via X-Ray Computerised Tomography that the density at fill is likely to be lower in the narrower lower section of a two-level component, see Figure 3.7.

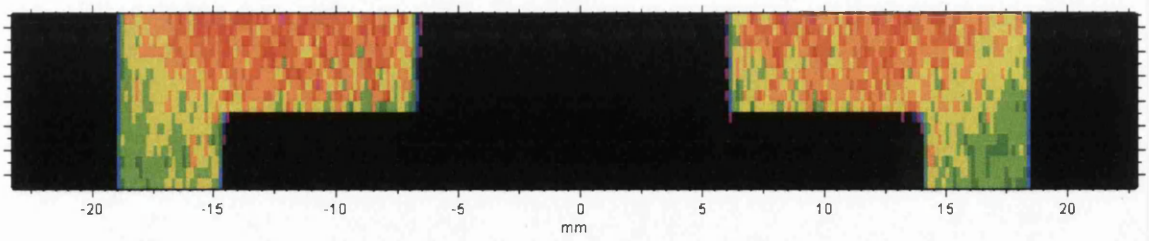

Figure 3.7 X-Ray Computerised Tomography of a filled die

Double ended compaction kinematics were used for each geometry and the punch displacements were selected to provide the required compaction ratio. The neutral plane was at the middle of the cylindrical compact and was located on the plane of the top surface of the outer lower punch for the Dienet configuration and on the plane of the top surface of the inner lower punch for the Modnet configuration, as indicated on the images in Figure 3.8. The punch travel was set such that the compaction ratio on each side of the neutral plane would remain the same.

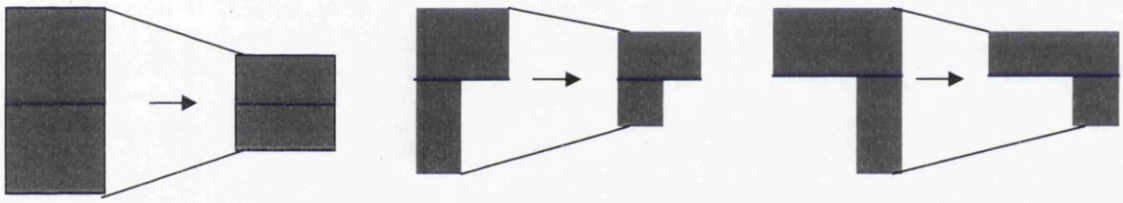

Figure 3.8 Compaction kinematics a) cylindrical part b) Dienet geometry, c) Modnet geometry

3.2.3 Sensitivity study - Cylindrical geometry

The sensitivity study began with the cylindrical geometry. Distaloy powder was the material chosen for the simulation, as its rough surface and irregular shape would be most likely to encourage bridging.

Fill density was taken to be 3.3 g/cm^3 for the uniform fill case. The compaction ratio was 2.0. For the non uniform fill case the compact was divided into two regions of equal density – the top and bottom halves. The density in the top part was set at a 10% higher value than that in the lower part. Mass balance was maintained to keep the average fill density at 3.3 g/cm^3, see Figure 3.9. The compaction was then simulated for both the uniform and non uniform

distributions. In each case identical double ended compaction kinematics, as shown in Figure 3.8, were employed. The resultant density distribution is plotted in Figure 3.10

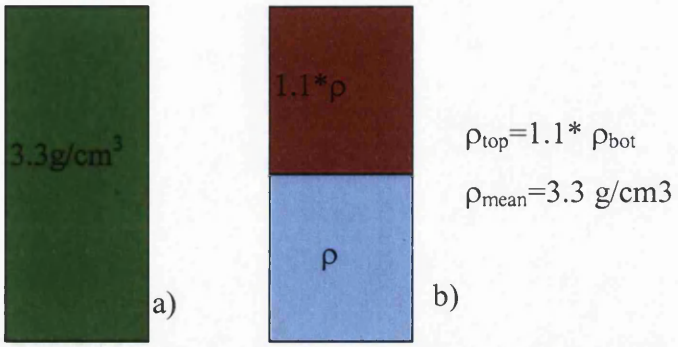

Figure 3.9 a) Uniform fill density b) Two regions with balanced mass.

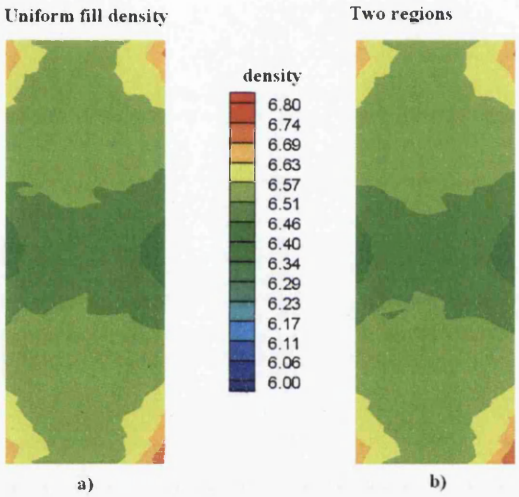

Figure 3.10 Distaloy AE, cylindrical geometry, compacts with a) uniform fill density and b) higher initial density in the top half (ρ_{top}=1.1* ρ_{bot})

It is apparent from Figure 3.10 that, in a compact of simple shape, variations in fill density distribution along the axis of compaction play an insignificant role. This was due to the powder in the region of lower density being initially compressed until it reached a similar density to that of the other parts of the compact. Thereafter compaction would proceed as normal, resulting in nearly identical final density distribution. This is illustrated in Figure 3.11.

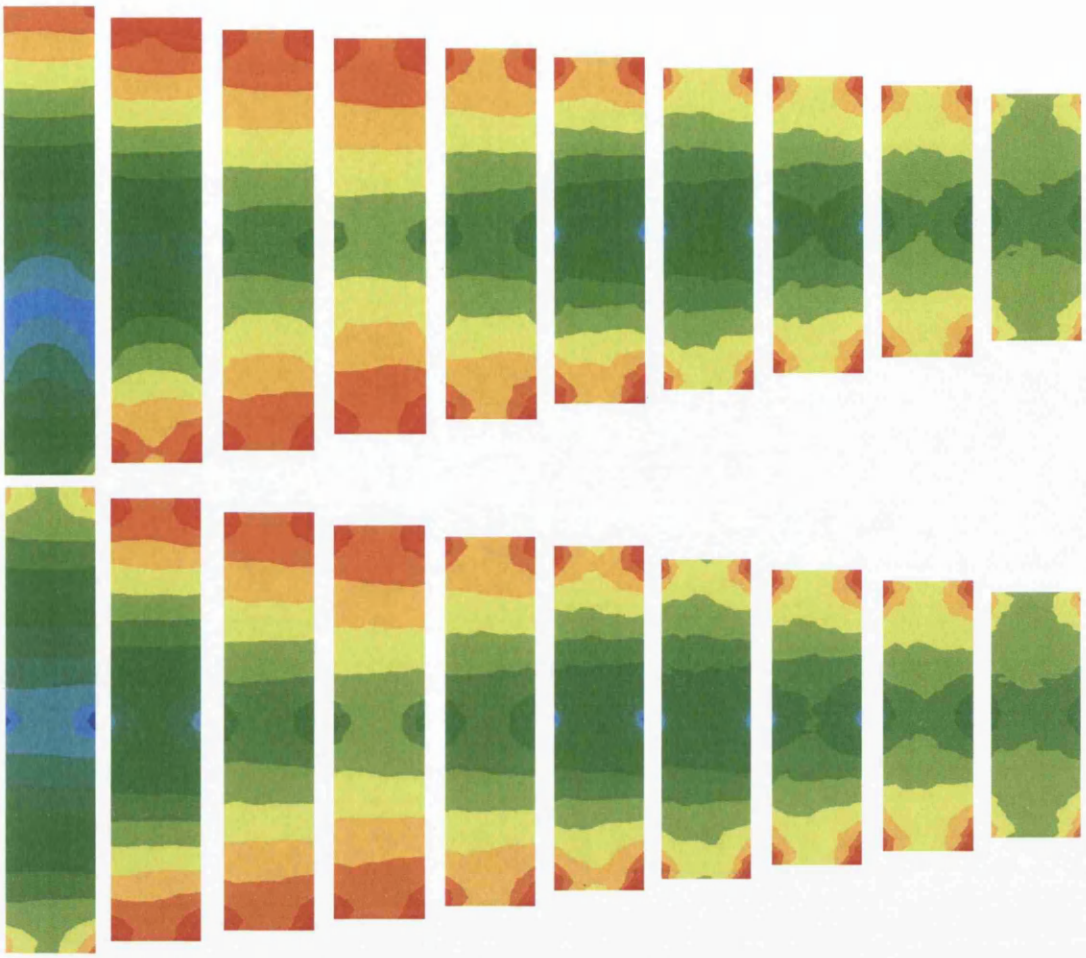

Figure 3.11 Compaction of a ringed compact of non-uniform (top) and uniform (bottom) fill density. Compaction stages in 10% increments starting at 10%. Colour scales independent for each stage.

3.2.4 Sensitivity Study – Dienet geometry

Having established that, for simple geometries, the fill density distribution had no significant influence on the pressed density, the next step in the study was to consider a more complex stepped geometry.

After exploring the factors affecting fill density distribution, and having consulted X-Ray CT scans available for filled dies, four fill density configurations were proposed for the Dienet geometry. First, a compact with a uniform fill density of 3.09 g/cm^3 was modelled as the benchmark simulation. The remaining configurations each consisted of two regions of different density at fill - a region of higher density in the upper section and of lower density in the

lower section, so that density in the upper region was 10% higher than that in the lower region, i.e. $\rho_{top}=1.1*\rho_{bot}$, see Figure 3.12. The mean density remained at 3.09 g/cm^3. The configuration shown in Figure 3.12 b) was selected as it was reasonable to assume that the powder flow into the narrow lower section may be impeded by the escaping air and particle bridging. Configuration c) represents a case similar to configuration b), with the assumption that a denser state may be obtained at the top of the lower section due to the weight of powder above it. Configuration d) may be produced as a result of local densification near the top of the die, caused by repeated passes of the feed shoe over the die.

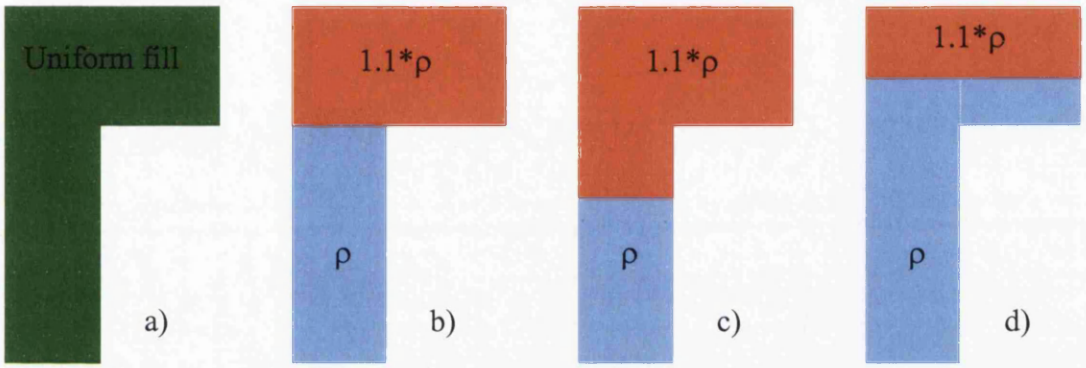

Figure 3.12 a) Uniform fill density b), c) and d) Two regions with balanced mass

As mentioned previously, proportional double ended compaction kinematics were used, see Figure 3.13.

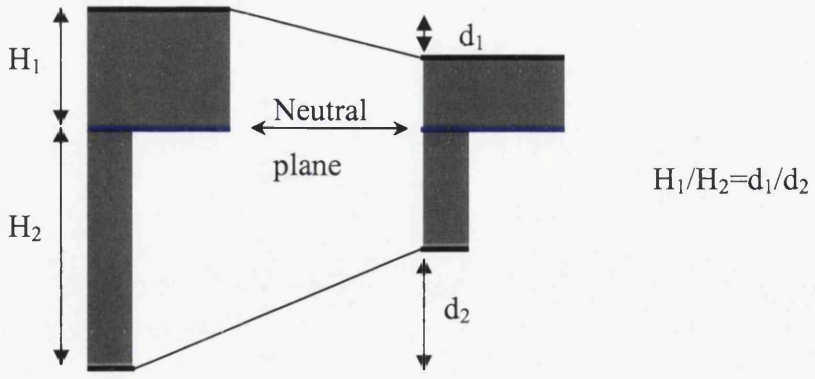

Figure 3.13 Double ended kinematics

The pressed density contour plots are shown in Figure 3.14 and Figure 3.15. The same levels for contour colours were used in all four cases.

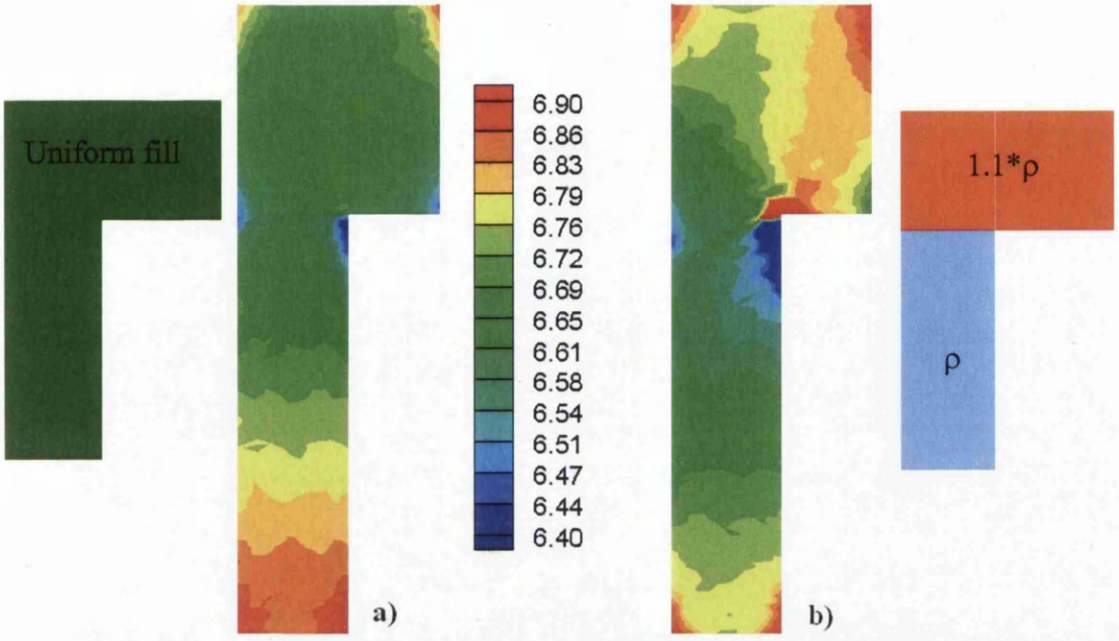

Figure 3.14 Distaloy AE, Dienet geometry, compacts with a) uniform fill density and b) higher initial density in the top region ($\rho_{top} = 1.1 * \rho_{bot}$)

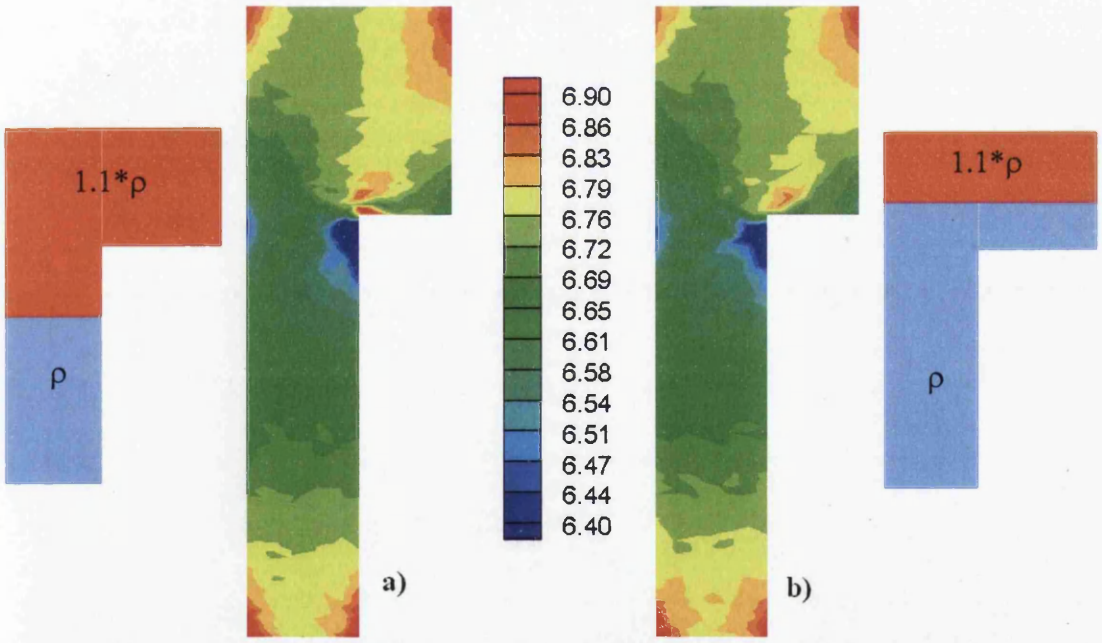

Figure 3.15 Distaloy AE, Dienet geometry, compacts with a) higher initial density in the top region ($\rho_{top} = 1.1 * \rho_{bot}$) with region border in pipe section b) higher initial density in the top region ($\rho_{top} = 1.1 * \rho_{bot}$) with region border in flange section.

In order to be able to interpret and compare the results a simpler density distribution diagram was required. In order to construct such a diagram the

density data from the simulation was interpolated onto a rectangular mesh (Figure 3.16). Then, the data was imported into an Excel spreadsheet, where weighted averages of density, taking into account the distance from the axis of symmetry, were calculated for each region. The final diagrams are presented in Table 3.3.

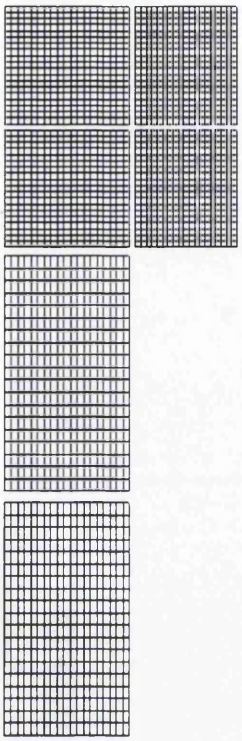

Figure 3.16 Rectangular mesh grid for Dienet geometry

The compact in Figure 3.14 a) exhibits behaviour which is normally expected when double ended compaction takes place. The regions of lowest density are located along the neutral plane and near the die walls. Regions of higher density are at the top and bottom punch surfaces near the die walls, where the displacement and wall friction are greatest. The compact in Figure 3.14 b) exhibits some similar features. In the lower narrow region the trends are the same, but the density is lower. The low density region on the neutral line is greater with the density values being even lower than for the uniform density case. In the upper region the density is much greater than in the uniform case. There is a new region of higher density at the base of the flange, where powder was pushed along the surface of the punch and then round the corner into the tube. There appears to be little powder flow from the upper into the lower section of the part. Compacts in Figure 3.15 exhibit similar density distribution patterns

to that in Figure 3.14 b) but with slightly less pronounced regions of high and low density near the flange-pipe interface.

The following diagram further illustrates the results:

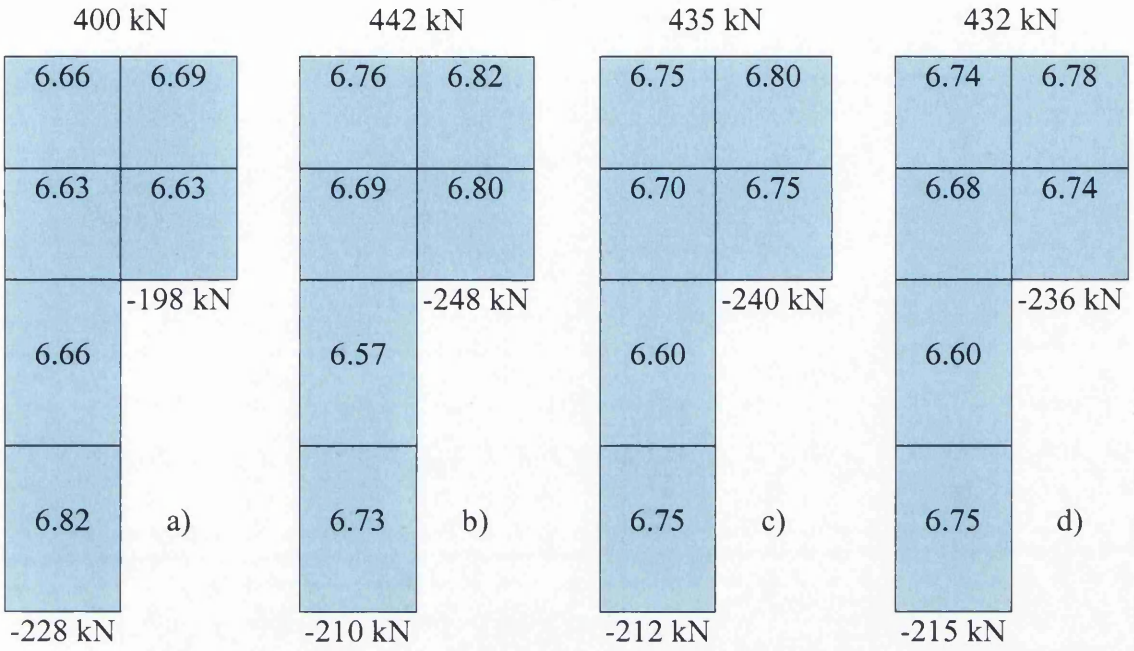

Table 3.3 Block diagram of density distribution: Dienet part, Distaloy AE

The density variation between the maximum and minimum values of the density in the compact was 10.3% of the final average density for the compact with uniform fill density and 35.2% for the non-uniform fill distribution case b). For cases c) and d) the density range was 14.8% and 10.5% respectively.

The tool forces acting on the punches are summarised in Table 3.4. For case b) there was a 10% increase in the force acting on the top punch and a 25% increase in the forces acting on the lower outer punch. The force acting on the lower inner punch was reduced by 8%. This is due to the increased amount of material in the top section of the part. For cases c) and d) the increase in top punch force was 8.7% and 8% respectively. The increase in load on the lower outer punch was 21% and 19% and the decrease on the lower inner punch was 7% and 5.7% respectively.

Table 3.4 Tool forces: Distaloy AE, Dienet geometry.

	Uniform fill	Two regions	Two regions lower border	Two regions upper border
Top punch, kN	400	442 (+10%)	435 (+8.7%)	432 (+8%)
Lower outer punch, kN	-198	-248 (+25%)	-240 (+21%)	-236 (+19%)
Lower inner punch, kN	-228	-210 (-8%)	-212 (-7%)	-215 (-5.7%)

3.2.5 Results - Tungsten Carbide

Having compared the four fill density configurations for the irregular ferrous Distaloy powder it was appropriate to test whether the conclusions would be valid for other powders. As mentioned previously and demonstrated in the material model validation work, the compaction behaviour of the three powders was different because of different material strength and particle shape and roughness. As Configuration b) was found to result in the most severe final density variation this was chosen, alongside configuration a), to be simulated again for the tungsten carbide and Zirconia powders.

Additionally, a configuration similar to that seen in Figure 3.7 with a diagonal interface between the two regions was explored, see Figure 3.20. The same fill dimensions as used for the ferrous powders were used. The compaction ratio was 2.5. See Table 3.5 and Figure 3.17

Table 3.5 Hardmetal geometry

Nominal geometry	
H1, mm	10
H2, mm	20
Target press density	7.8
Assumed fill density	3.15
Compaction ratio	2.5
Part internal radius, mm	1.0
Fill geometry	
H1, filling, mm	25
H2, filling, mm	50

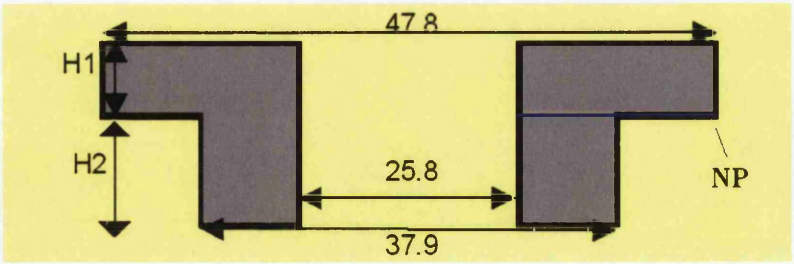

Figure 3.17 Dienet Hard Metal Geometry

The fill density was set at 3.15 g/cm^3 for the uniform fill configuration. As before, double ended compaction kinematics were used, see Figure 3.18. The displacements for the top and bottom punches were chosen to achieve a compaction ratio of 2.5. The displacements were proportional to avoid powder flow around the corner at the interface of pipe and flange (this is only true for the uniform fill case).

The resultant density distribution is presented in the form of a contour plot in Figure 3.19 and the block diagram is presented in Table 3.6.

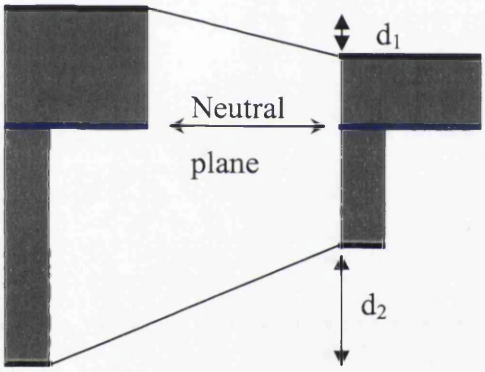

Figure 3.18Double ended kinematics

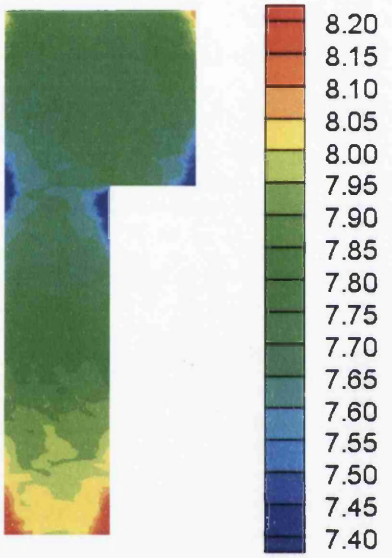

Figure 3.19 WC-Co Dienet part. Uniform fill density at 3.15 g/cm3

7.74	7.78
7.68	7.68
7.70	
7.95	

Table 3.6 Density distribution diagram for WC-Co Dienet part with uniform fill density at 3.15 g/cm^3.

Once the reference model had been analysed two further configurations of fill density were simulated, Figure 3.20. In each case the fill density in the upper region was 110% of the fill density in the lower region, with the average density remaining at 3.15 g/cm^3.

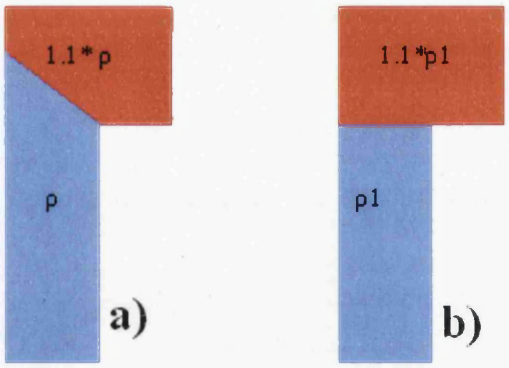

Figure 3.20 a) Diagonal and b) flat region configurations.

The results of the simulation follow:

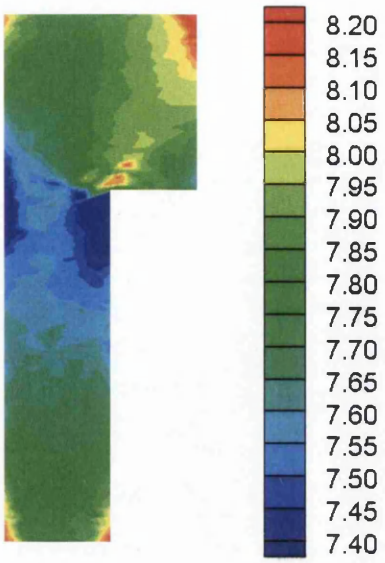

Figure 3.21 Final density distribution in a Dienet WC-Co compact with two regions of varying fill density (Figure 3.20 a)).

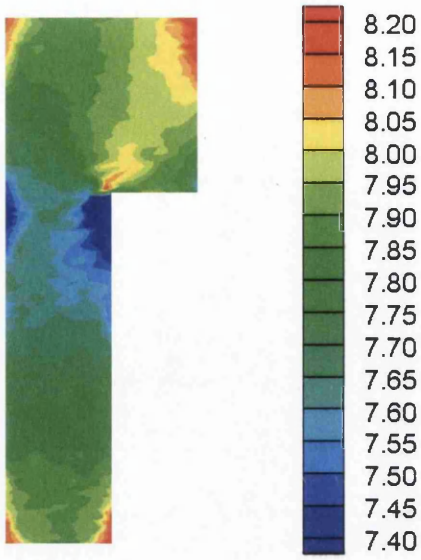

Figure 3.22 Final density distribution in a Dienet WC-Co compact with two regions of varying fill density (Figure 3.20 b)).

Comparing the results it is clear that the pressed density distribution was significantly more uniform for the compact with uniform fill. Regions of lower density near the neutral plane (NP) and of higher density near the punches are a lot more prominent for the cases with non-uniform fill. There was also a region of higher density immediately above the pipe/flange interface.

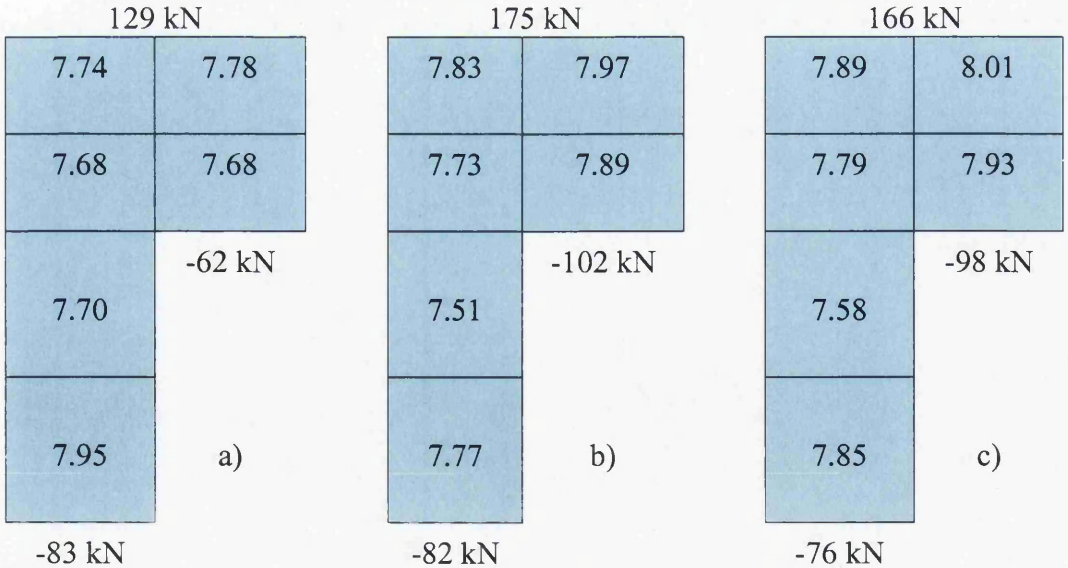

Table 3.7 Density distribution block diagram. a) Uniform fill density.

b) Two regions with a diagonal border. Figure 10(a)

c) Two regions horizontal border. Figure 10(b).

The density variation between the maximum and minimum density values in the compact was 15.9% of the final density for the uniform fill, 34.1% for the diagonal border case and 34.2% for the horizontal border case.

The tool forces acting on the punches are summarised in
Table **3.8**. There was an increase in the force acting on the top punch of 29% for the diagonal region case and of 36% for the horizontal region case. For the lower outer punch the figure was 57% and 64% respectively. The force acting on the lower inner punch was reduced by 9% and 1.5% respectively. The load increase on the upper and the lower outer punches was due to the increased amount of material in the top section of the part.

Table 3.8 Tool forces on punches: Dienet part, Tungsten Carbide

Tungsten Carbide	Uniform fill	Two regions diagonal	Two regions flat
Top punch, kN	129	166 (+29%)	175 (+36%)
Lower outer punch, kN	-62	-98 (+57%)	-102 (+64%)
Lower inner punch, kN	-83	-76 (-9%)	-82 (-1.5%)

Similar to the ferrous powder there was an increase in loads on the punches, however these were proportionally much larger for the tungsten carbide powder. This may be due to the higher friction coefficient of the tungsten carbide powder. Although the patterns of density distribution were similar for the ferrous and the hardmetal powder the percentage increase in the values of the tool forces was different. It was therefore appropriate to consider the ceramic powder, a material with significantly different compaction loads, to explore these effects.

3.2.6 Results – Zirconia

Once again the Dienet geometry was used, with fill heights identical to those used for the ferrous and hardmetal powders. The dimensions of the geometry, including punch displacements are presented in Figure 3.23.

Nominal geometry	
H1, mm	11.36
H2, mm	22.72
Target press density	2.8
Assumed fill density	1.27
Comp ratio	2.2
Fill geometry	
H1, filling, mm	25
H2, filling, mm	50

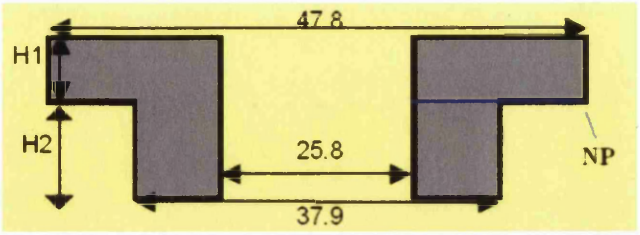

Figure 3.23 Dienet Zirconia geometry

As before, two compacts, one with a uniform fill density (configuration a)) and the other with two regions of different fill density (configuration b)), were considered. In both cases the mass of powder was the same. Double ended compaction was used with a compaction ratio of 2.2. The interface between the regions was on the plane of the top surface of the lower outer punch, see Figure 3.24 b).

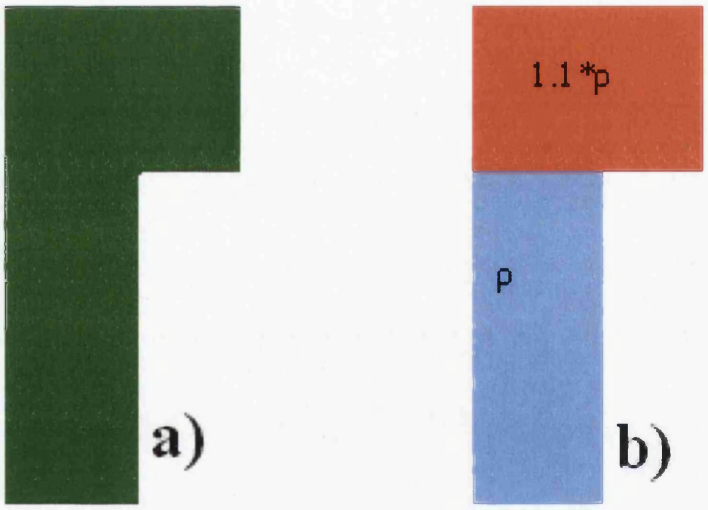

Figure 3.24 a) Uniform fill density b) Two regions with the same total mass as in a)

The density contour plots for both simulations are presented in Figure 3.25 and the corresponding block diagrams in Table 3.9.

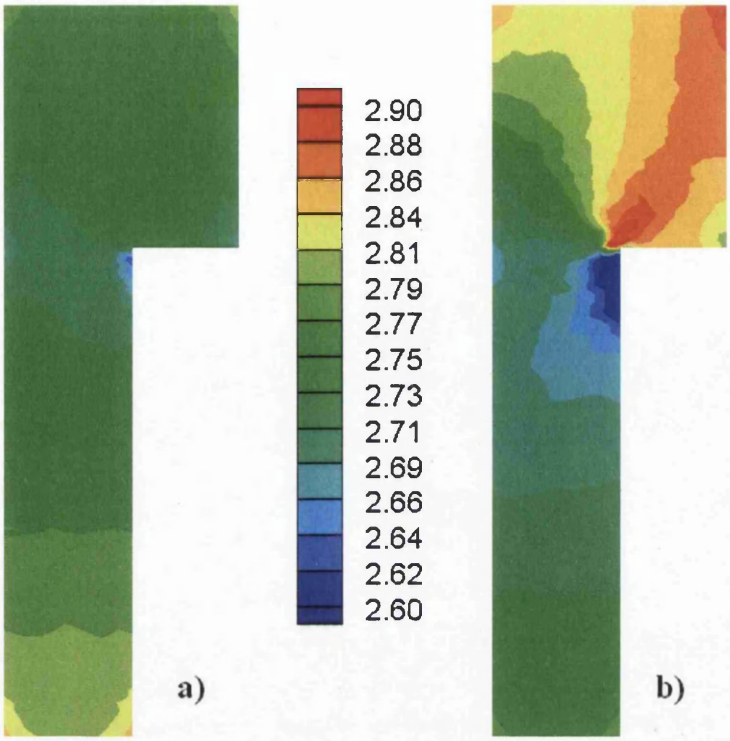

Figure 3.25 Zirconia. Dienet geometry, compacts with a) uniform fill density (Figure 24(a)) and b) higher initial density in the top region (Figure 24(b))

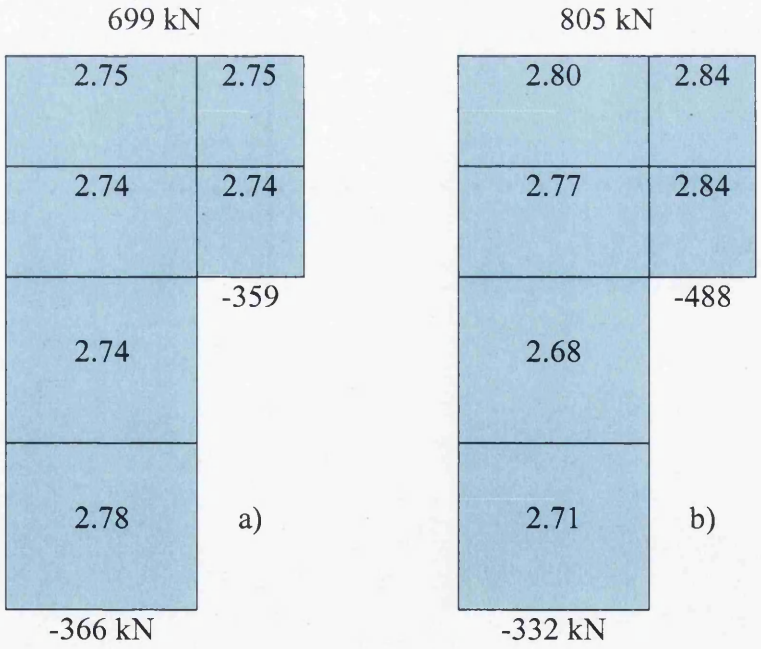

Table 3.9 Block diagram of density distribution: Dienet part. Zirconia. a) uniform fill density and b) higher initial density in the top region.

A similar behaviour to other powders was observed for this geometry. For the non-uniform fill part the lower section's density was lower overall. The region of low density near the neutral line was greater, with a lower minimum density. There was a general increase in density in the flange region and an area of high density just above the flange/pipe interface. The density variation between the maximum and minimum densities in the compact was 8.3% of the final density for the compact with uniform fill density, and 28.9% for the multi-region case.

The tool forces acting on the punches are summarised in Table 3.10. There was a 15% increase in the force acting on the top punch, and a 36% increase in forces on the lower outer punch. The force acting on the lower inner punch was reduced by 9%. This was due to the increased amount of material in the top section of the part.

Table 3.10 Tool forces on punches: Dienet part, Zirconia.

Zirconia	Uniform fill	Two regions
Top punch, kN	699	805 (+15%)
Lower outer punch, kN	-359	-488 (+36%)
Lower inner punch, kN	-366	-332 (-9%)

3.2.7 Modnet Part

The Modnet stepped geometry differed from the Dienet geometry in having the lower section on the outside of the part, rather than on the inside. This was significant as it meant that more volume would be occupied by the lower section of the Modnet part than that of the Dienet part. As the upper section of the die was expected to have a higher density value then some of the powder from the top section would be transferred to the lower section. In the case of the Modnet geometry there would be more capacity to accommodate such powder transfer than in the Dienet geometry, see Figure 3.26.

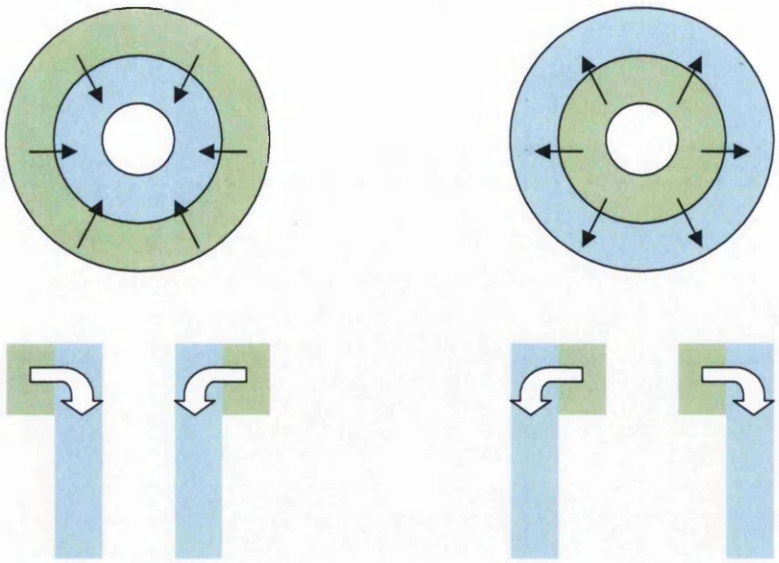

Figure 3.26 Possible powder transfer direction in Dienet and Modnet parts

It was therefore appropriate to include the Modnet geometry into the study. Similar fill configurations were used for the Modnet part, i.e. uniform fill density for the first model and the second model with two regions of different fill density which were balanced to produce the same mass compact as in the uniform fill case. Once again, the difference between the density in the upper and lower parts was taken to be 10%. The border between the regions and the neutral plane was along the top surface of the inner lower punch, see Figure 3.27.

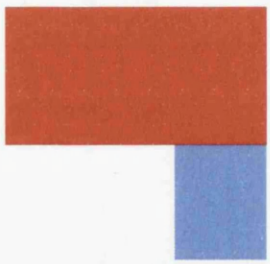

$\rho_{top}=1.1*\rho_{bot}$

$\rho_{mean}=3.3\ g/cm^3$

Figure 3.27 Modnet part fill conditions. Distaloy AE

Double ended kinematics were used in both cases with a compaction ratio of 2. Results are shown in Figure 3.28 and Table 3.11.

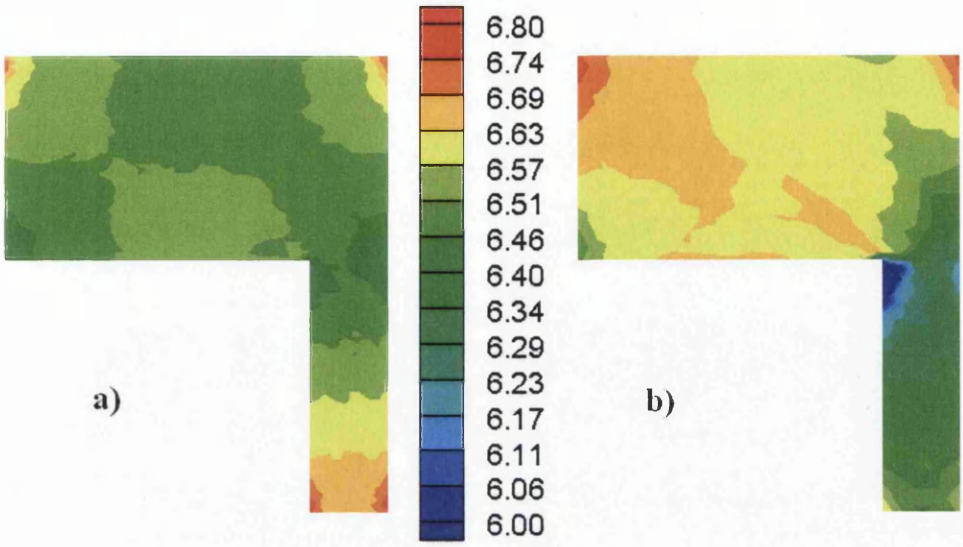

Figure 3.28 Distaloy AE, Modnet geometry, compacts with a) uniform fill density and b) higher initial density in the top region ($\rho_{top} = 1.1 * \rho_{bot}$)

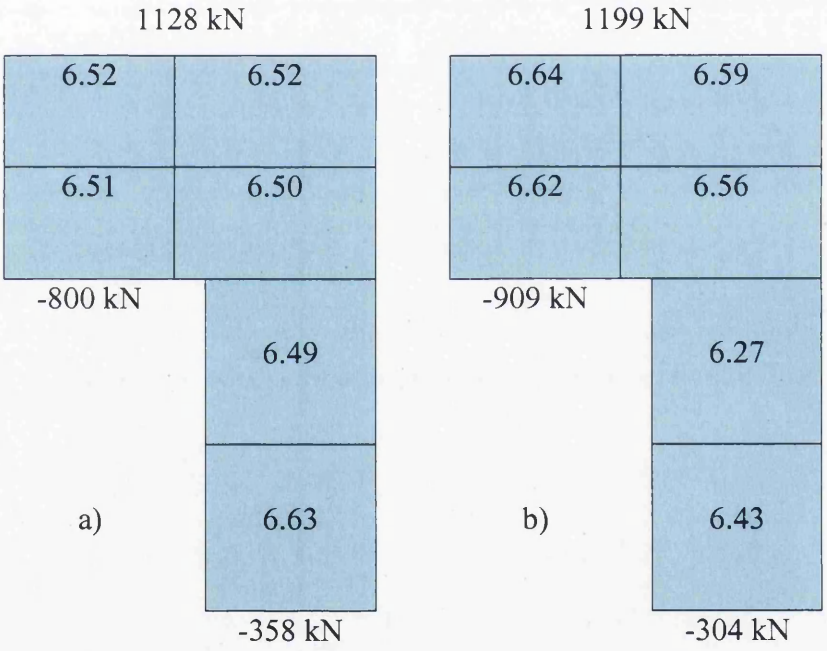

Table 3.11 Block diagram of density distribution: Modnet part. Distaloy AE. with a) uniform fill density and b) higher initial density in the top region ($\rho_{top} = 1.1 * \rho_{bot}$)

As in the Dienet configuration the part with the uniform fill density exhibits a smaller variation in density. Most of the part appears to have an almost uniform density, with regions of high density in the areas of contact between the top and bottom punches and die walls. The block diagram in Table 3.11 a) shows an

almost uniform density distribution, with only the bottom section of the tube being significantly denser than for most of the compact.

However, the compact with the variations in fill density was a lot less uniform in density in the pressed state. The lower density region near the neutral axis was a lot more pronounced and the density in the upper region was significantly higher overall. This is apparent from both the contour plot and the block diagram.

As a result of the non uniform fill condition there was an increase of 6.4% in loads on the top punch, a decrease of 15% in loads on the lower punch, which was caused by the lower densities in the lower section, and an increase of 13.6% in loads on the lower inner punch. The increase in forces on the top and lower inner punches were caused by the higher densities in the top part of the compact.

3.3 Discussion

This study assessed the impact of fill density distribution on pressed density.
It has been demonstrated that for simple shapes, such as hollow cylinders, the variations in fill density along the direction of compaction did not significantly affect the final pressed density distribution in the compacted part.

However, for more complex geometries, such as the Dienet and the Modnet flanged pipe shapes, the difference in both final density distribution and tool forces was significant. Typically, the range of density values in the final compact was higher, with more extreme maximum and minimum densities, which would result in a lower quality for the final product.

Forces on the top and the lower outer punch of the Dienet part were also found to increase significantly, which may lead to a reduced lifespan of the punch, or in extreme cases, failure. The percentage increase varied for different powders – this can be attributed to different material behaviour for each of the powders.

Future work may be required to investigate the combined effect of more complex kinematics and non-uniform fill density conditions.

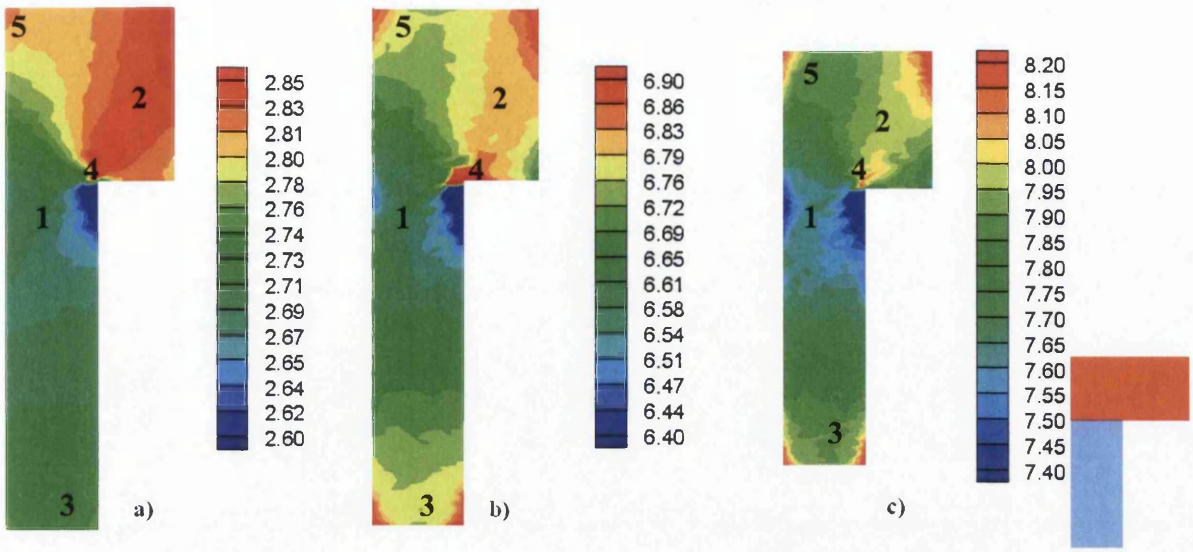

Figure 3.29 Comparison between density distribution for Zirconia, Distaloy, Tungsten Carbide powders (non uniform fill condition, region border on the level of the lower outer punch)

The different densities of each powder prohibit a direct comparison of the density distribution. Additionally, the compaction ratio for the Tungsten Carbide powder was different to that of the Zirconia and Distaloy powders. However, some common features can be observed in all three compacts. There is an area of low density, designated as "1" on Figure 3.29, just below the level of the lower outer punch. This is the area most distant from the top and bottom punches, and the presence of a low density area there agrees well with expectations. There is a region of higher density common to all three of the compacts, designated "2", which connects the tip of the lower outer punch with the top right corner of the compact. It is difficult to compare the intensity of zone "2" between the different compacts because of varying densities and contour colour indexation. Section "3" is a region of higher density, which was caused by the friction between the tools and the powder. This is a feature commonly seen in compacts. At the lower end of area "2", marked as "4", there is a very local region of high density which is common for all three compacts. The high density area marked as "5" is a common feature for all three compacts and like feature "3" correlates well with expectations from experience.

The above features are also present in the density distribution of the Modnet geometry part, see Figure 3.30. The region of lower density "1" is just below the level of the lower inner punch. There is a band of higher density, designated as "2", which connects the inside top of the compact with the tip of the lower inner punch. However there is not a prominent region of high density around point "4", unlike the compacts of the Dienet geometry. This is likely because the top part of the Modnet geometry is a lot bulkier. The difference between the initial density in the top section and the mean fill density had to be smaller for the Modnet part than for the Dienet part to keep the 10% top to bottom variation because of the relative volumes occupied by the top and bottom sections in each part. The size of the top section of the Modnet part would also result in a less varied distribution as powder is less constrained. The high density areas "3" and "5" are also less pronounced. The former because the fill density was low in the lower section, and the latter because the powder in the top section was less constrained, allowing for more uniform density distribution than in the Dienet shaped part.

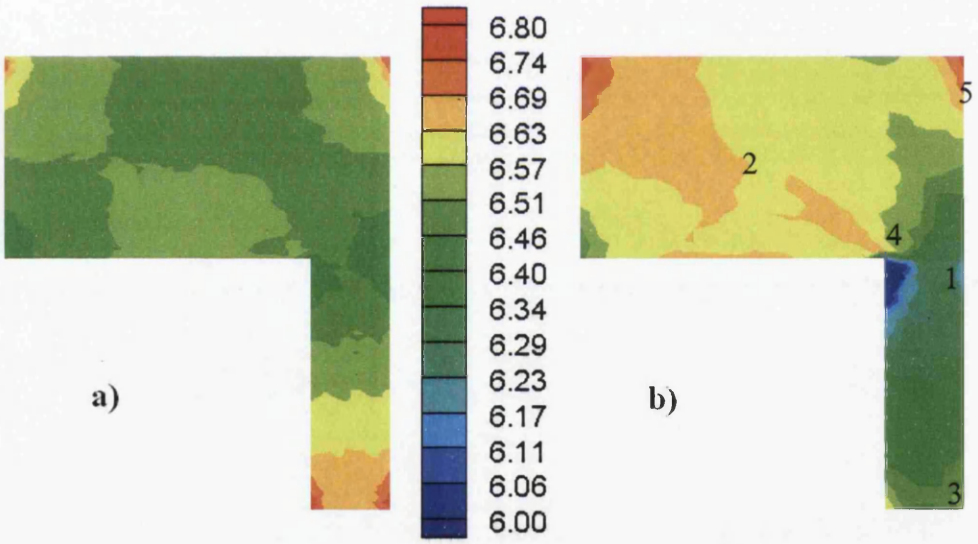

Figure 3.30 Density distribution in green compacts for Modnet geometry, ferrous powder: a) uniform fill b) non-uniform fill

Coube, Cocks et al. (2005) have also performed a study of the effect of variations in density prior to compaction, caused by filling and powder transfer, on the final pressed density. These authors considered an H section part with a range of different fill conditions inspired by filling and transfer simulations. The fill density variations considered included a depression at the top of the die caused by

powder settlement after transfer. They concluded that the variations in fill density distribution were of secondary importance compared to the presence of a depression at the top of the compact. However, some variation between the reference uniform fill and the non-uniform fill cases was reported. Only one powder type and geometry was considered in the investigation.

3.4 Closure

Three powders were characterised and a sensitivity study on the effect of fill density distribution was performed for a range of geometries. Simple ring geometries were found to be unaffected by variations in the axial direction. Final density distributions for flanged geometries (both internal and external flange) proved to be less uniform in cases of a non-uniform fill density. High density variations were found – these would compromise the structural integrity of the compact. Tool forces were found to increase for some of the tools when the fill density was non-uniform.

All of the trends observed were true for all three materials, suggesting that the variations are a true consequence of the part shapes and fill density variations.

The numerical code used for this work, could be used to predict the final density distribution and tool forces resulting from a non-uniform fill density. This would enable the manufacturer to be more aware of the effects of the filling process and may lead to finding ways of rectifying problems caused by the resulting fill distribution.

Chapter 4 Friction measurement

4.1 Introduction

Powder-die friction is an important consideration for the powder compaction process. Inhibiting the sliding of powder against the die surface influences the tool force levels and for multilevel parts it determines the maximum achievable density and its distribution, as discussed in Chapter 3. Friction is also important during ejection. High friction leads to increased ejection loads and tool wear and can also impact on the surface finish of a compact and in some cases may result in compact failure. Friction also limits the maximum size of PCM parts that can be produced and is even more inhibiting for large height parts. If the value of the powder-die friction is high, galling may occur, leading to scratches on compacts, increased ejection loads and in some cases seizing of the die and punches (Sandberg and Jönson 2005).

For the reasons stated above it is important to reduce powder-die friction, this results in higher density, more uniform compacts produced at lower loads and with lower tool wear. Reducing friction may also allow faster production rates.

There are many practical ways of reducing powder-die friction: through die wall surface finish, by using a different die material, applying a coating, by mixing in powder lubricants and through die wall lubrication. The effect of powder-die friction can be reduced through the use of appropriate compaction kinematics – for example using double ended compaction instead of compaction in a single direction. This is advantageous for large height compacts and the choice of kinematics is especially important for multilevel compacts.

It is clear that in order to select an optimal combination of the above solutions, a quantitative understanding of the merits of each approach is required. It is important therefore to be able to measure accurately and reliably the coefficient of friction for any combination of powders, tools and other process parameters.

Such measurements also form the basis for improving the understanding of the friction phenomena in powder compaction: its causes, its evolution and further ways of reducing it. Additionally, comprehensive friction measurements are required as input data for a numerical simulation of the compaction process.

Currently, there is not a single standard method for measuring the coefficient of friction during compaction. Existing measurement techniques can be classified into two categories: indirect or direct. In a compaction experiment on a simple cylinder, there is a loss of pressure in the compact between the top punch and the bottom punch. When combined with the radial stress this leads to an indirect technique for measuring the friction coefficient. Direct techniques allow for the friction force to be recorded during the experiment and often involve the sliding of a compact against a target surface. This will be referred to as a shear plate apparatus.

Of the existing techniques the two most commonly used are the instrumented die test (Mosbah, Bouvard et al. 1997) and the shear plate test (Cameron, Gethin et al. 2002), (PM Modnet Methods and Measurements Group 2000). The former being an indirect friction measurement device and the latter being an example of a direct friction measurement system. An overview of some alternative measurement equipments can be found in Chapter 2 of this thesis.

4.1.1 Instrumented die

During instrumented die tests the complete balance of the top and bottom stresses together with the radial stresses is recorded. This data can be used to determine both the friction characteristics and yield behaviour of a powder (Mosbah, Bouvard et al. 1997).

The main feature of the instrumented die test equipment is a die equipped with sensors to measure radial stresses during compaction, see Figure 4.1. Typically, an array of sensors records either die deflections or the pressure directly at different points over the height of the die. In the case of the former some derivations are required to obtain the radial stress.

The axial stress at the top and bottom of the compact can be measured by load cells or by incorporating strain gauge sensors on the punches. In the case of the particular equipment used here the axial load on the bottom of the compact was obtained from a custom made load cell and the axial load on the top was recorded from the press load cell via the press control unit.

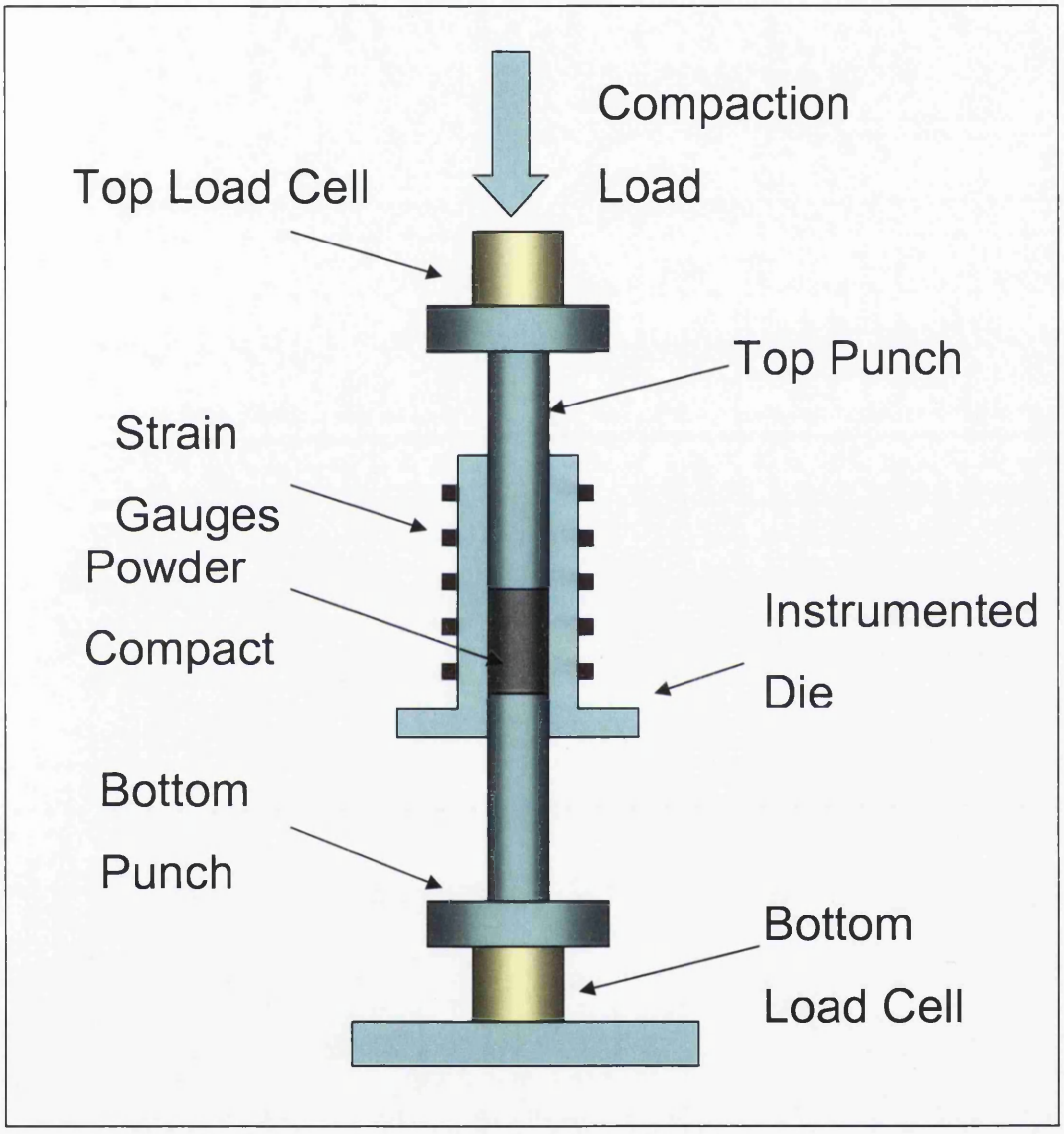

Figure 4.1 Instrumented Die

The specific details on how the friction coefficient can be obtained from the instrumented die test will be set out later in this chapter.

The main advantage of the instrumented die friction test is that friction data can be obtained during general powder characterisation tests. However, instrumented die

friction tests are very limited in scope. The friction surface (in this case the die) material, coating, finish and orientation cannot be readily altered. Such process parameters as sliding speed, distance and normal force cannot be controlled independently. These issues are easily addressed by use of a dedicated friction testing system, such as a shear plate apparatus.

4.1.2 Shear plate

The main feature of the shear plate apparatus is a die with a target surface at the bottom, see Figure 4.2. During the test, the top punch presses powder against the target surface until the desired density, or pressure, is reached. The normal load can then be adjusted if desired. In the next stage the target surface, normally supported by linear bearings, is forced to slide against the bottom of the compact. The friction coefficient is then obtained from the ratio of the sliding force required and the normal force. To eject the compact the sliding block that houses the target surface is removed and the compact is pressed out downwards by the top punch. Ejection forces may also be recorded for completeness.

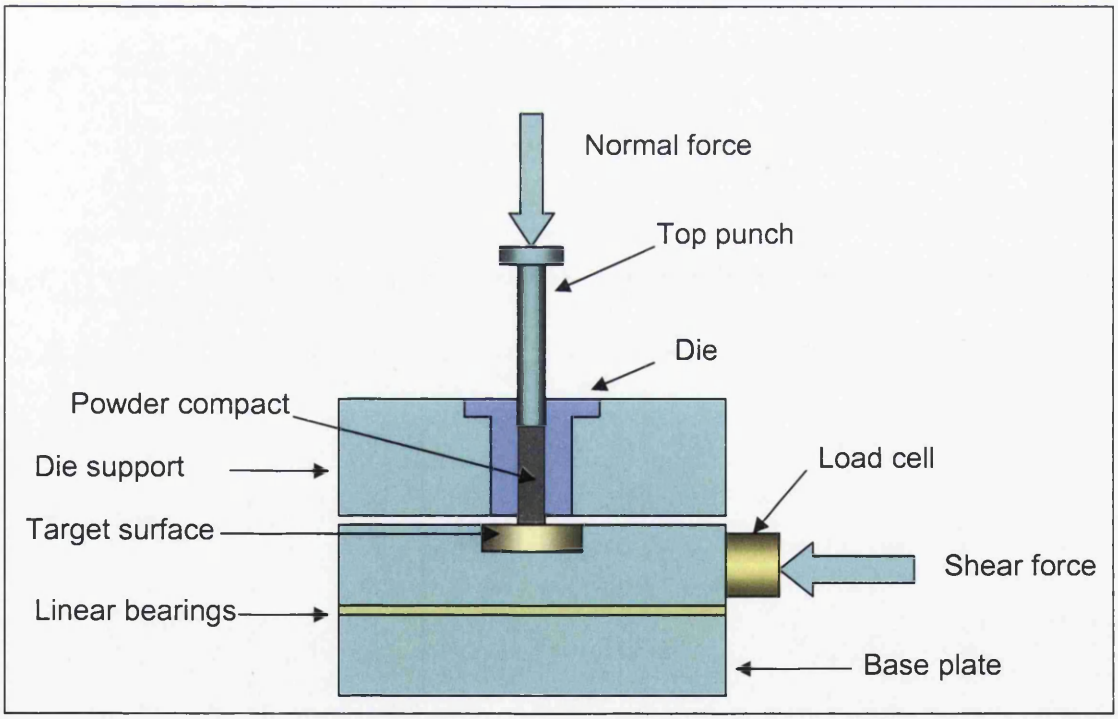

Figure 4.2 Shear plate apparatus

The target surface can be easily changed between tests, allowing different materials, coatings, finishes and orientations to be freely explored.

The main drawback of this apparatus is the loss of normal load through powder-die friction – i.e. the load on the target surface is lower than the applied axial force at the top of the compact. This has to be accounted for if the calculated friction coefficient is to be correct. This is typically achieved by performing a complementary instrumented die test to obtain the pressure transmission information.

4.1.3 Shear plate with floating die

In this chapter a modification to the shear plate apparatus is proposed, with its merits compared with the other two techniques mentioned. The purpose of the modification was to facilitate full transmission of the axial load applied at the top of the compact to the target surface. To achieve this, the die and its supporting mechanism have been replaced with modified parts, see Figure 4.3. At the start of the test the die is supported by means of a supporting ring and behaves in the same manner as the die in the conventional shear plate apparatus. A small gap is maintained between the die and the target surface so that only the protruding compact is in contact with the surface during the sliding phase of the test. The compaction then starts.

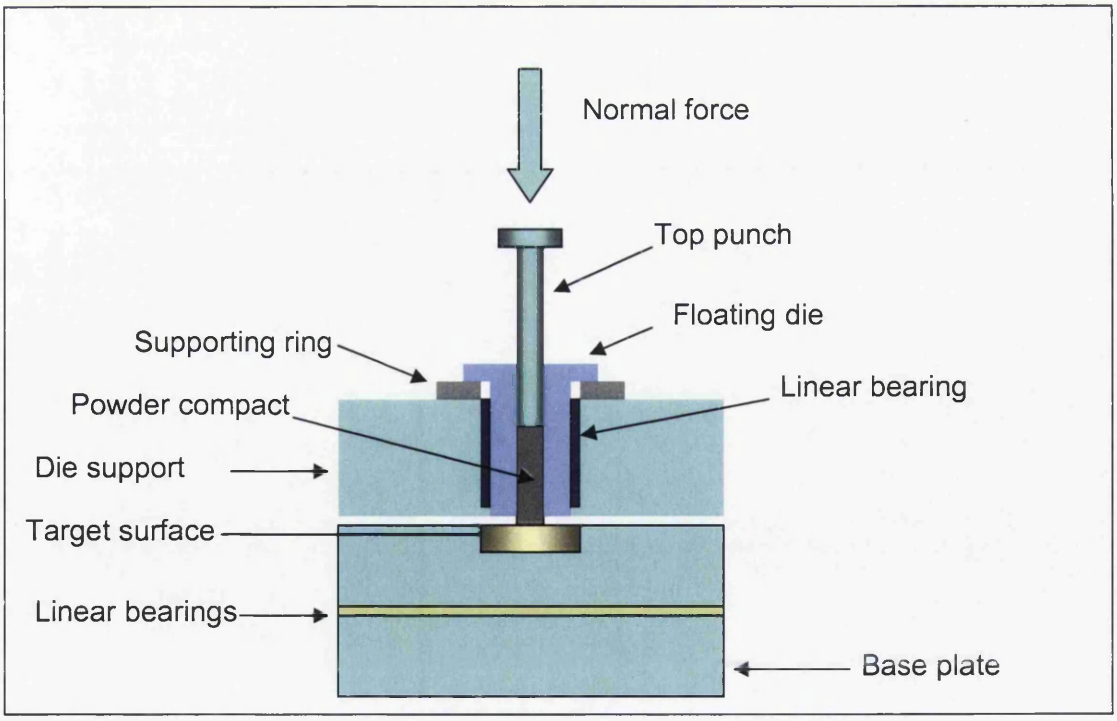

Figure 4.3 Shear plate apparatus with floating die – compaction stage

Once the desired density, or displacement, have been reached the load is removed, which allows the removal of the supporting ring, Figure 4.4. At this point a linear bearing permits the die to descend freely until the bottom of the protruding compact touches the target surface. The normal load required for the test can then be applied. The load is fully transmitted to the target surface as the bearing prevents any pressure loss. The sliding test is then performed in the same manner as for the conventional equipment. For ejection, the supporting ring is reinstalled, the target surface and the sliding block are removed and the compact is ejected downwards.

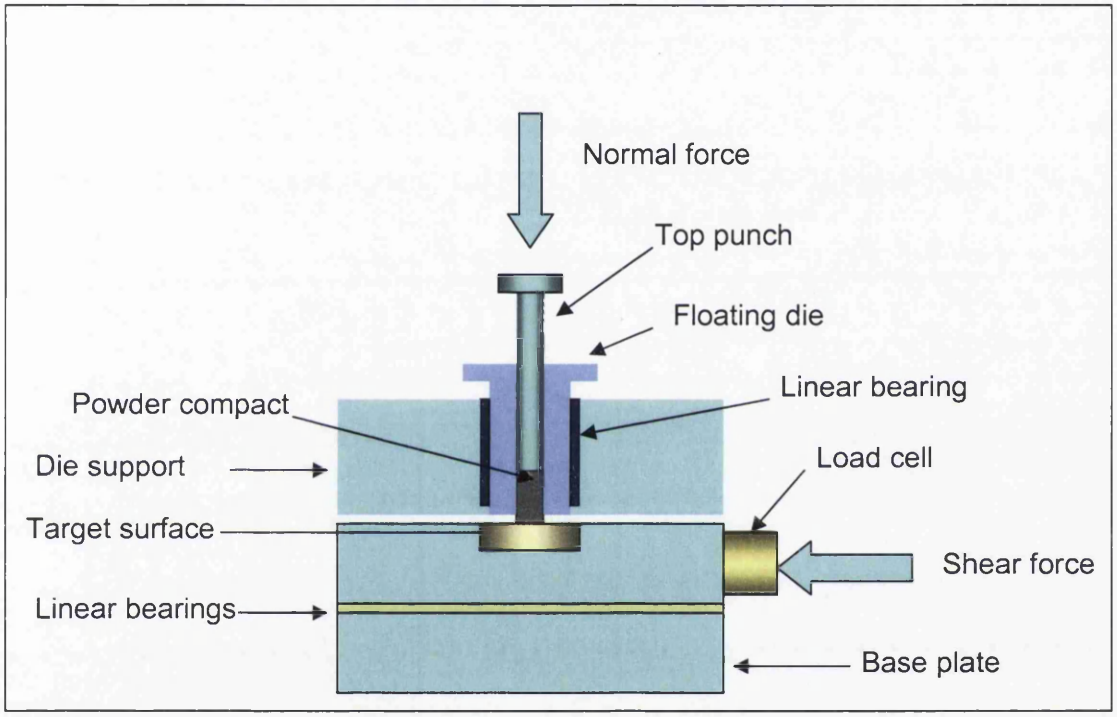

Figure 4.4 Shear plate apparatus with floating die – sliding stage

Some examples of measurements made with both the established techniques and the new floating die shear plate apparatus will be presented and compared. This will be followed by a study of powder lubricant content effects, which was performed on the new equipment.

4.2 *Friction measurement – instrumented die*

In the closed die compression tests the parameters needed to obtain the friction values are the axial pressure on the top and bottom punches, radial stress, compact diameter and height. The axial pressures are readily recorded, while some derivations are required to obtain the radial stress from the strain gauge

measurements. The compact height is recorded from the punch displacements for the compaction stage. Recording the compact height allows the estimation of friction as a function of either stress or average density during compaction. The die is assumed to be sufficiently rigid for the radial strain to be negligible and hence the compact diameter is taken to be equal to the internal diameter of the die.

4.2.1 Instrumented die – test equipment

The closed die tests were performed using an instrumented die rig mentioned in the introduction to this chapter, see Figure 4.5. The rig was used with a Dartec hydraulic press, capable of providing up to 250kN load. The press could be operated in either load or displacement control modes. The former was typically used for the compaction stage, for safety reasons, and the latter for the ejection stage.

A die was manufactured out of tool steel and instrumented as described in Section 4.1.1. The die height available was 77mm, however, complete filling was not possible due to the clamping arrangement – this limited the height of compacts that could be tested. The die was installed onto a support that provides precise guidance and held down by a plate, bolted to the assembly. During the installation the whole assembly was lined up with the crosshead of the press so that the top punch had minimal interference with the die. Typically, a resistance of 100-500N was recorded when the punch was lowered into the die cavity. Also, when the plate that clamps the die was installed the strain gauge readings on the die were logged. These reflect the stress state in the die due to axial clamping and were recorded for completeness. The strain gauges were zeroed prior to calibration and experiments, thus removing the need for a complex data reduction process to remove the strain induced by the clamping.

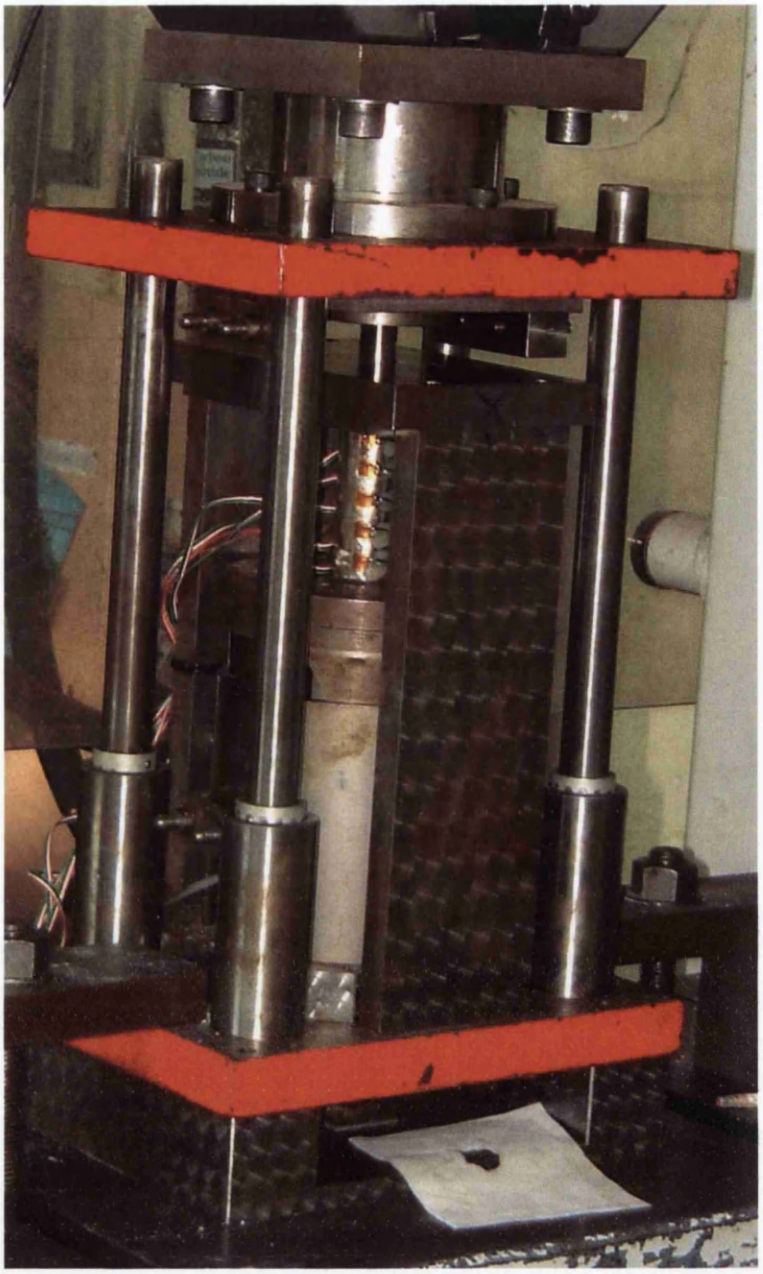

Figure 4.5 Instrumented die equipment

The Dartec press was capable of providing displacement and load output signals, with output voltage being between 0 and 10V. The press instrumentation was calibrated prior to the experiments taking place.

In this test configuration a load cell was used to measure the load on the bottom punch during compaction. It was directly calibrated by transmitting a load from the top punch to the bottom punch with a lubricated metal cylinder having a diameter slightly smaller than that of the die to avoid friction. Additionally, an LVDT was used to complement the displacement data for the press. It was

attached at the same level as the top punch and the difference between the readings from the LVDT and the press displacement data accounted for the deflections in the press frame. The punch deflections were accounted for by simple calculations, where the punch was assumed to be a cylinder in compression. These corrections become important when axial stress levels in the compact become high – axial stresses in excess of 490MPa were achieved in some of the tests with ferrous powders.

The instrumented die used in this work, shown in Figure 4.6, was equipped with five sets of strain gauges, with each set connected in a modified full bridge configuration to maximise sensitivity. The bridges consisted of two hoop gauges (i.e. gauges fixed having their measurement axis in the circumferential direction), which were bonded at diametrically opposite positions on the die. The remaining two gauges were bonded to a separate metal plate made of the same grade of steel as the die. The common steel grade was used to negate any influence of ambient temperature variations. The measurements from these sensors needed to be processed before the radial pressure could be obtained. The details of the calibration and processing are presented in Appendix 2.

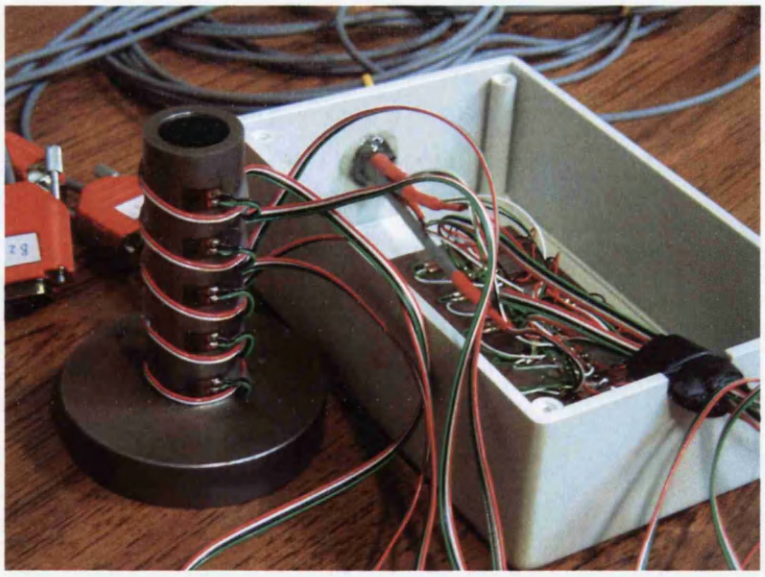

Figure 4.6 Instrumented die and metal plate for bridge balance

All the signals were fed into a Vishay System 5000 data acquisition unit, with a maximum sampling rate of 100Hz. A sampling rate of 10Hz was found to be sufficient and was used during the tests as a good compromise between being able

to capture the detail of the process and being able to manage the amount of data recorded. Ten channels were recorded in total: five strain gauge bridges from the die, press load and displacement, load on the bottom punch load cell, LVDT displacement and LVDT excitation voltage. A test campaign included a calibration check followed by a series of tests. Thus, both the calibrated values and the voltages were recorded for each of the channels. Raw data was then reduced and saved as MS Excel and text files for analysis.

4.2.2 Instrumented die – Experimental procedure

At the start of the experiment the top punch was withdrawn and the bottom punch was resting on the load cell. The desired quantity, by weight or volume, of the powder being tested was then poured into the die opening via a funnel. Initial experiments were based on powder volume, whereas later experiments were based on mass. This gave improvements in consistency which will be discussed further below. The top punch was then lowered into the die, the process variables, such as compaction rate and maximum load, were set and the data acquisition system was set to record. A low loading rate of 1kN/s was typically used since precise press control could be achieved, especially when pressing softer powders. The compaction process then began. When the desired load was reached the press stopped. Load was then gradually removed at the same rate as it had been applied. The top punch was then completely withdrawn and the crosshead was connected to the bottom punch for the ejection phase. Ejection was typically performed at the rate of 1mm/s. Once the compact was ejected it was measured, bagged and labelled.

When measuring the friction coefficient in the instrumented die test the contact surface between the powder slug and the die was the one considered. In the context of the experiment the stress normal to the friction surface was the radial stress. The compaction stress, i.e. stress applied to achieve desired density, was the axial stress. These definitions are important to note, as in Section 4.4.4 the results from the instrumented die tests will be compared with those from the floating die.

The equation for the evolution of the friction coefficient for long cylinders has been derived in (Bocchini 1995) and has the following form:

$$\mu(h) = \frac{D}{4kh}(\ln\sigma_{zt} - \ln\sigma_{zb})$$

Where D is the compact diameter, k is the ratio of radial to axial stress, h is the compact height, σ_{zt} is the axial stress at the top of the compact and σ_{zb} is the axial stress at the bottom of the compact. It was implemented into the MS-Excel spreadsheets which contained the test data.

4.2.3 Results – Instrumented Die

To demonstrate some typical friction measurements from the instrumented die experiment a Distaloy AE ferrous powder with 0.5% Kenolube lubricant by weight was chosen. The powder and the lubricant were placed to fill a 0.72 litre jar to approximately 30% and mixed using a Stuart Scientific Rotor Drive STR4 tumbling machine, run for a duration of 30 minutes. Based on the work by Guyoncourt (2004), this is a more than an adequate duration for the mixing, as about 10minutes should normally sufficient be. The same procedure was used for mixing the other powders and lubricants used in other experiments, unless otherwise stated.

The die used was made of D2 tool steel having Vickers hardness of 790 and had a smooth polished inner surface having an average roughness of 0.04μm (Ra). The powder was compacted in quantities of 10cc and 15cc and the friction coefficient between the powder and the die was obtained from the measurements of stress and displacement via the equation introduced in Section 4.2.2. Although metered volumetrically, the weight loading was also checked and was found to be consistent within 3% for a ferrous powder (with non lubricated powder showing the largest variations) and 2.5% for a ceramic powder.

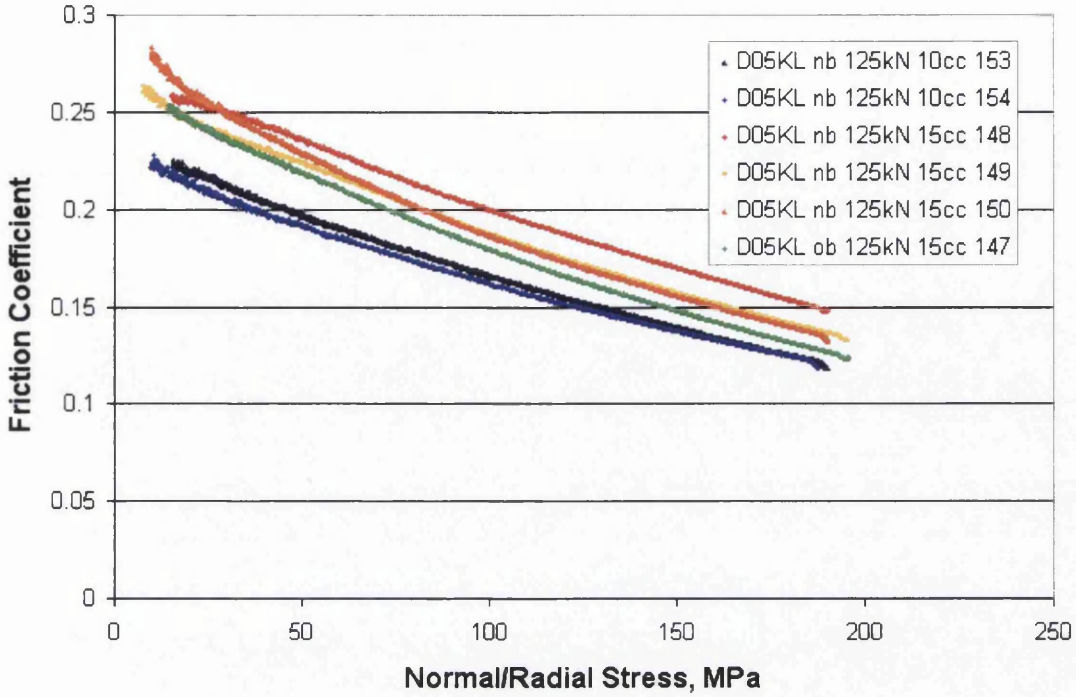

Figure 4.7 Friction coefficient vs. normal (radial) stress, Instrumented Die

A plot of the friction coefficient relative to the radial stress, which in this case is also the stress normal to the friction surface, can be seen in Figure 4.7. The first two series represent the test with 10cc of powder (153 and 154), the next three were performed with 15cc of powder. The final series was done with 15cc of an older batch of Distaloy and provides some insight regarding both the batch to batch variations and repeatability. In each case the powder was compacted until the load of 125kN (486MPa) was reached. The friction coefficient follows a decreasing trend and at later stages is almost linear with an increase in normal stress. The friction coefficient is lower for the 10cc tests than it is for 15cc tests.

Figure 4.8 shows the relationship between the friction coefficient and the axial stress applied to the top of the compact. It is appropriate to consider such a representation of friction as in the floating die experimental equipment, which will be presented in Section 4.4.1, the normal and axial loads can be controlled independently. As in Figure 4.7 a trend of reduction in the friction coefficient with an increase in stress can be observed. Again, the friction coefficient was lower for the compacts with 10cc of powder, i.e. for shorter compacts.

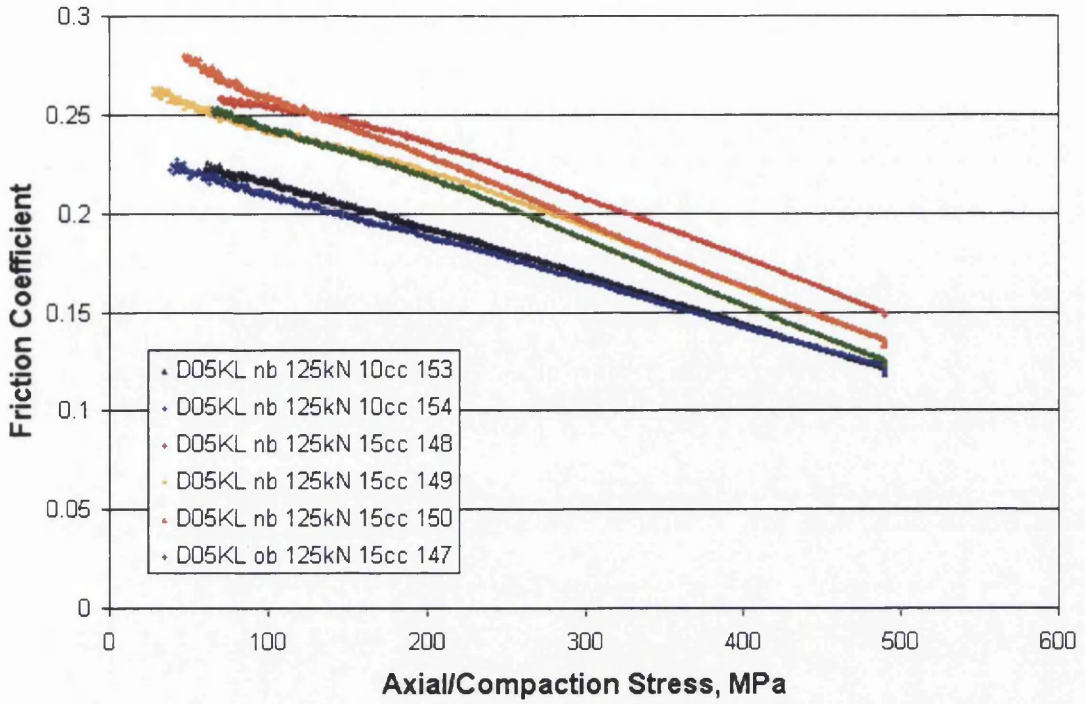

Figure 4.8 Friction coefficient vs axial (compaction) stress, Instrumented Die

An examination of the literature shows that for compacts pressed at the same compaction load, the ejection forces are greater for longer compacts, (Briscoe and Rough 1998). A comparison of the compaction conditions for the samples tested here shows that the density was nearly identical for the same stress level for both sets of compact heights, see Figure 4.9.

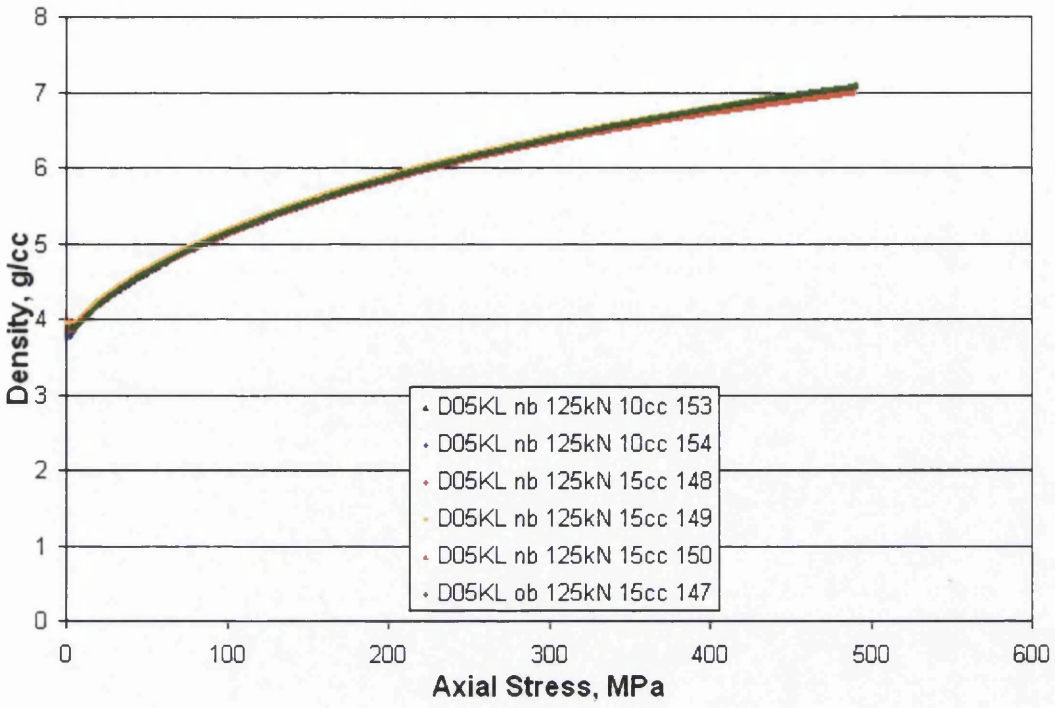

Figure 4.9 Evolution of Density with Axial Stress, Instrumented Die

The variations in radial stress with respect to the axial stresses were greater, see Figure 4.10. However, this is still insufficient to fully explain the consistent difference in the friction coefficient between the 10cc and 15cc compacts. It appears that the most significant element in the difference is the compact height to radius (aspect) ratio. The likely mechanism involved is that a less uniform density field can be expected in a compact of a higher aspect ratio. This would result in a greater proportion of the compact being at a lower density, which is shown to result in higher friction, see Figure 4.11. Other authors (Doremus, Toussaint et al. 2001), (PM Modnet Methods and Measurements Group 2000), (Solimanjad 2003) have similarly reported the friction coefficient to be higher at lower densities. In this case, the net effect is the apparent dependence of the friction coefficient on compact aspect ratio.

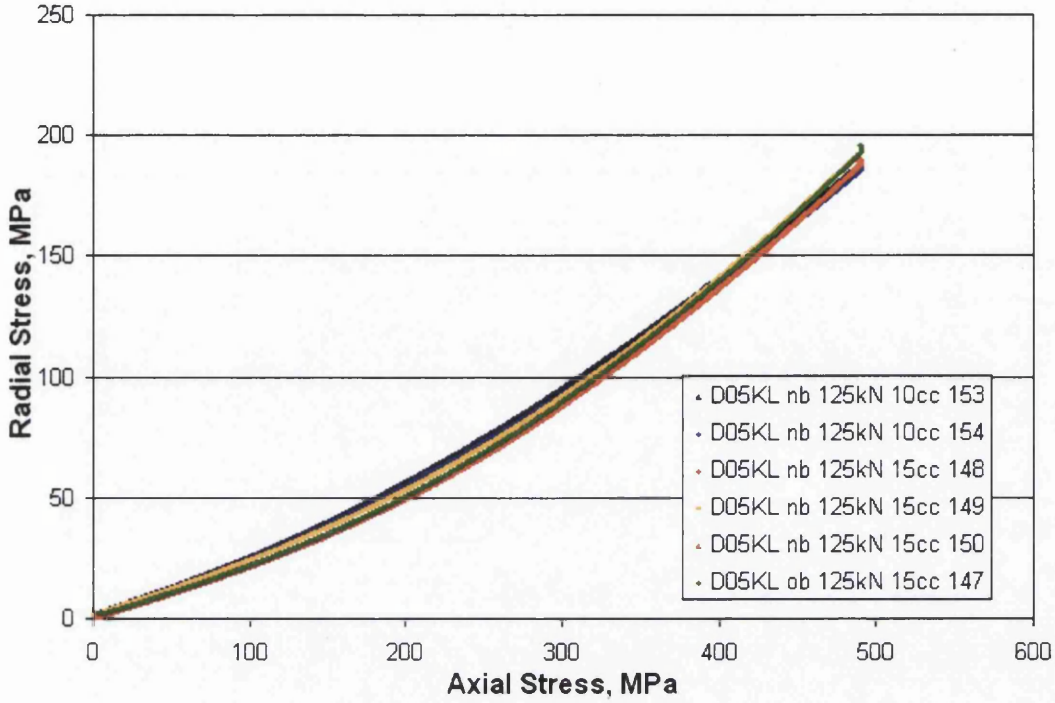

Figure 4.10 Evolution of Radial Stress with Axial Stress, Instrumented Die

In our numerical simulations the friction is typically represented as a function of either stress, as depicted in Figure 4.8, or density. The latter is plotted in Figure 4.11, where the reduction in friction with increasing density can be observed.

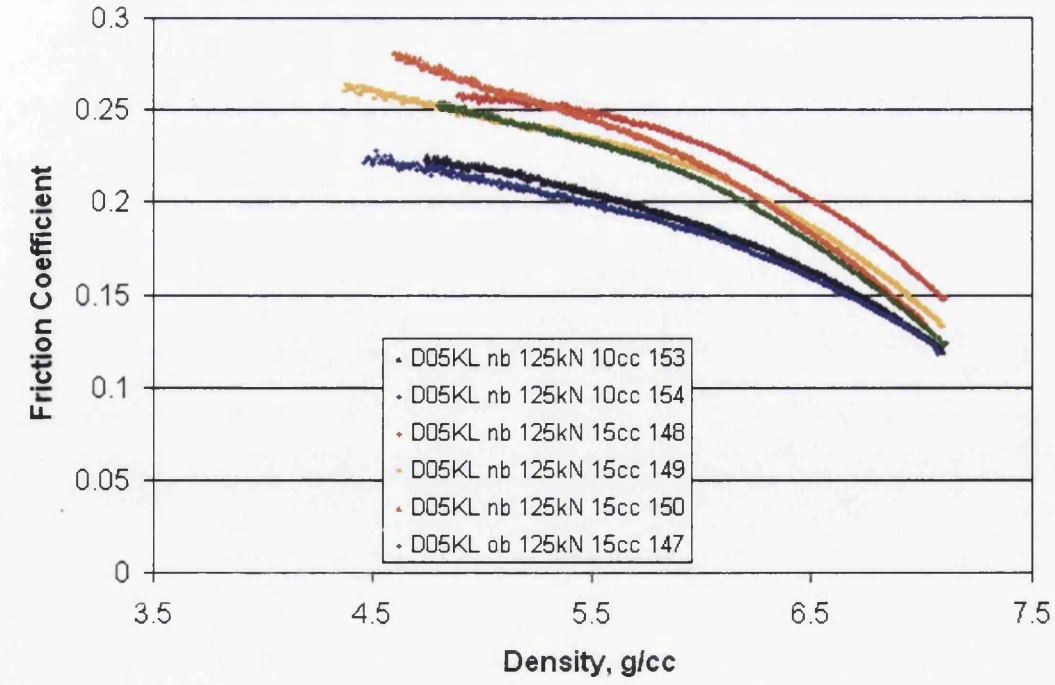

Figure 4.11 Friction coefficient vs density, Instrumented Die

When plotted against density the friction coefficient for the shorter 10cc compacts was again seen to be lower than for the 15cc ones.

The evolution of the friction coefficient with compact height is plotted for completeness in Figure 4.12. This relationship is not direct, but governed by the change in compact density and applied pressures required to achieve the required height.

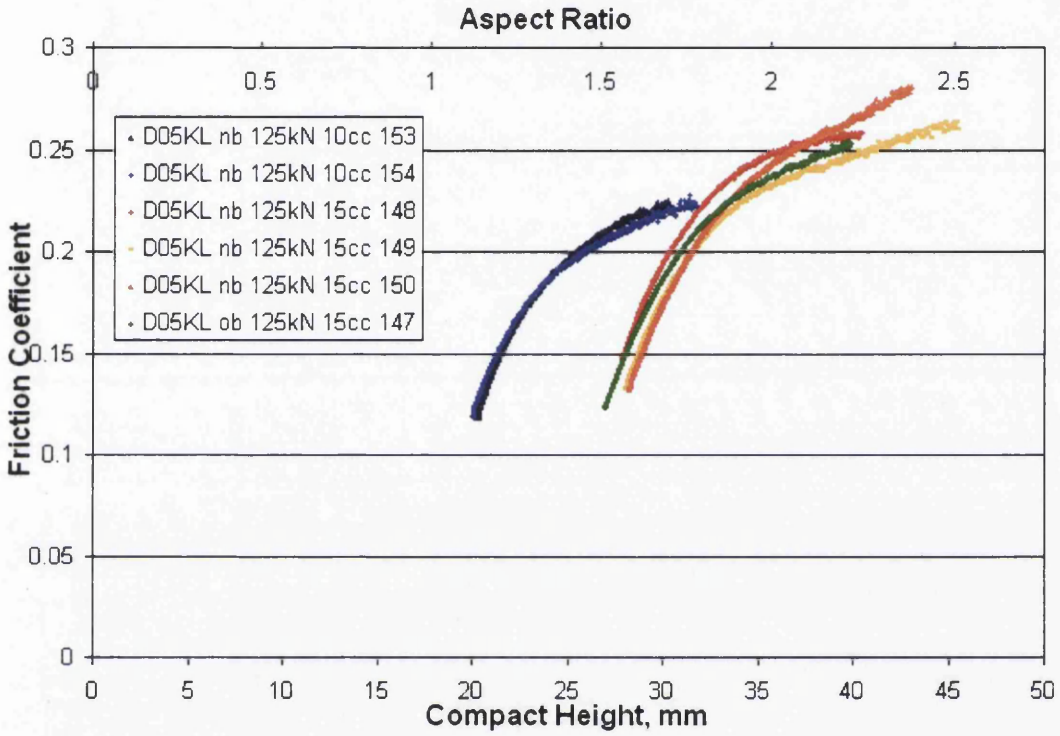

Figure 4.12 Friction Coefficient vs Compact Height, Instrumented Die

Overall, the friction coefficient was seen to reduce with increasing density values and normal and axial stress. It was also found to be lower for compacts of lower aspect ratio, as indicated indirectly in Figure 4.12, i.e. for a given compact height X of the 10cc sample the friction coefficient at an equivalent compact height of 1.5*X of the 15cc sample is higher, despite similar stress and density values.

4.3 Shear plate

It is impossible to evaluate all of the parameters independently during an instrumented die test. Continuous curves can be produced during the experiment showing the relationship between the coefficient of friction and parameters such as density, stress and aspect ratio. However, the latter are linked and cannot be

varied independently. The shear plate apparatus presented herein went some way towards providing greater control during the experiments. Modifications to the equipment, which will be introduced later in this chapter, allowed for these process parameters to be separated, making independent control and study of their effects possible.

4.3.1 Shear plate – test equipment

The shear plate apparatus used in this work was previously used to investigate the effect of surface hardness and roughness on powder friction (Cameron, Gethin et al. 2002). The authors demonstrated the suitability of the shear plate technique for measuring friction and produced results detailing the effect of target roughness and hardness on friction for ferrous and alumina powders.

It was also one of the items of equipment which was used in the PM Modnet Methods and Measurements Group (2000) study comparing a range of friction measurement devices. There was found to be generally good agreement between the shear plate devices and more variability of data from those centres using instrumented die equipment. This was possibly in part due to a more specialised design of the shear plate equipment, and in part to the variety of designs and dimensions among the instrumented dies tested.

The main features of the shear plate apparatus can be seen in Figure 4.13 and Figure 4.14. The target surface disc is located at the bottom of the die. The disc is mounted in a sliding plate, which in turn rests on linear bearings to minimise parasitic friction (friction coefficient of 0.002-0.003, INA Bearings). The target surface disc can easily be replaced and usually represents a typical die surface. The gap between the die and the target surface was necessary to avoid rubbing between the two. It is exaggerated on the diagram – it was typically set to 0.01mm with position being adjusted by placing shims underneath the target surface.

Above the die is a bronze bushing, which is used to support and align the punch. This is especially important when the die is filled to the top and the punch is inserted to a very shallow depth. The maximum fill height was 50 mm, which was

deemed sufficient to be able to avoid end effects that are associated with low aspect ratio compacts that approximate a disc.

The shear force was generated by a hydraulic system. This consisted of a mechanical screw, driven by an electric motor with variable speed control, which forced a piston into a master hydraulic cylinder. The hydraulic pressure was transmitted through a pipe to the work cylinder, which in turn applied the load to the sliding plate through the load cell.

The normal force was generated by the Dartec hydraulic press, capable of loads of up to 250kN in either compression or tension. Load control was used during compaction and a loading rate of 1kN/s was used.

The instrumentation consisted of the shear force load cell, an LVDT that measured the movements of the sliding plate and the punch displacement and load readings were obtained from the Dartec press. Additionally, LVDT excitation voltage and ambient temperature were recorded. The signals were routed through a data acquisition pod and into a PC. A custom program was used to record the data in text format with a sampling rate of approximately 1Hz.

Before any experimentation took place the LVDT and the load cells were calibrated. Different load cells were used for different load ranges in order to maintain sensitivity. Each of the load cells was instrumented with 4 strain gages in a full bridge configuration and calibrated prior to use with subsequent calibration checks being made during the test campaign.

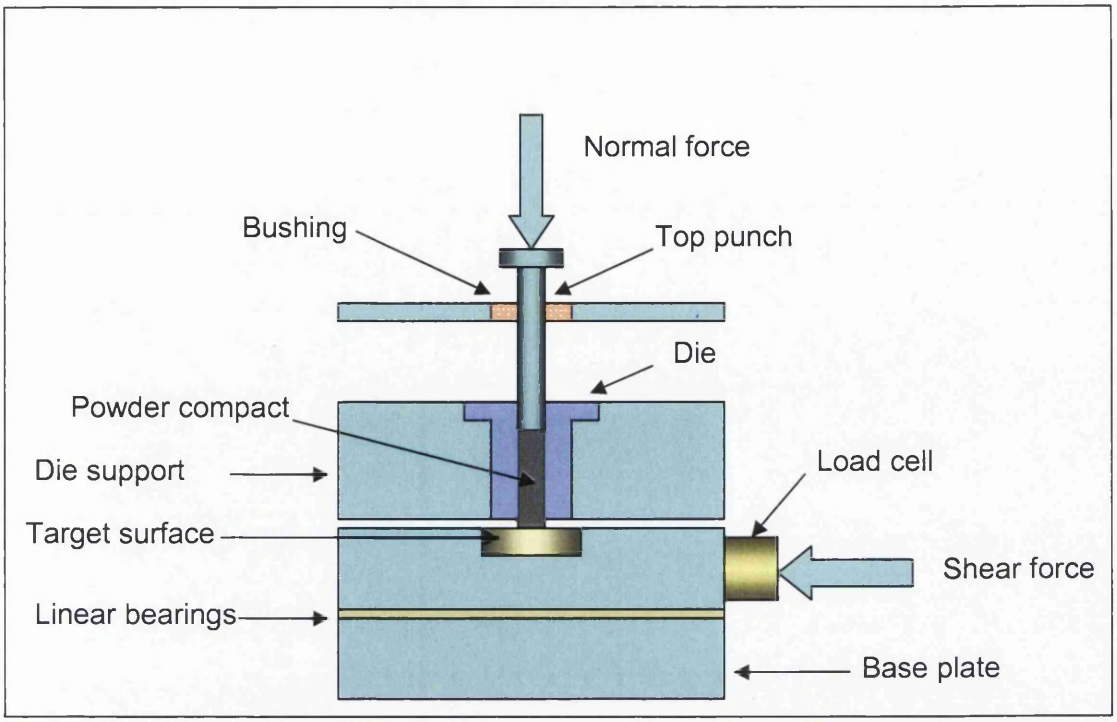

Figure 4.13 Shear plate apparatus

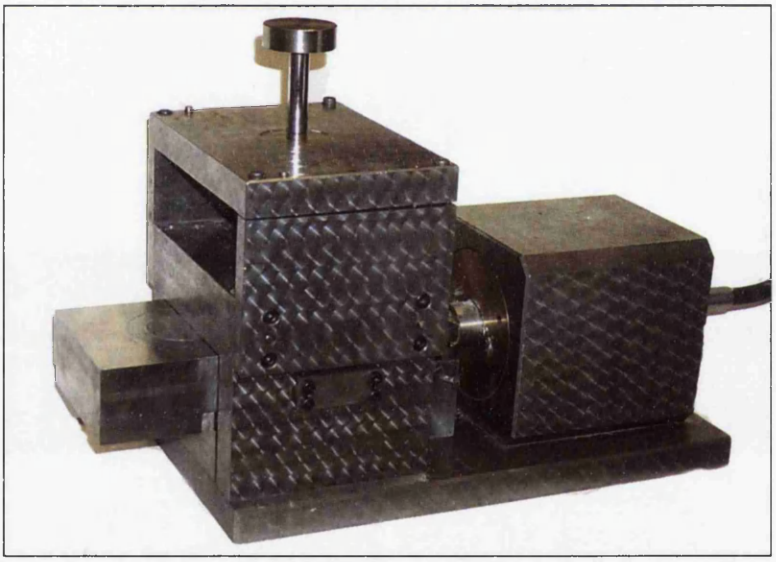

Figure 4.14 Shear plate apparatus (Cameron 2000)

4.3.2 Shear plate – experimental procedure

The experimental procedure started with the target surface in position underneath the die, with the hydraulic ram fully withdrawn. The die was then filled to the top through a funnel and the powder levelled off. The punch was then inserted through the bushing and into the die. Data recording was started and the powder compacted to a set load. Load control was used for safety, as without experience

of the powders being tested, displacement control could have resulted in extremely high loads. Once the desired load was reached the motor activating the hydraulic system was switched on. The motor reached its maximum running speed before the ram came into contact with the load cell. This ensured that the displacement of the shear plate occurs at nearly constant velocity. Once the shear plate was displaced by approximately 5mm the shear load was stopped and the normal load gradually removed. The sliding plate was then removed from the apparatus and the downwards ejection of the compact was performed. The data recording was then halted.

4.4 Floating die shear plate

4.4.1 Floating die shear plate – test equipment

The floating die shear plate apparatus is a modification of the shear plate equipment described above. The parts below the target surface have remained unchanged. The principal innovation is the new die support, which incorporates a linear bearing. The bearing removes the rigid link between the die and its support and allows forces from the top punch to be fully transmitted to the target surface, see Figure 4.15. The dimensions of the new die were modified – the diameter has been brought in line with that of the instrumented die equipment used elsewhere in this thesis. The height of the die has also been increased to improve the height range of the compacts that can be tested. The die is typically filled with a set weight or volume of powder. Sufficient space is then left at the top of the die to ensure an adequate depth for the top punch insertion thus ensuring that the correct alignment is achieved. This made the bushing system used in the previous shear plate design unnecessary. Its removal has improved access to the die when filling and, together with the floating design, allowed for easy removal and refitting of the die, which also facilitated its cleaning and maintenance.

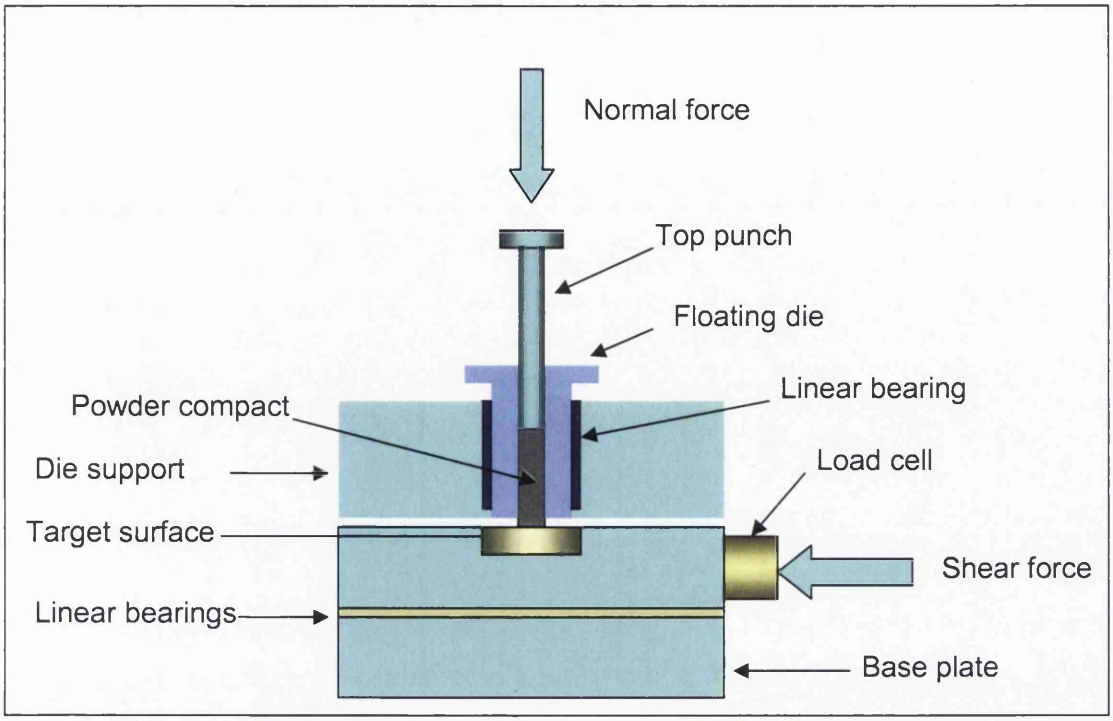

Figure 4.15 Floating die shear plate apparatus

The same instrumentation and data acquisition system as used in the original shear plate set up were employed. The top punch load and displacement were obtained from the press control unit, the shear force and displacement were measured using a load cell and a LVDT.

4.4.2 Floating die shear plate – experimental procedure

The experimental procedure for the floating die shear plate test is similar to that of an ordinary shear plate test. The only difference is that after initial compaction the sample has to be unloaded, to allow for removal of the support half-rings. The load can then be reapplied, either to the same level as the compaction load previously, or to a lower level if a test at higher density, but with lower normal force, is desirable. The support half-rings are reintroduced for the ejection stage. A check of the bottom surface of the die was performed to confirm that the die did not come in contact with the target during the sliding stage with support rings removed. No striations, which would have been inevitable if such an event occurred, were found, confirming that only the compact was sliding against the target surface.

The overall sequence can be traced in the recorded data, a sample of which is shown in Figure 4.16. Here, press displacement was zeroed when the punch was level with the top of the die. At the start of the test the punch was resting on top of the powder approximately 26mm into the die. The process started with the compaction of the sample – the press load rose linearly until the desired compaction load was reached and the press displacement increased nonlinearly with a visible hardening behaviour (0-100s). After the maximum load was reached the compact was then unloaded at the same rate and the displacement curve shows corresponding springback (100-200s). The support rings were then removed and the compact rested on the target surface. The normal load was then applied (220-280s). Once the compact was loaded the motor powering the sliding plate was turned on. The friction load increased to a peak value and then dropped off to an almost constant value. The motor was then stopped and reversed in preparation for the next test. Simultaneously, the normal load was removed (350-420s). The sliding plate was then removed (~445s) and the die supports reinstalled. The compact was then ejected downwards into the space vacated by the sliding plate (530-580s). Ejection was performed in two stages – initial pressing under displacement control and final ejection under manual control, the switch from the former to the latter accounts for the pause in punch displacement (~560s).

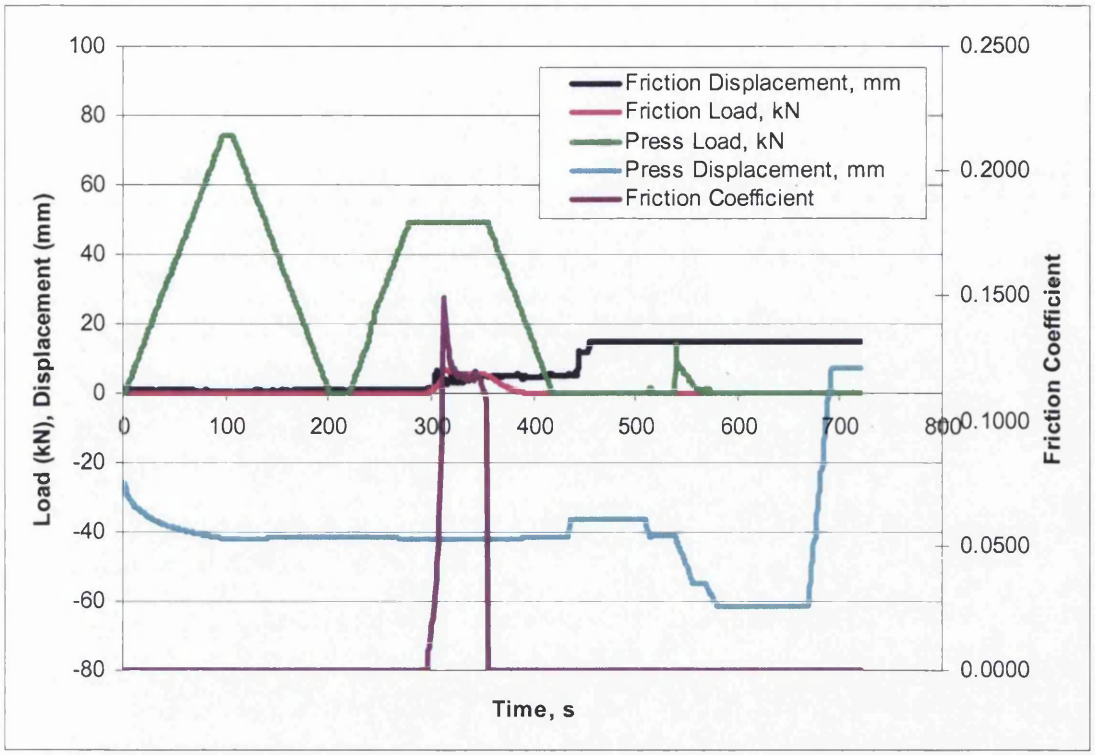

Figure 4.16 Data from a typical test on the floating die shear plate equipment

The primary results from a floating die shear plate test are the static and dynamic friction coefficients. The ejection force required can also provide useful insight into powder friction behaviour, but this will be explored more fully in Chapter 7.

4.4.3 Floating die shear plate – repeatability

When performing friction tests two approaches to treating the test surface can be taken. The first aims to mimic the industrial conditions as closely as possible and the second is geared to ensure consistency. The first approach involves performing a series of preliminary test runs to recreate the industrial conditions by either coating the target with the lubricant present in the powder, or by allowing for any residual lubricant to be removed, if non-lubricated powder is used. This approach is very time consuming and was found to be impractical for this work due to the high number of powder/lubricant mixes used. Consequently, the second approach was used and the target surface was cleaned thoroughly with wipes soaked in an alcohol-based solvent prior to each test to ensure the consistency throughout the test programme.

Before the full test program could go ahead it was necessary to perform a trial exploring the repeatability of the experiments on the new equipment. Three tests with the same powder type and quantity were performed under identical loading conditions. Non-lubricated powder was chosen for these tests as, based on previous experience (Cameron 2000), it was expected to provide the most variable results. The powder was compacted until a load of 75kN (295MPa) was achieved and which was applied at the rate of 1kN/s. The normal load during the sliding stage was 50kN (196MPa). The plots of friction coefficient obtained in these tests can be seen in Figure 4.17.

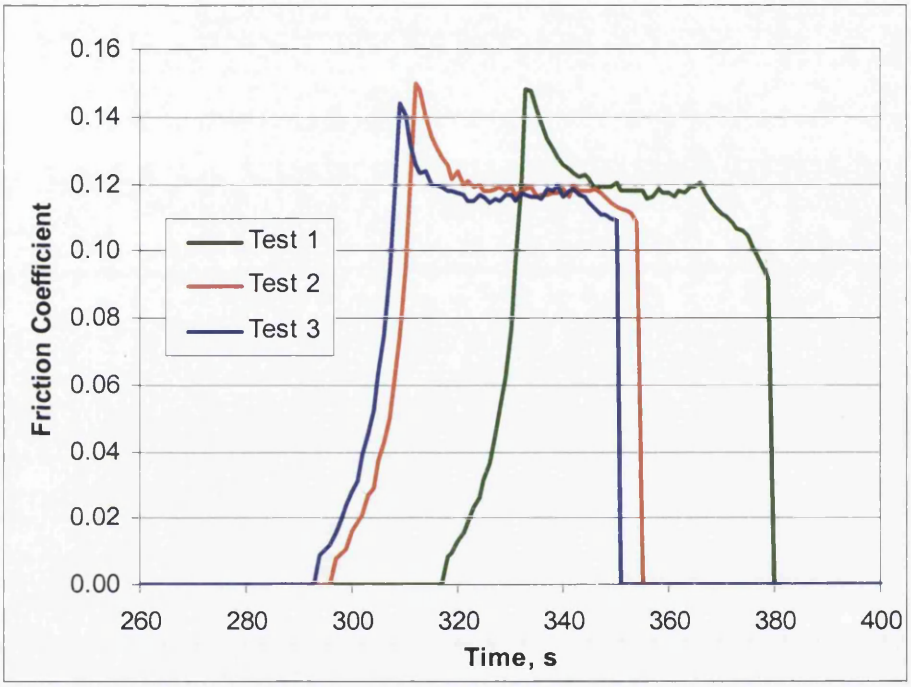

Figure 4.17 Floating die shear plate – repeatability

The initial peaks represent the static friction coefficient, reached just before the shear plate starts moving. This is accompanied with a drop in friction and the resulting plateau represents the dynamic friction coefficient. The initial fall off from the plateau corresponds to stopping of the motor driving the hydraulic ramp and its reversal, the steep drop at the end was an artificial device used for data analysis and presentation. Of interest here are the values of the static and dynamic friction coefficients. The former is taken to be the maximum value recorded, while the latter is a result of averaging the values recorded between ten and thirty seconds after the initial peak.

The relative positions of the tests on the timeline are irrelevant and depend on the operator caused delay between the stages of the experiment. With that in mind the timeline can be normalised and the same tests are then presented in Figure 4.18. The loading path almost completely coincides for all the tests until the static friction limit is reached. Once the sliding stage is underway a very small variation between the tests exists, but essentially they are very close. The consistency achieved is significantly better than that achieved by Cameron (2000), highlighting a superior performance of this new equipment.

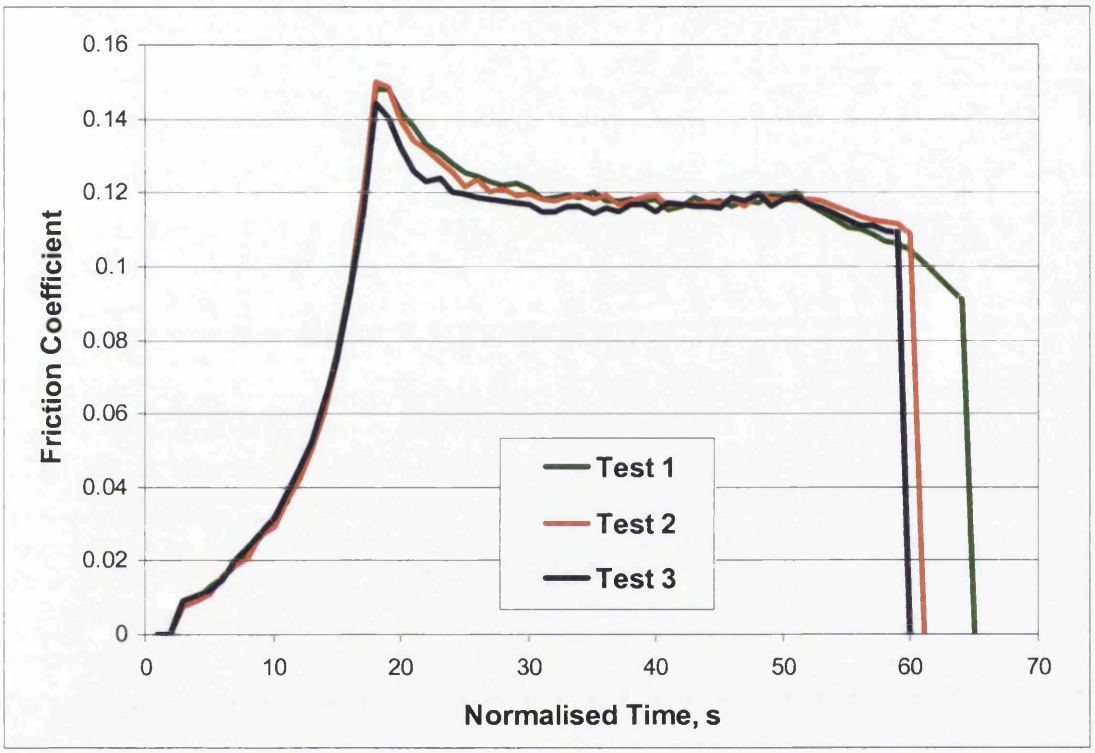

Figure 4.18 Floating die shear plate – repeatability (normalised time)

Statistical analysis was also performed using Student's 't' distribution (Kreyszic 1988) to quantify the variability in the results. The findings can be seen in Table 4.1. Error values presented are for the 95% confidence level and signify that with 95% probability the true mean would lie within ±3% of the calculated mean for the static friction coefficient and within ±1.3% for the dynamic friction coefficient. Variation from the mean in the sample was ~2% for the static friction coefficient and 1% for the dynamic friction coefficient. This is comparable, or better than, the repeatability of tests with iron powders reported previously for tests with conventional shear plate equipment (Cameron 2000).

Table 4.1 Floating die shear plate – repeatability, statistical analysis

	Test 1	Test 2	Test 3	Mean	Std Dev	%Error
Static	0.1479	0.1499	0.1440	0.1473	0.0030	2.9776
Dynamic	0.1184	0.1182	0.1165	0.1177	0.0011	1.3328

Where $Error = A * \frac{S_n}{\sqrt{n}}$

The above procedure was repeated for a faster loading rate of 5kN/s. The results are presented in Table 4.2. The results exhibit some sensitivity with respect to loading rate and this is consistent with expectations, as a higher rate is more likely to introduce dynamic effects. In this instance, variability is the focus and although less variability in the static friction coefficient was observed, the variability in the dynamic friction coefficient was higher (4.1% instead of 1.3%). Thus, a 1kN/s loading rate was chosen for the subsequent experiments.

Table 4.2 Floating die shear plate – repeatability, 5kN/s, statistical analysis

	Test 4	Test 5	Test 6	Mean	Std Dev	%Error
Static	0.1548	0.1511	0.1554	0.1538	0.0023	2.2201
Dynamic	0.1238	0.1205	0.1274	0.1239	0.0035	4.0931

The conclusion of the repeatability trial was that sufficient consistency was demonstrated for the non-lubricated powder. Based on previous work by Cameron (2000), it was expected that repeatability would be better for lubricated powders as they would be less likely to exhibit stick slip behaviour. It was therefore decided that the study could go ahead with a single sample being tested for each powder and loading condition.

To further ensure test repeatability when powders with a different lubricant content were tested, the tests were performed in such a sequence that the difference in lubricant content was minimised between each batch.

4.4.4 Floating die – results

An instrumented die experiment (Section 4.2) produces a representation of the continuous relationship between the friction coefficient and such parameters as stress and density. In contrast, the floating die shear plate experiment shows the relationship between the friction coefficient and the target displacement for specific density and stress conditions. These are constant throughout the sliding stage of the experiment. To obtain a representation of the friction-density, or friction-stress relationship, a whole series of experiments would need to be performed. For the instrumented die and the conventional shear plate equipment the relationship between stress and density cannot generally be controlled; in the case of the floating die apparatus those parameters are uncoupled. This makes it possible to simulate different equipment configurations and process conditions.

For example, compacts of the same density (identical quantities of powder compacted to the same height/load) can be tested at a range of normal loads. The limitation here being the requirement for those loads to be lower than the initial compaction load, as otherwise further compaction would take place.

Throughout this work tests with a wide range of normal loads and densities were performed. It is therefore important to highlight the distinction in the different types of stress considered here. The axial stress is taken to be the current stress on the top punch. Depending on the stage of the experiment this stress will also represent the compaction stress or the normal stress.

In this work the compaction stress is defined as the maximum axial stress applied via the top punch in order to densify the powder. Once the compaction stage of the experiment was complete the compact was unloaded to allow for the die support rings to be removed.

The next stage of the floating die experiment consisted of loading the compact to a desired level of normal load or normal stress. This is the stress at which the compact was pushed against the target surface during the sliding stage of the experiment.

A series of tests was performed for the Distaloy AE ferrous powder mixed with 0.5% Kenolube. This was the same powder as was used in the above instrumented die tests. The experiments were performed with a tool steel surface – this material was chosen as it is similar to the die material in the instrumented die apparatus.

The matrix of experiments is presented in Table 4.3. The tests at 10kN compaction load could not be completed as no cohesive compact was formed and powder spilled from the die when the support rings were removed.

Table 4.3 Matrix of experiments, Distaloy AE +0.5% Kenolube, floating die shear plate, tool steel target

Normal Load, kN	Compaction Load, kN				
	10	25	40	50	75
10					√
25		√			√
40			√		√
50				√	√
75					√

A different behaviour was observed for the tool steel target surface compared to that of the Zirconia tool surface used in the repeatability studies and elsewhere in this thesis. For this combination of powder and target surface, there was no prominent time when the static coefficient of friction, as seen in Figure 4.16, could be determined. Instead, once a sufficient load was reached to initiate the sliding of the target surface, then the friction load continued to increase with only a small spike present to indicate the beginning of sliding, see Figure 4.19. The dynamic friction coefficient obtained was an average value taken over an interval of up to 20 seconds.

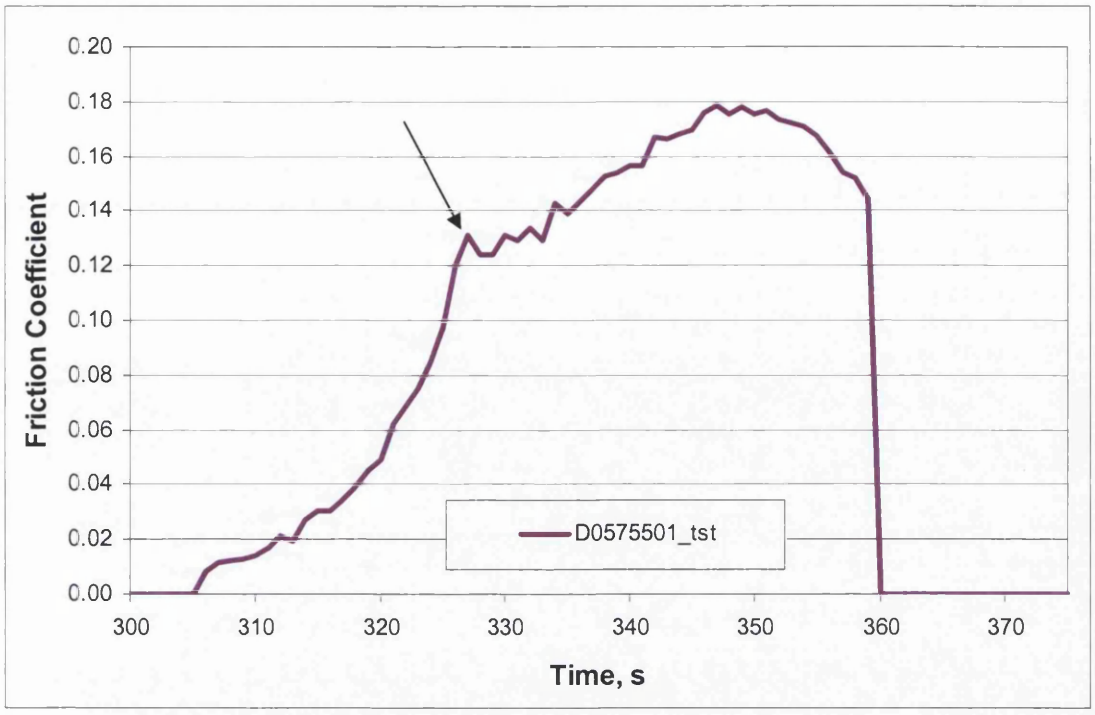

Figure 4.19 Evolution of friction coefficient during a floating die shear plate test on tool steel target

When looking at the evolution of the friction coefficient (static or dynamic) with stress, the same trends as seen in the instrumented die tests and work undertaken by others (Doremus, Toussaint et al. 2001), (PM Modnet Methods and Measurements Group 2000), (Solimanjad 2003) are apparent. That is the friction coefficient reduces as the stress increases. Figure 4.20 shows this reduction for a series of tests in which the normal stress was equal to the compaction stress. Thus, the friction coefficient was also found to reduce with increasing density.

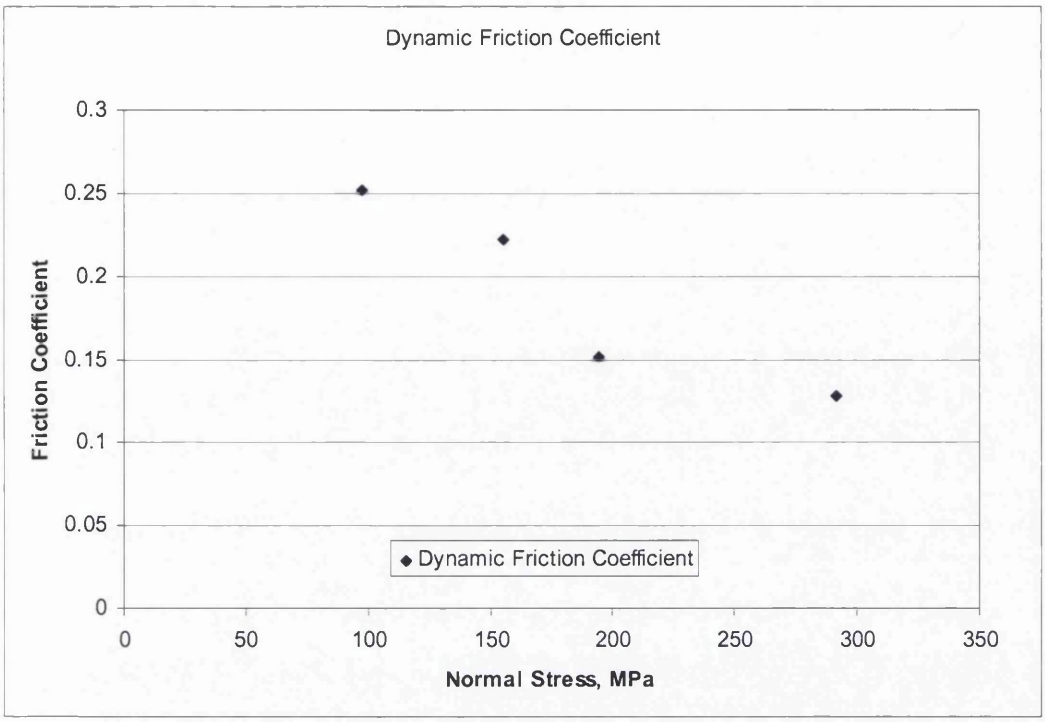

Figure 4.20 Evolution of friction coefficient with stress, floating die test, tool steel target

As mentioned previously, both the normal and compaction stresses were the same, resulting in density changes throughout the series of tests. The new equipment, however, allows for the two stresses to be uncoupled, thus enabling compacts which had been pressed to the same density to be tested at different normal loads. An example of tests where the stresses were uncoupled is shown in Figure 4.21. In this case all of the samples were first pressed to 75kN (290MPa), unloaded, and after removing the support rings loaded again to 10, 25, 40, 50 and 75kN. The trend of reduction in friction coefficient with increasing stress is again present. However, this time it can be singularly attributed to the normal load as the density remained constant.

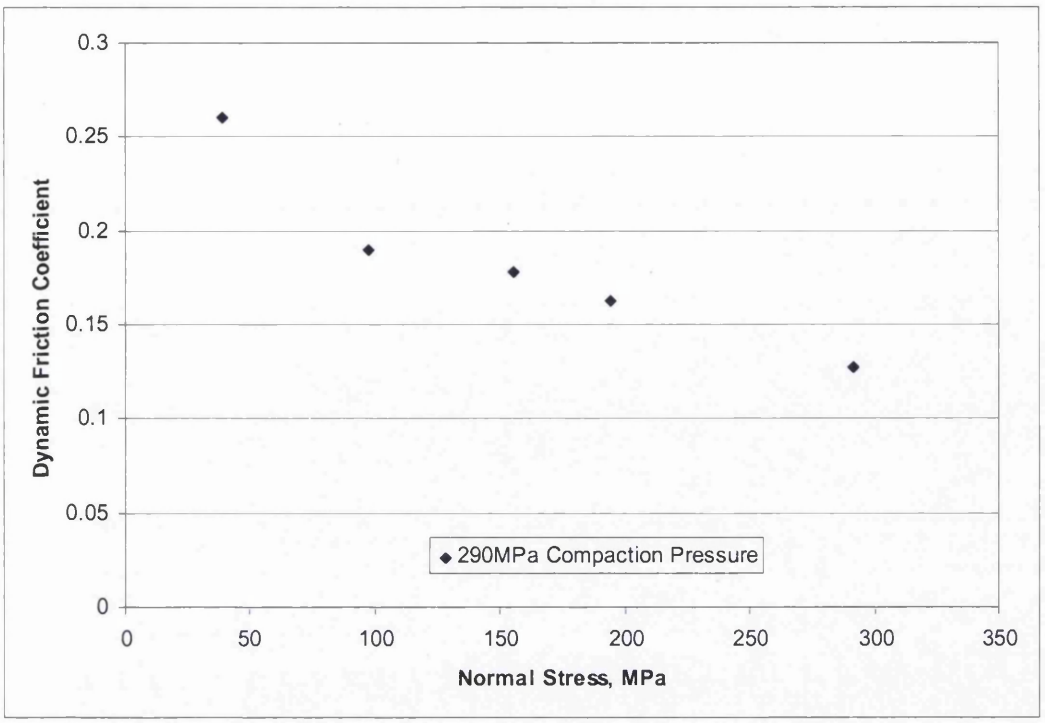

Figure 4.21 Evolution of friction with normal stress, floating die test, tool steel target, all compacts pressed at 290MPa

Combining the two series on the same graph allows for the differences to be observed, see Figure 4.22. The points representing the sample with the highest pressure coincide as they come from the same compact. However, at a lower normal stress the friction coefficient was lower for the compacts pressed to a high density. This mechanism has not been fully explored before. The high level of friction at low density is generally attributed to a 'ploughing' model of friction (Cameron 2000). However, it may also be attributed to different boundary lubrication regimes and this is considered below.

It may be hypothesised that for a constant high compaction pressure, the powder particles will be deformed to the same extent and that a similar amount of lubricant will be extruded. Where compacts are pressed to lower density, the particles will not be deformed in the same way and they will remain as individual particles. Further, the lubricant may not be extruded from the compact to the same extent. This leads to different lubrication regimes as the compact slides against the target surface. For the low density compact, the level of lubricant at the surface is lowest and consequently the friction is high. At a higher normal stress

there comes a point for the compact that shares a common compaction pressure and normal stress when sufficient lubricant is extruded to achieve a regime that is common to both compacts and the friction coefficient achieves a similar level. This mechanism is particularly relevant to the process of ejection where admixed lubricant is extruded to the die surface and therefore aids ejection through a reduction in the friction coefficient.

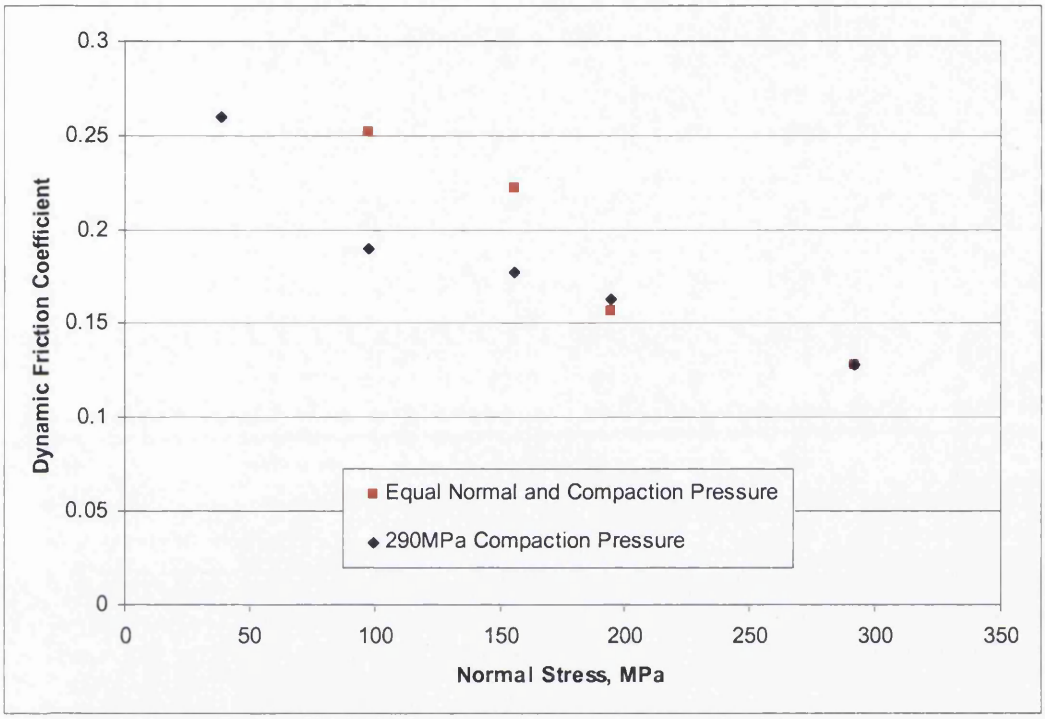

Figure 4.22 Evolution of friction with normal stress, floating die test, tool steel target

4.4.5 Energy Dispersive X-Ray analysis of compact surfaces

In order to establish, or explore, the presence of lubricant on the compact surface, selected compacts were examined using X-ray analysis. To achieve this, the sliding surfaces of three compacts, two with 0% and one with 0.5% admixed lubricant were scanned with a Scanning Electron Microscope capable of Energy Dispersive X-Ray analysis. The EDX analysis is a technique capable of identifying the chemical elements present on the surface of the test sample. The aim of the scan was to identify elements present in the admixed lubricant and by comparing their levels to estimate the amount of lubricant present on the surface.

A test sample of pure lubricant was scanned first to identify any possible marker elements present in it, see Figure 4.23. Very high levels of Carbon were identified (off the scale in Figure 4.23) along with smaller quantities of Zinc, Oxygen and Silicon. However, Carbon could not be used as a marker element as it is already admixed in the base Distaloy AE powder. This quantity is comparable to the total amount of admixed lubricant added and would make exact comparisons impossible. Additionally, it is readily present in many forms in the environment – e.g. in the atmosphere and in the plastic bags which contained the powder samples. Thus, carbon contamination of the samples could be possible.

Figure 4.23 Spectral analysis of admixed lubricant (Carbon is off the scale)

As Zinc is not present in the base powder, see Figure 4.24, it was selected as the marker element. As expected, the base Distaloy AE material contains a high proportion of iron, some nickel, copper and a small quantity of carbon.

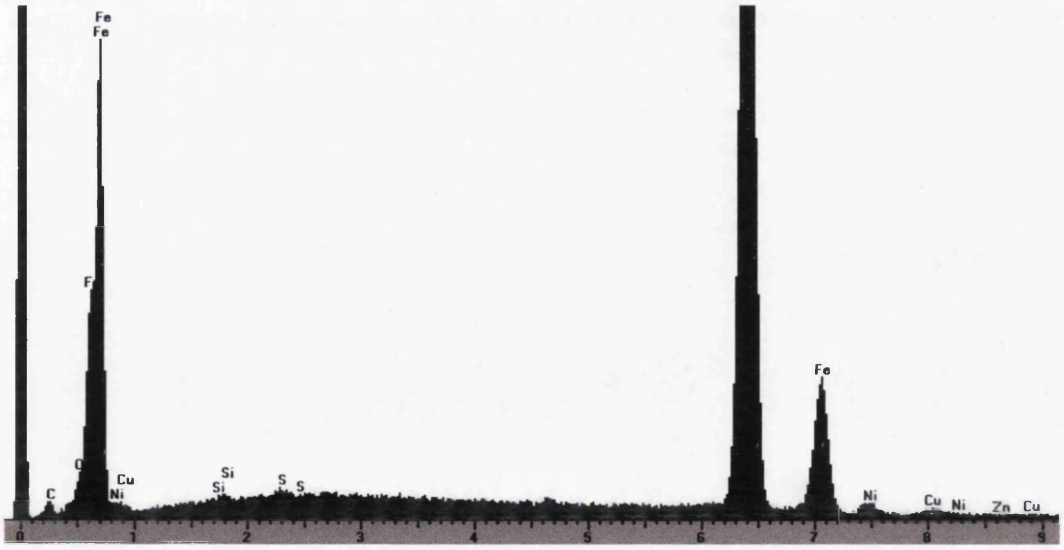

Figure 4.24 Spectral analysis of the Distaloy AE material (Iron is off the scale for convenience)

A series of scans were made from different areas on the sliding surface of the compact containing 0.5% admixed lubricant. Three distinct types of area were identified – the raised metal surface and two types of pits – light and dark. These are shown on the micrograph, see Figure 4.25.

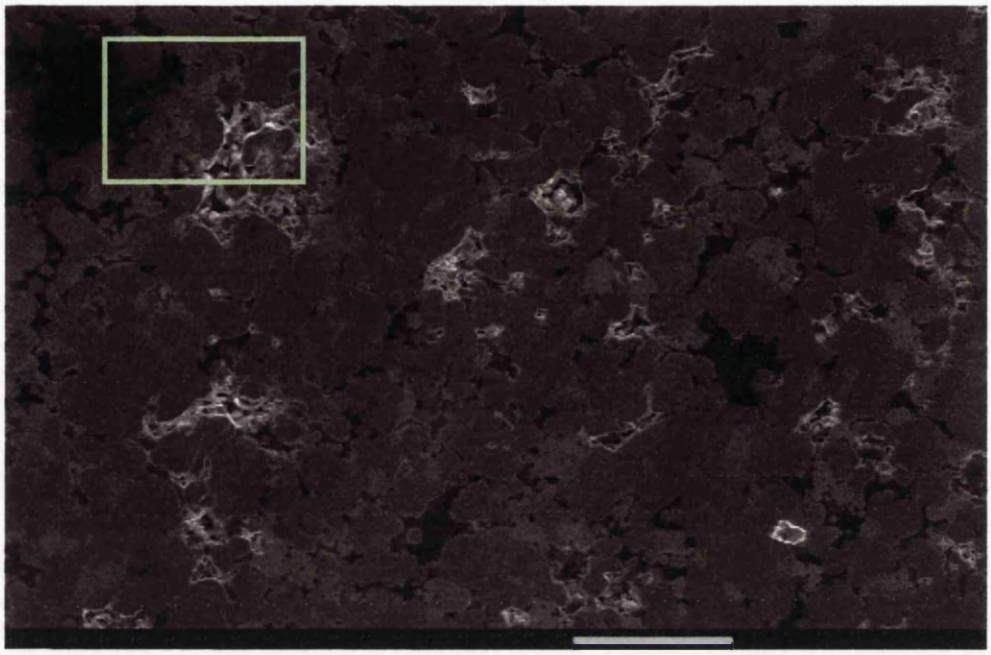

Figure 4.25 Sliding surface of a Distaloy AE compact with admixed lubricant. 200x magnification, the scale line is 100μm. See Figure 4.26 for the close up image of the selection.

The three specific areas considered were the section in the dark pit, the flattened raised area and an area in the bright pit as shown in Figure 4.26.

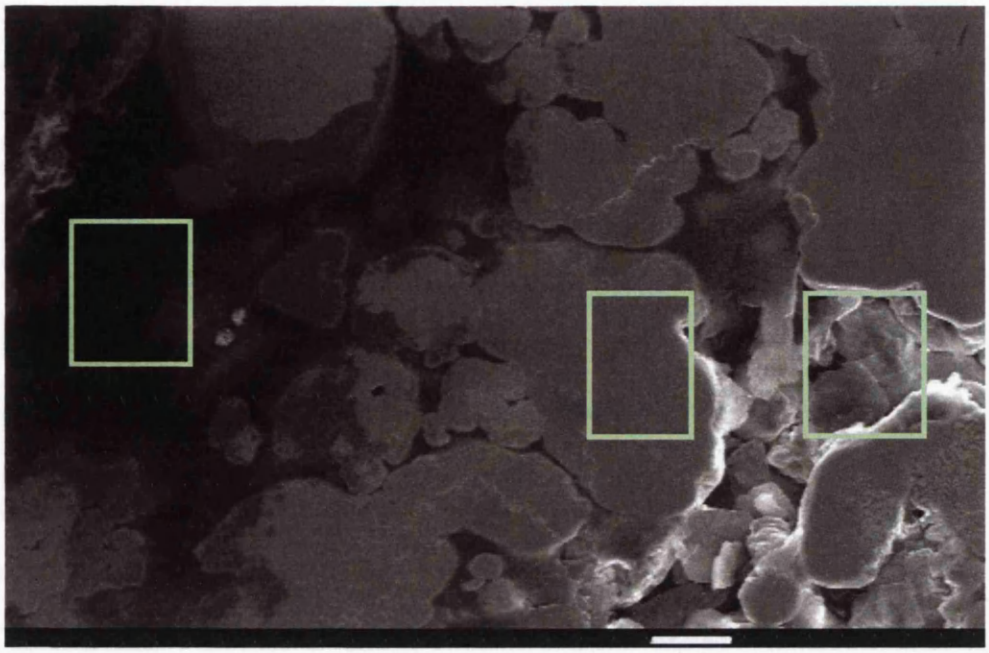

Figure 4.26 Sliding surface of a Distaloy AE compact with admixed lubricant. 1000x magnification. The scale line is 10μm long. Areas considered for EDX testing are highlighted

The scan in the dark pit area reported high quantities of carbon with a small amount of iron. None of the other elements could be seen in significant quantities. The scan of the raised area is dominated by iron, with small quantities of nickel, copper and carbon also present, see Figure 4.24. The surface of the bright pit was found to contain a lot of iron, carbon and nickel, the latter being in higher proportion than seen previously.

No significant amount of Zinc could be detected at any of the locations. The possible reason for this is the small overall proportion of zinc in the mixture. Only 0.5% lubricant was mixed in with the powder tested, of which Zinc was already a small proportion.

Scans of larger areas comprising a selection of surface features reported high quantities of iron, significant quantities of carbon, and identifiable quantities of nickel and copper. No identifiable amounts of Zinc could be detected.

There was a small difference in the amount of carbon detected for large area scans of lubricated and non-lubricated compacts, however this difference was not significant enough and could possibly be attributed to the proportions of surface pits seen on each individual scan section. As mentioned previously, carbon contamination was also likely to occur.

Thus, the EDX measurement did not identify quantities of lubricant extruded to the surface for the particular admixed lubricant used here. However, with a different lubricant, i.e. one which is not carbon based and has a high proportion of an easily detected element not present in the base powder mixture, may lead to more conclusive results. This remains as a future work requirement.

The scans have revealed a different surface structure for lubricated and non-lubricated compacts, see Figure 4.25 and Figure 4.27. There were fewer pits on the lubricated samples, and a higher proportion of the pits were of the "dark" variety. The surface porosity of the samples will be further explored in Chapter 5 where a more detailed study of admixed lubrication will be presented.

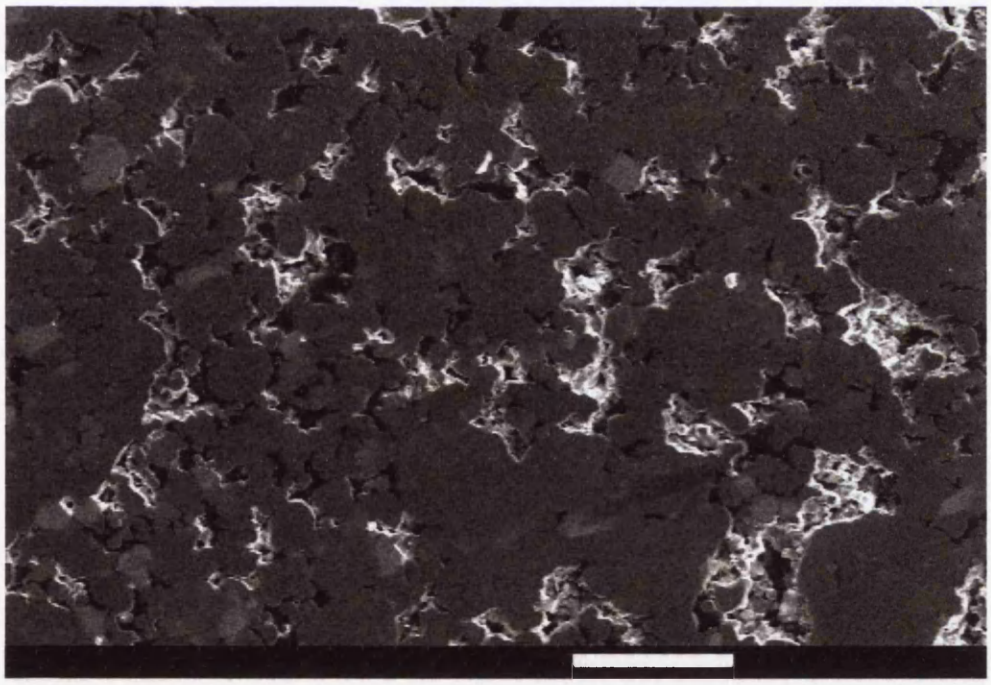

Figure 4.27 The sliding surface of a non-lubricated compact. 200x. Marker length 100μm.

4.4.6 Floating die shear plate – results, comparison to other techniques

It is now appropriate to compare the results of the instrumented die tests presented earlier with the results of the floating die shear plate tests. A tool steel target was used to best mimic the surface of the die and allow as direct a comparison as possible. The same Distaloy AE powder with 0.5% lubricant was used in both cases.

The relationship between the friction coefficient and the normal stress in both the instrumented die and the floating die shear plate experiment is presented in Figure 4.28. Similar trends can be observed. However, it is necessary to point out that some of the stress conditions of the floating die experiment differed slightly from those of the instrumented die test and a direct correlation could not always be expected. These differences are outlined below.

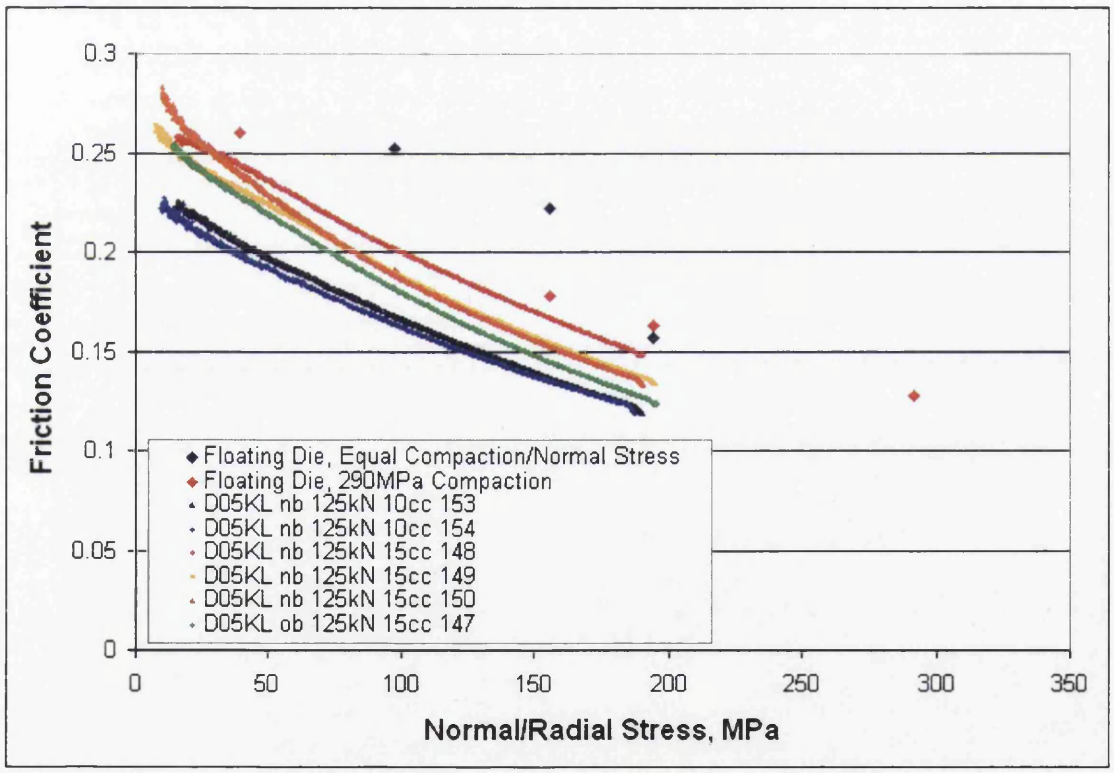

Figure 4.28 Evolution of friction coefficient with stress: instrumented die and floating die shear plate experiments

As mentioned previously, in Section 4.2.2 in the context of the instrumented die test, the stress normal to the friction surface was the radial stress and the

compaction stress was the axial stress. At any point in time the stress conditions were those of a certain radial stress, normal to the die surface and inducing the friction, and of a significantly higher axial stress, which densified the powder and provided a confining pressure. The ratio of the normal (radial) stress to the compaction (axial) stress varied from 0.2-0.26 at the beginning of the test to 0.37-0.4 at the end of compaction, see Figure 4.29. In the first series of the floating die shear plate tests presented in Figure 4.28 (also shown in Figure 4.22) the normal stress was equal to the compaction stress, i.e. after pressing the compact was reloaded to the level at which it was pressed. Therefore, the first series of tests shown in Figure 4.22 was performed with normal to axial stress ratio of unity. In the second series, the ratio varied as the compaction stress remained constant between tests and the normal stress was increased for each subsequent test. This variation can be seen in Figure 4.29.

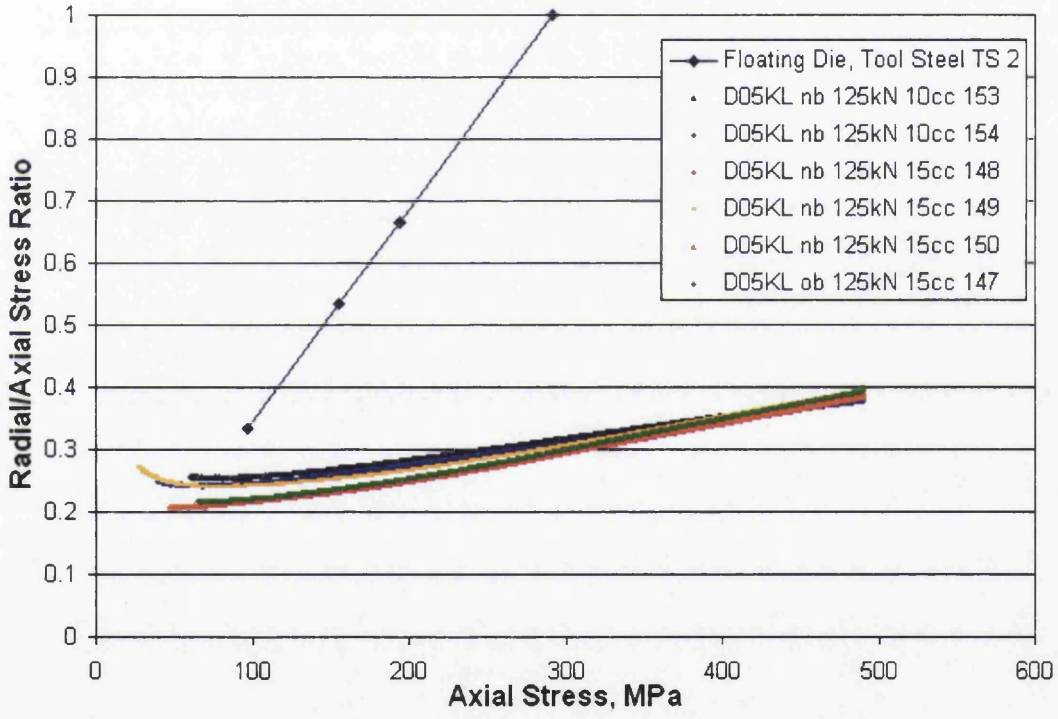

Figure 4.29 Ratio of radial to axial stress, floating die shear plate and instrumented die, Distaloy with 0.5% lubricant

As seen from Figure 4.22 the friction coefficient varies with normal stress even if the compaction stress remains constant. Since the normal/compaction stress conditions were different between the instrumented die and the floating die tests, identical friction values cannot be expected. Additionally, in the instrumented die

tests the axial pressure, which is greater than the radial pressure, is present throughout the test. In the floating die shear plate test the axial pressure during the test is always equal to the normal pressure, which in turn is lower or equal to the compaction pressure. Thus, the confining axial pressure in the floating die shear plate test is typically lower than that in the instrumented die test.

Nonetheless, the results from the second series of the floating die shear plate tests in Figure 4.28 are much closer to the instrumented die results than those from the first series. This is due to the stress conditions being closer to those encountered during the instrumented die test, and shows that if an appropriate stress state is obtained good correlation with the instrumented die test is possible.

4.4.7 Closure

A floating die modification to the shear plate equipment has been introduced with the aim of removing friction losses which occur in conventional shear plate equipment. This removes the need for complementary instrumented die tests, as required if a conventional shear plate is used. The new equipment allows independent control of normal and compaction loads – thus the loading conditions encountered in other equipments, such as in the instrumented die or as encountered during ejection, can be recreated.

The repeatability of the new equipment was tested and found to be very good. Early results were compared with those of other authors and those obtained in a series of instrumented die tests and were found to be in good agreement.

The EDX technique was used in an attempt to detect the lubricant on the compact surface. The results were inconclusive, however a better understanding of the surface topology was achieved.

In the next chapter the floating die shear plate will be used in a series of tests aimed at investigating the effect of admixed and die wall lubrication. Simultaneously, the friction mechanisms will be explored with special attention being paid to the effect on friction of normal and compaction loads. These will be

considered separately, as the new equipment allows for normal load and compact density to be explored independently.

Chapter 5 Exploration of Admixed and Die Wall Lubrication

5.1 Introduction

In the preceding chapter a modified shear plate apparatus was introduced. Its repeatability was tested and this was found to be very good. Further a comparison was made with the instrumented die tests performed here at Swansea and other friction measurement results published elsewhere. Overall good agreement was found between the trends exhibited for friction expressed as functions of either stress or density.

In this chapter the new equipment will be used to assess the effectiveness of admixed lubrication. Powders with varying quantities of lubricant and non lubricated powder will be tested at a range of loading conditions. These will enable a deeper analysis of the friction mechanisms, with normal stress and density being controlled separately. Finally, die wall lubrication will be briefly explored with the aim of applying the shear plate apparatus to quantify its effectiveness.

5.2 Admixed Lubricant – Experiment Layout

For this series of experiments the powder used was Distaloy AE and the lubricant was Kenolube. A highly polished Zirconia target surface was used. This had a surface roughness (Ra) of ~50nm, see Figure 5.1, and a Vickers hardness of 1182. No directional pattern could be observed on the surface of the target.

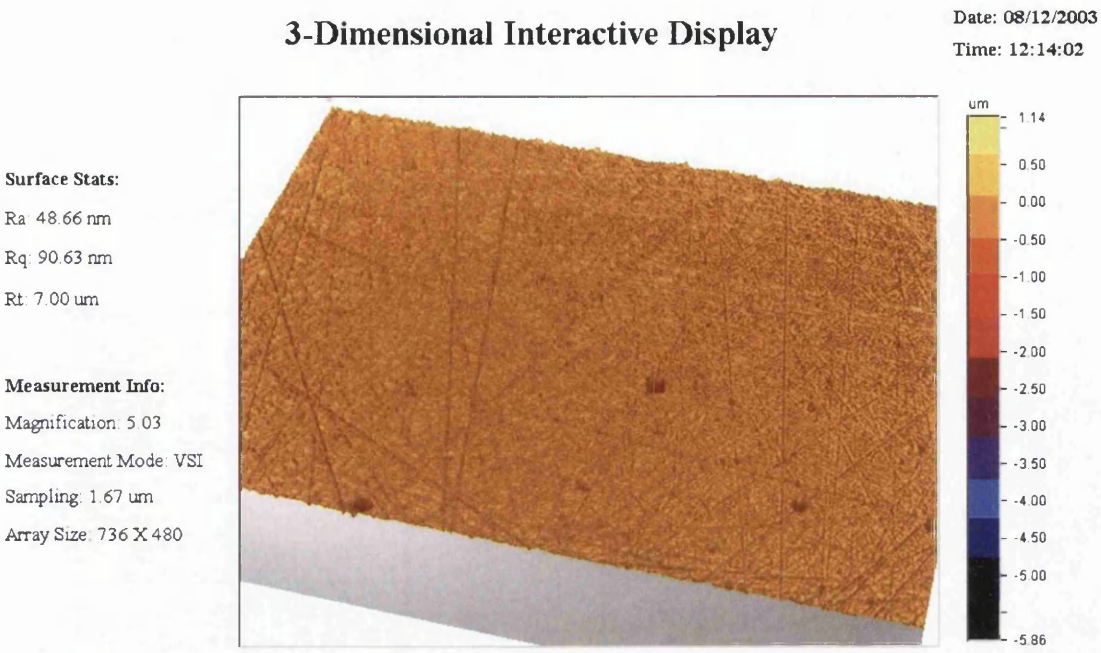

Figure 5.1 White light interferometer scan of the Zirconia target surface

Four powder mixes, three with lubricant (0.25, 0.5 and 1% by weight) and one without lubricant were tested over a range of pressures up to 777MPa (200kN compaction load). For most of the compaction loads considered, tests at all the lower normal load values were also carried out, see Table 5.1. This was done in order to evaluate independently the effect of the compaction pressure (and therefore density) and normal stress on friction.

Table 5.1 Matrix of Experiments - lubricant content study, floating die

Normal Load/*Pressure*, kN/*MPa*	Compaction Load/*Pressure*, kN/*MPa*							
	10 / *39*	25 / *97*	40 / *155*	50 / *194*	75 / *291*	100 / *389*	150 / *583*	200 / *777*
10 / *39*	√	√	√	√	√			
25 / *97*		√	√	√	√		√	
40 / *155*			√	√	√		√	
50 / *194*				√	√		√	
75 / *291*					√		√	
100 / *389*						√	√	
150 / *583*							√	
200 / *777*								√

The powder mix with 1% lubricant was only tested at loads of up to 75kN. It was observed in the course of the experiments that at higher pressures, a 0.5% addition of lubricant was almost as effective. Indeed at lower normal loads, 0.25% lubricant addition is equally effective in reducing the friction coefficient and this will be discussed further below.

5.3 Results

5.3.1 Evolution of friction under different loading conditions

First the results were considered from the perspective of a fixed compaction load, i.e. the tests from the columns of the experimental matrix. The compaction load for each of the columns was the same, and the static and dynamic friction coefficients measured at each of the different normal loads were plotted for each powder mix, see Figure 5.2 and Figure 5.3.

For compacts pressed to 10kN (39MPa) only a single data point was recorded therefore these results are more conveniently presented as a table rather than on a graph, see Table 5.2. Here both the static and the dynamic friction coefficients were lower for the mixtures having a higher amount of lubricant, while the static friction was always higher than the dynamic friction.

Table 5.2 Friction coefficients for compacts pressed to 10kN (39MPa)

	0% Lubricant	0.25% Lubricant	1% Lubricant
Static Friction	0.22	0.20	0.18
Dynamic Friction	0.21	0.17	0.14

For the rest of the tests, shown in Figure 5.2, some common trends were observed. The static friction coefficients were typically higher than the corresponding dynamic friction coefficients, as was expected from experience. The addition of lubricant resulted in lower friction coefficients, for both the static and dynamic cases. Even small amounts of admixed lubrication yielded significant improvement, however lubrication beyond 0.5% appears unnecessary as loads rise. For compacts pressed at 75kN there was very little difference between the friction coefficients for powder with 0.5% and 1% of lubricant.

Another common trend observed in all the tests was that of the friction coefficients reducing as the normal load rises. Note that in this case the compacts presented in each graph have been pressed to the same load and hence density. Thus, the reduction in friction is due to just the normal load and not density.

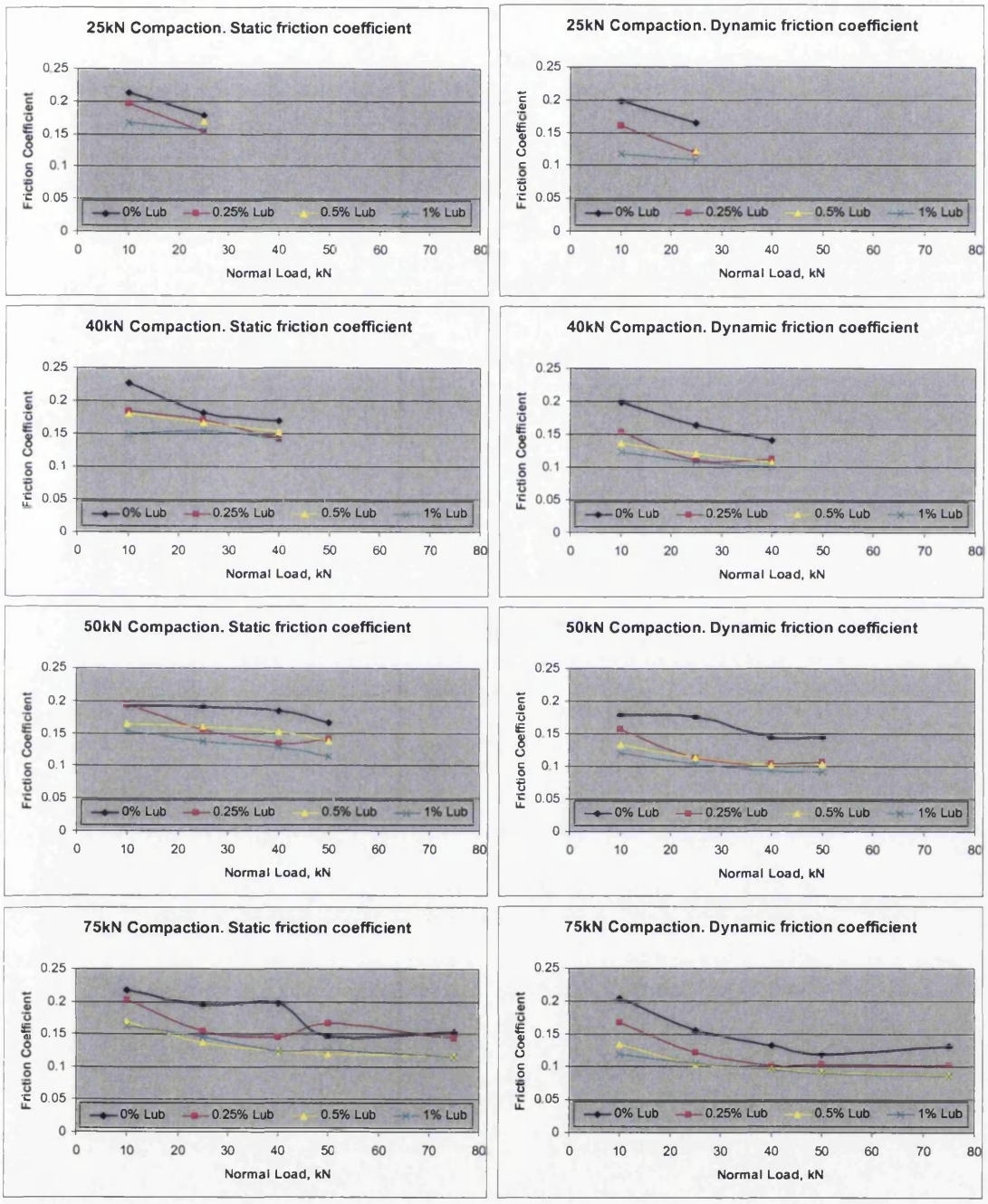

Figure 5.2 Static and dynamic friction coefficients for compacts pressed at set load.

As the above tests showed, at high compaction pressures the differences in performance between the powders with 0.5% and 1% of lubricant were very

small. Thus, the powder with 1% lubricant was excluded from tests at higher pressures.

The results of the tests from samples compacted to 150kN (583MPa) again show a significant reduction in friction when a mixture with lubricant is used, see Figure 5.3. However, instead of decreasing at higher normal loads the friction coefficient appears to be rising. Note here that the friction coefficient is very low and so it becomes difficult to measure precisely due to its small value, hence the scatter. There may be a slight upward trend for increasing normal load, but the dominant effect is that lubricant still reduces the friction level, the extent depends on the content. To further explore the slight increase in friction with normal load, a surface analysis of the compacts pressed to 150kN will be presented in Section 5.3.2.

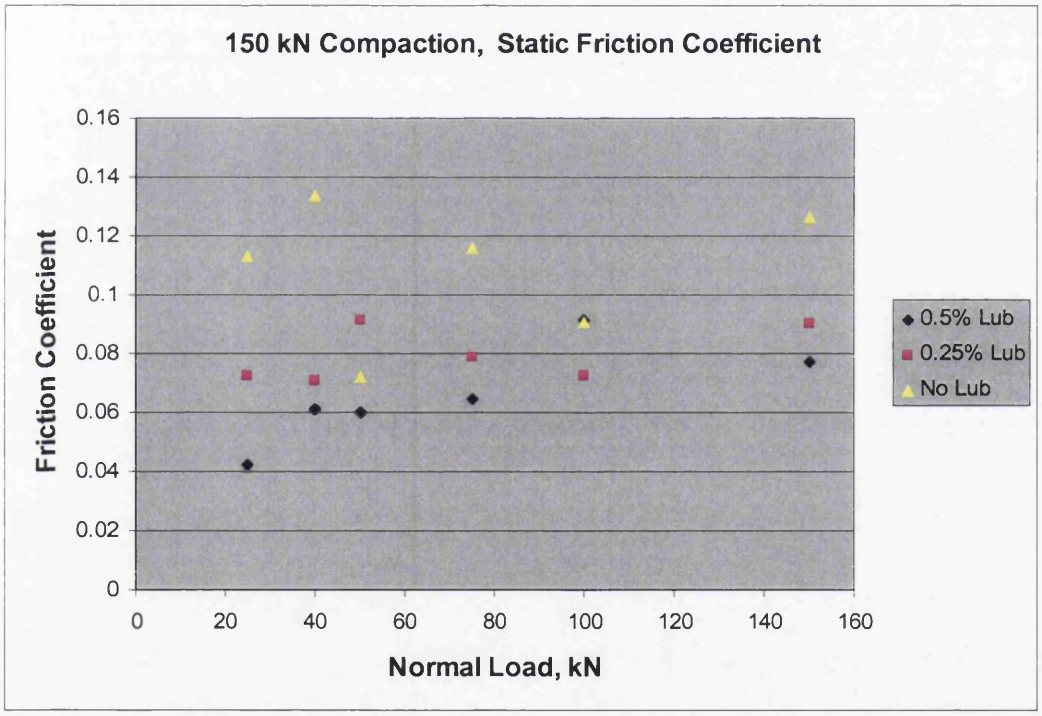

a)

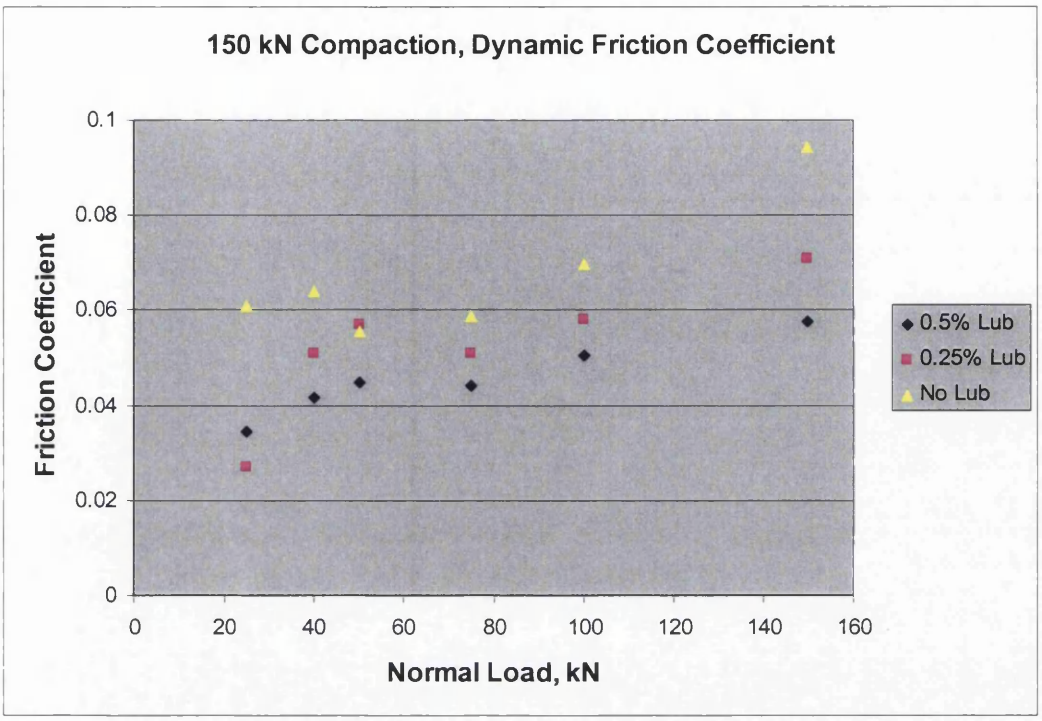

b)

Figure 5.3 Static and Dynamic Friction Coefficients for 150kN Compaction Load

Having determined the effect of normal load on friction coefficients the effect of density on friction was considered. By studying data from the experiments with identical normal load the influence of compact density can be studied independently. Thus, the effectiveness of lubricant content can also be assessed in relation to compact densities.

The friction coefficient is seen to reduce as the compaction load grows, Figure 5.4. Note that each pair of graphs represents static and dynamic friction coefficients at a set normal load. Thus, any trend in the way friction evolves depends purely on compaction load and hence density.

As seen previously, the addition of admixed lubricant greatly reduces friction with even small quantities proving effective. At higher compaction loads the addition of lubricant beyond 0.5% becomes unnecessary as no noticeable improvement was achieved. As before, static friction coefficients were higher than dynamic friction coefficients – a trend that was consistent with expectations.

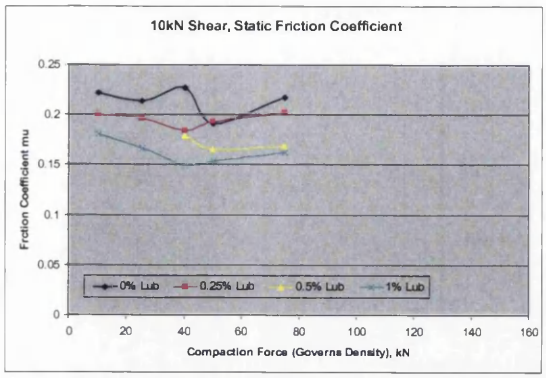
10kN Shear, Static Friction Coefficient
Friction Coefficient mu
0.25
0.2
0.15
0.1
0.05
0
0% Lub
0.25% Lub
0.5% Lub
1% Lub
0
20
40
60
80
100
120
140
160
Compaction Force (Governs Density), kN

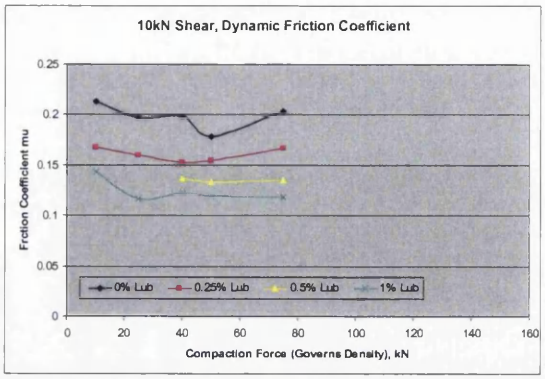
10kN Shear, Dynamic Friction Coefficient
Friction Coefficient mu
0.25
0.2
0.15
0.1
0.05
0
0% Lub
0.25% Lub
0.5% Lub
1% Lub
0
20
40
60
80
100
120
140
160
Compaction Force (Governs Density), kN

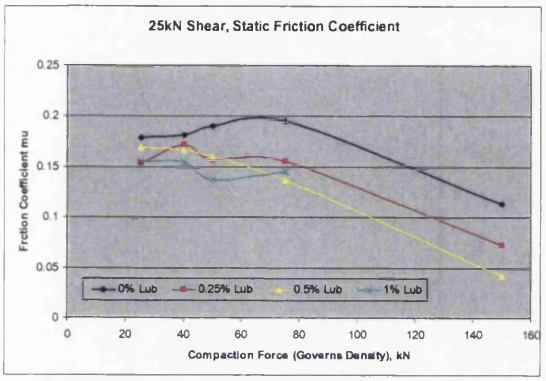
25kN Shear, Static Friction Coefficient
Friction Coefficient mu
0.25
0.2
0.15
0.1
0.05
0
0% Lub
0.25% Lub
0.5% Lub
1% Lub
0
20
40
60
80
100
120
140
160
Compaction Force (Governs Density), kN

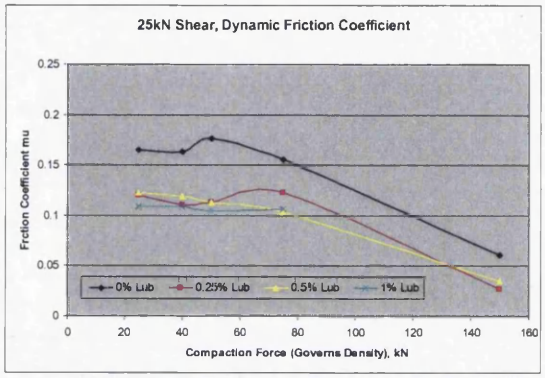
25kN Shear, Dynamic Friction Coefficient
Friction Coefficient mu
0.25
0.2
0.15
0.1
0.05
0
0% Lub
0.25% Lub
0.5% Lub
1% Lub
0
20
40
60
80
100
120
140
160
Compaction Force (Governs Density), kN

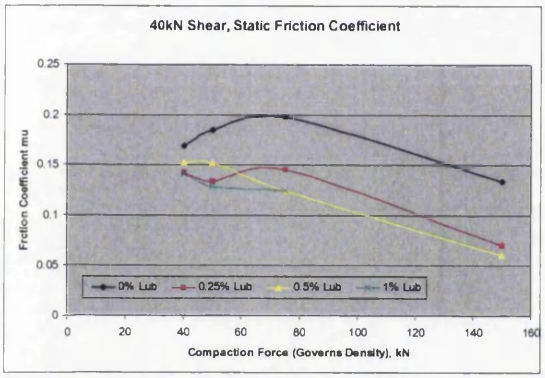
40kN Shear, Static Friction Coefficient
Friction Coefficient mu
0.25
0.2
0.15
0.1
0.05
0
0% Lub
0.25% Lub
0.5% Lub
1% Lub
0
20
40
60
80
100
120
140
160
Compaction Force (Governs Density), kN

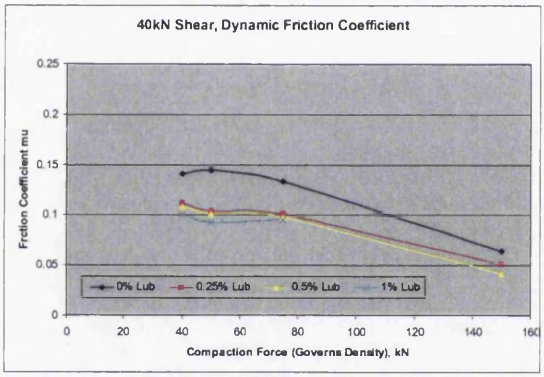
40kN Shear, Dynamic Friction Coefficient
Friction Coefficient mu
0.25
0.2
0.15
0.1
0.05
0
0% Lub
0.25% Lub
0.5% Lub
1% Lub
0
20
40
60
80
100
120
140
160
Compaction Force (Governs Density), kN

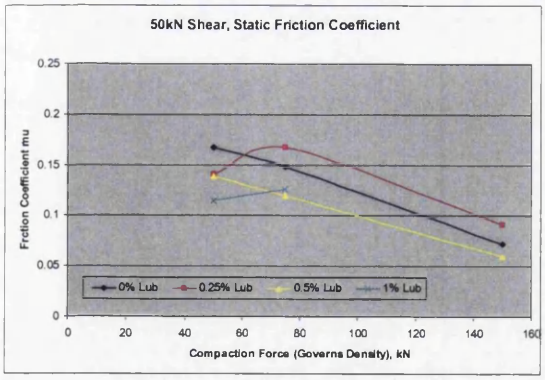
50kN Shear, Static Friction Coefficient
Friction Coefficient mu
0.25
0.2
0.15
0.1
0.05
0
0% Lub
0.25% Lub
0.5% Lub
1% Lub
0
20
40
60
80
100
120
140
160
Compaction Force (Governs Density), kN

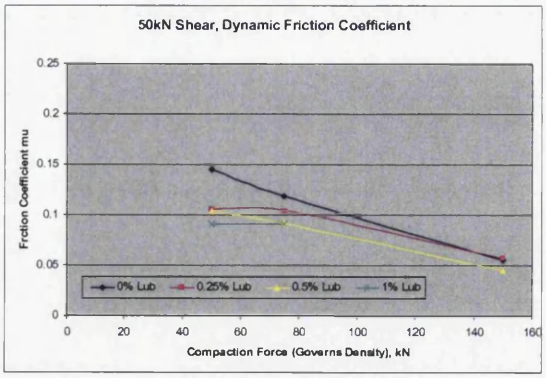
50kN Shear, Dynamic Friction Coefficient
Friction Coefficient mu
0.25
0.2
0.15
0.1
0.05
0
0% Lub
0.25% Lub
0.5% Lub
1% Lub
0
20
40
60
80
100
120
140
160
Compaction Force (Governs Density), kN

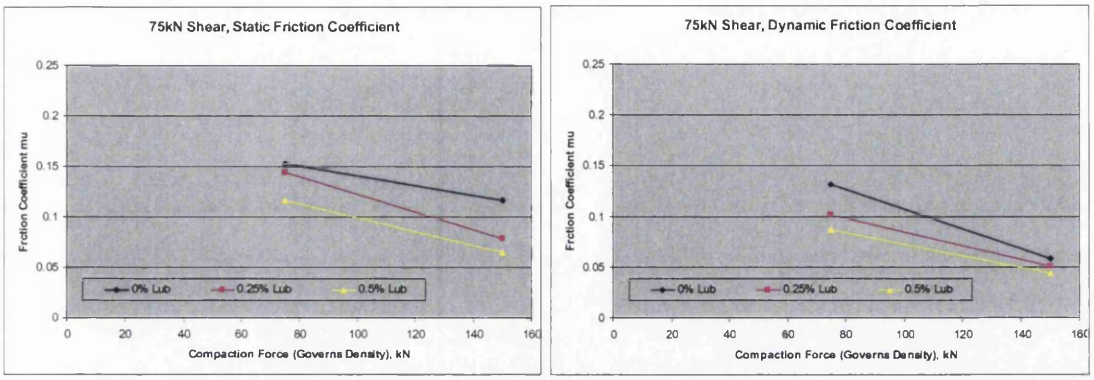

Figure 5.4 Static and dynamic friction coefficients for compacts tested at set normal loads.

Next, in order to further assess the overall significance of compact density, the friction values were averaged for a given compaction load, see Figure 5.5. Each data point represents an average value of respectively the static or dynamic friction for compacts for all four powder mixes with identical compaction load. The series denote varying normal load conditions during the test. There is a trend of reduction in both the static and the dynamic friction coefficients with an increase in compaction load and hence compact density. The figures also confirm the reduction in friction with increase in normal load. This is most evident at lower compaction loads. At higher compaction loads there appears to be a crossover point, when the effect of normal load appears to be reversed – leading to higher friction coefficient at greater pressures.

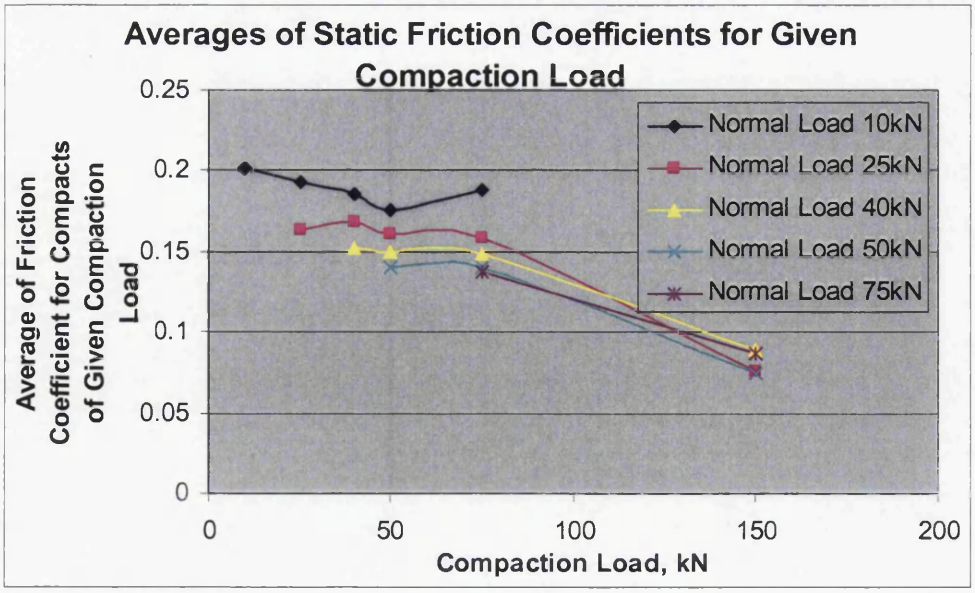

a)

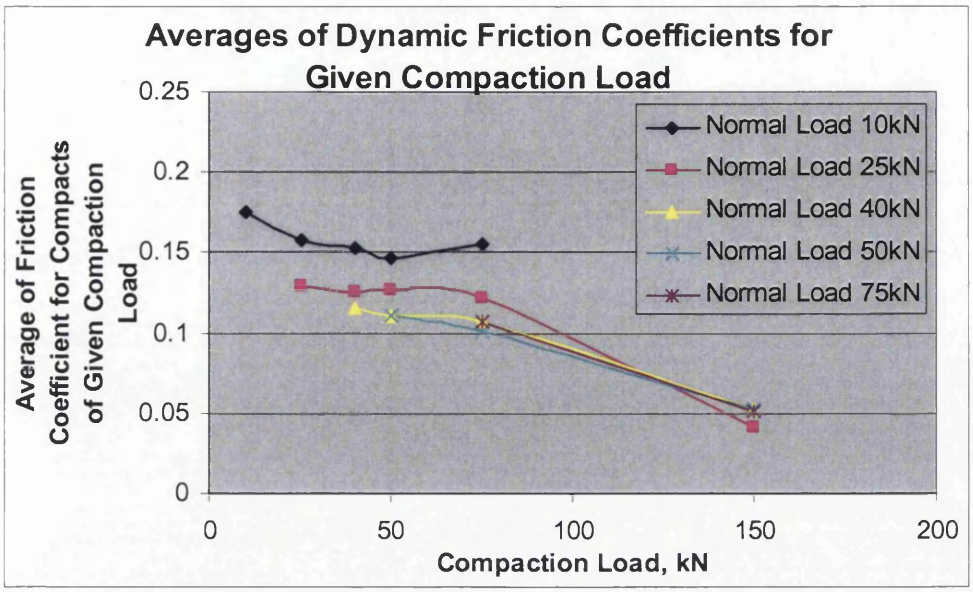

b)

Figure 5.5 Averages of Static and Dynamic Friction Coefficients for Given Compaction Load

To summarise – the friction coefficient was found to decrease with increasing normal stress and to decrease with increasing compaction load, and hence the density. The exception to this can be seen at the highest compaction pressures, where the normal load appears to lead to a slightly higher level of friction.

From Figure 5.2 to Figure 5.4, the addition of lubricant was shown to reduce friction significantly, often with just a small addition being sufficient. The difference between friction levels for differently lubricated powders was highest at lower normal loads. At high normal loads there was a big difference between lubricated and non-lubricated powders, but the distinction between the more lubricated powders was diminishing. At higher pressures, 0.5% of admixed lubricant appeared to provide nearly as much reduction in friction as the mix with 1% lubricant. This is in agreement with other authors (Mallender, Dangerfield et al. 1974), who found that the addition of 2% of Zinc Stearate resulted in only a minor reduction of friction over a 1% mix. Having established this in the earlier stages of the programme the powder with 1% lubricant was excluded from further high pressure tests as that amount of lubricant was considered redundant. The overall effectiveness of lubrication is shown in Figure 5.6, where the data from all

of the tests with compaction loads below 75kN (291 MPA) was averaged for each powder mix.

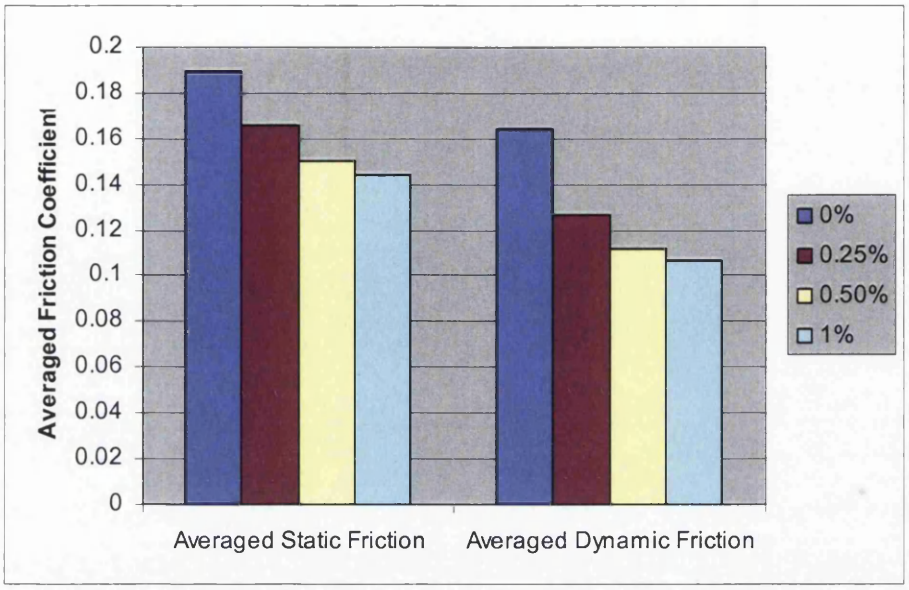

Figure 5.6 Averaged friction coefficient, low pressure floating die tests

The averages of the friction coefficients for the full range of common loads are presented in Figure 5.7 (here the powder with 1% lubricant was excluded as no high pressure tests were performed with this powder). As seen previously, lubrication reduces friction, with higher quantities providing better results, however the rate of improvement reduced as more lubricant was added.

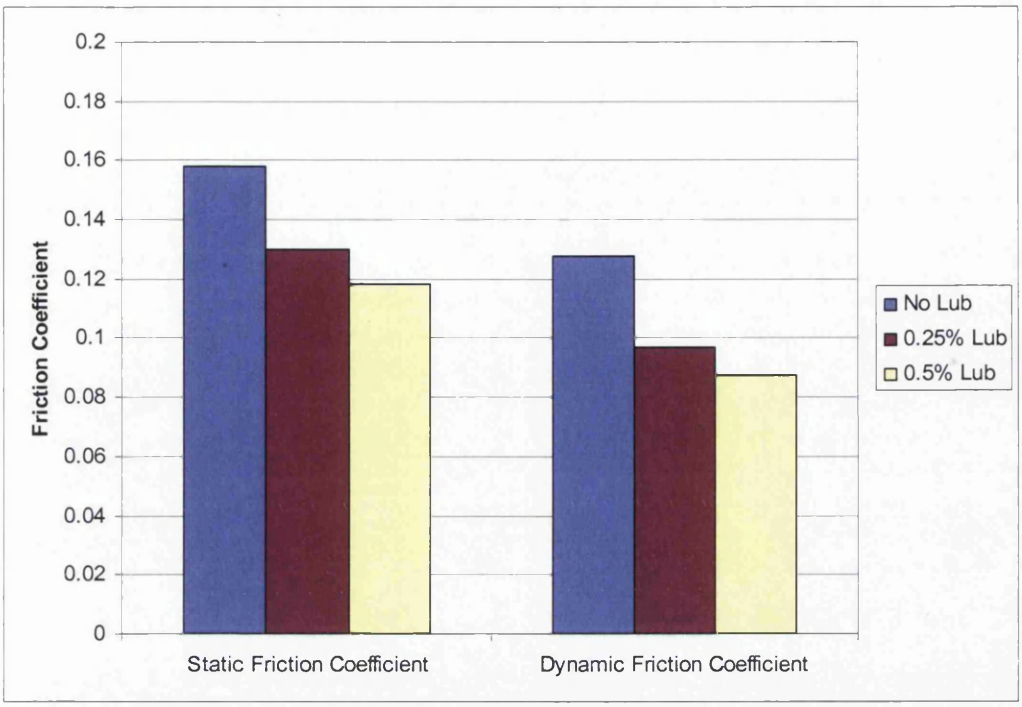

Figure 5.7 Averaged friction coefficient, floating die tests

As seen from the literature (Cameron 2000) the friction tests are sometimes performed with the compaction and normal load claimed as being nominally identical (for shear plates without a floating die system some of the normal pressure is lost through friction between the die wall and powder). Such an interpretation of the results is presented in Figure 5.8 and Figure 5.9.

At lower pressures there is little to choose between the two lubricated powders, both provide a small improvement over non-lubricated Distaloy AE. However, this improvement becomes very significant when high pressures are applied. The differences between the two lubricated powders are smaller at high pressures than between non-lubricating powder and slightly lubricated (0.25% powder). This supports the previous findings, which indicated that the effectiveness of admixed lubricant suffered from diminishing returns once a certain level of lubricant was reached. Additionally, at pressures beyond 400-600MPa the friction coefficient started to rise for powder with no lubricant.

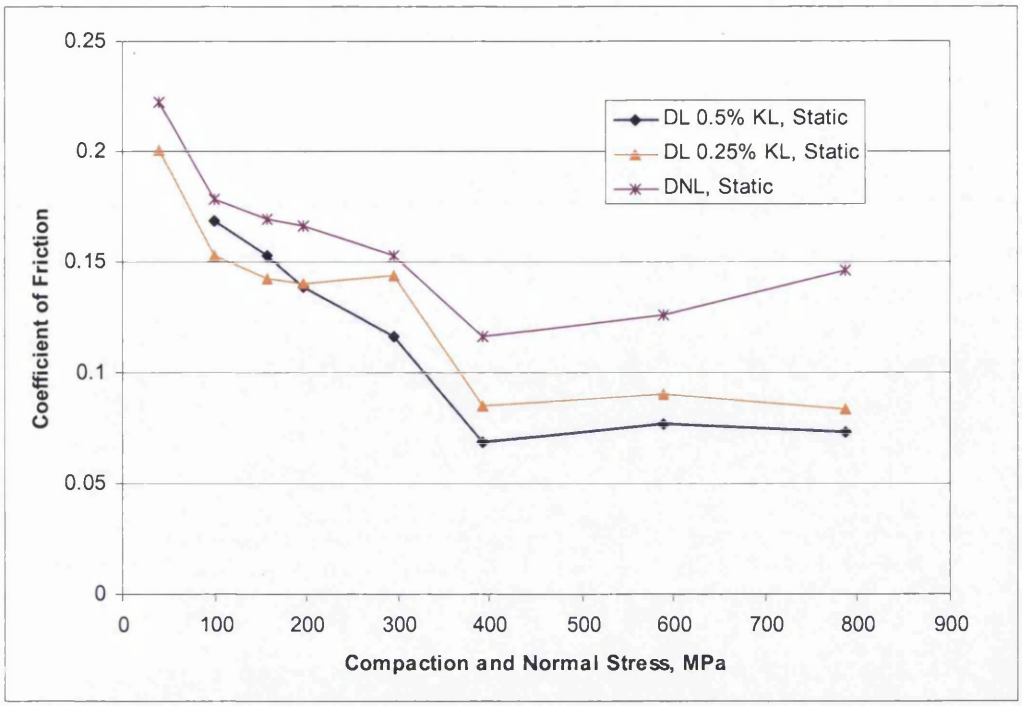

Figure 5.8 Evolution of static friction with pressure, floating die, Distaloy AE, Zirconia target surface

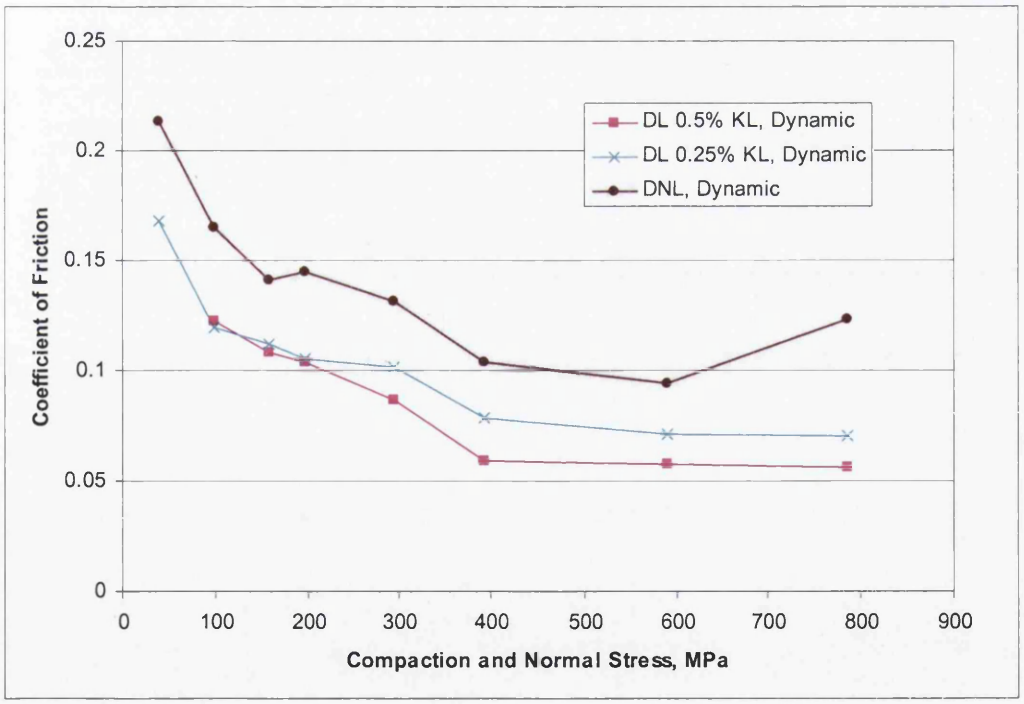

Figure 5.9 Evolution of dynamic friction coefficient with pressure, floating die, Distaloy AE, Zirconia target surface

It is important to note that not only was the friction typically higher for non-lubricated compacts, but at very high pressures galling (the adherence of powder

to the target surface) had occurred, see Figure 5.10. The adhered particles are in an arc indicated by the arrow. Galling is a very undesirable effect as it increases tool wear and the forces involved in the compaction process and negatively affects the finish of the final product. At its extreme, galling can lead to seizure of the tooling. This leads to delays in production while the tooling is refurbished.

Whenever galling had occurred during the experimental program the adhered particles were removed from the target surface with a gentle polishing agent (jeweller's rouge). The target surface was then examined to ensure that its condition was satisfactory for further experiments.

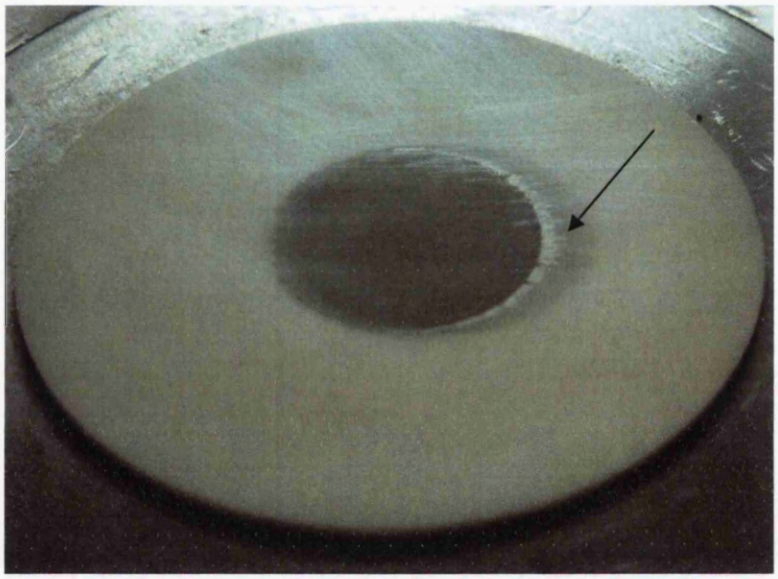

Figure 5.10 Galling, high pressure floating die, non-lubricated Distaloy, Zirconia target surface

5.3.2 Surface analysis of powder compacts tested

In this section the compacts pressed at 150kN will be analysed closer in order to expand the understanding of the effect of the high compaction pressure on compact surface and subsequently on friction.

In Chapter 4, EDX analysis was used in an attempt to determine the amount of lubricant on the compact surface. The surface was found to be a plateau of particles with pits, some of which appeared to contain a lot of carbon, this carbon content originating partly from the admixed carbon powder and partly from the admixed lubricant. The proportion of the surface area of the pits to that of the

raised particles may be an important factor, as these provide a measure of the area that is in direct contact with the target surface.

In order to further examine the sliding surfaces of the compacts from the floating die tests the ends were scanned with a white light interferometer (Wyant 2002). This device is capable of producing a contour map of a section of the compact surface, making possible identification of the pits on the surface. Nine samples were considered. They were all compacted to the same load (150kN). There were three samples studied for each of the powder mixes (non-lubricated, 0.25% and 0.5% lubricant), each of these three were tested under a different normal load. Thus, a comparison can be made of the evolution of the surface due to sliding for the same normal loads and differently lubricated powders as well as the evolution of the surface of the compact of the same powder mix under different normal load conditions. Additionally, scans of the tops of the compacts, where no sliding took place, were taken as a reference of zero sliding. Note that the top surfaces of the compacts were in contact with the top punch rather than with the target surface. These two surfaces have different roughness. Additionally, due to the nature of single ended compaction kinematics the density at the top surface of the compact can be expected to be higher than that at the bottom surface. The latter explains the slightly lower surface porosity observed in scans of the compact's top surface for powders with 0.25% and 0% lubricant, see Figure 5.11. The images of the sliding (bottom) surfaces are presented in Figure 5.12, where the light areas represent the surface of the compact and the dark areas are the pores on the surface. Three dimensional representations of Figure 5.12 can be seen in Figure 5.13-Figure 5.15.

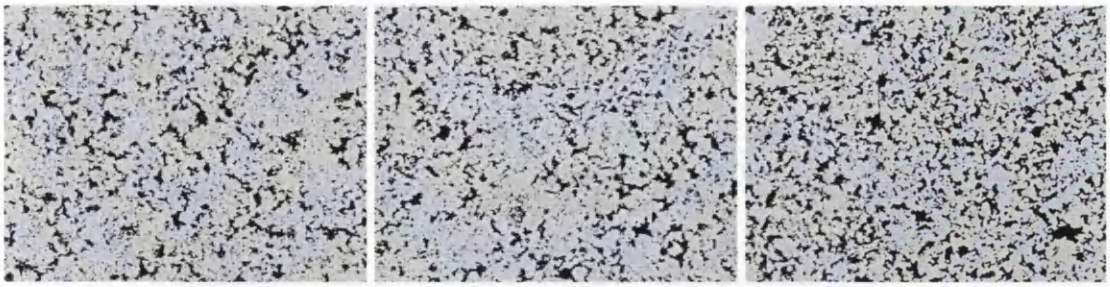

a) 0.5% Lub, p=14.3% b) 0.25% Lub p=14.1% c) No Lub, p=21.1%

Figure 5.11 White light interferometer images of the top surfaces of the compacts pressed at 150kN. Lubricant content and the percentage of the pores (p) on the compact surface are given for each image

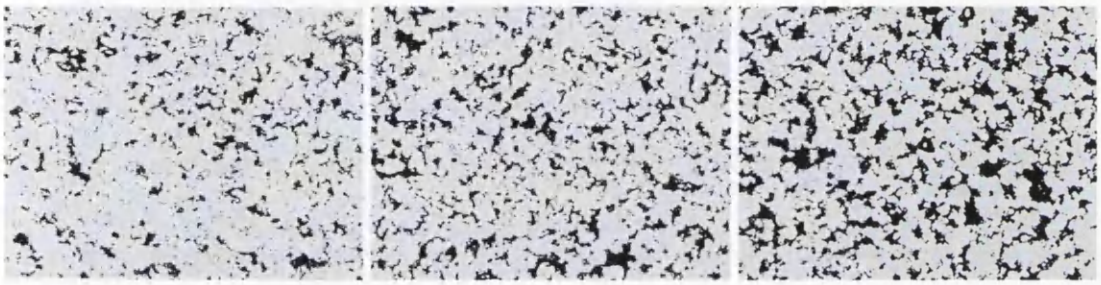

a) 25kN, 0.5% lub, p =10% b) 25kN, 0.25% lub, p=15.3% c) 25kN, no lub, p= 22%

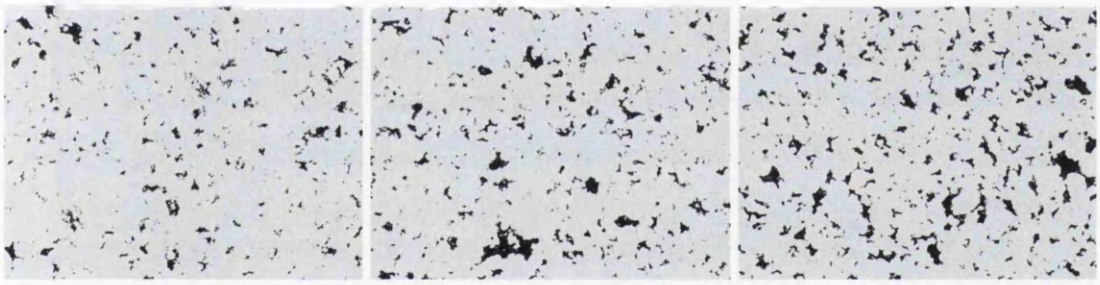

d) 75kN, 0.5% lub, p=4.1% e) 75kN, 0.25% lub, p=6.8% f) 75kN, no lub, p=9.4%

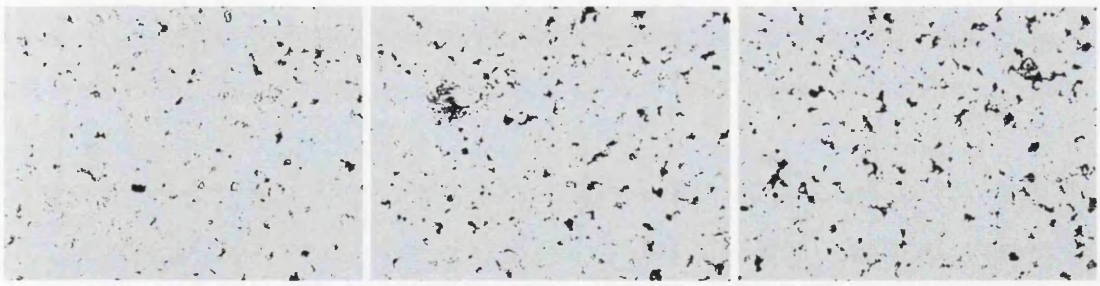

g) 150kN, 0.5% lub, p=1.9% h) 150kN, 0.25% lub, p=4% i) 150kN, no lub, p=5.3%

Figure 5.12 White light interferometer images of the compacts' sliding surface, 150kN compaction load. Normal load, lubricant content and the percentage of the pores (p) on the compact surface are given for each image

The limitation of the interferometry measurement is the inability to obtain a complete profile deep within the pores. This is in part due to the interferometer's

inability to scan steep vertical walls and partly because the surface of the pores is not sufficiently reflective. However, because the surface of the compact was generally very smooth, level and highly reflective, sufficient information about the proportion of the total area occupied by the open pores could be gathered. The percentage of this area is given for each of the interferometer images in Figure 5.12.

Consistent trends of pore coverage can be seen both visually and from the percentage data provided by the software image analysis. The surface porosity was lower when more lubricant was added to the powder (right to left in Figure 5.12). This was true for all three normal load conditions and reflects the higher densities, and therefore lower porosities, typically obtained for more lubricated powders and agrees well with expectations based on experience. The porosity also decreased as the normal load applied during the sliding stage of the experiment was increased (top to bottom in Figure 5.12). This was also consistent for each of the three powder mixes. The latter reflects pore closure as a consequence of sliding against the target surface. The high porosity on the reference images taken at the top of the compacts further confirms this.

The white light interferometry technique also allows for a three-dimensional representation of the scanned surface to be created. Such three-dimensional maps of compact ends are shown in Figure 5.13-Figure 5.15 for the three different powder mixes. As the normal load increased the porosity decreased and the plateau areas became larger as pores closed – this was common for all of the powder mixes with and without admixed lubricant. The dimensions of the remaining pores also reduced. Thus, a greater area of the compact was in contact with the target surface.

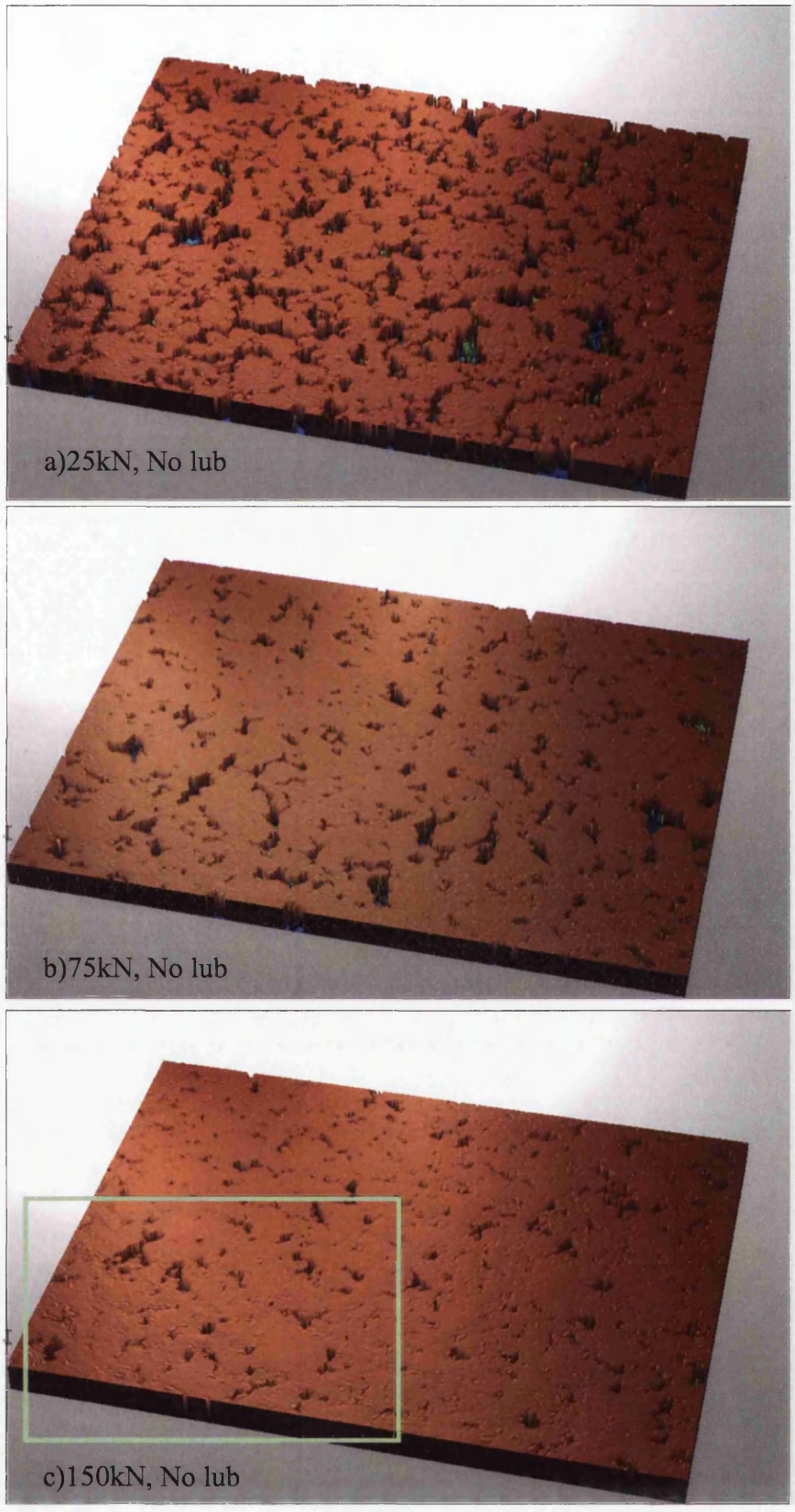

Figure 5.13 Three dimensional representation of the bottom surface of the compacts pressed at 150kN for powder without lubricant; normal load and lubricant content are given for each image.

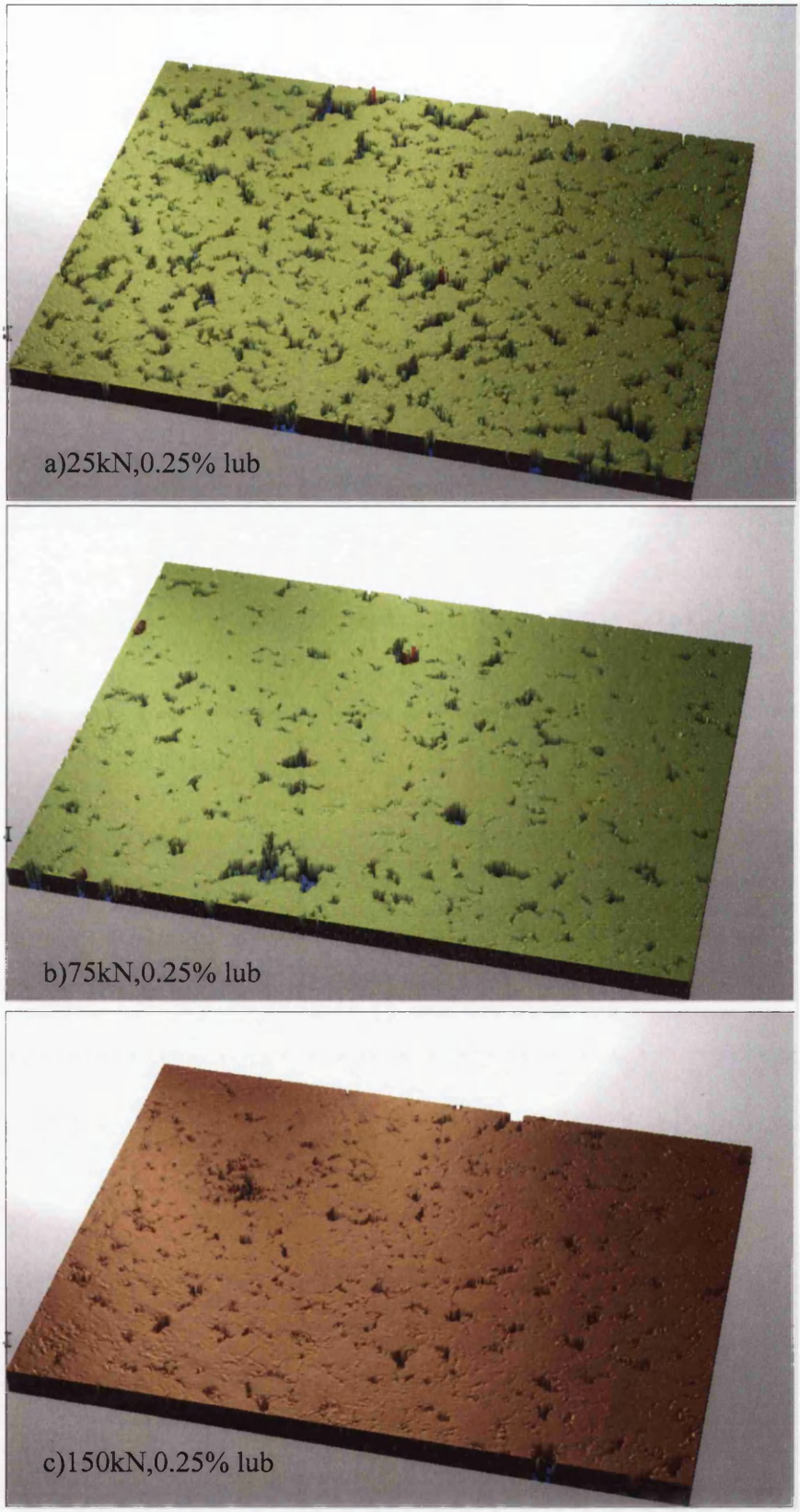

Figure 5.14 Three dimensional representation of the bottom surface of the compacts pressed at 150kN for powder with 0.25% lubricant; normal load and lubricant content are given for each image.

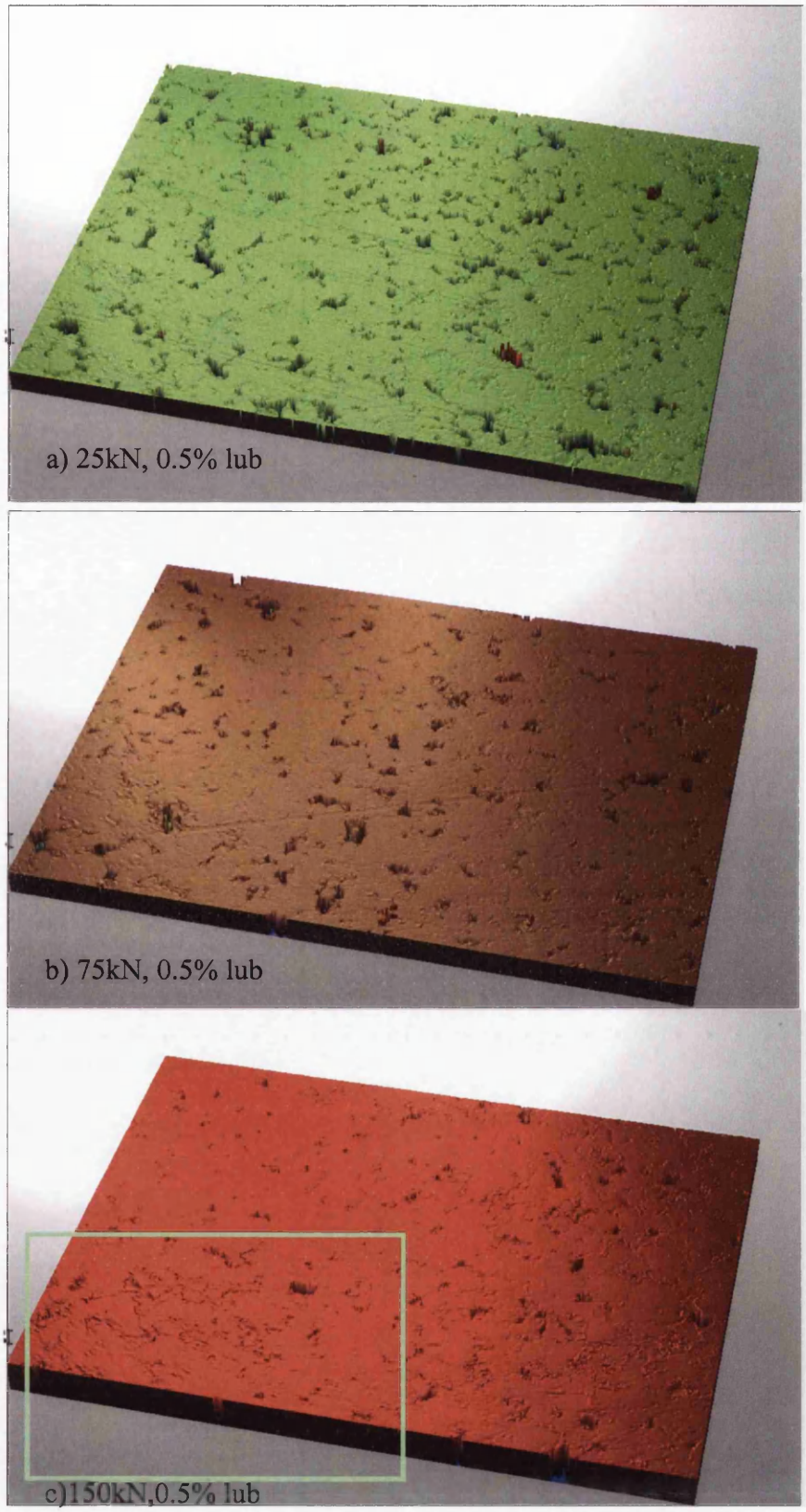

Figure 5.15 Three dimensional representation of the bottom surface of the compacts pressed at 150kN for powder with 0.5% lubricant; normal load and lubricant content are given for each image.

Closer inspection of the surface of the compact in Figure 5.13 c), a magnified view of which is shown in Figure 5.16, reveals features that can be identified as the lines of contact between the powder particles, as they are deformed by first the compaction pressure and then the sliding. The open pores, which are also present on the surface, are connected by these lines, indicating that these are indeed the closed "valleys" or gaps between individual plateaus of particles.

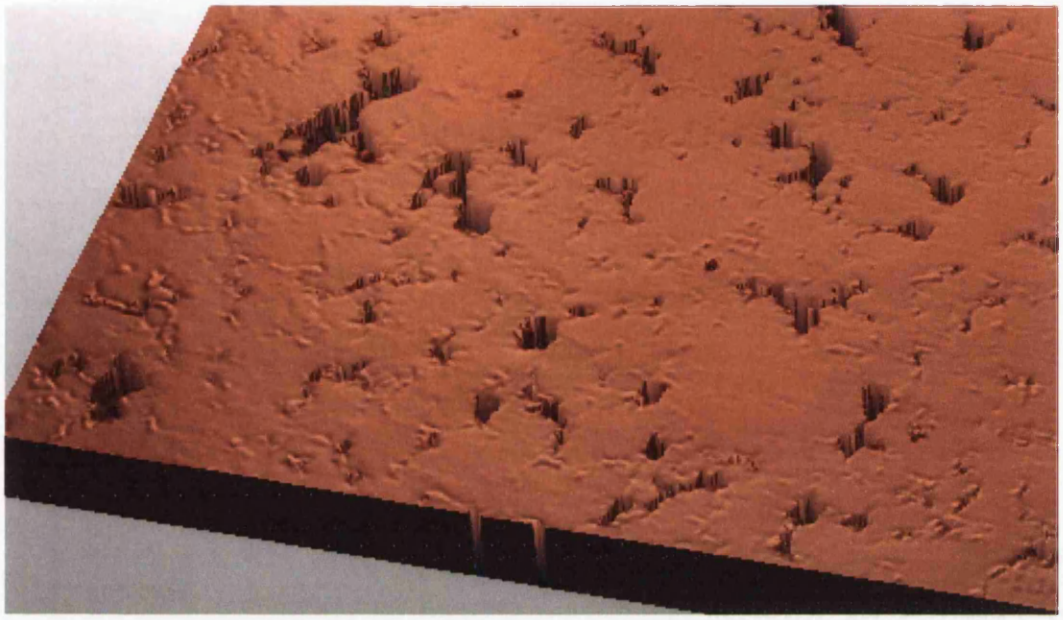

Figure 5.16 An enlargement of the section of the compact in Figure 5.13 c). 150 kN Normal load, No Lubricant

Close examination of Figure 5.15 (c) reveals some of the same features: inter-particle contact borders and pits. These can be seen in detail in the magnified view presented in Figure 5.17. However there are features which look like pits filled with a substance. As reported previously in Chapter 4 some of the pores were found to be filled with a carbon rich substance, likely a mixture of carbon additive and admixed lubricant (in cases where the lubricant was added). It is possible that some of the shallow pores seen here are in fact deeper pores which contain lubricant. During the surface porosity analysis, as seen in Figure 5.12, only the empty pores were identified as pores and the filled pores were counted as the solid surface. For non-lubricated powder the total amount of pores was counted, but this was not the case for lubricated powders.

Figure 5.17 An enlargement of the section of the compact in Figure 5.15 c). 150 kN Normal load, 0.5% Lubricant

The trends in the friction coefficient data for the above tests will now be considered in reference to the observations regarding the target surface, see Table 5.3. As expected, friction rises as the amount of lubrication is reduced. However, as seen in Figure 5.3, at high compaction loads the friction coefficient was found to increase with the normal load, this trend is opposite to that observed for lower compaction loads. The possible mechanisms involved are now considered.

Table 5.3 Friction Coefficients for compacts in Figure 5.12

Static Friction Coefficient	Lubricant Content		
Normal Load	0.50%	0.25%	No Lub
25 kN	0.042	0.072	0.113
75 kN	0.065	0.079	0.116
150 kN	0.077	0.090	0.126
Dynamic Friction Coefficient	Lubricant Content		
Normal Load	0.50%	0.25%	No Lub
25 kN	0.035	0.027	0.061
75 kN	0.044	0.051	0.059
150 kN	0.058	0.071	0.094

At high compaction pressure the porosity of the compact surface reduces, see Figure 5.18. As mentioned above, particle deformation during the sliding stage

also leads to a reduction in surface porosity. Thus, the contact area on the compact surface becomes greater. The "filled pore" features, shown in Figure 5.17, suggest that at high pressures the lubricant present between the compact and die is pushed into the pores, thus becoming less effective. It is also possible that when the high normal loads (e.g. 150kN) are applied they are sufficient to cause fusing of the powder particles to the die as indicated in Figure 5.10, thus increasing the resistance to sliding. A combination of these effects may lead to the friction coefficients rising at higher normal pressures for compacts pressed at high compaction loads.

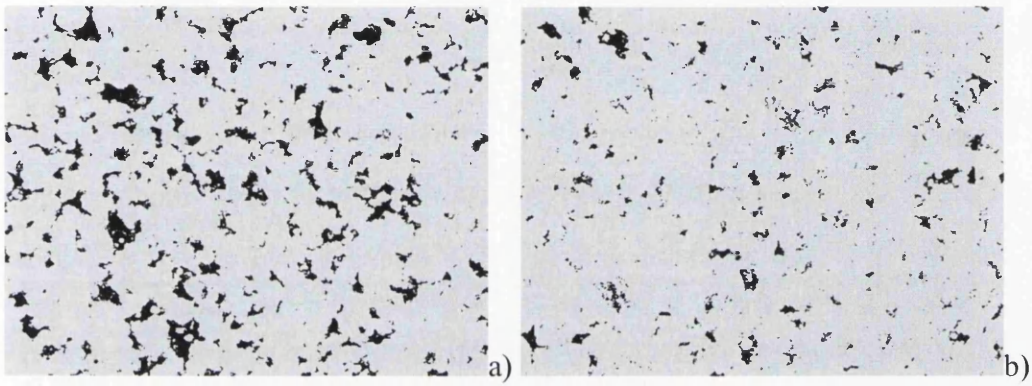

Figure 5.18 White light interferometer images of the compacts' sliding surface: a) 75kN compaction load, 75kN normal load, 0.5% lubricant, 10.3% surface porosity b) 150kN compaction load, 75kN normal load, 0.5% lubricant, 4.1% surface porosity

5.3.3 Die wall lubrication

Die wall lubrication is an alternative way to reduce friction during the compaction process. The main advantage of die wall lubrication is the application of the lubricant directly to the areas where it is most needed, allowing for a smaller quantity of the lubricant to be used. Additionally, as the lubricant is on the surface of the compact it is easier to remove during sintering. Overall, a large reduction in friction can be anticipated with a reduced amount of lubricant without the density limitations caused by admixing the lubricant. However, the advantage measured quantitatively remains unknown and the present section seeks to quantify this advantage.

The drawbacks of the technique mainly comprise the technical challenges encountered when trying to apply a consistent lubricant coating to dies of complex geometries. Additional and often complex equipment is also required to apply the lubricant, making the initial expenses higher.

The new floating die equipment being proposed in this chapter was tested to establish if it could also be used to measure friction between the powder and the lubricated die wall and hence establish its effectiveness quantitatively.

There are a number of methods of applying die wall lubrication, these range from application by brushing of lubricants dissolved in solvents (Li, Ngai et al. 2002) to a spray deposition of electro-statically charged lubricant particles (Ball, Hibner et al. 1997), (Yang, Gui et al. 2006).

In this work the admixed lubricant used in the previous sections was dissolved in methanol and a small quantity of blue dye was added to improve the coating's visibility against the white surface of the target. It was then deposited onto the target surface with a handheld atomizer (brushing was also attempted but was found to be inconsistent). The solvent was then allowed to evaporate. The target was then visually inspected and additional lubricant was sprayed on if required. Once an acceptable coverage was achieved the target surface was placed into position underneath the die, with two metal shims protecting the coating from contact with the die and its support plate. Examples of typical lubricant coverage before and after the sliding test can be seen in Figure 5.19 and Figure 5.20.

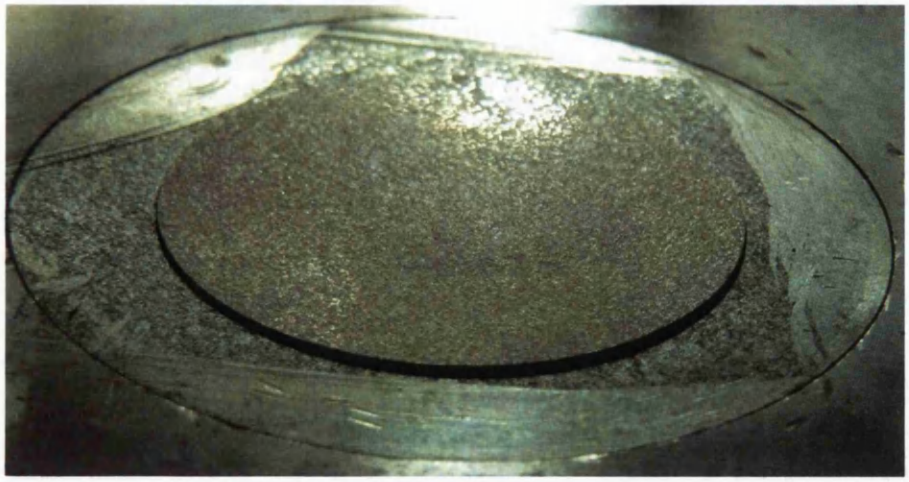

Figure 5.19 Lubricant Coating on the Zirconia Target (Spray Deposition)

Figure 5.20 Lubricant Coating on the Zirconia Target after Friction Test

While the spraying method does not allow for a consistent coating to be deposited every time it should still allow for the general impact of the coating to be investigated.

It is possible to measure the amount of lubricant deposited onto the surface using white light interferometry, however, this was not done for every test due to the amount of time such measurements require. Figure 5.21 shows a white light interferometer scan, taken on the boundary between the lubricant coating and the clean section of the target. The lubricant particles are easily distinguishable against the flat surface of the target. Additionally, data from the white light interferometer can readily be used to calculate the volume occupied by the lubricant on the surface of the target.

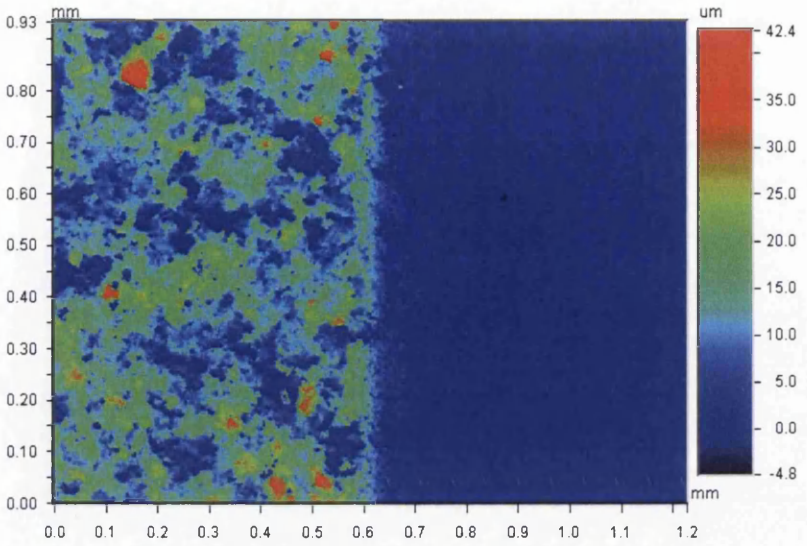

Figure 5.21 A white light interferometer scan of the Zirconia target surface with a die wall lubricant coating.

After the procedure for applying the lubricant coating was developed a set of experiments to investigate the effect of die wall lubrication was performed on the floating die apparatus. Some of the same powders as in the admixed lubricant study were used. Powders with 0%, 0.25%, and 0.5% admixed lubricant were compacted to 25, 40, 50 and 75kN and the friction tests were then performed with the same normal load.

Values of static and dynamic friction coefficients were obtained for die wall lubricated samples in the same manner as described previously. These results were compared with equivalent tests performed previously against a clean target. Static and dynamic friction coefficients are plotted in Figure 5.22 and Figure 5.23 respectively. From these graphs it is clear that the use of die wall lubricant significantly reduces friction. Figure 5.24 summarises these results by averaging the results for each powder mix. Compared with non-lubricated powder, die wall lubrication is approximately twice more effective. Even in comparison between powders with 0.5% lubricant die wall lubrication reduces friction by a further 30%.

The trend of friction reducing at higher loads is still present when die wall lubrication is employed.

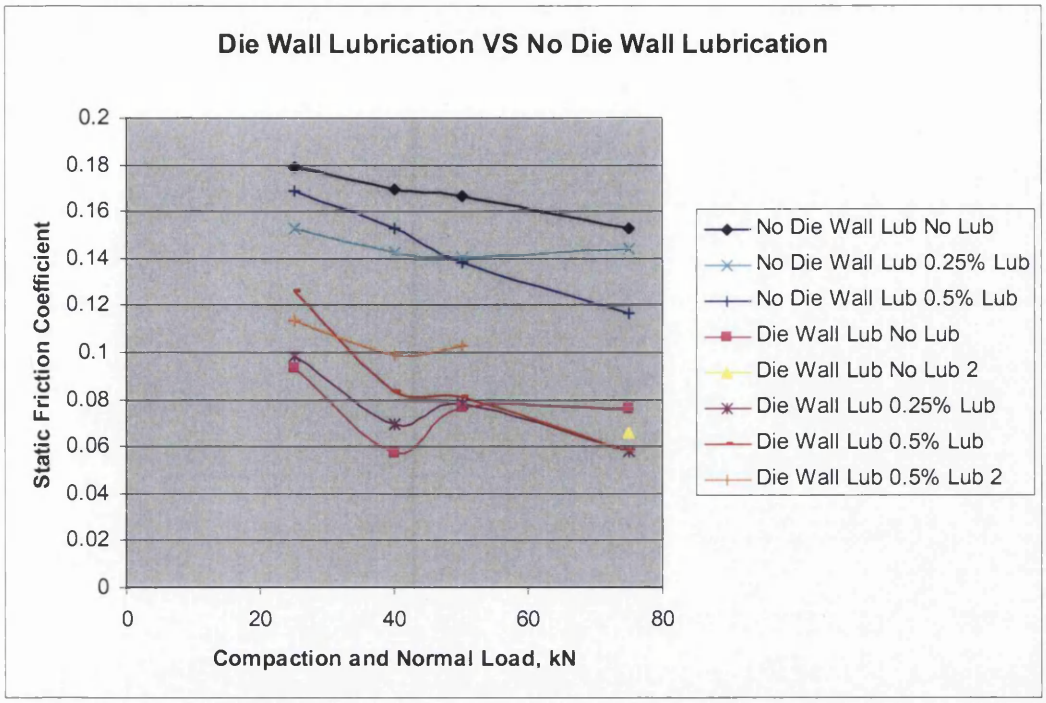

Figure 5.22 Static Friction Coefficients for Tests With and Without Die Wall Lubrication

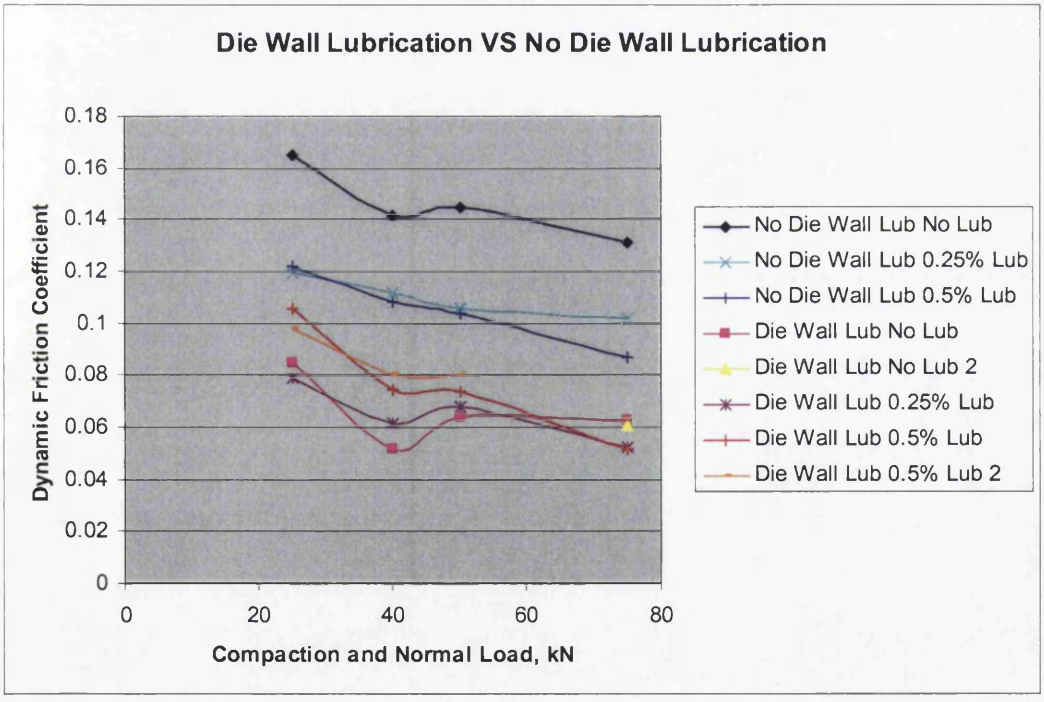

Figure 5.23 Dynamic Friction Coefficients for Tests With and Without Die Wall Lubrication

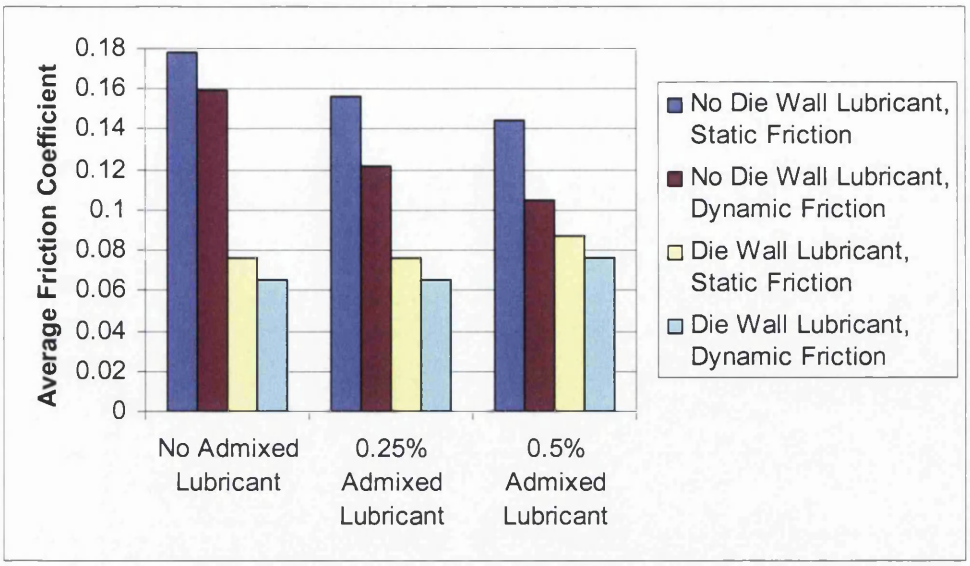

Figure 5.24 Average Friction Coefficients from Die Wall Lubrication Tests

Somewhat unexpectedly, among the tests with die wall lubrication the friction coefficient was highest for the powder with 0.5% admixed lubricant. It is not completely clear whether this is indeed an accurate reflection of physical phenomena, or has been caused by the die wall lubrication procedure used. The coating applied to the target surface may have differed in thickness and coverage throughout the test programme. This could be caused by operator dependency of the application procedure on one hand and the change in concentration of the lubricant solution as it was used up on the other. This can only be explored fully by performing measurements to establish the coverage of each coating as it is applied and remains as a future task. The purpose of the tests was to establish if the floating die apparatus could be used to measure friction with die wall lubrication in principle rather than to perform an in depth study. The equipment was found to be sensitive enough and with a consistent lubricant application system the effect of die wall lubrication can be comprehensively explored.

5.4 Conclusions

The floating die shear plate apparatus, which was introduced in Chapter 4, was used in a series of experiments assessing the effectiveness of different lubricant quantities under a wide range of both compaction and normal loading conditions. Simultaneously, analysis of the effect of compact density and normal stress on friction was performed.

The results confirm a correlation between the rise in normal load and reduction in friction for compaction pressures below 300MPa. This trend was consistently present for all powders tested. For compacts pressed at 583MPa the friction coefficient was found to rise as the normal load increased.

A correlation was also found between the compact density and the friction, which was found to reduce at higher densities.

As regards the lubricant performance it was established that at higher loads there is no noticeable benefit in increasing lubricant content above 0.5%. The addition of 1% lubricant would be more justifiable at lower loads, as there is a significant gain in performance under those conditions. However, it is likely that at lower loads the friction will be of less concern. It was also observed that the addition of even 0.25% lubricant was often sufficient to significantly reduce friction. In cases where high percentage of lubricant is undesirable the addition of lower quantities of lubricant may still provide a significant reduction in friction.

The sliding surfaces of the compacts were examined using a white light interferometer in order to explain the phenomenon of higher friction coefficients for increasing normal loads for compacts pressed at high pressures.

The examination revealed a more open structure for compacts pressed at lower compaction loads. Higher normal loads during shear appeared to result in a more polished appearance of the contact surface with a smaller area occupied by pits. However, some of the pits appeared to be filled with lubricant and were not detected as pits during the scan. A larger contact area and fusing of the particles were suggested as possible explanations for the higher friction values found in high pressure tests.

A brief study on die wall lubrication showed the significant impact that die lubricant plays on friction. A reduction in friction of between 27% and 58% was observed for a range of powders and loading conditions.

A method of measuring the die wall lubricant coating was proposed, based on an analysis of white light interferometer scans. These are capable of providing detailed information about the lubricant coating, such as surface coverage and even volume of lubricant.

Further experiments with a more appropriate lubricant and lubricant deposition technique may give a better indication of friction coefficient values in industrial applications.

Chapter 6 Ejection and unloading - elastic parameters

6.1 Introduction

In Chapter 1 it was demonstrated that the formation of a powder compact can be divided into five identifiable stages; filling, transfer, compaction, unloading and ejection where the part is ejected from the die and these are shown schematically in Figure 6.1. The processes involved at each stage are markedly different and so are the numerical models employed to simulate these stages. These models require a variety of material parameters and the measurement of those for the unloading and ejection stages will be the focus of this chapter.

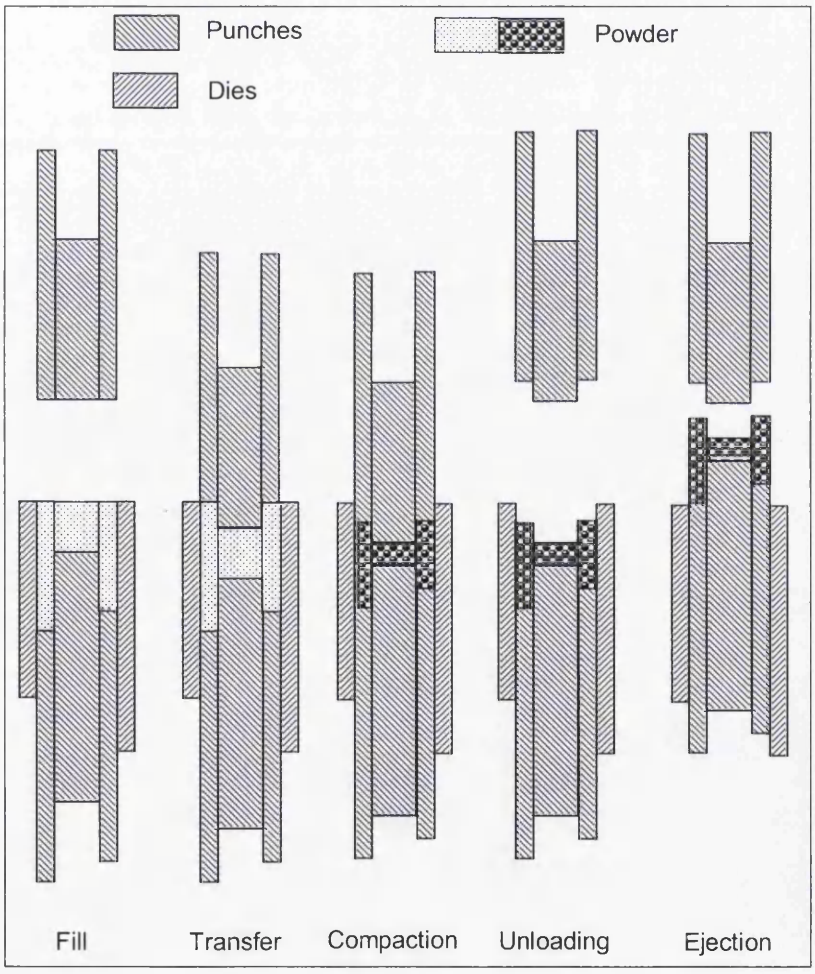

Figure 6.1 Schematic of the powder forming cycle broken into five distinct stages

6.1.1 Unloading

When the punch loads are relaxed at the end of the compaction stage, there will be some recovery associated with elastic mechanisms because of the deformation in the compact and in the press itself. For the case of long punches, the relaxation can be significant, especially when compacts are formed at high pressures (e.g. 800MPa for iron) and a recovery in the press of the order of 1mm is typical. In the case of multilevel parts, different loads on different punches can lead to differential recovery, thereby leading to tensile stresses within the compact and possible tension induced cracks. This is mitigated in complex multilevel parts via appropriate press controls. Further complexity is introduced through the presence of friction between the powder and tool set. As the axial pressure on the compact is reduced, there will also be a reduction in radial pressure. Slippage between the die and powder will occur where the elastic recovery force exceeds the restraining force due to friction. Thus, it is expected that relative movement between the powder and die will occur over only a section of the compact as the punch loads are relaxed. Evidence of this mechanism is presented in some early work described in (Gethin, Lewis et al. 1995), (Gethin, Ariffin et al. 1994).

6.1.2 Ejection

The ejection process involves moving the part out of the die, principally by means of the lower punch set. During this process the confinement offered by the die is removed and the part is free to expand in a radial direction as sections emerge from the die. Where radial strains are large, this can also lead to shear bands being formed in the compact, manifesting in failure by delamination under extreme circumstances. In multilevel parts, ejection is completed by effectively removing the lower punch set progressively, punch by punch and through downward movement of the die set. This effectively relaxes the radial loads and ultimately allows the part to be removed easily without inducing stress levels within the part that may lead to failure.

During ejection, friction is also present between the powder and the surfaces in relative motion, such as the die and sections of punch sides (as opposed to their faces).The frictional properties are likely to be affected to some extent by the preceding compaction history. Also, for the case of long compacts, the friction

force due to the contact between the powder and the die may be sufficient to cause further bottom end compaction as the lower punch forces the compact out of the die (Gethin, Lewis et al. 1995), (Gethin, Ariffin et al. 1994).

6.1.3 Ejection Model Requirements

An ejection model that encompasses the unloading and ejection process needs to reflect the mechanisms that have been identified in the preceding sections. It requires material information in terms of elastic properties (Young's modulus and Poisson's Ratio), information about the frictional behaviour of compacted powders (as opposed to frictional behaviour during compaction), plastic response of the powder when further densification occurs during ejection and information about the cohesive and tensile strength of the powder. In this instance, cohesion represents the 'collection of particle bonding mechanisms, e.g. mechanical interlocking, welding, etc' and the tensile strength represents the maximum stress that a powder compact will sustain before failing. Tests need to be devised to establish each of these properties and these tests need to be relevant to allow incorporation into a numerical scheme to model the process.

6.1.4 Tests for Measuring Elastic Parameters that are Relevant to Unloading and Ejection

A number of tests may be devised, or adapted, to measure the elastic behaviour in a compact. These include the instrumented die test, the unconfined compression test, the bending test, the Brazilian disc test and the use of ultrasonic techniques.

Details of experiments that use the instrumented die to measure Young's modulus and Poisson's ratio using an unloading test procedure are set out in (Guyoncourt 2005). An assumption is required concerning the axial strain, namely that recovery is assumed to take place over the full compact height. The extent to which this occurs is not known at this time, but liberal pre-lubrication of the die wall may assist in realising this. Another data reduction procedure is outlined in (Cunningham, Sinka et al. 2004), with the authors making assumptions regarding die rigidity, negligible friction and porosity variation, and the elastic nature of material. If this test can be implemented successfully, it provides a further

application of the instrumented die to characterise powder elastic properties as well.

An unconstrained compression test may be used to characterise the Young's modulus of a compact. This test eliminates the constraining influence of die friction, but it does require a free standing compact and therefore it can not be undertaken at low compaction densities. This test will be adapted and explored as a method of measuring the Young's modulus of the compact. This will supplement its application for measuring yielding by a shearing mechanism.

The Young's modulus may also be derived from a three point bending test and this can similarly be extended to establish the tensile strength of the compact. Three point bending tests are already employed to measure the green strength of powder compacts (ISO3995 1985).

The Brazilian disc test involves the diametrical compression of a cylindrical compact between two flat rigid plates (Procopio, Zavaliangos et al. 2003). This test effectively induces a tensile failure within the compact. The test has been used principally for brittle powder systems and so its application to more ductile systems needs further investigation.

Another possible technique is the application of ultrasonic measurements to establish elastic modulii (ISO3312 1987). There are published examples of this method and the measurement relies on the ability of the porous compact to transmit ultrasonic signals without undue attenuation (Hentschel and Page 2001). The contact between the transmitter and the receiver is an inherent problem. This technique was not pursued further in this work.

6.2 Young's Modulus

The instrumented die unloading test, the compression test of an unconfined compact and the three point bending test were investigated as techniques to measure the Young's modulus. The techniques and sample results will be compared in the following sections.

6.2.1 Instrumented Die Test

The same instrumented die as described in Chapter 4 was used for these tests. It was designed to have an internal diameter of 18mm, a wall thickness of 7mm, the bottom punch length was 108mm and the top punch length was 100mm. In conducting the test, displacement may be obtained from the transducer system on the press, or through a transducer on the test head. The latter eliminates any press deflection due to loading, but only includes the effect of punch deflection that may be accounted for analytically or through calibration. The test was conducted using Distaloy AE having a 1% Kenolube addition. Dependent on the test, the die was filled with either 10 or 15ml of powder and then compressed through stages to a high density. At the end of each stage, an unloading sequence was applied and the compact recovery measured at each stage. This facilitates the measurement of the modulus through consideration of the stresses and strains during the recovery process. A number of test runs were performed to establish repeatability and, furthermore, tests were carried using different powder samples for each density level, thus eliminating any influence of loading history from the powder. Tests were also performed for powders having different lubricant content.

Figure 6.2 shows the results from a single compact loaded successively so that the powder experiences a loading history. The relaxation was measured across the die set and so includes the elastic recovery of the punch itself. This may be compensated for analytically, but this has not been included at this stage. The figure illustrates three sets of results that confirm the repeatability of this test. In examining the details of any relaxation curve it maintains a linear form down to low force levels, at which point the compact appears to recover at a higher rate. As a first approximation, the axial stress and strain data only has been used to estimate the material Young's modulus and the consequent trend is shown in Figure 6.3 as a function of compact average density.

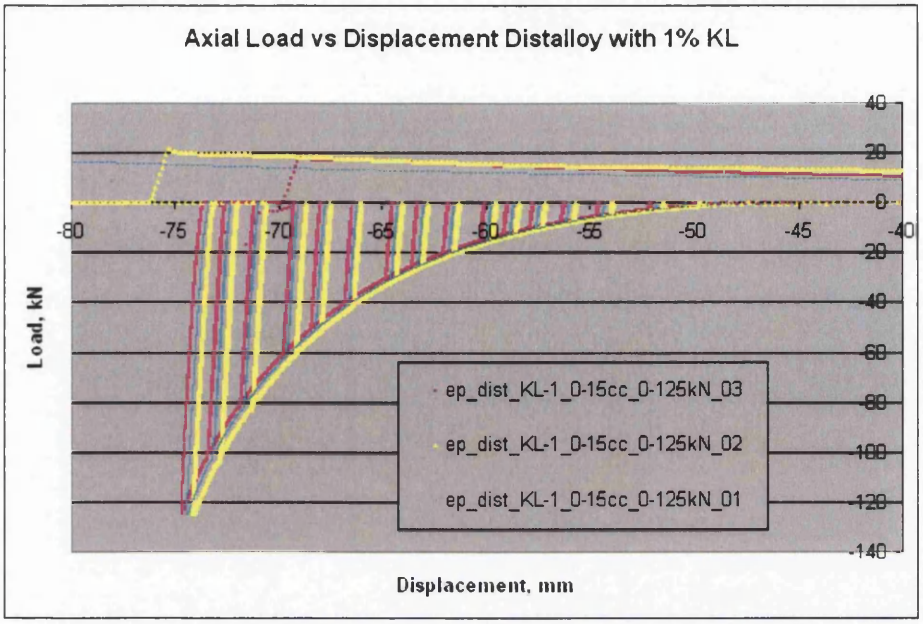

Figure 6.2 Instrumented Die Load Unload Test on a Single Sample (repetition to confirm consistency)

The trends in Figure 6.3 have been computed based on displacement measurements from the press (designated Dartec) and across the die set (designated LVDT). The 'Dartec' values are smaller since the figure includes the press deflection and consequently the strains appear to be large. The LVDT figures are clearly higher since the strains now appear to be smaller, but this will be discussed further in connection with the tests on the free standing compacts. It is not clear why the modulii decrease at higher densities. While a lower rate of increase is expected for densities approaching that of the solid material this reduction was unexpected.

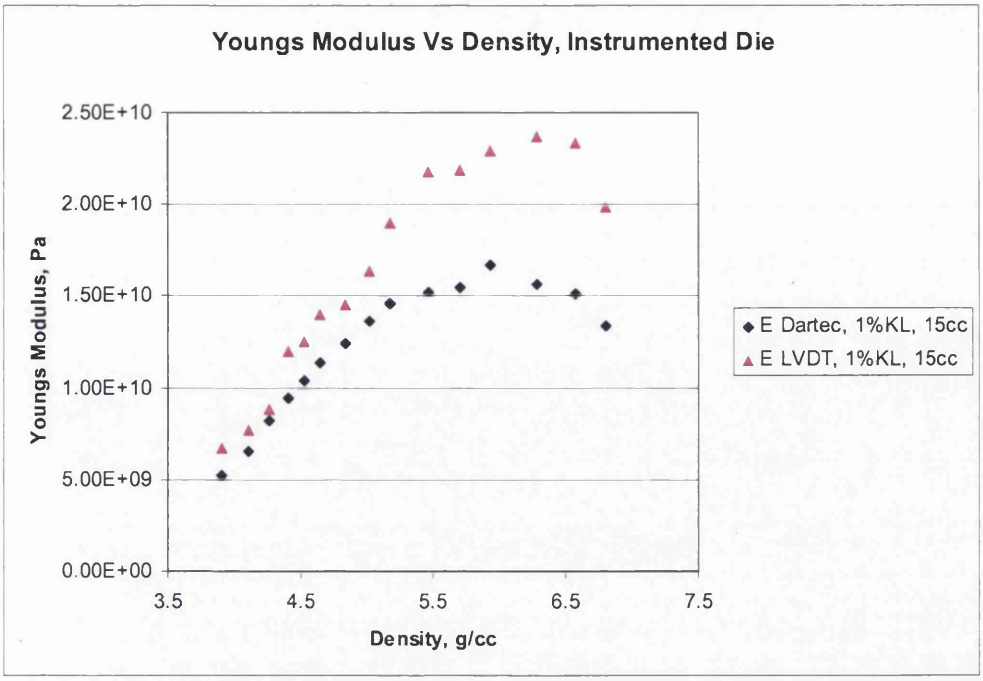

Figure 6.3 Young's Modulus from an Instrumented Die Test

Figure 6.4 shows the data set when fresh powder was used to perform the tests at different loading levels. This effectively eliminates the effect of loading history on the powder. The results are closely similar to those presented in Figure 6.2 and are overlaid in Figure 6.5.

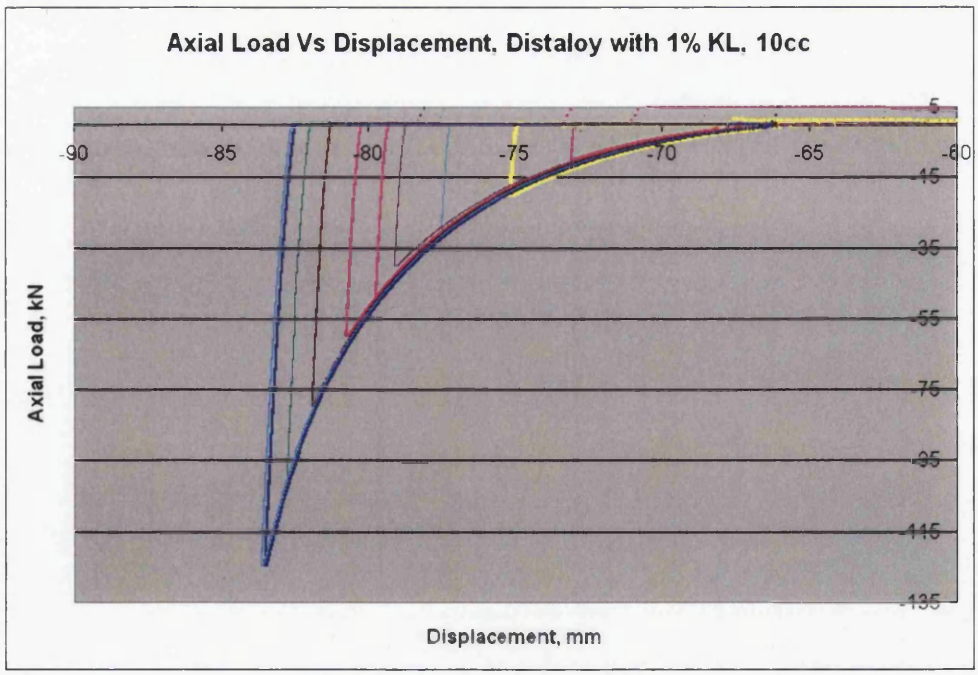

Figure 6.4 Instrumented Die Load Unload Test Using Fresh Powder Samples

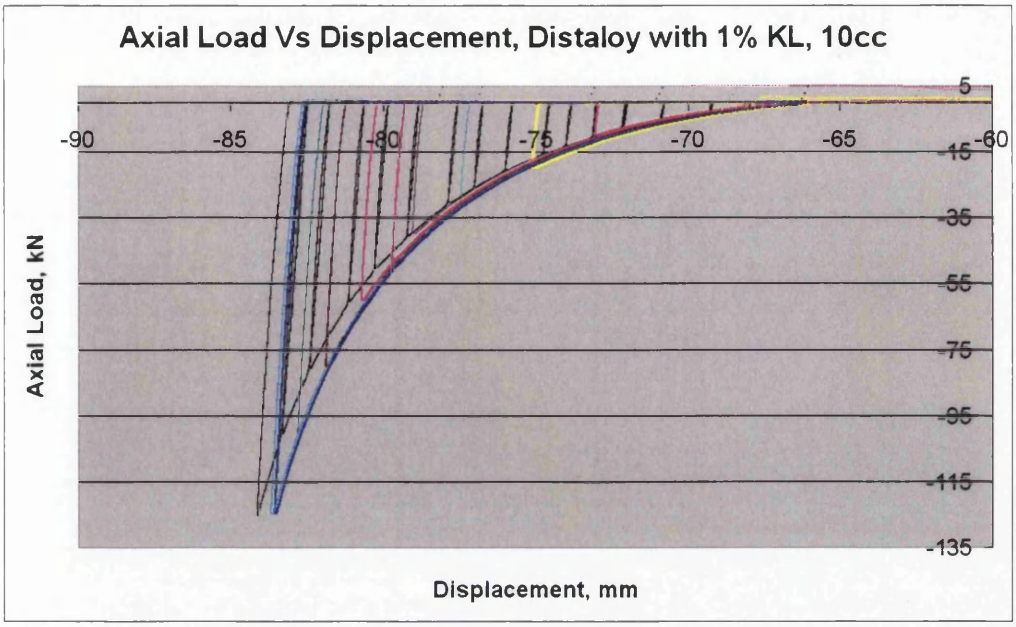

Figure 6.5 Relaxation Tests for Fresh and Reused Powders

From Figure 6.5 it can be seen that the characteristics are virtually identical. Notably, the relaxation slopes are closely parallel at each density. This implies that for ferrous powder, the modulus data may be derived from tests performed through repeated loading of a single powder sample. This may not be the case for granulated materials where the loading cycle may induce breakdown of the granulate.

Tests were also performed on powders having different levels of admixed lubricant and these are shown in Figure 6.6.

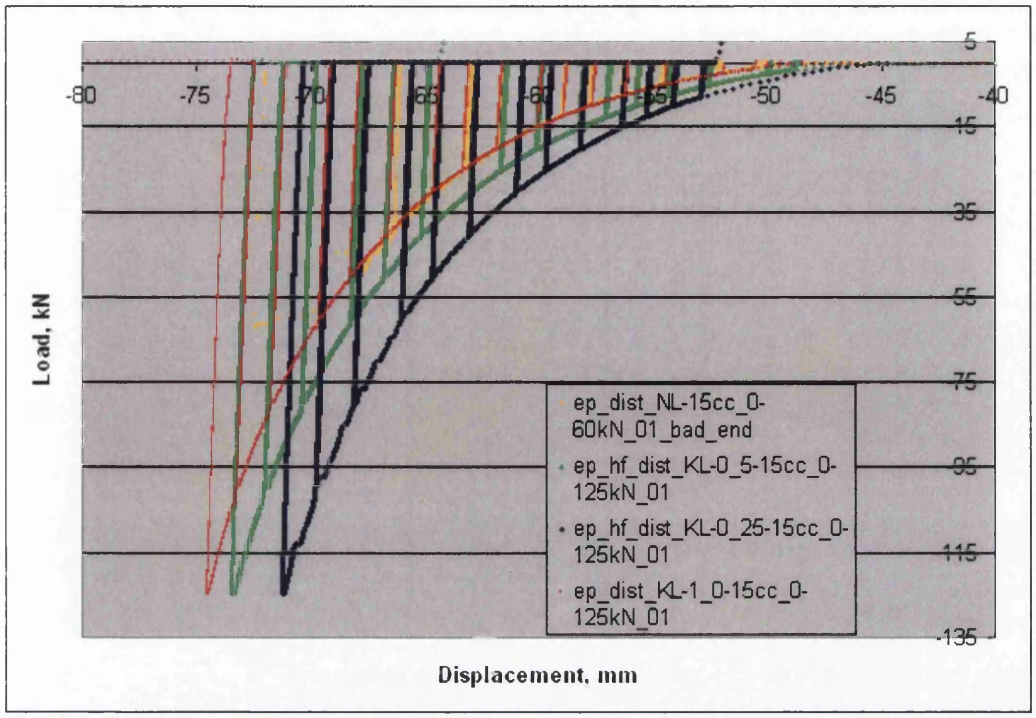

Figure 6.6 The Impact of Lubricant Addition of the Load Unload Cycle

The compaction characteristics exhibit the expected trends in that lubricant addition leads to increased compact density. The effect of lubricant addition on Young's modulus was found to be small since the unloading characteristics shown in Figure 6.6 are nearly parallel for the different lubricant additions. This result is confirmed in Figure 6.7, where little difference is observed in the evolution of Young's modulus with density for each powder.

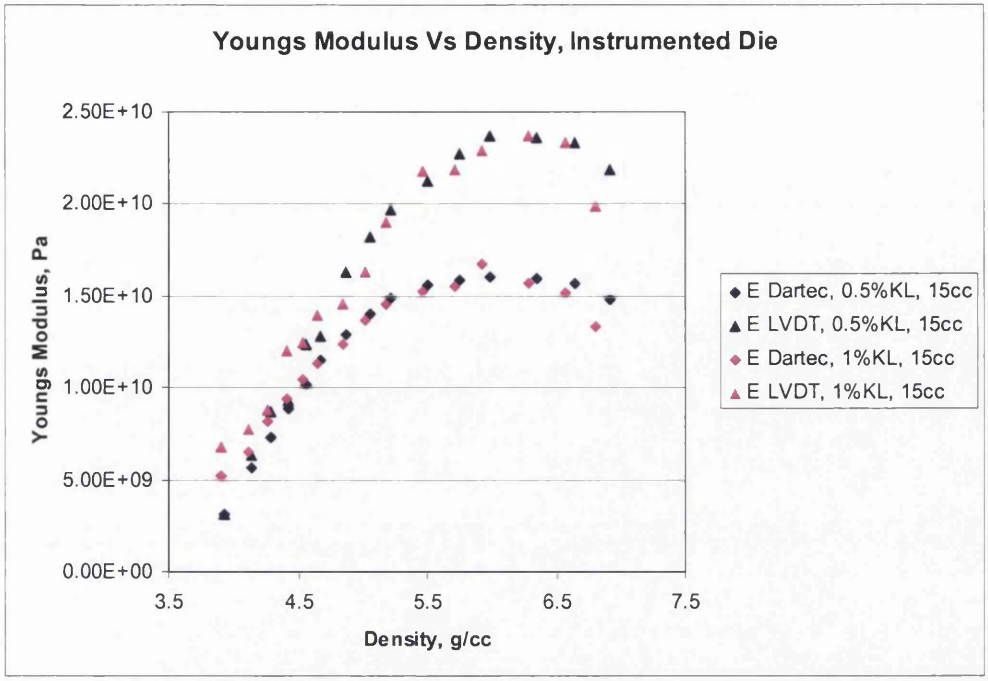

Figure 6.7 Lubricant Addition and its Effect on Young's Modulus

Next, the alternative reduction technique proposed by Cunningham, Sinka et al. (2004) was used. The following assumptions were made:

- The die wall is perfectly rigid
- Friction is ignored and no porosity variation exists in the specimen
- The compact can be represented by a linear elastic isotropic material

From Hooke's law the change in strain can then be written in cylindrical coordinates as:

$$d\varepsilon_{zz}^{e} = \frac{d\sigma_{zz}}{E} - \frac{\nu}{E}(d\sigma_{rr} + d\sigma_{\theta\theta})$$

$$d\varepsilon_{rr}^{e} = \frac{d\sigma_{rr}}{E} - \frac{\nu}{E}(d\sigma_{rr} + d\sigma_{zz})$$

Where ν is Poisson's ratio, E is Young's modulus, σ denotes stresses and ϵ^{e} elastic strains and indices zz, rr and $\theta\theta$ indicate axial, radial and hoop directions respectively. Given that the radius of the compact remains constant during unloading (this follows from the assumption of a rigid die) and that $d\sigma_{rr}=d\sigma_{\theta\theta}$ due to equilibrium,

$$\nu = \frac{d\sigma_{rr}}{d\sigma_{rr} + d\sigma_{zz}} \text{ and } E = \frac{d\sigma_{zz}}{d\varepsilon_{zz}^{e}} - 2\nu\frac{d\sigma_{rr}}{d\varepsilon_{zz}^{e}}$$

The resultant Poisson's ratio for the Distaloy AE with 0.5% Kenolube powder is shown in Figure 6.8.

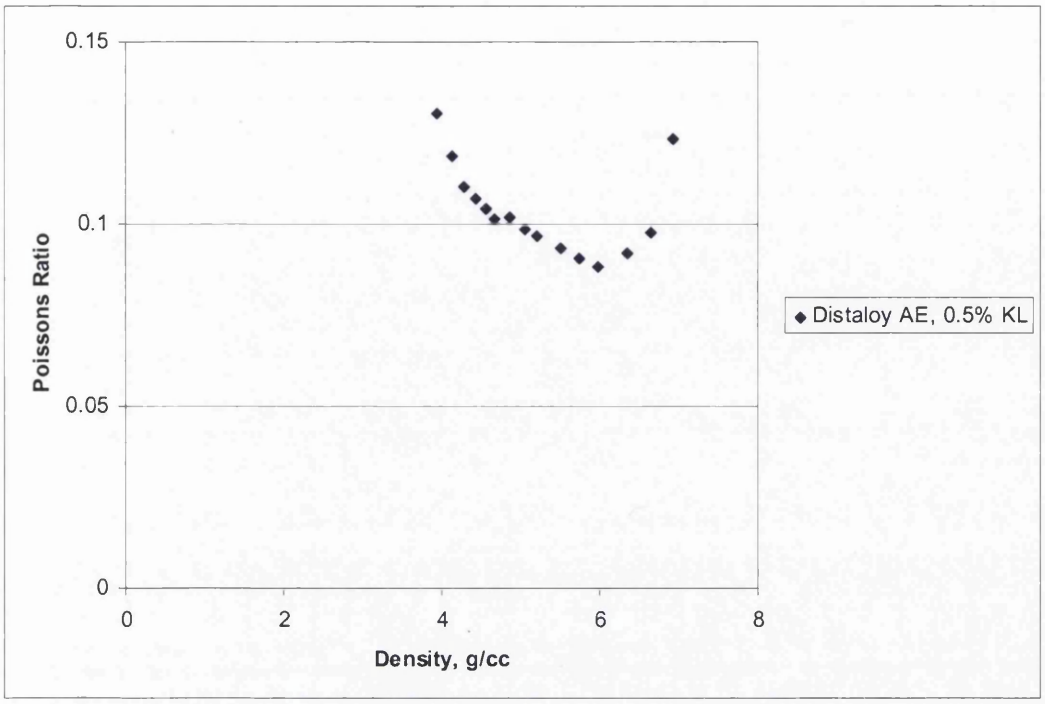

Figure 6.8 Poisson's Ratio, Instrumented Die Test

The values of Young's modulus obtained by following the above calculations are plotted in Figure 6.9 together with values obtained using the simple analysis as introduced in Figure 6.7 (designated as E LVDT in Figure 6.9). Values obtained by using both the "nominal" strain and the "natural" strain in the equations proposed by Cunningham, Sinka et al. (2004) are plotted and are very close to those obtained using the simple analysis. Additionally, the values of Young's modulus obtained when accounting for top punch deformations are also plotted for completeness – no significant influence was observed.

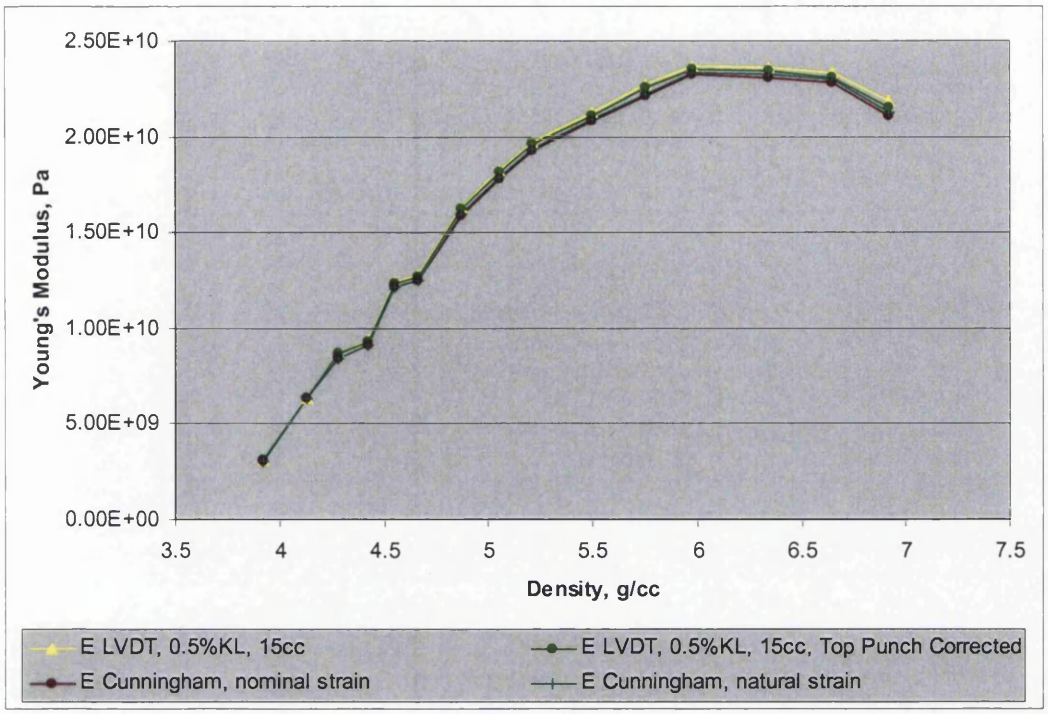

Figure 6.9 Comparison of Young's modulus obtained by different reduction techniques

In Figure 6.10 the values of Young's modulus derived from the instrumented die test are compared to those derived via an analytical equation based on triaxial tests of Distaloy AE powder with 1% wax addition (Doremus 2002). However, according to the equation the value of Young's modulus at 7.5g/cc (i.e. at solid density) is 285GPa, which is significantly greater than that of the solid parent material. Thus, the equation cannot be applied with confidence at high densities.

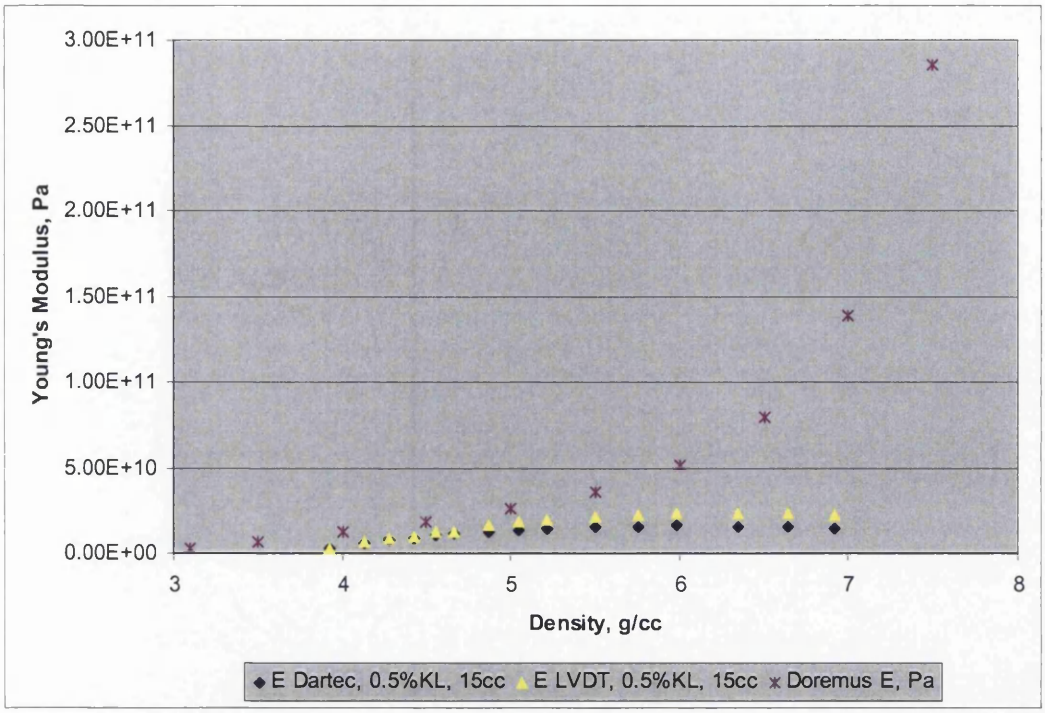

Figure 6.10 Comparison of Elastic modulus data

Guyoncourt (2005) reported calculated values of Young's modulus in the region of 15.4-18GPa for two blends of metal powders with densities between 6 and 6.85g/cc. The corresponding measured values were in the region of 29-50GPa. For these densities the values of elastic modulus calculated from both the simple analysis used in this chapter and the equations suggested in (Cunningham, Sinka et al. 2004) lie between 20 and 25GPa.

The values of the Poisson's ratio, as obtained earlier following the equations set out in (Cunningham, Sinka et al. 2004), are compared to those predicted by the analytical equation in (Doremus 2002), see Figure 6.11. While in both cases there is an increase in Poisson's ratio at densities above 6g/cc different results were obtained for lower densities. It is not clear why the measured Poisson's ratio remains high at lower densities, as logically it is expected to increase with density.

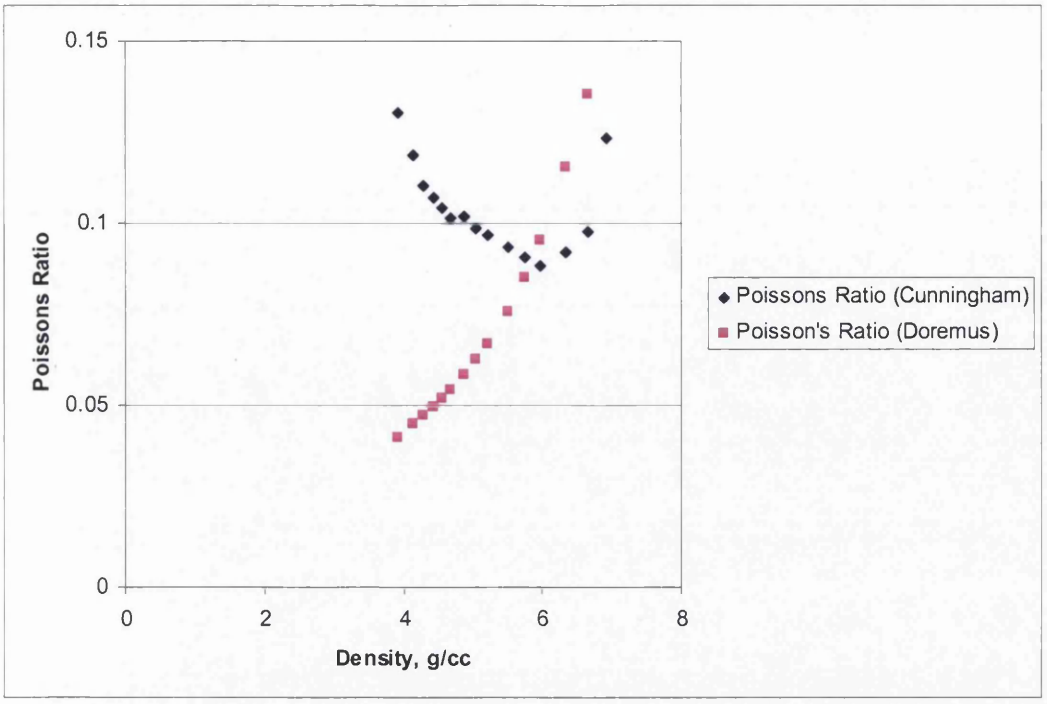

Figure 6.11 Comparison of Poisson's ratio data

6.2.2 Unconfined Compression Test

Two series of unconfined compression tests were performed. The first one was with Distaloy AE powder having 1% Kenolube addition. Compacts were prepared at different densities and dependent on the density, the compacts were compressed using load cells having a working range of 1kN, 10kN and 250kN. This provided sufficient resolution for determining the stress strain relationship for a range of densities. Also, each compact was loaded to failure and an example of a typical failure is shown in Figure 6.12, which exhibits a typical shear mechanism. The associated stress strain characteristics are shown in Figure 6.13. The initial stage corresponds to the displacement over which the press engages the compact and this is followed by a build up of stress to a maximum at which point the compact begins to crumble. By ignoring any end effects due to friction between the powder and press platen, the Young's modulus is established over the zone for which there is a continuous build up of stress and the consequent variation with relative density is shown in Figure 6.14. It should be noted that the failure stress for the most dense compact (pressed to a load of 125kN) is significant and that tests on two samples (albeit prepared using a single and multiple loading cycle) show excellent repeatability.

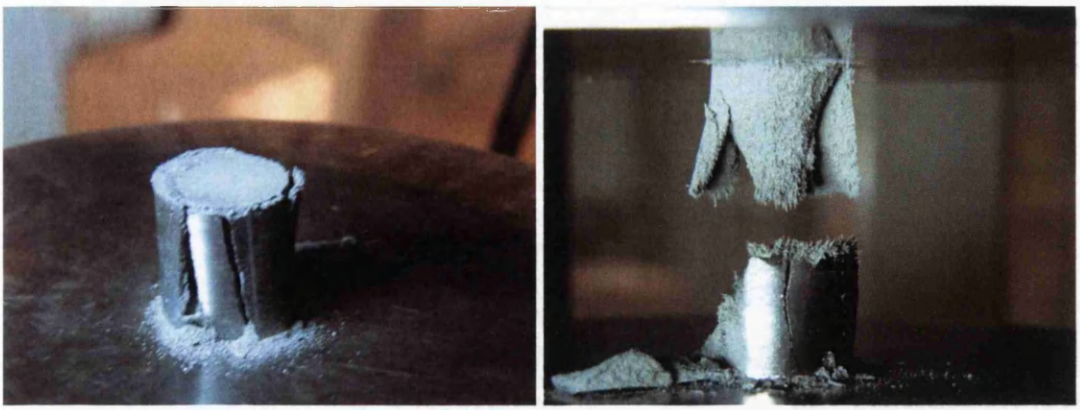

Figure 6.12 Typical Failure of Freestanding Compacts

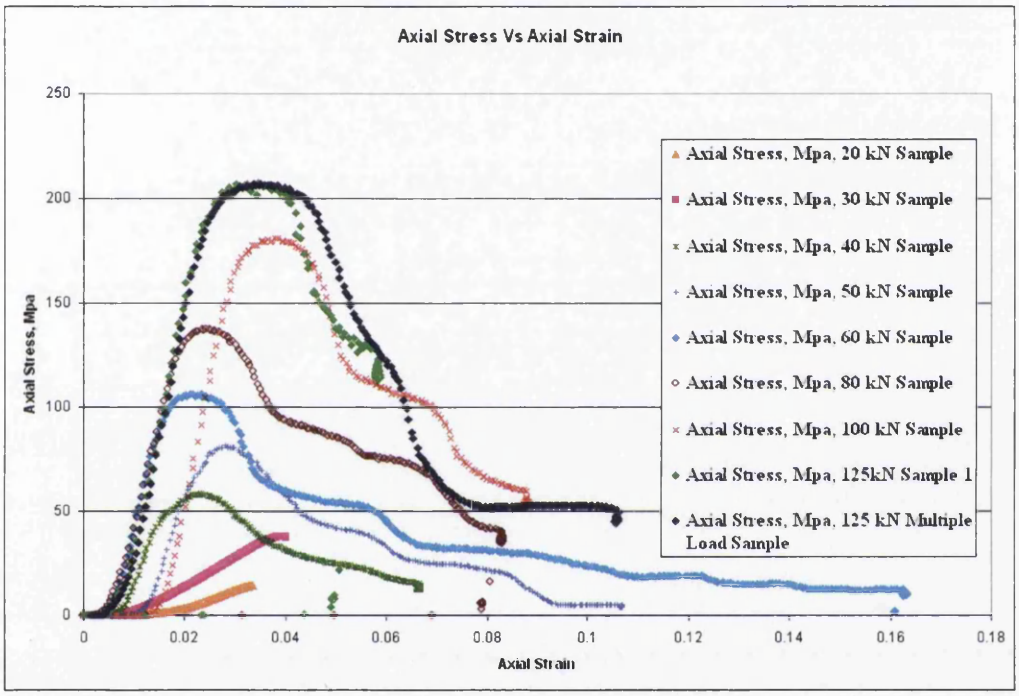

Figure 6.13 Axial Stress vs Axial Strain, Freestanding Compacts

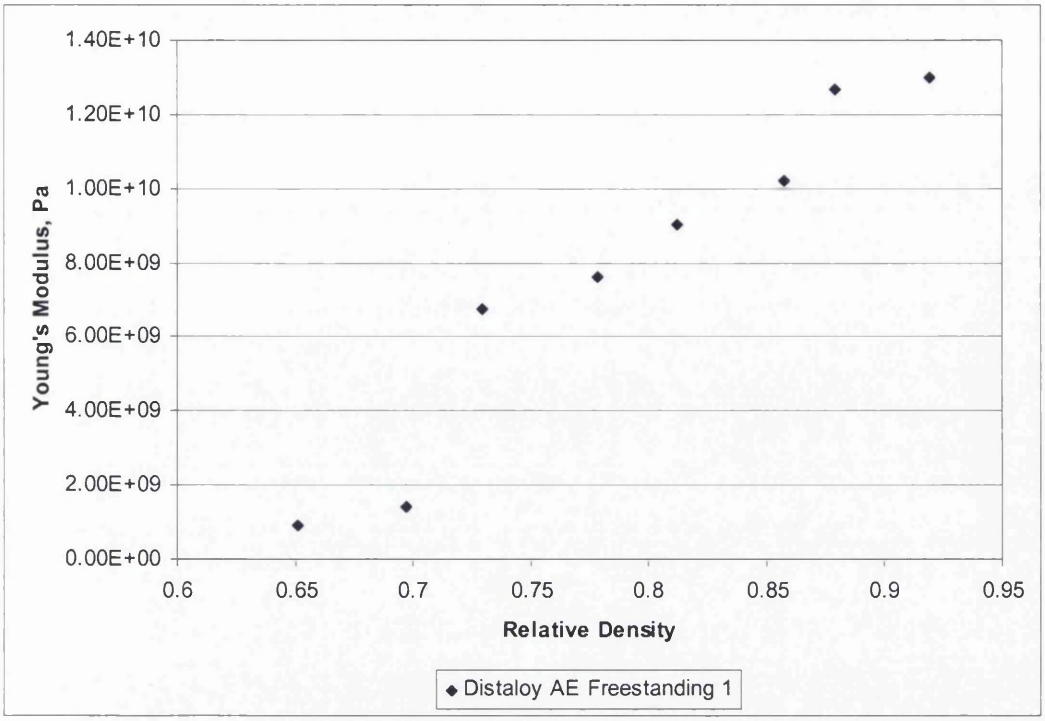

Figure 6.14 Young's Modulus vs Density, Freestanding Compacts 1

The results in Figure 6.14 exhibit an approximately linear increase in Young's modulus as the compact density is increased.

The second series of tests was performed with Distaloy AE powder with 0.5% Kenolube. This time the compacts were pressed to target densities of 5.5, 6, 6.5 and 7g/cc, with three compacts being prepared for each density. The mass of powder at fill was selected to produce compacts with an aspect ratio of 1. The press platens were lubricated to reduce the friction at the contact and minimise end effects. Otherwise, the same procedure as used previously for the uniaxial compression tests and the same technique was used to obtain the Young's modulus data. The results are plotted in Figure 6.15 together with those for the first series of tests.

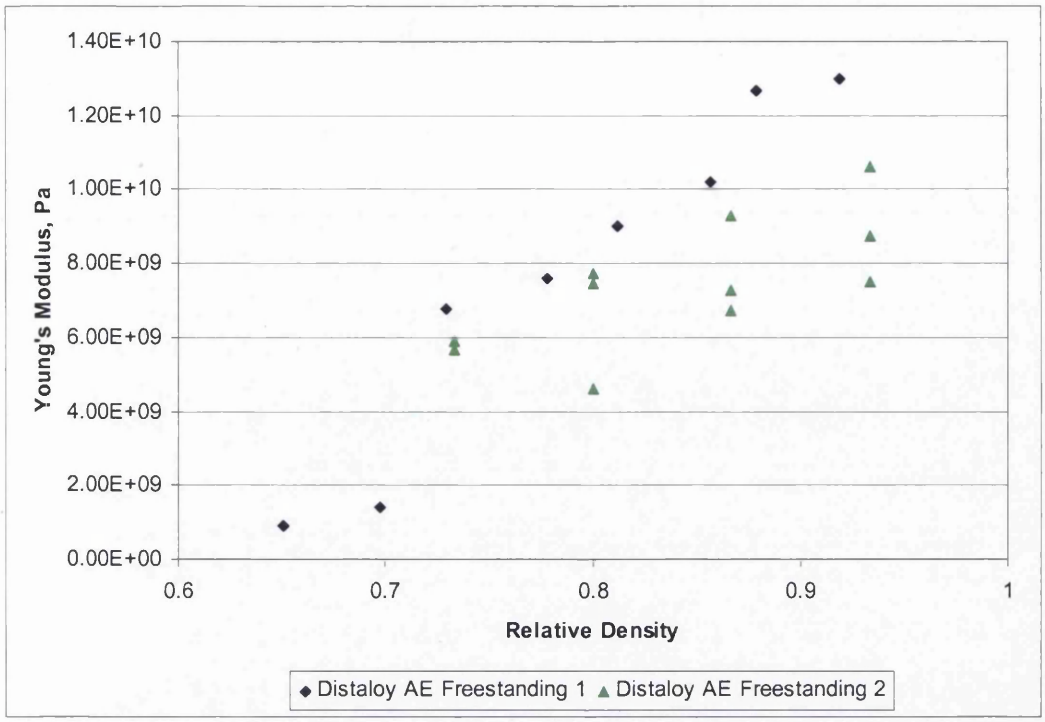

Figure 6.15 Young's Modulus vs Relative Density, Freestanding Compacts 1 (Distaloy AE with 1%Kenolube) & 2 (Distaloy AE with 0.5%Kenolube, lubricated platen)

There is a common trend of an almost linear increase in Young's modulus with density, with the second series of tests having lower values of Young's modulus.

However, when the values are compared with those derived from the tests when the powder was confined within the die, then it can be seen that the values are clearly lower, Figure 6.16. There also does not appear to be a downturn in Young's modulus at higher densities, as observed in the instrumented die tests (Figure 6.16 and Figure 6.7).

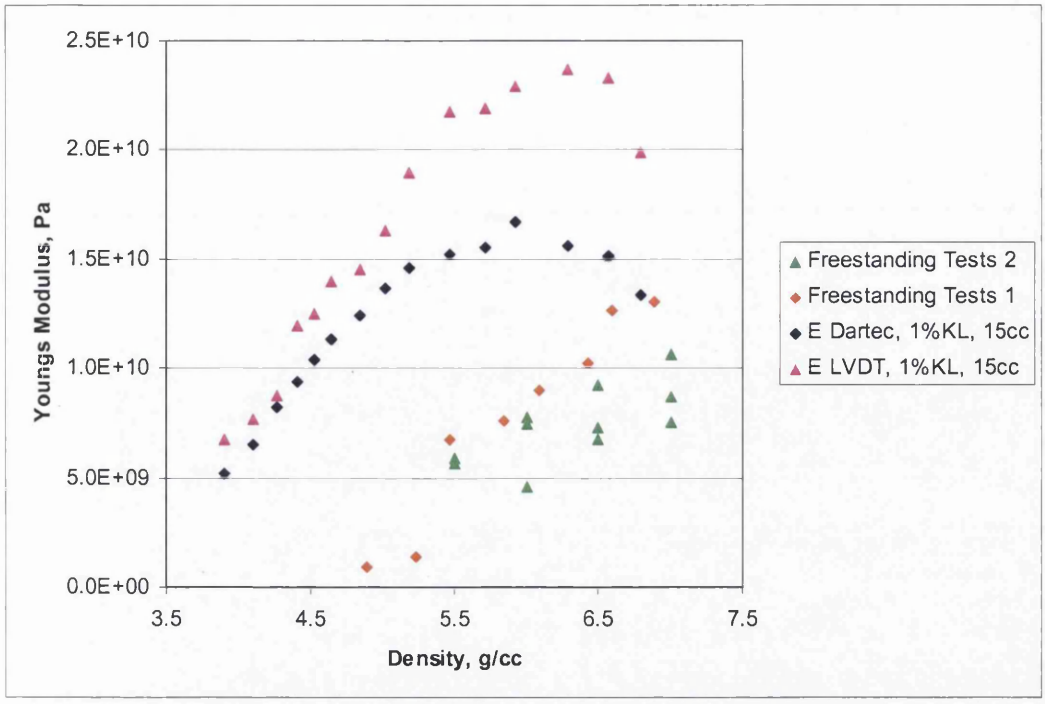

Figure 6.16 Evolution of Young's modulus with density, ferrous powder with 1% lubricant, data from freestanding tests and instrumented die (series 2 and 3)

The difference in values of Young's modulus for constrained and unconstrained compacts is due to the level of strain that is measured in the compact which is affected by the friction between the compact and die wall. As discussed in the introductory remarks, the strains are smaller in the confined compact since only a portion of it actually recovers when the load is removed, see Figure 6.17 (c). However, in the calculations the reduced recovery is taken to represent a complete compact recovery as if it was uniform throughout, Figure 6.17 (b). Thus, the Young's modulus is overestimated when calculating the value from instrumented die tests. Further work is still required to reconcile these differences in the measurement of the modulus. Potential solutions to this problem include performing the tests on lower aspect ratio compacts (at the cost of decreased density uniformity) or to thoroughly lubricate the die wall (possibly by pressing a lubricant slug) prior to performing the confined test.

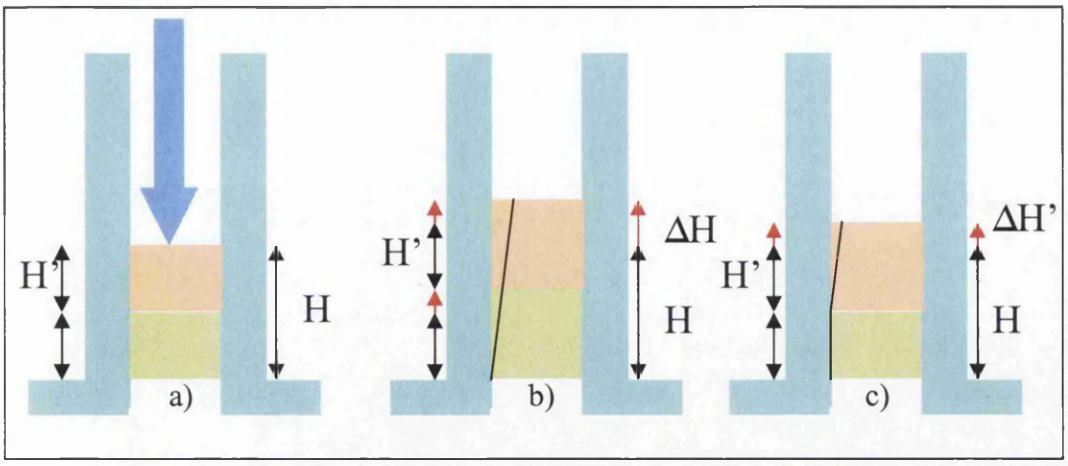

Figure 6.17 Schematic of compact relaxation in die

6.2.3 Three point bending test

Another experiment that can be performed in order to determine the elastic properties of powder compacts is the three point bending test. The layout of the test is shown in Figure 6.18 and the equipment design complies with the guidelines set out in (ISO7438 1985). The distance between the centrelines of the supports was 100mm, the diameter of the supports and the central loading cylinder was 30mm.

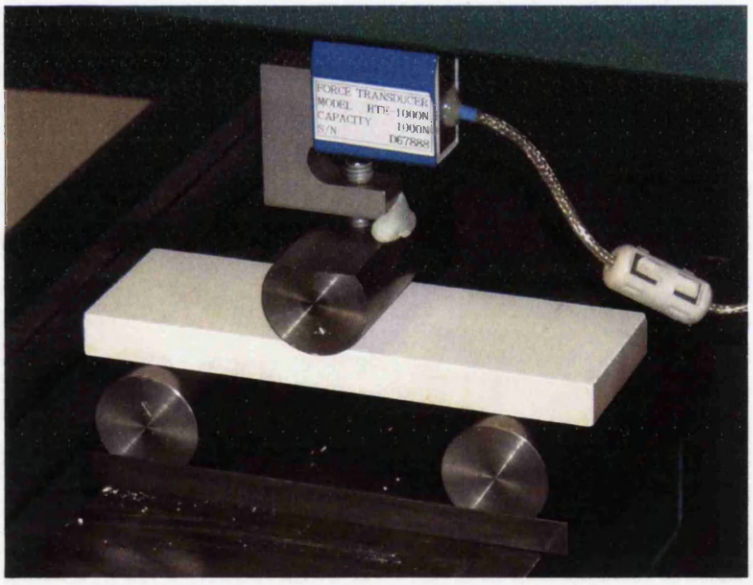

Figure 6.18 Three point bending test

The Young's modulus can be obtained from the equations of the simply supported beam theory (Stephens 1993). It can be obtained if the dimensions of the compact, the deflection and the applied load are known (Poquillon, Baco-Carles et al. 2002).

Using a simple bending model, the deflection at the centre is given by:

$$v = \frac{FL^3}{48EI}$$

Where v is the deflection at the centre of the beam, F is the load, L is the distance between the supports, E is the Young's modulus and I is the second moment of area of the section about the neutral axis.

For a rectangular section beam I is given as:

$$I = \frac{bd^3}{12}$$

Where b is the beam's width and d is its thickness. Combining these equations together E can be expressed as:

$$E = \frac{FL^3}{4vbd^3}$$

6.2.3.1 Materials and experimental procedure

Rectangular slabs where manufactured by single action compaction from Alumina and Zirconia powders (these contained organic binders). Ferrous powders could not be used at the time due to fears of damaging the press tools by overloading. Two compacts of each powder were produced for each of the following loads which were applied via the top punch: 22, 33, 44, 66 and 88 tons, these loads are equivalent to 31, 46, 61, 92 and 123MPa of axial pressure respectively. Additionally, ten more compacts of each powder, pressed initially at 61MPa were isostatically compressed to pressures of 10, 12, 14, 17 and 20 thousand Psi (69, 83, 97, 117 and 138 MPa). The dimensions of each compact were measured, with each dimension taken at three different locations. Averages of the dimensions from left, middle and right of the compacts were used during density calculations.

6.2.3.2 Results

The average and relative densities of the samples are shown in Figure 6.19 and Figure 6.20 respectively. Although the average density of Zirconia samples was higher than that of the Alumina ones, the relative densities were higher for Alumina compacts, due to the lower solid density of Alumina. For both powders the density values for isostatically pressed compacts were higher than those of the

compacts pressed in a closed die only. Overall, the density values were found to be very consistent between the pairs of compacts pressed at the same pressure.

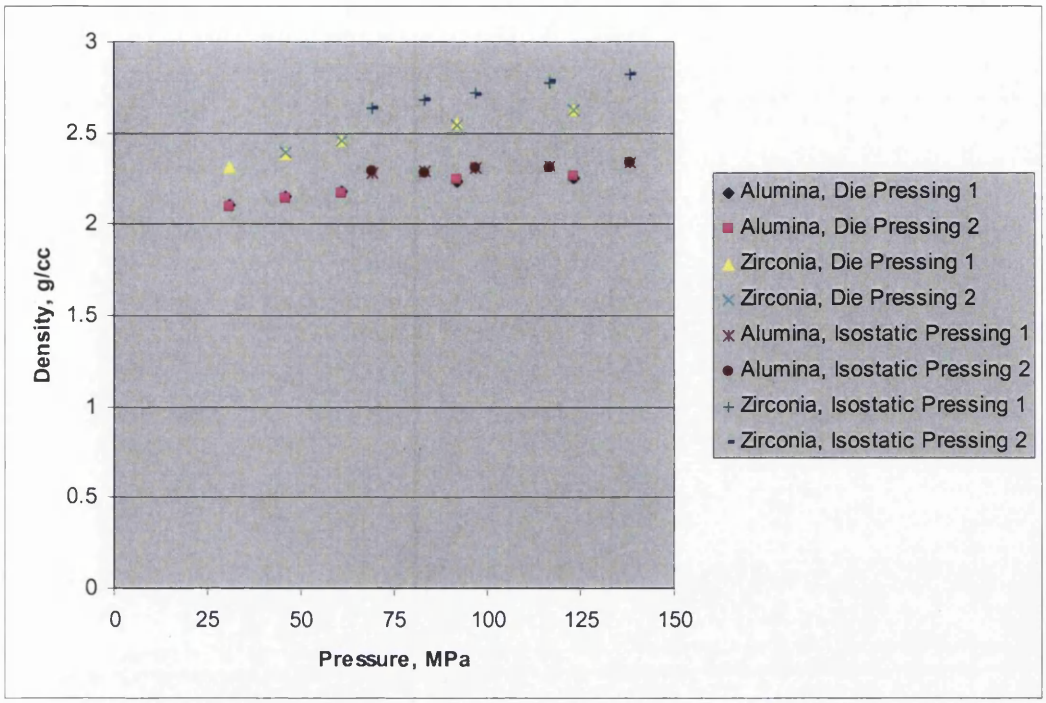

Figure 6.19 Sample densities, three point bending test

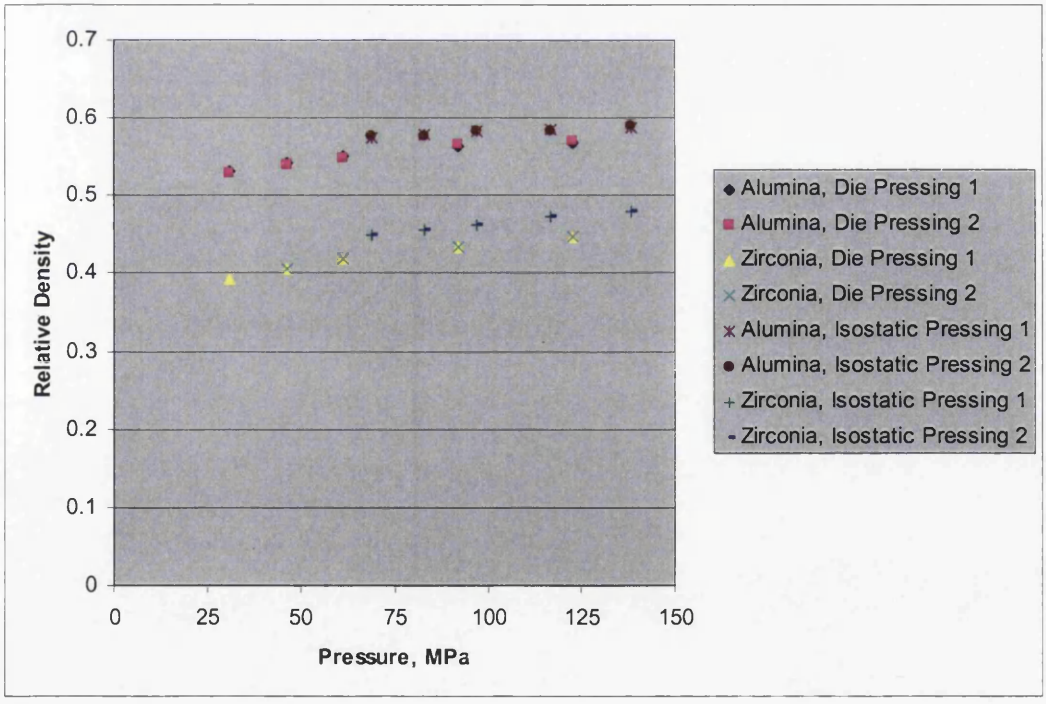

Figure 6.20 Sample relative densities, three point bending test

A Hounsfield mechanical screw press was used for the bending tests. Since the loads involved were small a sensitive 1000N load cell was used. The edges of the compacts were gently rubbed down before testing to remove sharp edges, thus preventing local stress concentrations. At the start of the experiment the compact was placed onto the supports with the top face down. This was done because, for compacts with single direction kinematics, the face that was nearest to the moving tool is denser. Therefore, such compacts are more capable of withstanding the tensile loads in one orientation and which are generated at the bottom surface during the three point bending test. Unfortunately, this implies that the modulus will reflect to some extent the anisotropy that must be present in the compact. Once the compact and the press head were positioned correctly the test was launched and the central cylinder descended onto the compact under displacement control. The load and the displacement were recorded. Once the compact failed the press was stopped. A pair of typical outputs from the test is shown in Figure 6.21.

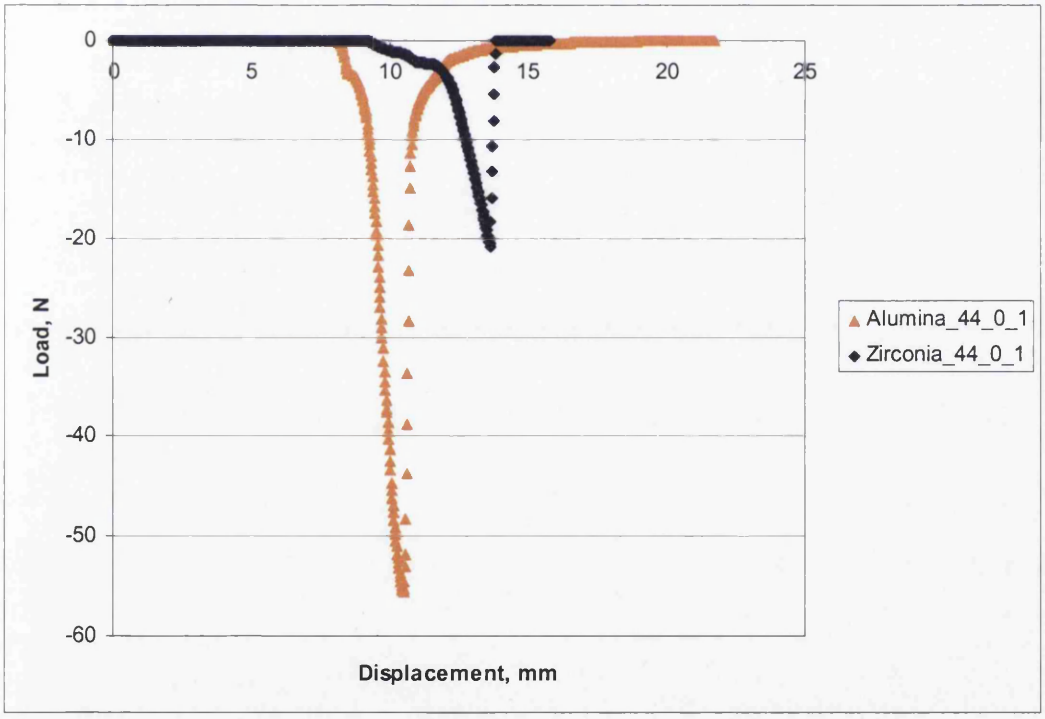

Figure 6.21 Typical output of the three point bending tests

The distinct stages of the three point bending test are demonstrated in Figure 6.22. At the start of the test the press crosshead was lowered so that the centre cylinder approached the compact – there was no load at that point. The cylinder then

engaged the compact and the slack in the loading cylinder's mounting was removed – this is noticeable through uneven loading pattern up to the load of approximately 3N on the graph. Once the loading cylinder was fully engaged with the compact, the load rose almost linearly until failure was reached. The two materials behaved differently at that point. The Zirconia compacts snapped immediately after the failure load had been reached, falling apart into two halves. This is indicated on the graph by the rapid reduction of the load to 0N after failure of the Zirconia sample. The Alumina compacts did not fall apart initially after failing and provided some resistance before completely falling apart. This is shown by a more gradual reduction in the load, starting at approximately -10N, as seen in Figure 6.21. No indentations were observed on the compacts at the support points, therefore the displacement during the bending phase can be attributed to the deflection of the compact.

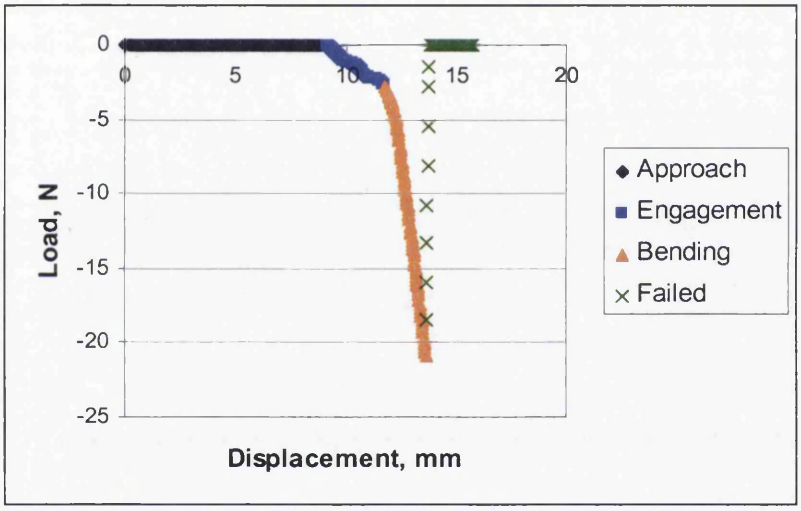

Figure 6.22 Stages of the three point bending test, Zirconia compact

First, the green strength of the compacts, in this case the maximum tensile stress achieved at failure, was considered. The expression for this follows from simple bending theory, where the maximum stress is given by:

$$\sigma = \frac{My}{I}$$

Where M is the bending moment, y is the distance from the neutral layer, which is equal to half of the thickness, and I is the second moment of area. The maximum bending moment is given by:

$$M = \frac{FL}{4}$$

Where F is the applied load and L is the distance between the supports.

Analysis of failure stresses for both die pressed and isostatically pressed samples shows greater consistency for the Zirconia compacts, see Figure 6.23 and Figure 6.24. The failure stresses are almost identical for the pairs of Zirconia compacts, showing good repeatability. There is more variation in failure stresses for Alumina samples, however adequate agreement can be observed, particularly for samples isostatically pressed to higher pressures.

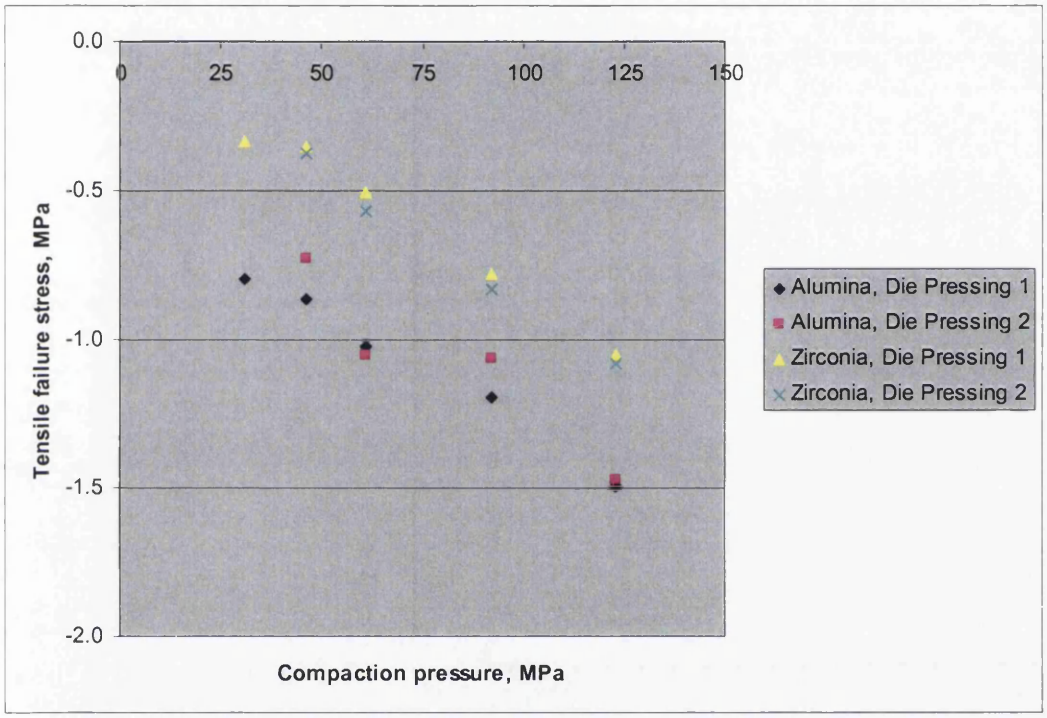

Figure 6.23 Failure stress, die pressed samples, three point bending test

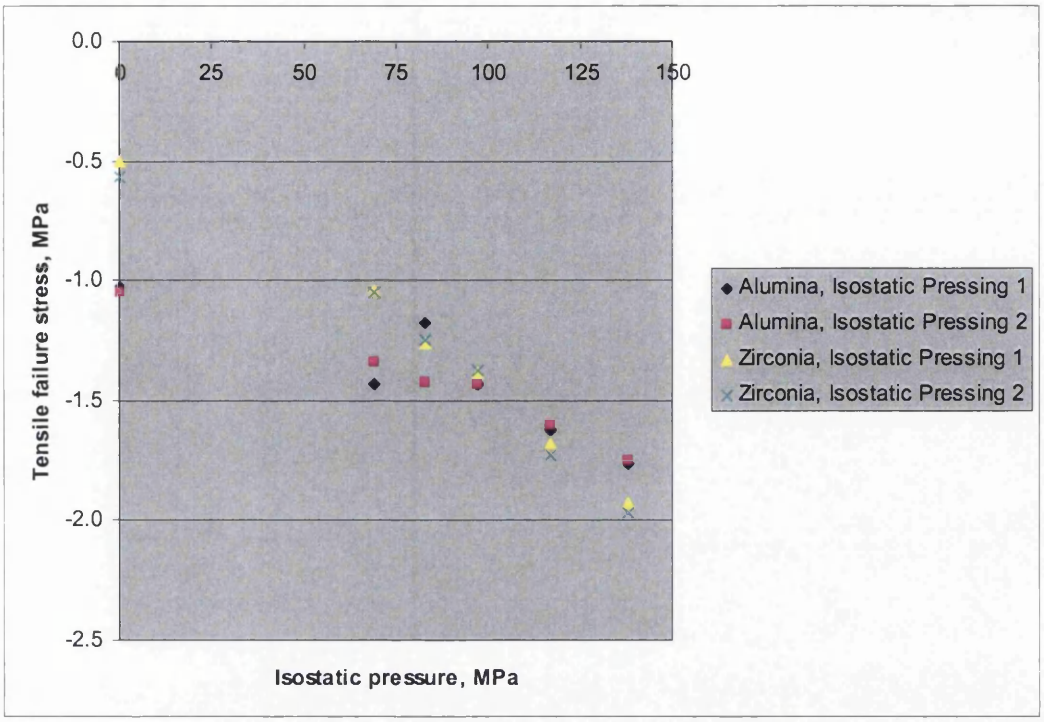

Figure 6.24 Failure stress, isostatically pressed samples, three point bending test

It is interesting to compare the trends of failure stress (Figure 6.24) with those of the failure load (Figure 6.25). The latter can be described as nearly parallel between the two powders, with Alumina compacts proving to be consistently stronger. However, due to different compression ratios achieved at the same isostatic pressure, and hence different cross-sectional areas, the Zirconia compacts experienced higher stresses even though the failure loads were lower than those for Alumina compacts.

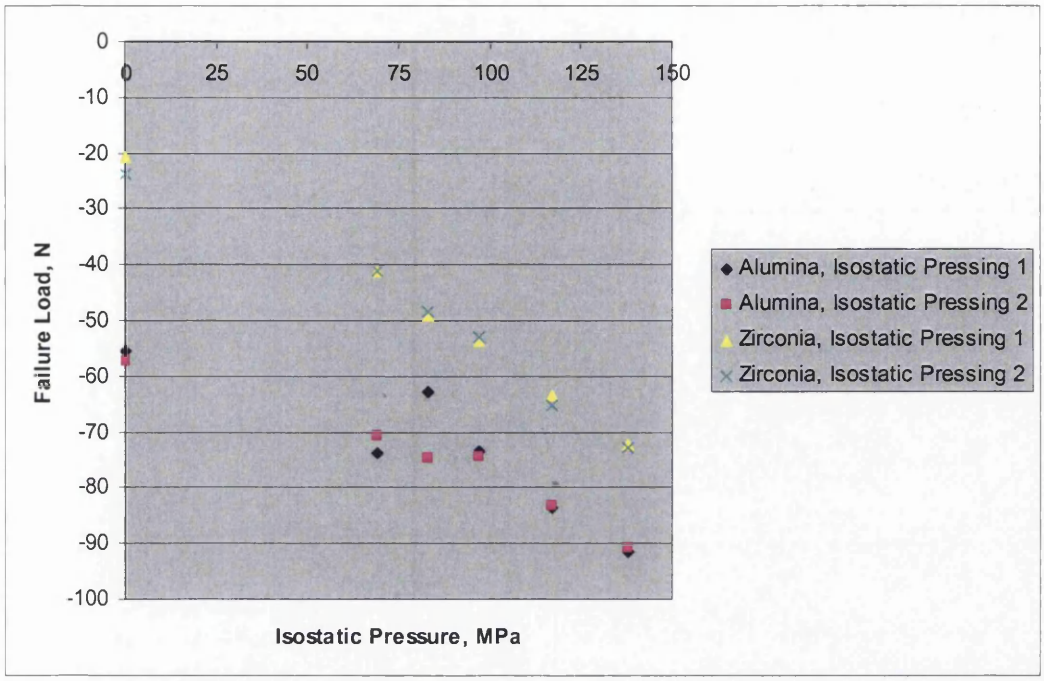

Figure 6.25 Failure load, isostatically pressed samples, three point bending test

When combining the results for both die pressed and isostatically pressed samples it is evident that the failure stress primarily depends on compact density, see Figure 6.26. The effect of isostatic pressing of the slabs can be approximately equated to that of further densification. Similar observations can be made when considering the Failure Load in relation to the apparent density of the compacts, see Figure 6.27. For Zirconia samples the failure loads for both the die pressed and the isostatically pressed (after prior die pressing) samples appear to lie on a continuous curve. This is also true for the Alumina samples, although more variability can be observed in the results.

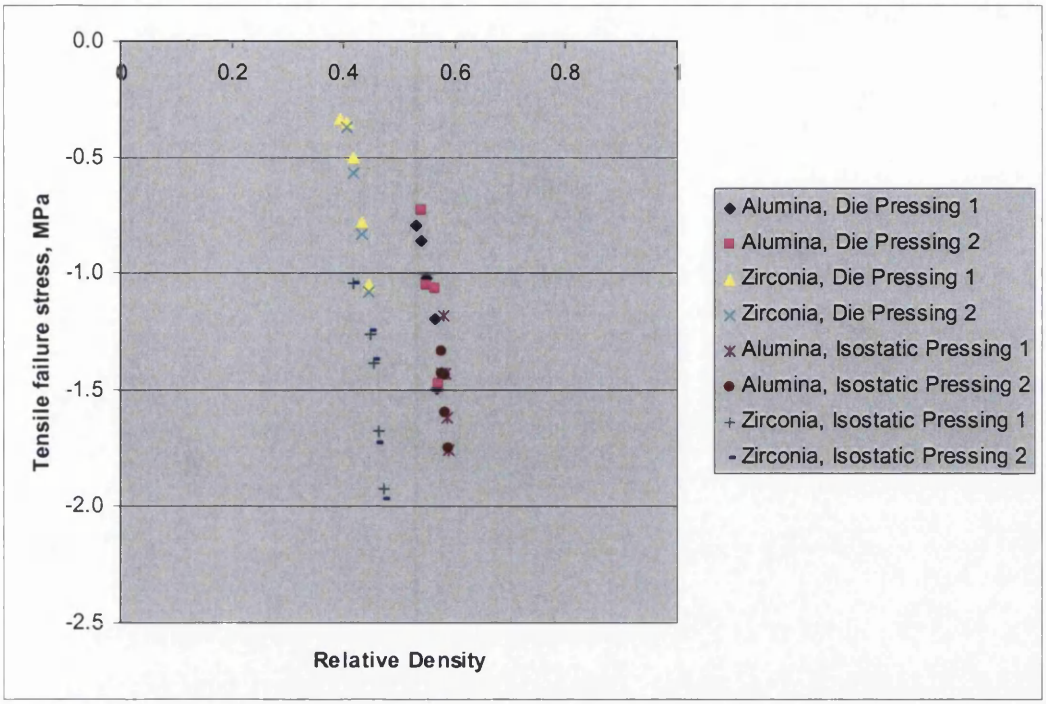

Figure 6.26 Failure stress vs. relative density, three point bending test

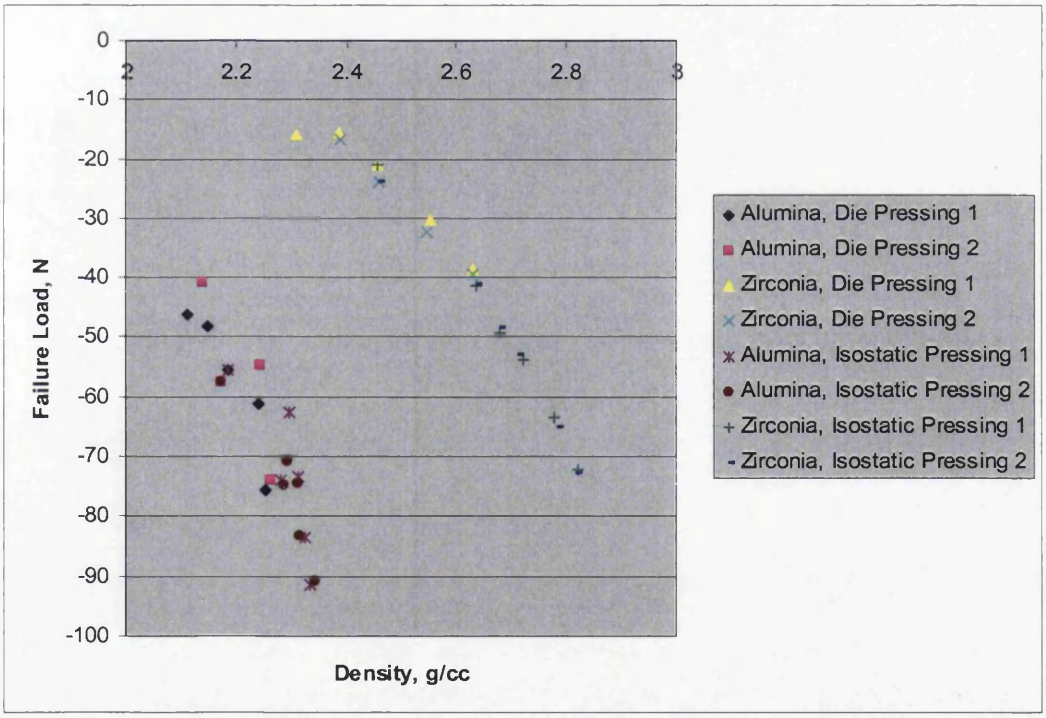

Figure 6.27 Failure load vs. density, three point bending test

In order to calculate Young's modulus for the samples tested, data in the linear loading region was considered, see "Bending" phase in Figure 6.22. Two points were selected from each test, one near the start and one near the end of the linear loading region. The differences between the load and deflection in the two points

were taken as the F and v values for the above formulae. Thus, the Young's modulus was obtained for each of the samples. The results are plotted in Figure 6.28.

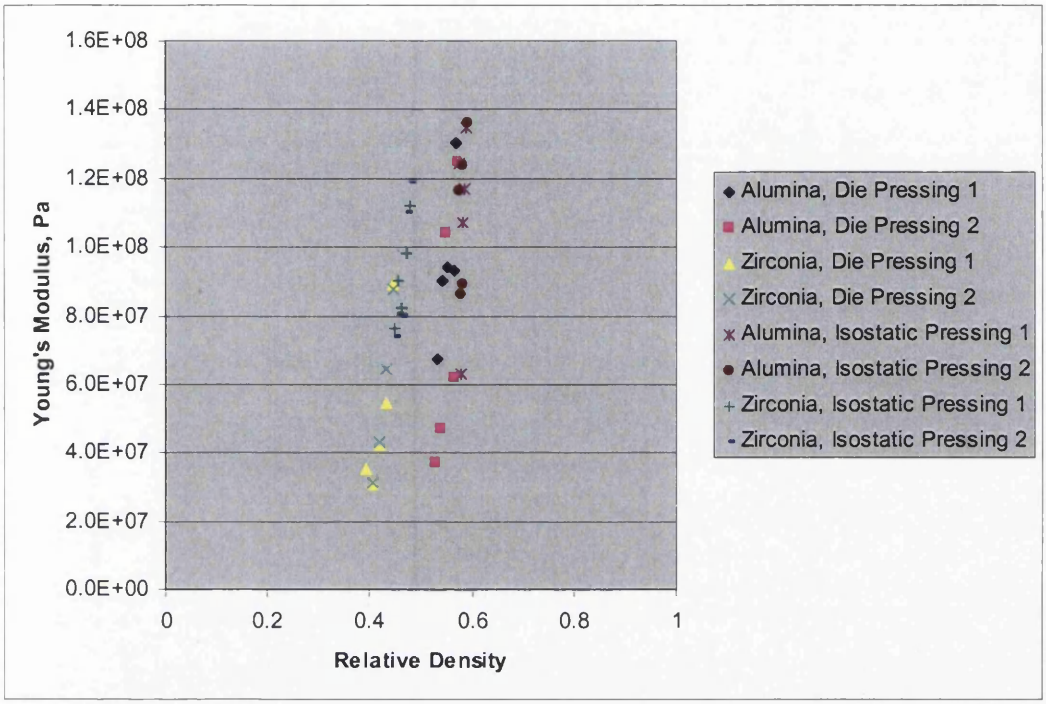

Figure 6.28 Young's modulus, ceramic bars, I

Young's modulus data from the perspective of average density is plotted in Figure 6.29. The locations for the two powders along the density scale have reversed, as, despite having a lower relative density the Zirconia compacts were actually denser than the Alumina ones. The results for the Alumina powder show more variation than those for the Zirconia powder.

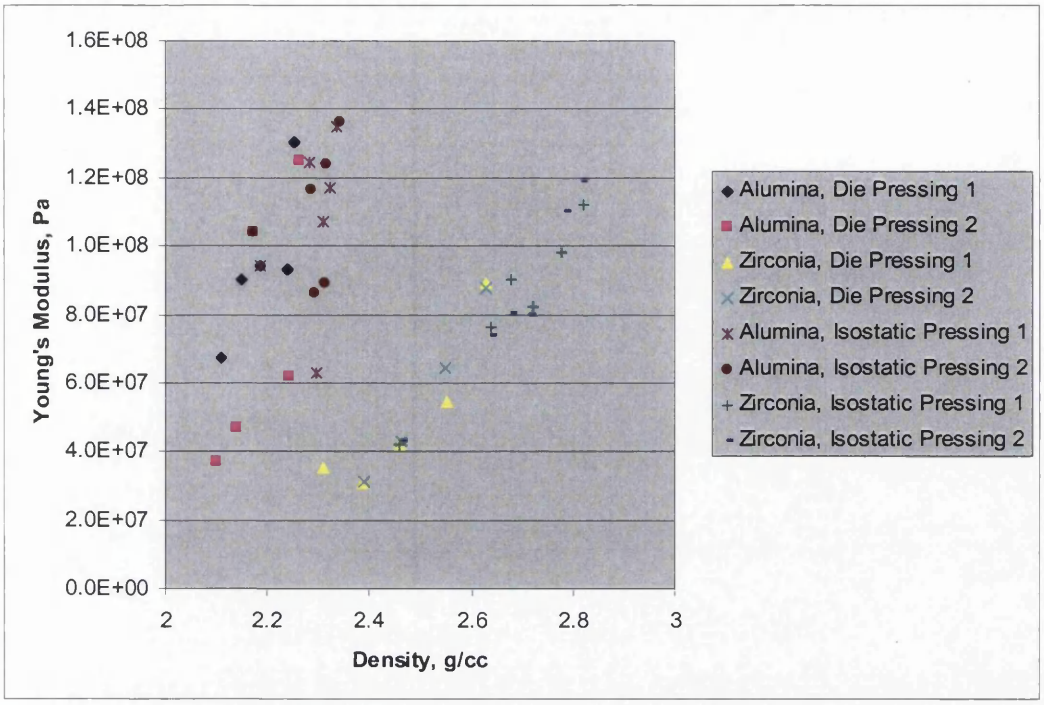

Figure 6.29 Young's modulus, ceramic bars, II

For the density levels considered here the relationship between Young's modulus and relative density can be represented by a linear function for both powders. Such a function can then be used to represent the elastic properties of the powder in a numerical simulation. It appears that the effect of isostatic pressing on the strength and elastic properties of Zirconia powders is equivalent to that achieved purely through further densification.

6.2.3.3 Alumina – uniaxial compression

In order to compare the three point bending tests to other techniques a series of uniaxial compression tests was performed with the Alumina powder. Compacts with the aspect ratio of 1 and having densities of 2.1, 2.17, 2.25 and 2.32g/cc were prepared. They were then tested in uniaxial compression following the procedure described in Section 6.2.2. The results are plotted in Figure 6.30. Values of Young's modulus obtained from the uniaxial compression tests were higher than those from the three point bending test. The exact reasons for this behaviour are not clear, however compact anisotropy is among the likely causes. During the uniaxial compression test the elastic modulus was tested in the direction of compaction, whereas during the three point bending test the loading direction was perpendicular to that of compaction.

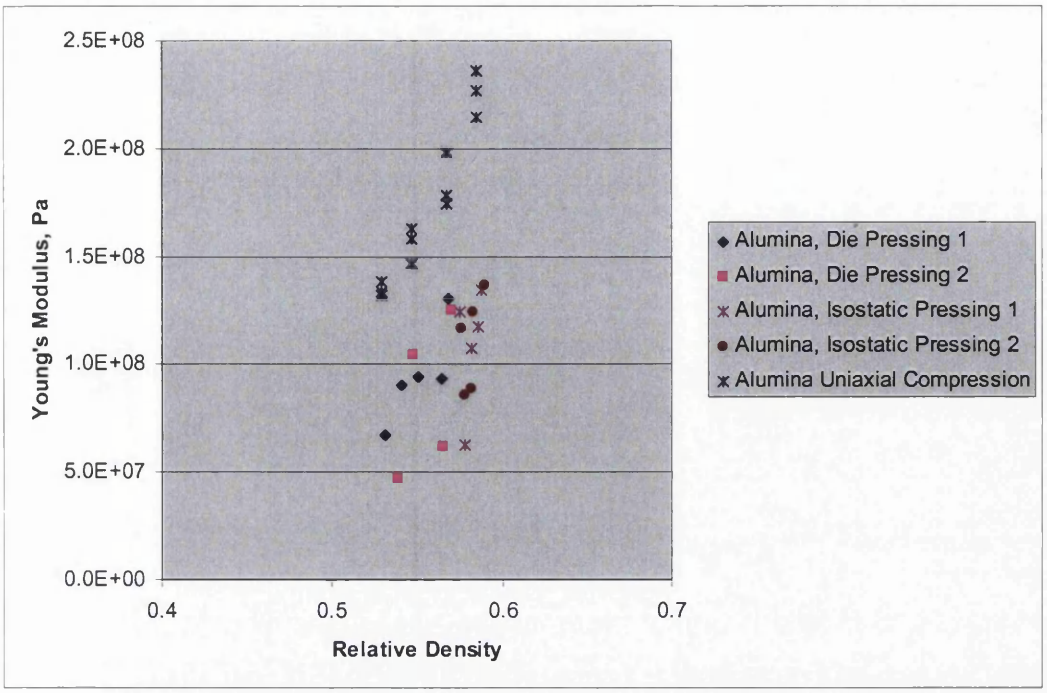

Figure 6.30 Young's Modulus, Alumina

6.3 Cohesion

In the numerical code used in Chapter 3 of this thesis the parameter representing cohesion is obtained from the diametrical compression tests, also known as a Brazilian disk test. Such tests were performed for compacts made with Distaloy AE and Alumina powders. Note that for ductile powder systems the Brazilian disc test must be applied with caution, as the deformations of the contact surfaces affect the stresses in the compact (Procopio, Zavaliangos et al. 2003).

6.3.1 Distaloy AE – Brazilian disc test

For this test the compact samples were prepared in the same manner as the samples for "Freestanding Tests 2", as described in Section 6.2.2. The aspect ratio of 1 was chosen as a compromise – it is sufficiently small to reduce variations induced by the single-ended compaction kinematics and sufficiently large to reduce the impact of end effects. Compacts with densities of 5.5, 6, 6.5 and 7g/cc were prepared. The compacts were tested on the Dartec hydraulic press, with load and displacement data recorded. The behaviour of a compact during a typical test is shown in Figure 6.31

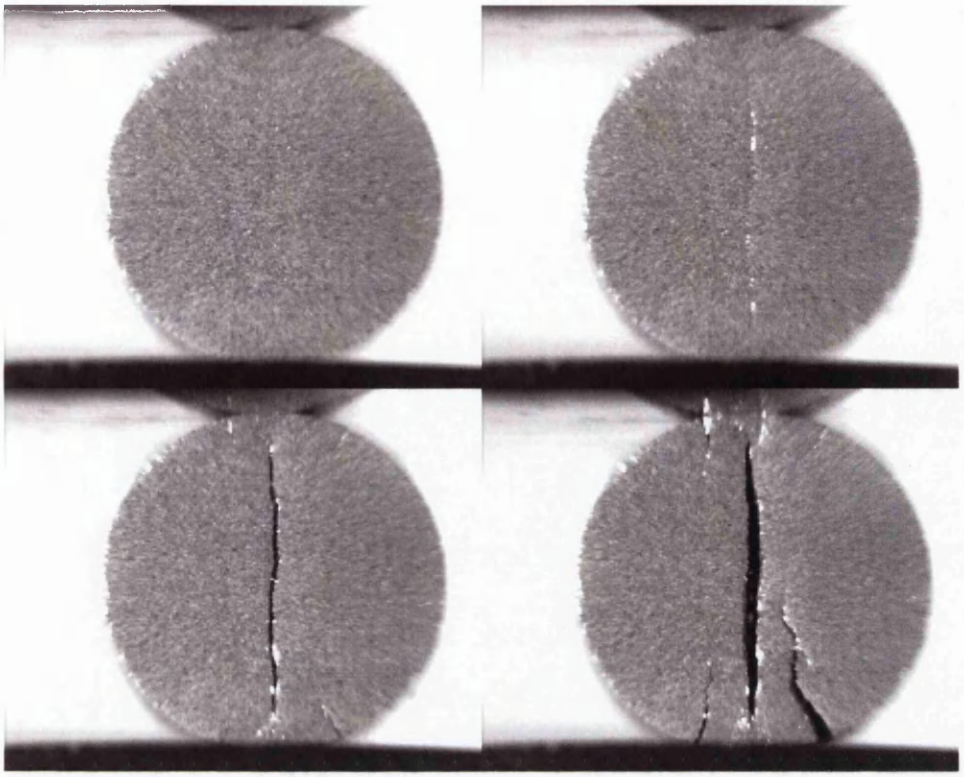

Figure 6.31 Brazilian disc test, Distaloy AE

The cohesion parameter required for the numerical code is equal to the tensile failure stress. If the material is assumed to be linear elastic up to failure and the point of contact between the sample and the compact is maintained (i.e. it does not flatten) then according to (Cunningham, Sinka et al. 2004) the tensile failure stress can be defined as:

$$\sigma_T = \frac{2P}{\pi D t}$$

Where P is the applied load, D is the diameter of the compact and t is its thickness. The results are plotted in Figure 6.32. A nearly linear increase in strength was observed at relative densities lower than 0.9 with a sharper increase beyond that.

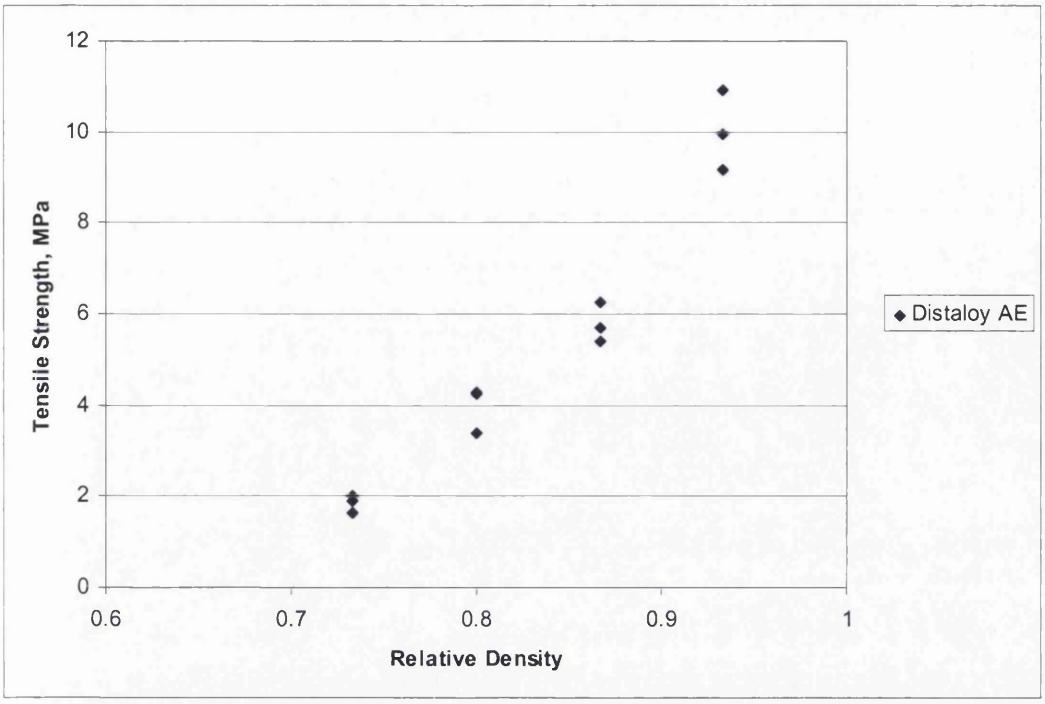

Figure 6.32 Cohesion parameter, Distaloy AE

6.3.2 Alumina – Brazilian disc test

The above procedure was also used to test the Alumina powder. Again, compacts with aspect ratio of 1 and densities between 2.1 and 2.32 g/cc were pressed using the instrumented die and the Dartec hydraulic press. The Brazilian disc tests were performed on the Hounsfield mechanical screw press, as a more sensitive load cell than that on the Dartec hydraulic press (10kN vs. 250kN) was required for the Alumina powder. The behaviour of a compact during a typical test is shown in Figure 6.33. The same data analysis procedure as in Section 6.3.1 was used and the results are plotted in Figure 6.34.

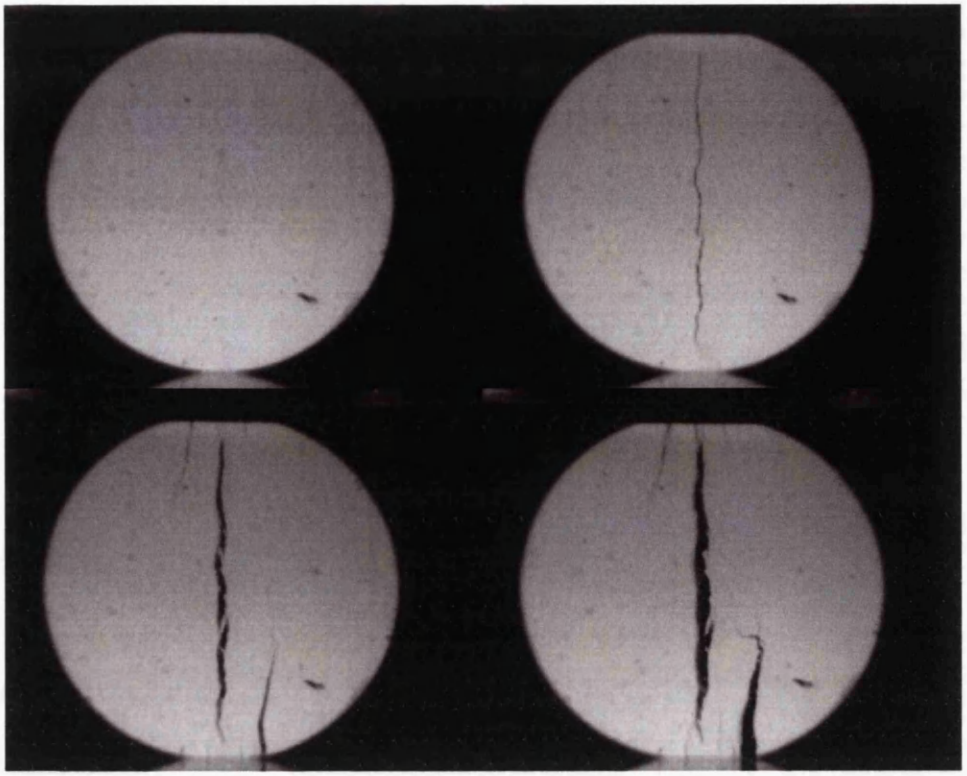

Figure 6.33 Brazilian disc test, Alumina

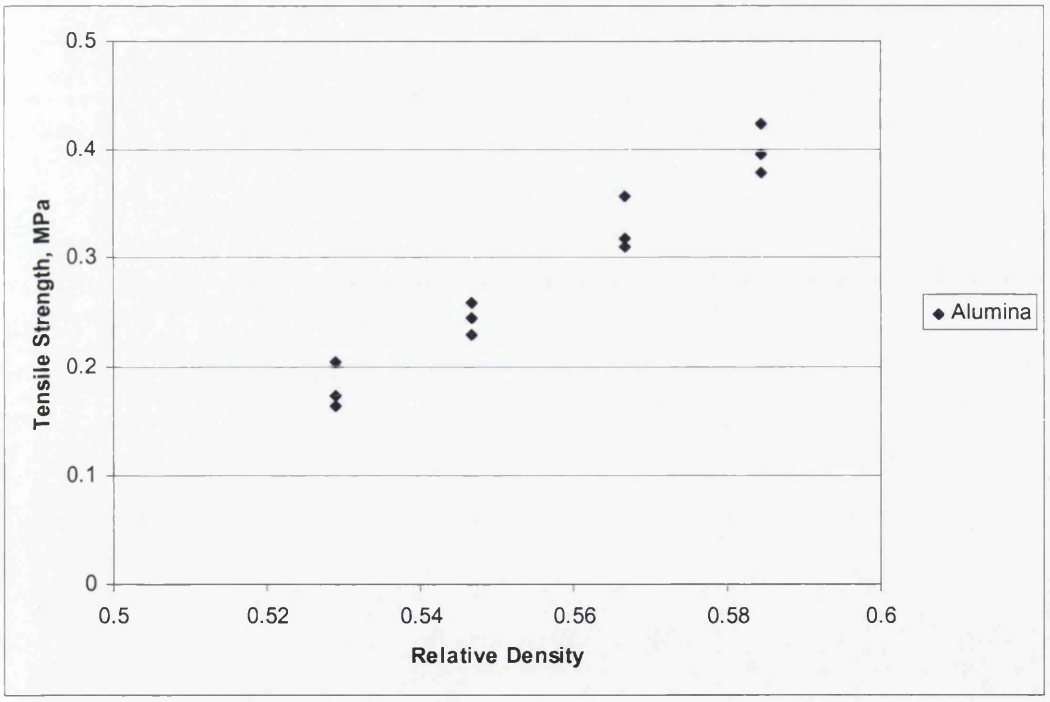

Figure 6.34 Cohesion parameter, Alumina

A linear increase in strength was observed for the density range considered. The results of the Brazilian disc test for the Alumina powder are compared to those from the three point bending in Figure 6.35

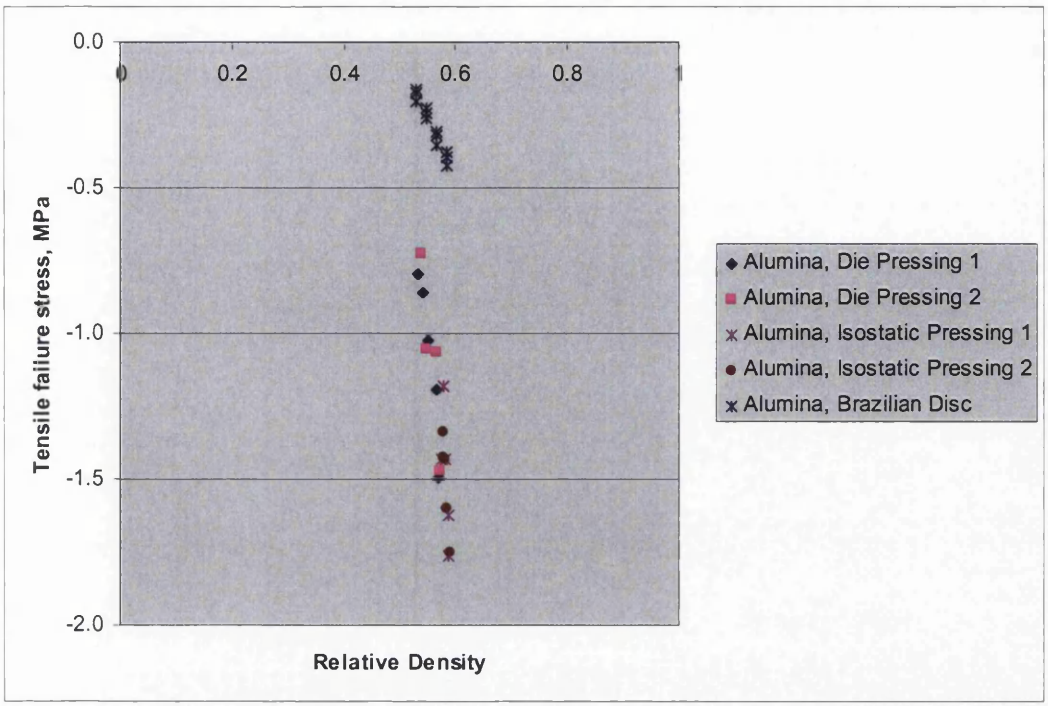

Figure 6.35 Tensile failure stress. Brazilian Disc and Three Point Bending Test

Both the Brazilian disc and the three point bending tests result in tensile failure. However, the tensile strength values for Alumina powder tested by both methods were different (~0.2-0.4 MPa during the Brazilian disc test and ~0.7-1.7 MPa during the three point bending test). One of the reasons behind this is the different density of the areas of the compact where failure originated for the different tests. During the three point bending tests the highest stresses were achieved on the bottom surface of the specimen. The compacts were placed so that the strongest surface, which was the top surface during compaction, was the bottom surface in the three point bending test. In contrast, during the Brazilian disc test failure originates inside the compact. From experience it is known that local densities are higher along the "skin" of the compact, where greater densification was achieved due to friction forces. Here the failure occurs over a vertical section of the compact and the crack originates at the less dense regions in the core of the compact.

It is also important to note that for the bending theory equations used in this work to be accurate certain assumptions need to be met. Among these is the requirement for the material to be homogenous and to have the same modulus of

elasticity in tension and compression. As was mentioned previously, the material was not completely homogenous and the elastic properties in tension and compression may also be different due to the nature of material.

6.4 Closure

The following different test procedures for obtaining the elastic modulus, Poisson's ratio and cohesion data in powder compacts have been considered:

- Instrumented die test
- Compression of freestanding samples
- Three point bending test
- Brazilian disc test

The instrumented die test is typically performed as part of the powder characterisation program. Its use as a method of obtaining elastic parameters has been explored. The advantage of the instrumented die test is its ability to provide data for a wide range of densities from a single test, thus reducing the cost of materials used. To achieve this, the compact needs to be pressed in stages of incremental densification, with the load being removed between each stage.

In the course of this work it was determined that some assumptions were required to enable the use of simplified data reduction techniques for the instrumented die tests. These result in Young's modulus values which appear overestimated in comparison to the unconstrained compression tests. The friction cannot be neglected as it impedes complete recovery of the compact and affects the reduction procedure. This effect may be reduced through generous lubrication of the die walls.

Freestanding compression tests can be readily used to obtain the Young's modulus. However, a range of tests needs to be performed for the whole spectrum of possible compact densities to be considered. These tests can only be performed over a limited range of densities – typically greater than 5.5g/cc for ferrous powders. One of the benefits of this method is the ability to use a simple cylindrical geometry for the samples.

It is important to note, however, that as the compact is not constrained radially it is free to expand under compression. This radial expansion will depend on the compact material and density and may not be significant in all cases. However, for a more accurate measurement of axial stress, monitoring of the radial strain is required. Such strain measurements will need to be recorded continuously throughout the test to be effective and will require accurate resolution, possibly through optical means.

Three point bending tests were also found to be a suitable tool for studying elastic parameters of the compacts. These require bar shaped samples, tooling for manufacture of which may not be readily available. As these tests have shown, the loads involved can be very low, depending on the materials used. Thus, a balance will have to be met between the sensitivity of the equipment used and the sample dimensions, which will determine the sample strength for a given material. For less dense materials the loads achieved may be outside the sensitive range of the load cell used. On the other hand it is desirable to test slender bars, as those are more compliant with the assumptions of simple beam theory. There will also be less top to bottom density variation in slender bars, thus reducing the effects of anisotropy. To further reduce anisotropy double ended compaction kinematics should be used.

The Brazilian disc test was used to obtained the cohesion parameter necessary for modelling of the ejection stage in the numerical code introduced in Chapter 3. In the case of the Alumina powder the cohesion parameter could be readily expressed by a linear function.

Both the Brazilian disc and the three point bending tests produce tensile failure. However, the results were not the same and the differences may be attributed to the non-homogenous nature of the material, this requires further investigation.

Chapter 7 Ejection

7.1 Introduction

The ejection phase of the PCM process involves the removal of the green compact from the die. This is typically achieved by either pushing it out with the punch set (both upwards and downwards ejection directions are commonly used) or by lowering the die and thus revealing the compact, which rests on the bottom punch set. In this work the compacts pressed during the instrumented die test were ejected upwards by raising the bottom punch, while the compacts produced in the course of the shear plate experiment were pushed out downwards into the space opened up by the removal of the sliding block.

7.2 Ejection – instrumented die

7.2.1 Introduction

During the instrumented die tests the stress state during ejection was recorded. Figure 7.1 shows an example of the evolution of the axial and average radial pressures during the compaction and ejection of a ferrous powder compact from the instrumented die. In this instance, the radial pressure has been computed simply by applying the calibration equation, derived in Section A2.1 of Appendix 2, to the average readings of the strain gauges, a more rigorous treatment of this measurement will be presented later in Section 7.2.2. The pressure loss between the top punch pressure (Axial Pressure) and the bottom punch pressure during the compaction stage was due to powder-die friction and the use of the instrumented die to measure friction was discussed in Chapter 4. During the unloading stage (~160s-280s) the top punch load was removed, but a residual load on the bottom punch remained, as friction forces prevented the compact from moving freely in the die.

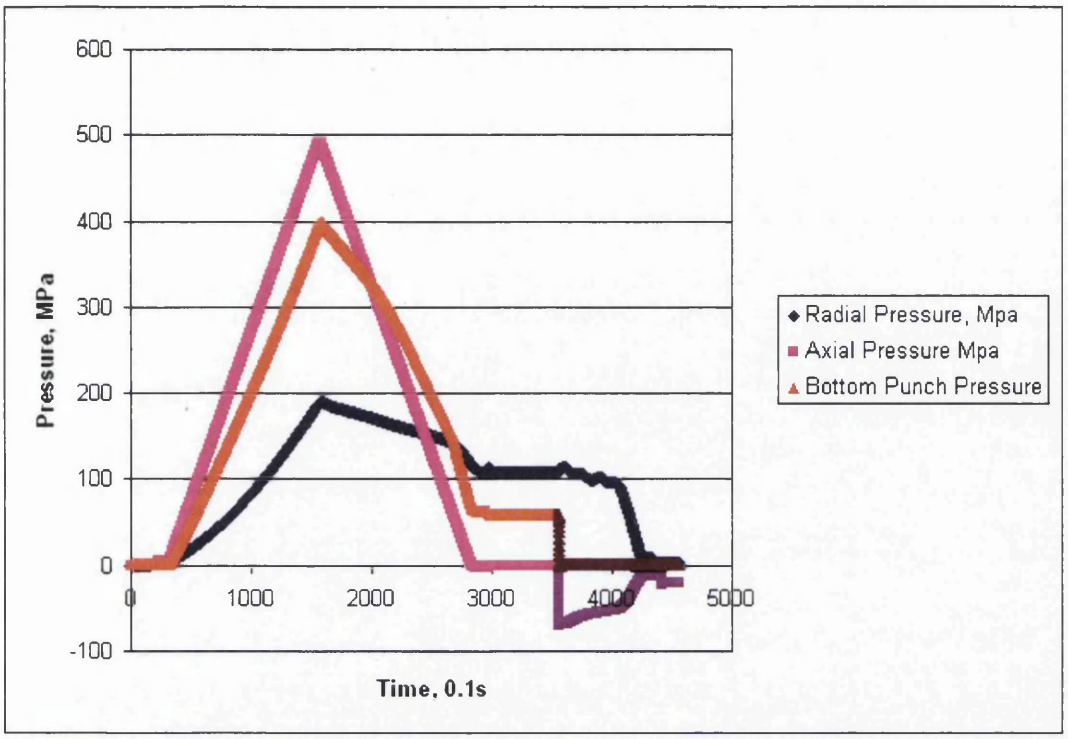

Figure 7.1 Pressures during compaction and ejection

Prior to the ejection phase the press cross-head was disconnected from the top punch and connected to the bottom punch. Thus, the axial pressure during ejection is the pressure acting on the bottom punch. The original "bottom punch pressure" data, was obtained via a load cell located underneath the bottom punch, which unloaded as the ejection started and the bottom punch started to rise. The ejection phase, which started around 350s into the test, is shown in more detail in Figure 7.2, where the average bottom axial and radial pressures are plotted against displacement. The compacts were out of the die at approximately 77mm displacement.

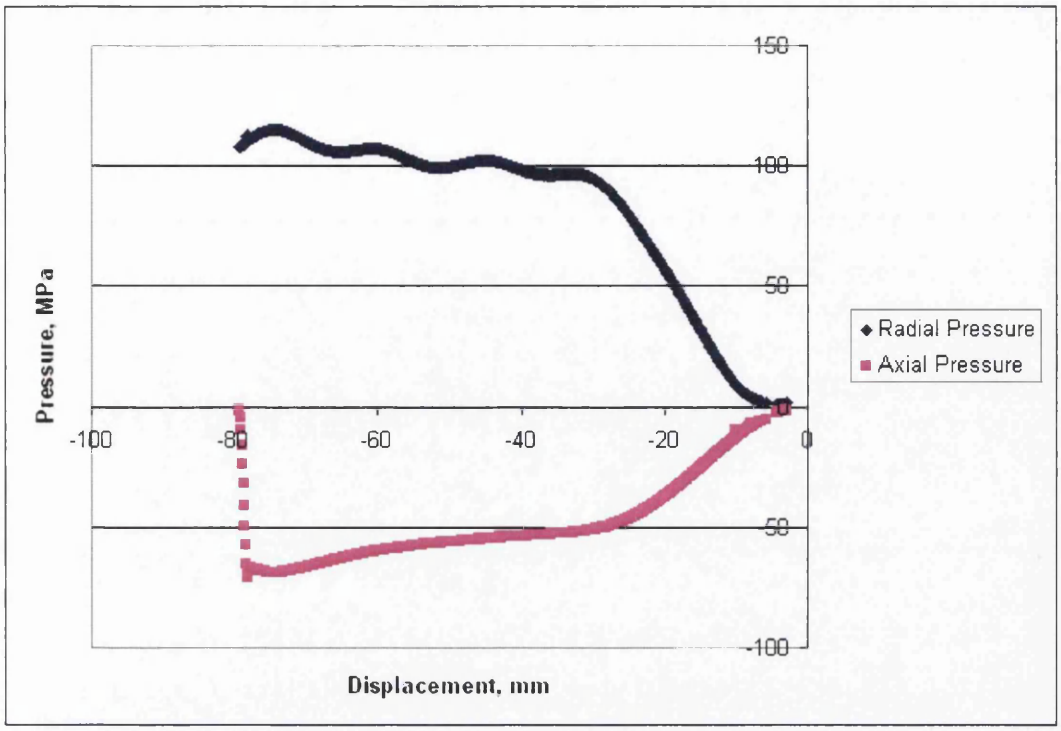

Figure 7.2 Pressures during ejection

7.2.2 Radial stress measurement during ejection

It is important to note that the problem of measurement of the radial stress during ejection is not trivial. Two primary issues can be identified.

Firstly, there are oscillations in the radial stress data, which are induced by the relative position of the compact and the strain gauge bridges on the die. While the calibration procedure outlined in Appendix 2 is effective for the complete range of heights of the compacts being tested some sensitivity to the position of the compact relative to the strain gauges cannot be avoided. As the compact travels through the die during the ejection stage, i.e. if it is relatively short (e.g. 20mm), there will be positions in the die where only one strain gauge will be directly opposite the compact. This effect is reduced for tests of the longer compacts, where the magnitude of these oscillations is lower.

This can be demonstrated by comparing the ejection data of the 10cc compacts (i.e. those created with 10cc of loose powder) to that of the longer 15cc samples, see Figure 7.3. The magnitude of the radial stress oscillations is smaller for the

longer compacts. Note that the frequency of the oscillations remains the same and is governed by the distance between the strain gauges.

While the radial pressure was only slightly higher for the 15cc compacts the axial pressure needed to eject it was considerably higher as the greater length meant higher forces.

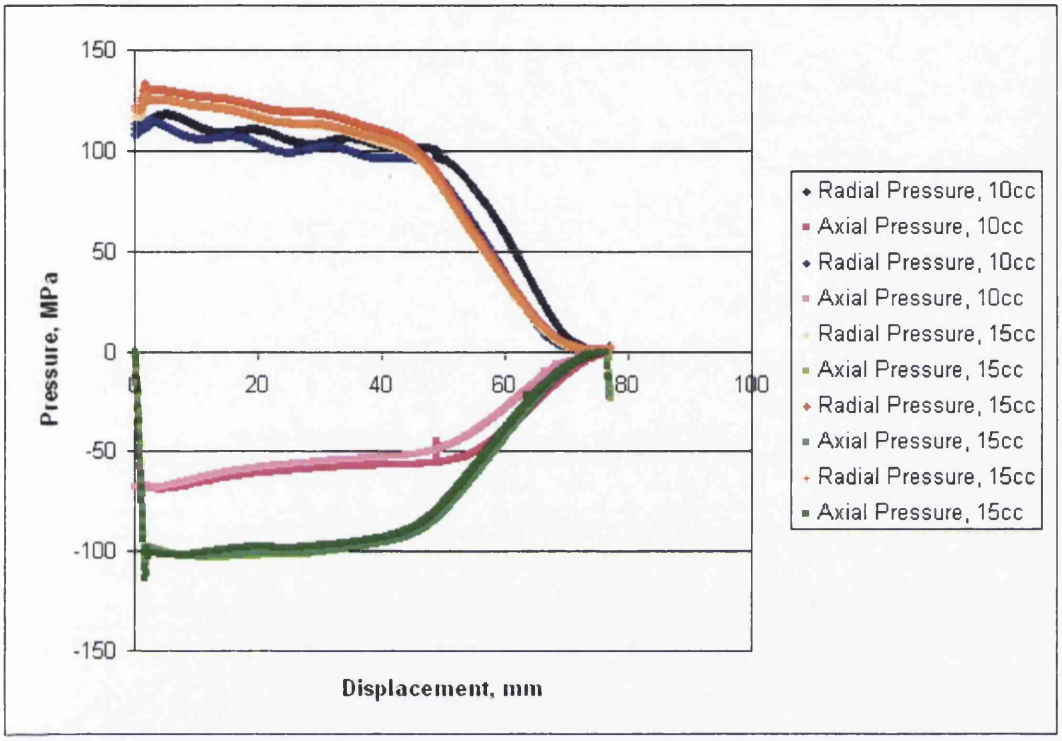

Figure 7.3 Pressures during ejection. 10cc and 15cc compacts

The second issue is that of the applicability of the calibration procedure outlined in Section A2.1 of Appendix 2 to the ejection stage. It is unrealistic to expect the calibration function to remain accurate as the bottom punch is raised and the relative position of the compact in the die changes. To counter any errors which may appear, an investigation into the effect of the bottom punch position was conducted, see Appendix 2 Section A2.2. The correction function thus obtained will be used alongside the original calibration function in the remainder of this chapter.

7.2.3 Ejection of compacts with different density

Figure 7.4 shows the radial and axial stress during the ejection of ferrous compacts of the same length but different density. The die was filled with a precise amount of powder by weight to achieve the desired density at a set

displacement. The displacement was set to result in 18mm tall compacts (as these have an aspect ratio of 1) and the target densities were 5.5, 6, 6.5 and 7g/cc. Six compacts were manufactured at each density, ensuring repeatability of the experiment. Although each of the compacts was pressed to the same punch displacement, small variations in compact height (within 0.5mm) were observed – this explains the variation within the batches.

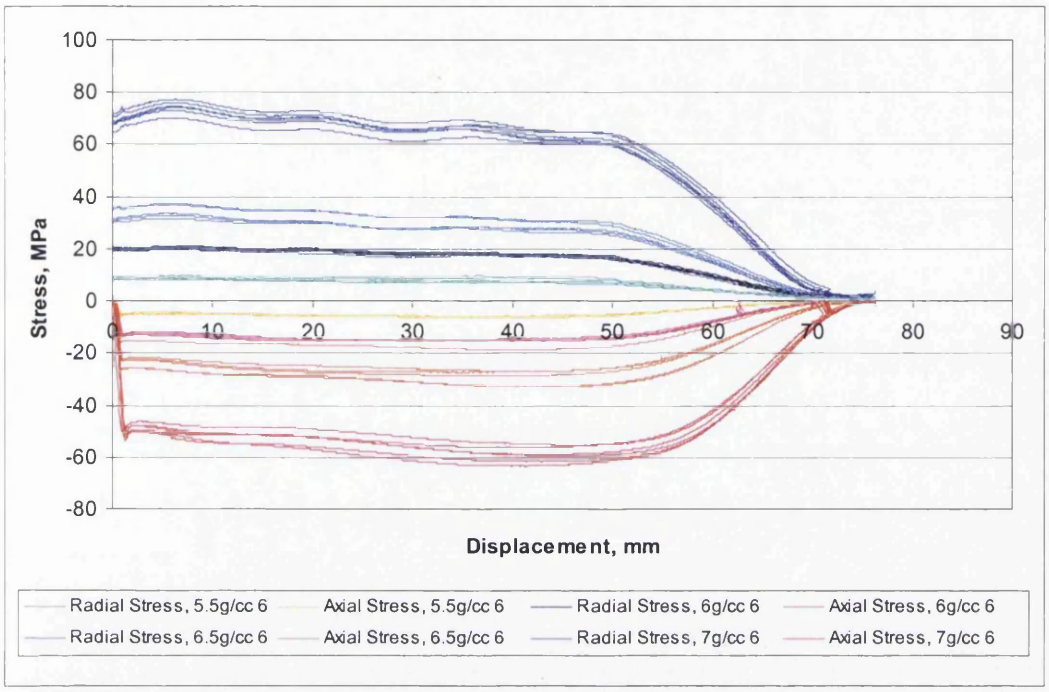

Figure 7.4 Radial and Axial pressure during ejection, ferrous powder, ~18mm high compacts.

When using the correction function presented in Appendix 2 Section A2.2 the radial stress values appear as shown in Figure 7.5 (only one test for each density is presented for clarity).

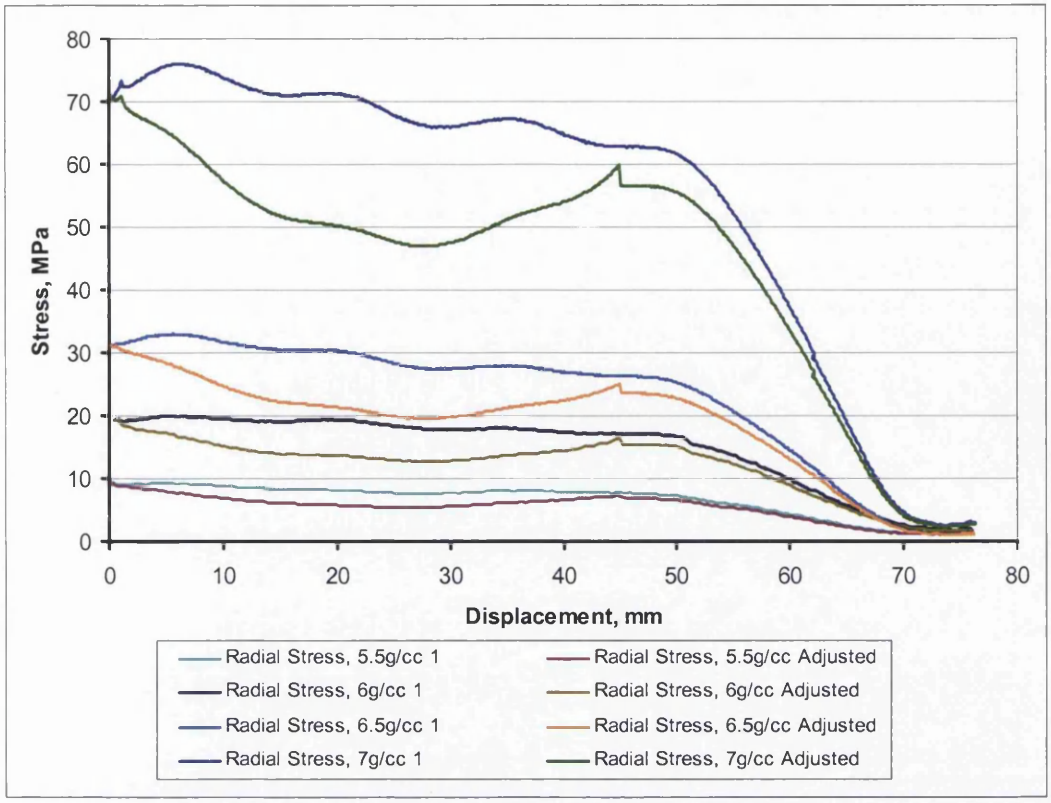

Figure 7.5 Radial pressure during ejection, ferrous powder, ~18mm high compacts, including corrected radial stress values.

The trends observed in Figure 7.4 were very consistent within each batch of six compacts. There were also trends common to all batches. As mentioned previously, the oscillations in radial stress were induced by the interpretation procedure. However, the trend of reduction in radial stress between 0 and 50mm displacement represents a physical effect and was present for all samples. The compacts were still fully within the die at that point and the reduction can be explained by partial relaxation of the compact[2]. During the unloading stage relaxation took place until friction forces prevented any further recovery. At that moment the friction was static. However, once the ejection phase began and the compact started moving through the die the friction became dynamic and decreased, allowing for further relaxation to take place.

[2] Relaxation was not associated with die geometry since the die was measured and found to be parallel within 0.02mm

The axial pressure, required to facilitate the ejection of the compact, peaked at the beginning of ejection, indicating the higher static friction and then after an initial reduction, began to rise again until approximately 50mm of the compact had been exposed. At this point the compact started to approach the end of the die and the radial pressure reduced to zero. The likely cause of this rise in axial pressure was the exhaustion of the lubricant layer with distance travelled. As the lubricant remained deposited on the lower sections of the die its effectiveness reduced and it was less able to reduce the friction at the higher part of the die. This observation is in agreement with findings in (Doremus, Toussaint et al. 2001). This is particularly important in cases when the ejection travel is long compared to the compact height, such as for hardmetal compacts, where large compression ratios are used, or when a long die is not completely filled thus resulting in shorter compacts.

Similar trends in axial stress were reported for iron powders in (Gethin, Ariffin et al. 1994) – a small peak indicating static friction was observed. For shorter compacts the ejection load reduced after reaching the initial static value, but for the longer compacts, where greater travel distance was required to remove the compacts from the die, the ejection load increased gradually until the compact approached the top of the die.

7.3 Ejection – floating die shear plate

In contrast to the instrumented die tests the ejection, after the shear plate tests, was performed downwards. Below follows the analysis of ejection of compacts after the high pressure floating die shear plate tests were performed.

Figure 7.6 shows the ejection loads for the compacts compacted to 150kN and which underwent the sliding tests at 40, 50, 75 and 100kN. The compacts were already at the bottom of the die (as was required for the sliding test) and thus began to emerge from the die as soon as the ejection process began. Although these compacts underwent the sliding test at different normal loads there appears to be good agreement in loads required for ejection between the samples. Note that due to slow data acquisition rate (1Hz) it was not possible to accurately capture the peak static load at the start of ejection.

The relative loads required to eject compacts with varying amounts of lubrication may appear to differ from expectations, however an exact comparison is not possible. The reason for this lies in the filling procedure for these tests. The compacts were made from 10cc of respective powder. However, the addition of admixed lubricant actually improved the powder flow and for lubricated compacts the fill density was between 3.5 and 3.6 g/cc, while for powder without lubricant the fill density was between 3.1 and 3.2 g/cc. The final compacts thus had different heights and densities and were subjected to different amounts of radial pressure. Thus, despite having a lower final density, the non-lubricated compacts were shorter as less material entered the die. They were also subjected to a lower value of radial stress (this was not measured but can be expected as more axial stress was consumed by frictional losses). Thus, in spite of having a higher coefficient of friction less force was required to facilitate their ejection. It is interesting to observe a reduction in gradient of the ejection load for non-lubricated compacts past the 10mm displacement. This trend was even more visible for the compact which underwent the sliding test at 150kN as well as being pressed to 150kN and for the compact pressed and tested at 200kN, see Figure 7.7. Galling was observed for these compacts and it is likely that the onset of galling was the mechanism behind the gradient change for the non-lubricated compacts pressed to 150kN and tested at40-100kN in Figure 7.6.

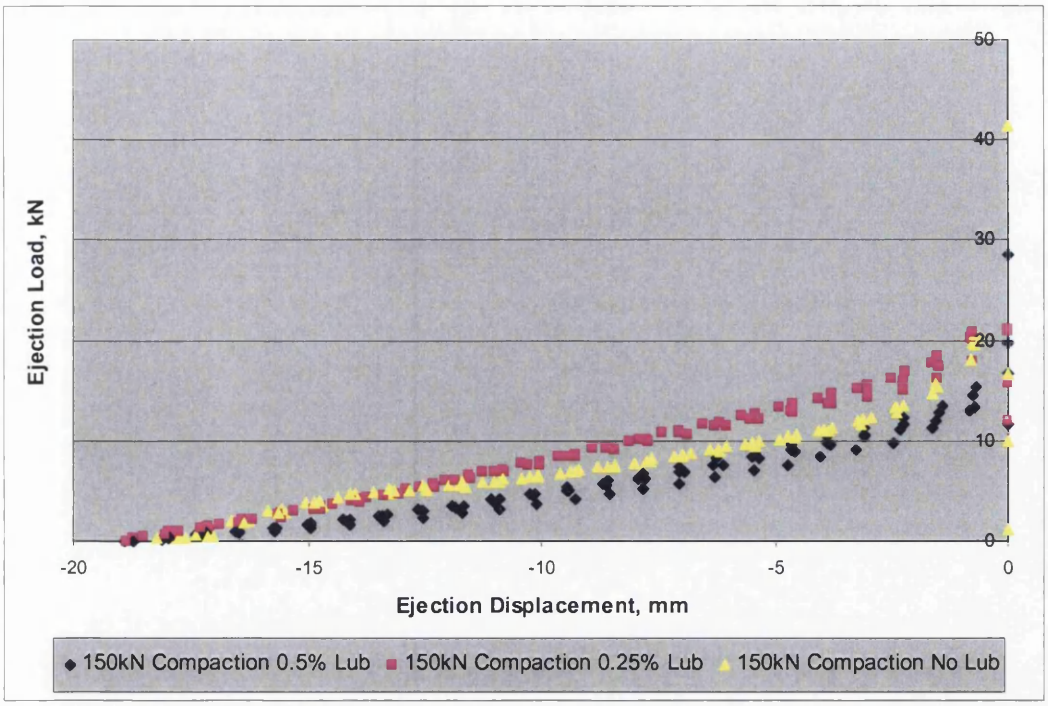

Figure 7.6 Ejection from the floating die shear plate apparatus. Compacts pressed to 150kN. Sliding tests at 40-100kN normal load.

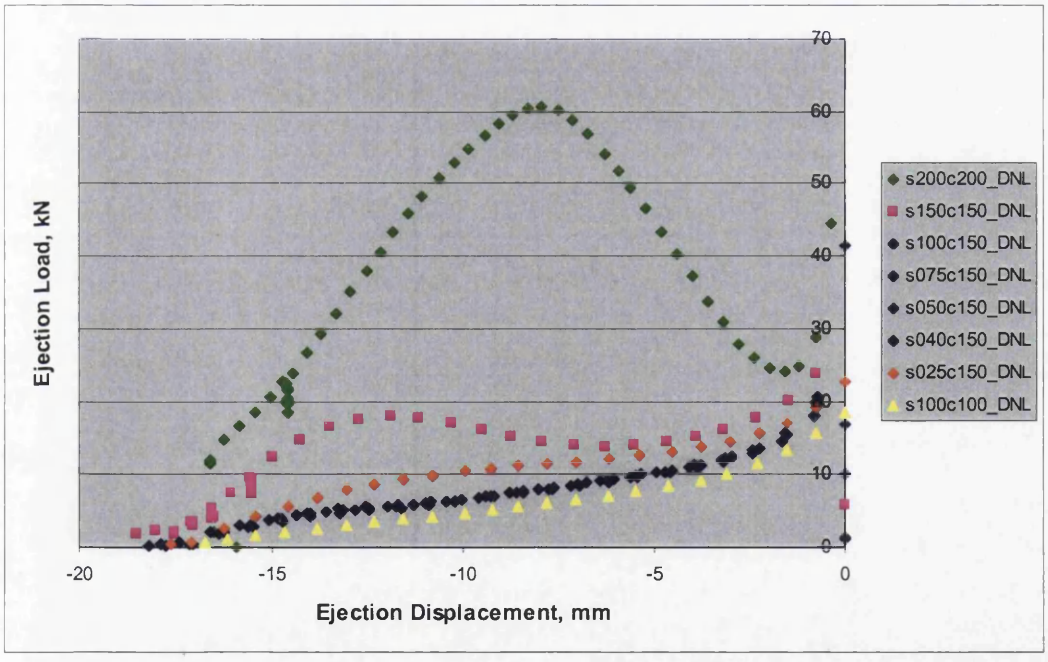

Figure 7.7 Ejection from the floating die shear plate apparatus, non-lubricated powder. In series labels s### denotes the normal load in kN during the sliding test, c### denotes the compaction load in kN.

For the lubricated compacts in Figure 7.6 the fill conditions were similar. It is therefore appropriate to consider the ejection loads required. As expected the

lower friction coefficient for the more lubricated powders resulted in lower ejection forces being required.

7.4 Split die

While it is relatively easy to record the stress state during ejection, the continuous measurement of compact height is a lot harder to achieve. This is due to one of the punches not being in contact with the surface of the compact after the unloading stage. In the case of the instrumented die used in this work the compacts were ejected through the top. Thus, at the end of compaction the top punch was removed from the die and the height of the compact during the ejection process could not be measured.

Such measurements, however, are needed in order to understand how the loads acting on the compact during ejection affect it throughout the ejection phase. For example, additional densification can occur during ejection. This is particularly likely if single ended kinematics are used and ejection takes place in the opposite direction to compaction, especially in the case of low density components.

It may also be valuable to be able to collect other information immediately after compaction before any ejection has taken place and from different periods of the ejection stage: such as compact surface condition and density. These typically cannot be obtained until the ejection is complete.

To allow for detailed analysis of the compact before ejection, or after the compact has been ejected a certain distance, a split die has been manufactured, see Figure 7.8. It has the same internal dimensions, material and surface finish as the instrumented die used in the current chapter and in Chapters 4 and 6 and can be mounted in its place. It consists of two halves, which are held together by bolts and can be separated after compaction before any ejection has taken place. It is also possible to obtain compacts after partial ejection. Due to the die's thickness it was impossible to instrument it with strain gauges in the manner seen on the instrumented die and thus no radial stress data could be recorded. This extra thickness was required to provide sufficient space for the bolts and to ensure sufficient strength of the join.

Figure 7.8 Split die

7.5 Split die – Results

The split die was used to explore the questions about compact relaxation raised in Section 7.2 where the radial stress was seen to reduce as the compact travelled through the die. The split die was used to study the differences in height of compacts ejected over different ejection distances in an attempt to identify if ejection promoted axial recovery of the compact. The tests were performed for both lubricated and non lubricated powders and at a range of different compaction loads. In each case the die was filled with a precisely measured mass of powder to ensure accurate comparison. Once the compaction stage was complete the compacts were unloaded and then ejected over a desired distance (or not ejected in some cases). The die was then removed from the press and its two halves were separated. The compact was then extracted and its height measured in two perpendicular orientations with digital callipers accurate to 0.02mm. The heights of these compacts are summarised in Table 7.1.

Table 7.1 Compact height comparison for different ejection distances

Ejection distance, mm	0.5% Lubricant			No Lubricant	
	Compaction Load, kN				
	75	**125**	**141**	**75**	**125**
0	22.25	20.34	19.83	20.15	17.985
20		20.45			18.14
40	22.27	20.41	19.91	20.25	
60/full		20.53			

Surprisingly, it was consistently found that the compacts which were ejected over a greater distance were longer than those which did not undergo ejection, or were ejected over a shorter distance. The only exception being the pair of lubricated compacts pressed to 125kN and ejected over 20 and 40mm respectively. These however were both consistently longer than the compact which did not undergo ejection and shorter than the compact which was ejected over the complete distance.

As mentioned in Section 7.2 the expected cause of this difference in compact length was the reduction in friction force during the change from static to dynamic friction as ejection begun, allowing for additional relaxation. This initial recovery then resulted in lower radial stress and thus promoted further recovery.

7.6 Closure

Data from the ejection stages of the instrumented die and the floating die shear plate experiments was analysed.

Measurement of radial stress during ejection is difficult, but a correction function was suggested.

During the ejection from the instrumented die trends indicating axial recovery were observed. These were confirmed with a series of split die tests.

The friction coefficient during ejection was found to increase with distance travelled. This was likely caused by exhaustion of lubricant, as indicated elsewhere in literature.

Analysis of ejection from the shear plate apparatus showed trends indicative of galling at high pressures for the non-lubricated powder. The ejection forces could not be compared between powders with and without lubricant because of different fill conditions. For lubricated powders the ejection forces were lower for powders with a greater amount of lubricant.

The split die was introduced and used to confirm the observations on compact relaxation. It can also be used for surface or density analysis of non-ejected or partially ejected compacts, although this was not done at this time.

Chapter 8 Conclusions and recommendations

In this thesis work has been undertaken in three main areas:

- The effect of fill density distribution on green density in pressed compacts
- Friction measurement and friction mechanisms with regard to loading conditions and lubrication
- Measurement of parameters relevant to unloading and ejection modelling and investigation into ejection mechanisms

The following sections draw out conclusions and propose recommendations for future work on the above topics.

8.1 The effect of fill density distribution on green density and tooling loads

A numerical investigation into the effect of fill density distribution on green density in powder compacts has been performed. In the course of the investigation three powders of different types (ferrous, hard metal and ceramic) were characterised – i.e. the parameters needed to represent the materials in the numerical simulation have been obtained. A simple bush geometry and two flange geometries with internal and external flange have been considered with a range of likely fill density distributions. These were derived following a review of work in the field of die filling, with both general behaviour during die fill and relevant specific cases being considered. The investigation was performed by carrying out compaction simulations of test cases with different fill density distribution but with identical mass. The resulting green densities and tool forces were then compared.

Density non-uniformity in the axial direction did not affect the final density for the simple bush geometry case. However, the final density distributions for flanged geometries (both internal and external flanges) proved to be less uniform in cases of a non-uniform fill density, typically rising from 8-16% difference between minimum and maximum densities in the compact to 28-35%. Such decreased homogeneity is likely to negatively impact sintering, particularly for

hard metal parts, where high levels of shrinkage are typical. At the same time, lower minimum densities mean weaker components even for ferrous parts, where shrinkage is low by comparison.

Greater quantities of powder in the upper regions of the flanged components also resulted in increased loads on the top punches (up to 36%) and on the raised lower punch (up to 64%), in the inner region for the Modnet geometry and the outer for the Dienet case. This leads to higher tool wear and also limits the final densities achievable on a press with a given loading capacity.

While some material based variations were evident, particularly in the actual values of density and load variations (e.g. the higher compression ratio for the tungsten carbide powder leading to a greater increase in tool loads for the non uniform cases), overall good agreement in trends was observed. This confirmed that the green density variations were caused by the different fill density distributions, highlighting the importance of the filling stage of the PCM process.

With the development of die filling models future work could take the output of fill simulations as the input conditions for the numerical simulation of the compactions stage. Thus, the more complex and realistic fill density variations could be explored for each specific application. This would allow informed practical decisions on tool kinematics or for a different filling mode to be suggested.

8.2 Friction measurement

A novel floating die modification to the proven shear plate apparatus has been proposed. A linear bearing ensures complete transmission of the axial pressure to the bottom of the compact and therefore the target surface. The equipment also allows independent control of compaction and normal loads. The repeatability of the modified equipment has been tested and was found to be very good. It was then compared to the instrumented die equipment and good agreement was observed. The ability to independently control the compaction and normal loads can be used to recreate the loading conditions of the instrumented die test.

The floating die shear plate apparatus was then used in a series of experiments assessing the effectiveness of different admixed lubricant quantities under a wide range of both compaction and normal loading conditions. Simultaneously, analysis of the effect of compact density and normal stress on friction was performed.

The results confirmed a correlation between the rise in normal load and reduction in friction for compaction pressures below 300MPa. For compacts pressed at 583MPa the friction coefficient was found to rise as the normal load increased.

A correlation was also found between the compact density and the friction, which was found to reduce at higher densities.

As regards the lubricant performance it was established that at higher loads there is no noticeable benefit in increasing lubricant content above 0.5%. It was also observed that even the addition of small quantities of lubricant was often sufficient to significantly reduce friction.

The sliding surfaces of the compacts were examined using a white light interferometer and a scanning electron microscope with EDX capability. The examination revealed a more open structure for compacts pressed at lower compaction loads. Higher normal loads during the sliding stage of the test resulted in a more polished appearance of the contact surface with a smaller area occupied by pits.

A brief study on die wall lubrication showed the significant impact that die lubricant plays on friction. A reduction in friction of between 27% and 58% was observed for a range of powder mixtures and loading conditions. A method of measuring the die wall lubricant coating was proposed, based on an analysis of white light interferometer scans.

In future the floating die shear plate equipment can be used to create a map of friction coefficients for the complete range of compaction and normal loads,

providing accurate friction data for the numerical simulations of the compaction, unloading and ejection stages.

The EDX technique can be used to study the lubrication mechanisms in compaction if a non-carbon based chemically distinctive lubricant is used.

Further experiments with a more appropriate die wall lubricant and lubricant deposition technique will give a better indication of friction coefficient values in industrial applications.

8.3 Measurements for unloading and ejection

The different test procedures for obtaining the elastic modulus, Poisson's ratio and cohesion data in powder compacts have been explored.

The instrumented die test was found capable of producing elastic data for a range of densities from a single compact if incremental densification and unloading were used. However, more accurate reduction procedures are needed as the assumptions required for the simpler techniques were not realistic. For the reduction procedures used the test was found to overestimate the elastic modulus when compared to the unconstrained uniaxial compression test and the reasons for this were explored.

Freestanding compression tests can be readily used to obtain the Young's modulus. However, a series of tests is required to cover the full range of densities. The test cannot be used at low densities as a free standing compact is required.

Three point bending tests were performed for two ceramic powders and were found to be suitable for measuring the elastic modulus of the compacts. For the two materials tested further isostatic pressing of green compacts had the same effect as an increase in density. Tensile strength was also measured.

The Brazilian disc test was used to obtain the cohesion parameter necessary for modelling the ejection stage for Distaloy AE and Alumina powders. In the case of

the Alumina powder the cohesion parameter could be readily expressed by a linear function.

Measurement of the radial stress during the ejection phase using the instrumented die has been explored and a correction procedure was suggested for the strain gauge calibration. The stress state during ejection has been explored and a split die has been manufactured to investigate axial recovery during ejection.

Future work should concentrate on developing an accurate data reduction procedure for elastic measurements using the instrumented die test. Such procedure should rely on realistic assumptions and account for powder-die friction. The split die can be used to explore the properties and surfaces features of the compacts obtained at different stages of ejection.

References:

Ariffin, A. K., D. T. Gethin, et al. (1998). "Finite element simulation and experimental validation for multilevel powder compact." Powder Metallurgy **41**(3): 189-197.

Ball, W. G., P. F. Hibner, et al. (1997). "New Die Wall Lubricant System." International Journal of Powder Metallurgy **33**(1): 23-32.

Bocchini, G. F. (1995). "Friction Effects In Metal Powder Compaction Part One - Theoretical Aspects,." Advances in Powder Metallurgy & Particulate Materials **1**(2).

Bonnefoy, V., P. Doremus, et al. (2003). "Investigations on friction behaviour of treated and coated tools with poorly lubricated powder mixes." Powder Metallurgy **46**(3): 224-228.

Brewin, P. and L. Federzoni (2006). "Dienet: conclusions and achievements." Powder Metallurgy **49**(1): 8-10.

Briscoe, B. J. and N. Ozkan (1997). "Compaction behaviour of agglomerated alumina powders." Powder Technology **90**: 195-203.

Briscoe, B. J. and S. L. Rough (1998). "The effects of wall friction on the ejection of pressed ceramic parts." Powder Technology **99**: 228-233.

Burch, S. F. (2004). Unpublished results from the MPM5.2 project, AEA Technology.

Burch, S. F., J. H. Tweed, et al. (2004). Measurement of density variations in Compacted Parts and Filled Dies using X-ray Computerised Tomography. Powder Metallurgy World Congress & Exhibition PM2004.

Cameron, I. (2000). Powder Characterisation for Compaction Modelling. Department of Mechanical Engineering. Swansea, University of Wales.

Cameron, I. M., D. T. Gethin, et al. (2002). "Friction measurement in powder die compaction by shear plate technique." Powder Metallurgy **45**(4): 345-353.

Cocks, A. C. F. (2005). SEM images of powders for MPM5.2 Project.

Cocks, A. C. F., L. Dihoru, et al. (2001). A fundamental study of die filling. EURO PM2001: 2001 European Congress and Exhibition on Powder Metallurgy, Nice, France.

Coube, O., A. C. F. Cocks, et al. (2005). "Experimental and numerical study of die filling, powder transfer and die compaction." Powder Metallurgy **48**(1): 68-76.

Coube, O. and H. Riedel (2000). "Numerical simulation of metal powder die compaction with special consideration of cracking." Powder Metallurgy **43**(2): 123-131.

Cunningham, J. C., I. C. Sinka, et al. (2004). "Analysis of tablet compaction. I. Characterization of mechanical behavior of powder and powder/tooling friction." JOURNAL OF PHARMACEUTICAL SCIENCES **93**(8): 2022-2039.

Demetry, C. a., F. S.Souto, et al. (1998). "Tactile sensing of density uniformity in powder beds after die filling." Powder Technology **99**: 119-124.

Denny, P. J. (2002). "Compaction equations: a comparison of the Heckel and Kawakita equations." Powder Technology **127**: 162-172.

Doremus, P. (2002). Characterisation of Distaloy AE, WC-Co, Zirconia. Input data, European thematic network Dienet.

Doremus, P., F. Toussaint, et al. (2001). "Investigation of iron powder friction on tungsten carbide tool wall." Powder Metallurgy **44**(3): 243-247.

Dunkley, J. (2005). "Euro PM 2005: cautious optimism in Prague." Powder Metallurgy **48**(4): 309-312.

Dynamic-Ceramic Ceramic PCM components.

EPMA (2004). www.epma.com.

Eurotungstene (2006). www.eurotungstene.com.

Fleck, N. A., L. T. Kuhn, et al. (1992). "Yielding of metal-powder bonded by isolated contacts." Journal of Mechanics and Physics of Solids **40**(5): 1139-1162.

Ge, R. (1991). International Journal of Powder Metallurgy **27**(3): 216-221.

German, R. M. (1994). Powder Metallurgy Science. Princeton, Metal Powder Industries Federation.

German, R. M. (2004). "Green body homogeneity effects on sintered tolerances." Powder Metallurgy **47**(2): 157-160.

Gethin, D. T., A. K. Ariffin, et al. (1994). "Compaction and ejection of green powder compacts." Powder Metallurgy **37**: 45-52.

Gethin, D. T., R. W. Lewis, et al. (1995). Modelling Compaction and Ejection Processes in the Generation of Green Powder Compacts. ASME International Mechanical Engineering Congress and Exposition, San Fransisco.

Guyoncourt, D. (2004). Review of potential measurement methods for powder mixedness. A report produced for DTI and the MPM5.2 Industrial Advisory Group.

Guyoncourt, D. M. M. (2005). Measurement of Friction on Part Ejection, AEA Technology Report.

Guyoncourt, D. M. M. and J. H. Tweed (2003). Measurement of powder flow.

Guyoncourt, D. M. M., J. H. Tweed, et al. (2001). "Constitutive data and friction measurements of powders using instrumented die." Powder Metallurgy **44**(1): 25-33.

Haeckl, R. S. (1968). "Automatic Lubrication of Powder Compacting Punches and Dies." International Journal of Powder Metallurgy **4**(1): 13-23.

Haskins, J. and W. Jandeska (1998). Powder flow and die filling studies using computed tomography. International Conference and Exhibition on Powder Metallurgy and Particulate Materials, Las Vegas, NV, USA.

Heckel, R. W. (1961). Density-Pressure Relationships in Powder Compaction. **221:** 671-675.

Hentschel, M. L. and N. W. Page (2001). Effect of particle shape on the elastic properties of powders during compaction. The 7th International Conference on Bulk Materials, Storage, Handling and Transportation, Newcastle, Australia.

Hirschhorn, J. S. (1969). Introduction to Powder Metallurgy. New York, American Powder Metallurgy Institute.

Hjortsberg, E. and B. Bergquist (2002). "Filling induced density variations in metal powder." Powder Metallurgy **45**(2): 146-153.

ISO3312 (1987). "Sintered metal materials and hardmetals - Determination of Young modulus."

ISO3995 (1985). Metallic powders -- Determination of green strength by transverse rupture of rectangular compacts.

ISO7438 (1985). Metallic materials - bend test.

Kachrimanis, K. and S. Malamataris (2004). "'Apparent" Young's elastic modulus and radial recovery for some tableted pharmaceutical excipients." European Journal of Pharmaceutical Sciences **21**: 197-207.

Kawakita, K. and K.-H. Lüdde (1971). "Some considerations on powder compression equations." Powder Technology **4**(2): 61-68.

Kehl, W., M. Bugajska, et al. (1983). "Internal or die wall lubrication for compaction of Al powders?" Powder Metallurgy **26**(4): 221-227.

Kim, K. T. and J. S. Kim (1998). "Stage 1 compaction behaviour of tool steel powder under die pressing." Powder Metallurgy **41**(3): 199-204.

Kraft, T. and H. Riedel (2002). "Numerical simulation of die compaction and sintering." Powder Metallurgy **45**(3): 227-231.

Kreyszic, E. (1988). Confidence Intervals. Advanced Engineering Mathematics. New York, John Wiley & Sons, Inc: 1248-1257.

Leopold, P. M. and R. C. Nelson (1965). "The Effect of Die-Wall Lubrication and Admixed Lubricant on the Compaction of Sponge-Iron Powder." International Journal of Powder Metallurgy **1**(3): 37-44.

Li, Y., H. Liu, et al. (1996). "Wall friction and lubrication during compaction of coal logs." Powder Technology **87**: 259-267.

Li, Y. Y., T. L. Ngai, et al. (2002). "Effect of die wall lubrication on warm compaction powder metallurgy." Journal of Materials Processing Technology **129**: 354-358.

Lordi, N. G., H. Cocolas, et al. (1997). "Analytical interpretation of powder compaction during the loading phase." Powder Technology **90**: 173-178.

Malamataris, S., T. Hatjichristos, et al. (1996). "Apparent compressive elastic modulus and strength isotropy of compacts formed from binary powder mixes." International Journal of Pharmaceutics **141**: 101-108.

Mallender, R. F., C. J. Dangerfield, et al. (1974). "The variation of coefficient of friction with temperature and compaction variables for iron powder stearate-lubricated systems." Powder Metallurgy **17**(34): 288-302.

Michrafy, A., J. A. Dodds, et al. (2004). "Wall friction in the compaction of pharmaceutical powders: measurement and effect on the density distribution." Powder Technology **148**: 53-55.

Michrafy, A., D. Ringenbacher, et al. (2002). "Modelling the compaction behaviour of powders:
application to pharmaceutical powders." Powder Technology **127**: 257-266.

Mosbah, P. and D. Bouvard (1996). "Finite element simulation of die compaction and ejection of iron powder." Advances in Powder Metallurgy & Particulate Materials **2**: 7.23-7.38.

Mosbah, P., D. Bouvard, et al. (1997). "Experimental techniques for analysis of die pressing and ejection of metal powder." Powder Metallurgy **40**(4): 269-277.

Nam, J., W. Li, et al. (2003). "Density gradients and springback: environmental influences." Powder Technology **133**: 23-32.

Niesz, D. E. (1996). Kona **14**: 44-51.

Panelli, R. and F. A. Filho (2001). "A study of a new phenomenological compacting equation." Powder Technology **114**: 255-261.

Park, C.-H., S.-J. Park, et al. (1999). "Model for uniaxial compaction of ceramic powders." Powder Metallurgy **42**(3): 269-274.

Peterson, J. E. and W. M. Small (1994). "Evaluation of metal powders using Arnold density meter and Hall flowmeter." Powder Metallurgy **37**(1): 37-41.

PM Modnet Computer Modelling Group (1999). "Comparison of computer models representing the powder compaction process." Powder Metallurgy **42**(4): 301-311.

PM Modnet Methods and Measurements Group (2000). "Measurement of friction for powder compaction modelling - comparison between laboratories." Powder Metallurgy **43**(4): 364-374.

PM Modnet Research Group (2002). "Numerical simulation of powder compaction for two multilevel ferrous parts, including powder characterisation and experimental validation." Powder Metallurgy **45**(4): 335-344.

Poquillon, D., V. Baco-Carles, et al. (2002). "Cold compaction of iron powders—relations between powder morphology and mechanical properties Part II. Bending tests: results and analysis." Powder Technology **126**: 75-84.

Procopio, A., A. Zavaliangos, et al. (2003). "Analysis of the Diametral Compression Test and its Applicability to Plastically Deforming Materials." Journal of Materials Science **38**(17): 3629-3639.

Ransing, R. S., D. T. Gethin, et al. (2000). "Powder compaction modelling via the discrete and finite element method." Materials and Design **21**: 263-269.

Sanchez, F., A. Bolarin, et al. (2001). "Effect of compaction process sequence on axial density distribution of green compacts." Powder Metallurgy **44**(4): 351-354.

Sandberg, O. and L. Jönson (2005). Properties of Powder Metallurgical and Spray Formed Tool Steels and Experiences in Powder Pressing Applications. EuroPM, Prague.

Schneider, L., D. Thomson, et al. (2003). Low & High Pressure Closed Die Compaction of Zirconia Powder, Tests carried out for European thematic network Dienet.

Schneider, L. C. R., A. C. F. Cocks, et al. (2005). "Comparison of filling behaviour of metallic, ceramic, hardmetal and magnetic powders." Powder Metallurgy **48**(1): 77-84.

Shapiro, I. (1995). "Cimpaction of Powders XII. Evaluation of Published Compaction Equations For Modeling Purposes." Advances in Powder Metallurgy & Particulate Materials **1**(2): 97-114.

Shima, S. and M. Oyane (1976). "Plasticity theory for porous metals." International Journal of Mechanical Sciences **18**(6): 285-291.

Simchi, A. (2003). "Effects of lubrication procedure on the consolidation, sintering and microstructural features of powder compacts." Materials and Design **24**: 585-594.

Sinka, I. C., J. C. Cunningham, et al. (2003). "The effect of wall friction in the compaction of pharmaceutical tablets with curved faces: a validation study of the Drucker–Prager Cap model." Powder Technology **133**: 33-43.

Solimanjad, N. (2003). "New method for measuring and characterisation of friction coeYcient at wide range of densities in metal powder compaction." Powder Metallurgy **46**(1): 49-54.

Stephens, R. C. (1993). Strength of Materials Theory and Examples. Newcastle upon Tyne, Edward Arnold.

Strijbos, S. (1977). "Powder-wall friction: The effects of orientation of wall grooves and wall lubricants." Powder Technology **18**(2): 209-214.

Sun, X.-K. and K.-T. Kim (1997). "Simulation of cold die compaction densification behaviour of iron and copper powders by Cam-clay model." Powder Metallurgy **40**(3): 193-195.

Tran, D. V., R. W. Lewis, et al. (1993). "Numerical Modelling of Powder Compaction Processes: Displacement Based Finite Element Method." Powder Metallurgy **36**(4): 257-266.

Tsukerman, S. A. (1965). Powder Metallurgy.

Turenne, S., C. Gode`re, et al. (2000). "Effect of temperature on the behaviour of lubricants during powder compaction." Powder Metallurgy **43**(2): 139-142.

Turenne, S., C. Gode`re, et al. (1999). "Evaluation of friction conditions in powder compaction for admixed and die wall lubrication." Powder Metallurgy **42**(3): 263-268.

Ullrich, W. J. (1998). Powder flow measurement techniques what's new? International Conference and Exhibition on Powder Metallurgy and Particulate Materials, Las Vegas, NV; USA.

Ward, M. and J. C. Billington (1979). "Effect of zinc stearate on apparent density, mixing, and compaction/ejection of iron powder compacts." Powder Metallurgy **4**: 201-208.

Wu, C.-Y. and A. C. F. Cocks (2004). "Flow behaviour of powders during die filling." Powder Metallurgy **47**(2): 127-136.

Wu, C.-Y., A. C. F. Cocks, et al. (2003b). "Die filling and powder transfer." International Journal of Powder Metallurgy **39**(4): 51-64.

Wu, C.-Y., A. C. F. Cocks, et al. (2003). "Experimental and numerical investigations of powder transfer." Powder Technology **138**: 216-228.

Wu, C.-Y., L. Dihoru, et al. (2003). "The flow of powder into simple and stepped dies." Powder Technology **134**: 24-39.

Wyant, J. C. (2002). White light interferometry. SPIE.

Yang, X., S. J. Gui, et al. (2006). "Electrostatic performance of various lubricant powders in P/M electrostatic die wall lubrication." Powder Technology **164**: 75-81.

Zahlan, N., D. T. Knight, et al. (2001). "Modelling powder compaction and pressure cycling." Powder Technology **114**: 112-117.

Zienkiewicz, O. C. and K. Morgan (1983). Finite Elements and Approximation, John Wiley & Sons.

Appendix 1 Powder characterisation for compaction modelling

Powder compaction modelling requires material response as a key input parameter. This Appendix summarises the material model data that has been used. This has been derived by drawing on data published in the literature (Guyoncourt, Tweed et al. 2001) and through private communication with other research groups (Doremus 2002).

Below follows an introduction to some of the parameters used in this Appendix:

ρ_0 – This represents the fill density at which the powder was characterised in the instrumented die test. The minimum level of density that may be used in the assignment of powder fill density in the simulation should not be significantly smaller than this value.

$\rho^\wedge$ – This is the maximum theoretical density for the powder mixture (when voids are closed).

E – This represents the Young's Modulus of the powder. It is an elastic parameter that must be supplied for calculation completeness although the calculation is dominated by plastic behaviour. Typically the modulus value is estimated as 70000Mpa

ν– This is the Poisson's Ratio for the powder and represents the relationship between strain components, for example the ratio between radial and axial strain in a free standing compact, typically 0.3 is an appropriate value.

Note that determination of the elastic parameters is not a trivial task and is explored in Chapter 6 of this thesis. For the purpose of compaction modelling the values of 80000 and 0.3 are used for the elastic modulus and Poisson's ratio respectively. For compaction, precise values are not required, since the elastic

component of deformation is small, it becomes an important factor for the unload and ejection stage within the cycle.

μ – Coefficient of friction between powder and tool surface

A1.1 Material Model

There are two main aspects to a material model for powder compaction - yielding and friction. These will be explained in the following sections.

A1.1.1 Material Yield Model

In the initial stages of the compaction process the densification of powder is achieved through rearrangement of powder particles. This is then followed by deformation of the particle once sufficient loads are reached. This deformation becomes increasingly difficult as the powder "hardens". The most common way to represent this in the model is by using the local density of the powder as a hardening parameter. This parameter can be established during an experimental procedure called powder characterization. This will be explained in Section A2 of this appendix.

Powder compaction models have originated in soil consolidation studies. There are a number of models that can be used. These can be divided into single and two surface yield models. Cam Clay and its variants, Shima and Gurson models are examples of the former, while Cap model with a "failure line" and a "cap" combination is an example of a two surface model. Figure A1.1a shows the Cam Clay yield surfaces and the stress path for a tabletting simulation. The Cap model is presented schematically in Figure A1.1b.

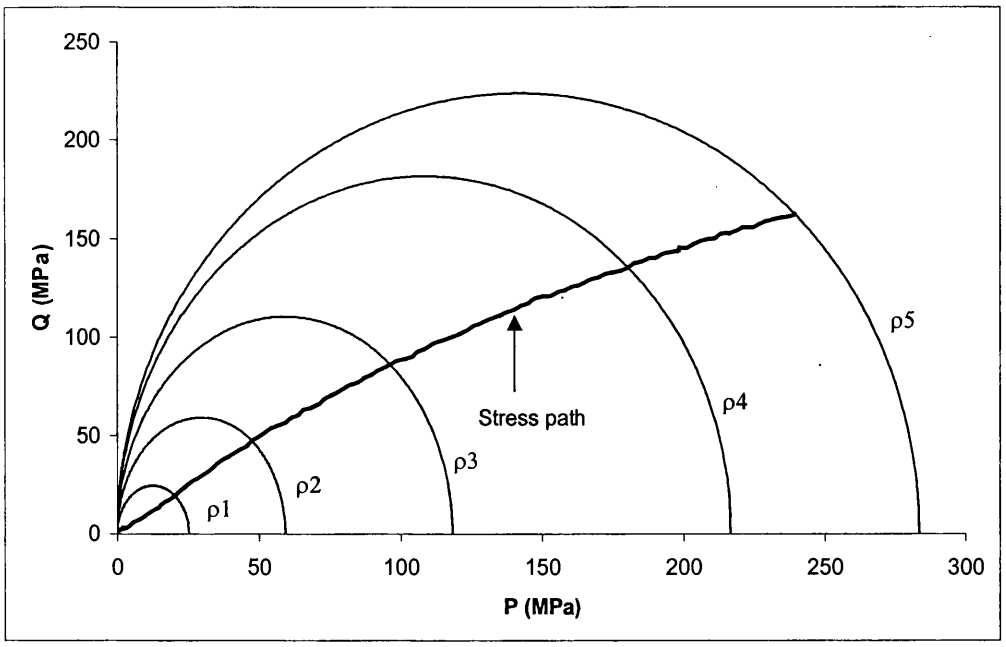

(a) Modified Cam Clay

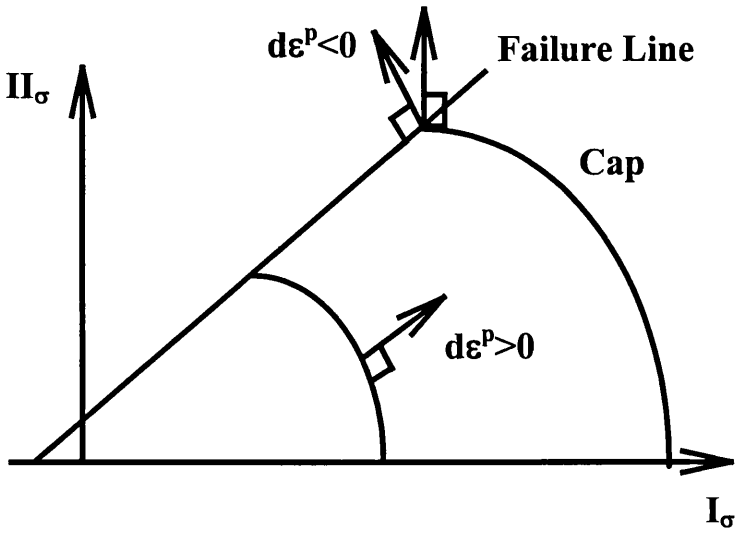

(b) Material Model Comprising Shear and Cap Surfaces

Figure A1.1 Examples of Material Models used to model the Powder Yielding Behaviour

Both models are expressed in the mean-deviatoric or P-Q plane (also known as I_σ-II_σ plane). The Cam Clay model is represented by ellipses in the P-Q plane, the size of which increases with density. The caps in Figure A1.1b can be either circular or elliptic in shape. The caps also increase with density due to material hardening. If the local stress state in the powder at its current level of density lies

within the boundaries of the yield surface for this density then the powder deforms elastically. If the stress state is on the boundary then powder consolidates through plastic deformation. The surfaces can be determined through experimental techniques, such as triaxial compaction of cylindrical samples, or through uniaxial compaction in an instrumented die. The schematics for both of the above sets of equipment are shown in Figure A1.2.

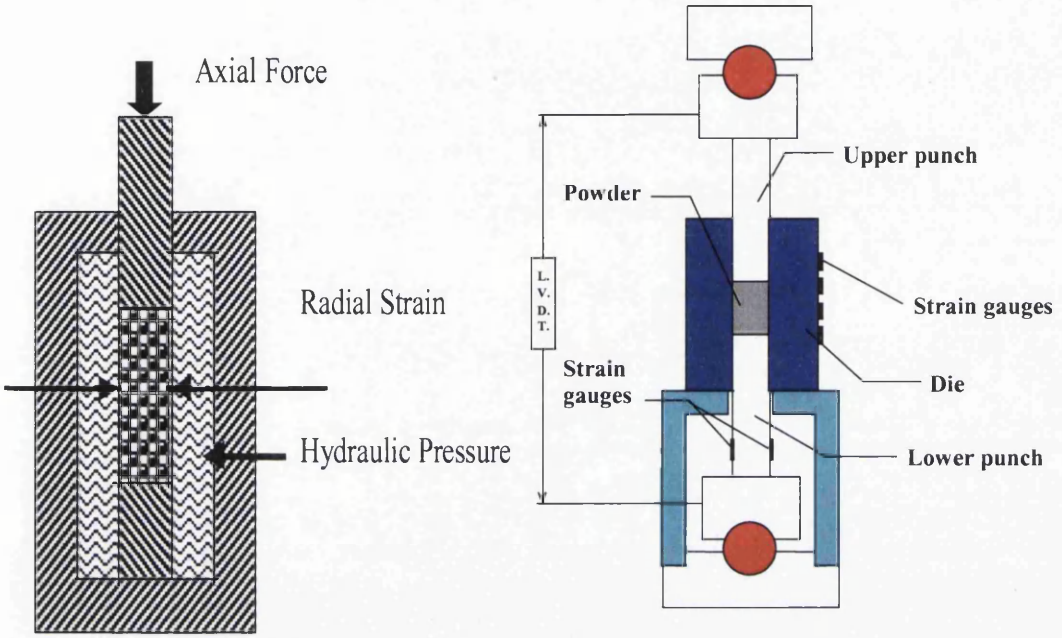

Figure A1.2 Schematic Arrangements of Triaxial and Die Compression Test Methods

The advantage of a triaxial facility (left) is that it allows for mapping of almost the entire stress field in the P-Q plane. However it is a more difficult and time consuming experiment to perform. The instrumented die compaction tests are simpler and also allow for friction data to be collected, as will be shown below. Experiments of this type are also closer to the industrial die compaction process. If a modified Cam Clay model can be used to represent a material then the instrumented die test can be used to fully characterise it. This is appropriate for many powders, the criteria being that the stress path is close to the "ideal" die pressing. This will be explained below. The objective of the characterisation process is to establish a mathematical relationship that represents the behaviour of the powder and can be incorporated into the finite element procedure.

As shown in Figure A1.1a the leftmost point of the ellipse that represents the yield surface in the modified form of the Cam Clay model passes through the origin in the P-Q stress plane. This represents the assumption of no cohesion in powder. Such an assumption is appropriate for the compaction process, but less so for the unloading and ejection processes. However, it is possible to modify the model to include the cohesive properties of the material by supplementing the model with some simple tests to establish the tensile properties of the compact.

From the basic equation representing an ellipse the yield equation can be presented in its general form as:

$$f = \frac{(P(\sigma_{ij}) - P_0)^2}{P_0^2} + \frac{Q^2(\sigma_{ij})}{Q_0^2} = 1 \qquad (1.1)$$

Where P_0 and Q_0 are the abscissa of the centre of the ellipse and its height respectively. These parameters vary with density to account for the hardening of the powder. Generally, in equation 1.1

$$Q^2 = \frac{3}{2} S_{ij} S_{ij} = 3J_{2D} \qquad where \qquad S_{ij} = \sigma_{ij} - \frac{\sigma_{ii}}{3}\delta_{ij} \qquad (1.2)$$

and

$$P = \frac{\sigma_{ii}}{3} = \frac{J_1}{3} \qquad (1.3)$$

If the stress state is axisymmetric, which is true for both the reduced triaxial and instrumented die pressing tests, P and Q are given by:

$$P = \frac{\sigma_z + 2\sigma_r}{3} \qquad (1.4)$$

$$Q = \sigma_z - \sigma_r \qquad (1.5)$$

Inserting 1.4 and 1.5 into 1.1 gives

$$f = \frac{\left(\frac{\sigma_z^d + 2\sigma_r^d}{3} - P_0\right)^2}{P_0^2} + \frac{(\sigma_z^d - \sigma_r^d)^2}{Q_0^2} - 1 = 0 \qquad (1.6)$$

where σ_z^d and σ_r^d are respectively the axial and radial stresses during die pressing

If no additional information is available it is commonly assumed that the model is associated and therefore the plastic strain rate tensor can be expressed as

$$\dot{\varepsilon}_{ij}^{p} = \dot{\lambda}\frac{\partial f}{\partial \sigma_{ij}}$$

For a die that's perfectly rigid there will be no radial displacement during die pressing and therefore the plastic radial strain will be zero at all times, which implies that

$$\left(\frac{\partial \mathrm{f}}{\partial \sigma_{\mathrm{ij}}}\right)_{i=j=r} = 0$$

Applying this to equation 1.6 results in

$$\frac{\partial f}{\partial \sigma_{ij}} = \frac{2}{3}\frac{(\frac{\sigma_z^d + 2\sigma_r^d}{3} - P_0)}{P_0^2} - \frac{(\sigma_z^d - \sigma_r^d)}{Q_0^2} = 0 \qquad (1.7)$$

From equations 1.6 and 1.7, the function P_0 and Q_0 are obtained as

$$P_0 = \frac{3P^{d^2} + 2P^d Q^d}{6P^d + 2Q^d} \qquad (1.8)$$

$$Q_0 = \sqrt{Q^{d^2} + \frac{\frac{3}{2}(P^d)^2 Q^d}{2P^d + \frac{2}{3}Q^d}} \qquad (1.9)$$

Therefore, for known σ_z^d and σ_r^d, P^d and Q^d can be calculated. Subsequently P_0 and Q_0 can be obtained from equations 1.8 and 1.9 and then curve fitted as functions of the density field. These can then be incorporated into the final element compaction model. The method for achieving this will be described in the following section of this appendix.

A1.2 Experimental Determination of Material Model Parameters

In this section the powder characterisation process, that is the die pressing experiments needed to obtain material parameters that describe the yield surfaces and friction, will be presented.

A1.2.1 Apparatus

A suitable testing apparatus is shown schematically in
Figure **A1.3**. Its main features are a die and two punches, of which only the top punch moves. The bottom punch and the die are instrumented in order to measure the bottom axial force and the radial force. The top axial force can usually be obtained from the press load cell.

The instrumented die equipment at University of Wales Swansea was designed to have the internal die diameter of 18mm and die wall thickness of 7mm. The latter was chosen as a good compromise between sensitivity and sufficient strength to withstand the stresses in compaction tests that approach solid density. The axial force on the top punch was measured by the press load cell, the forces acting on the bottom punch were measured by a load cell on which the bottom punch was resting. Radial stress between the powder and the die was recorded via a series of strain gauge bridges, bonded on to the die, and then reinterpreted through a calibration procedure. The die was installed onto a hydraulic press, capable of applying 250kN of force, which for the chosen die diameter is equivalent to the pressure of 960 MPa. The displacement of the top punch was measured both from the press and by an LVDT in order to account for press deflections. Accurate displacement measurement is known to be a critical factor in the powder characterisation process.

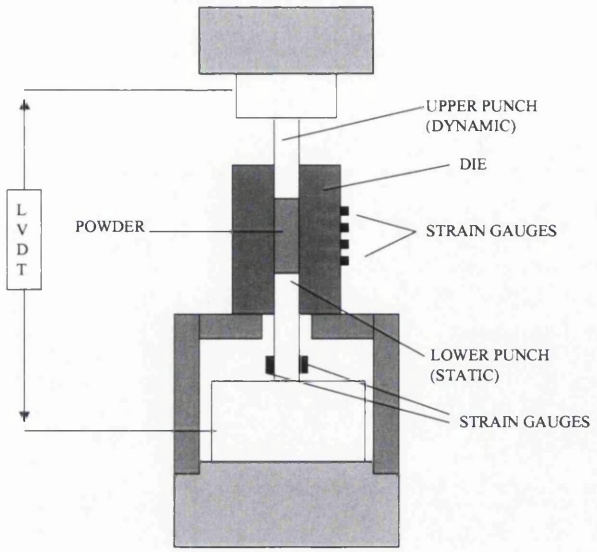

Figure A1.3 Schematic of Die Pressing Apparatus

An example result from a compaction test is shown in Figure A1.4 for a powder from the food industry

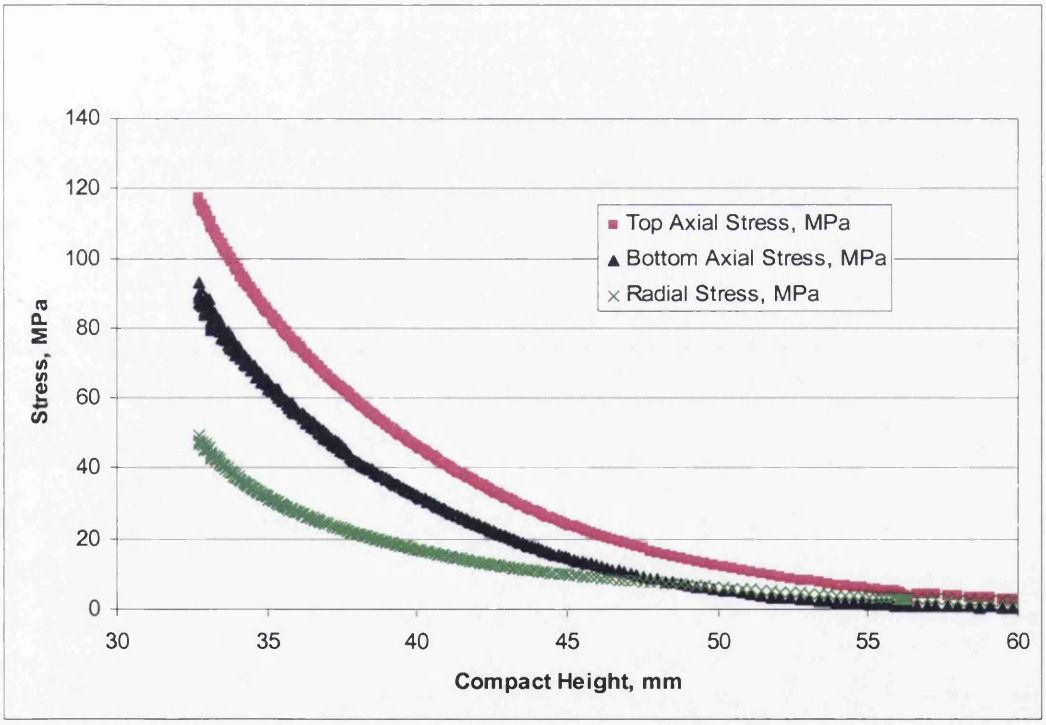

Figure A1.4 Typical result of compression of a powder from the food industry

A1.2.2 Derivation of Yield Surface Characteristics

As explained in Section A1.1.1 values of P_0 and Q_0 can be obtained at any time during compaction if the radial stress and the top and bottom axial stresses are known, Figure A1.4. However they need to be fitted by curves that correspond to various aspects of physical behaviour of the powder in order to be used in the finite element modelling software. Below follow equations proposed for P_0 and Q_0. Alternative equations can also be used.

$$P_0 = K_1 \left(\ln\left(1 - \frac{\rho - \rho_0}{\rho - \rho_{max}}\right)\right)^{K_2} \tag{2.1}$$

$$Q_0 = Q_{max} \tanh\left(\frac{K_3 P_0}{Q_{max}}\right) \tag{2.2}$$

Here K_1, K_2 and K_3 are curve fit constants; ρ_0 and ρ_{max} are the fill and maximum theoretical density of the powder respectively and Q_{max} is the maximum deviatoric stress sustainable by the fully dense powder. An example of a graph for P_0 is shown in Figure A1.5, where K_1=21.903 and K_2=1.3527

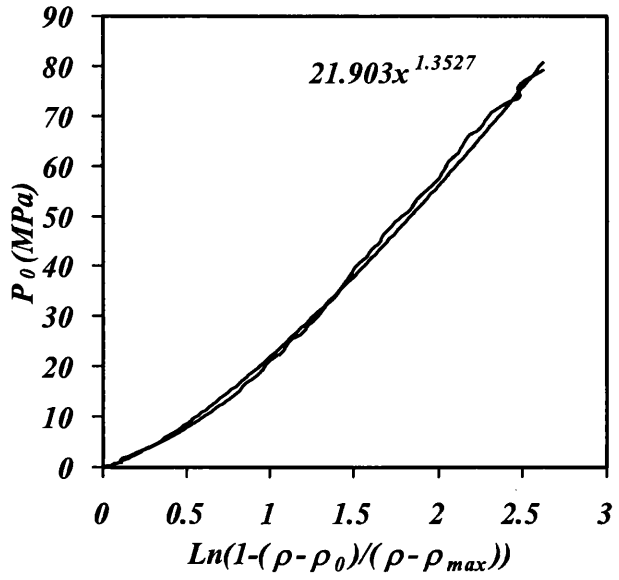

Figure A1.5 Functional Relationship Between P0 and Compact Density

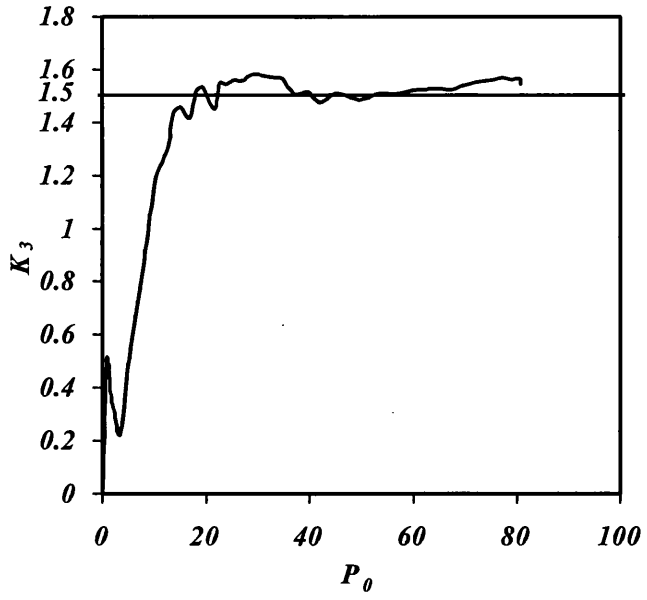

Figure A1.6 Functional Relationship Between K3 and P0

Similarly from Figure A1.6, $K_3 = 1.5$ and Q_{max} is determined as 170MPa.

A1.2.3 Derivation of Die Wall Friction Characteristics

The results shown in Figure A1.4 can be used to obtain the die wall friction coefficient and, if necessary, the pressure transmission coefficient. The latter is not used within the finite element simulation, but equations for both are shown for completeness.

$$\mu(\rho) = \frac{R}{2\sigma_{rr}H}(\sigma_{zz}(H) - \sigma_{zz}(0))$$

$$K = \frac{R}{2\mu H} Ln(\frac{\sigma_{zz}(H)}{\sigma_{zz}(0)})$$

Example results for these equations are shown in Figure A1.7

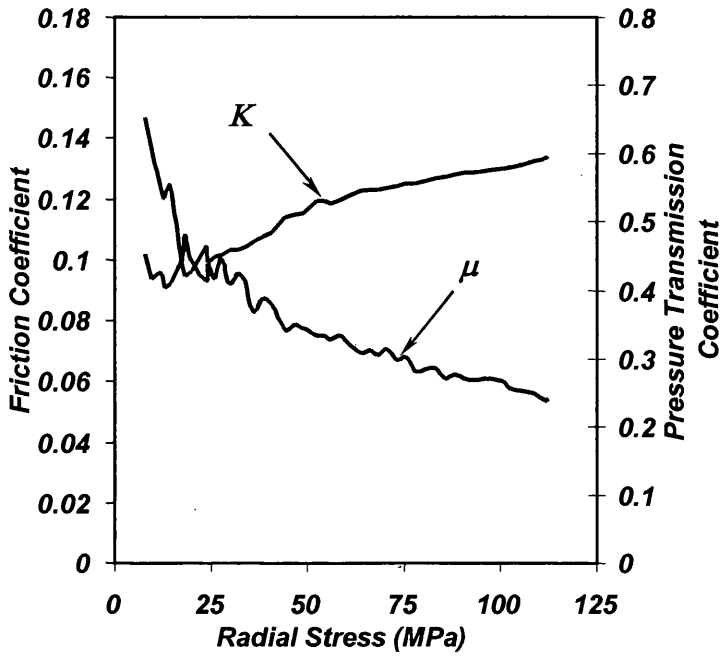

Figure A1.7 Example Trends in Friction and Pressure Transmission Coefficient

The parameters explained above are required for any simulation studies, as they define the material model data in the numerical code. The equations presented here are just some of the possibilities and can be replaced with others if necessary.

A1.4 Example of Powder Characterisation Procedure

Now that the origins of the characterisation procedure have been explained an example of a characterisation sequence for the Tungsten Carbide powder, used in the sensitivity study on die filling, will be presented.

The characterisation of a powder involves obtaining material parameters K_1 to K_3, Qmax and μ, which are needed to define the material yield and friction models in the simulation, from measurements taken during a die pressing test. An optimisation routine is then performed to fine tune the parameters. Once the parameters are obtained a validation simulation replicating the characterising experiment is performed. The results are compared against those obtained during the experiment and the material parameters may be adjusted again to achieve better agreement.

In the case of the Tungsten Carbide powder used in the sensitivity study the experimental data consisted of over a hundred lines of data recorded throughout the compaction process. Each line contained values of density, compact height, axial and radial stress, friction and pressure transmission coefficients.

The procedure started with determining of P and Q for each data point using equations 1.4 and 1.5. Substituting these into equations 1.8 and 1.9 then resulted in values of P_0 and Q_0. A graph of Q_0 vs. relative density was then plotted and a trend facility of MS Excel was used to predict the value of Q_{max}, which is the value of Q_0 at relative density of 1. The next step was to obtain values of K_1 and K_2 from equation 2.1. This was achieved by first taking a logarithm of equation 2.1:

$$\ln(P_0) = \ln K_1 \left(\ln\left(1 - \frac{\rho - \rho_0}{\rho - \rho_{max}}\right)\right)^{K_2}$$

$$= \ln K_1 + \ln\left(\left(\ln\left(1 - \frac{\rho - \rho_0}{\rho - \rho_{max}}\right)\right)^{K_2}\right) = \ln K_1 + K_2 \ln\left(\ln\left(1 - \frac{\rho - \rho_0}{\rho - \rho_{max}}\right)\right)$$

Then by plotting the relationship between $\ln(P_0)$ and $\ln(\ln(1-(\rho-\rho_0)/(\rho-\rho_{max}))$ the material parameters K_1 and K_2 could be obtained. In this case K_2 was the slope of the graph and $\ln(K_1)$ was the intercept, these were obtained by extending the trendline to the origin, see Figure A1.8.

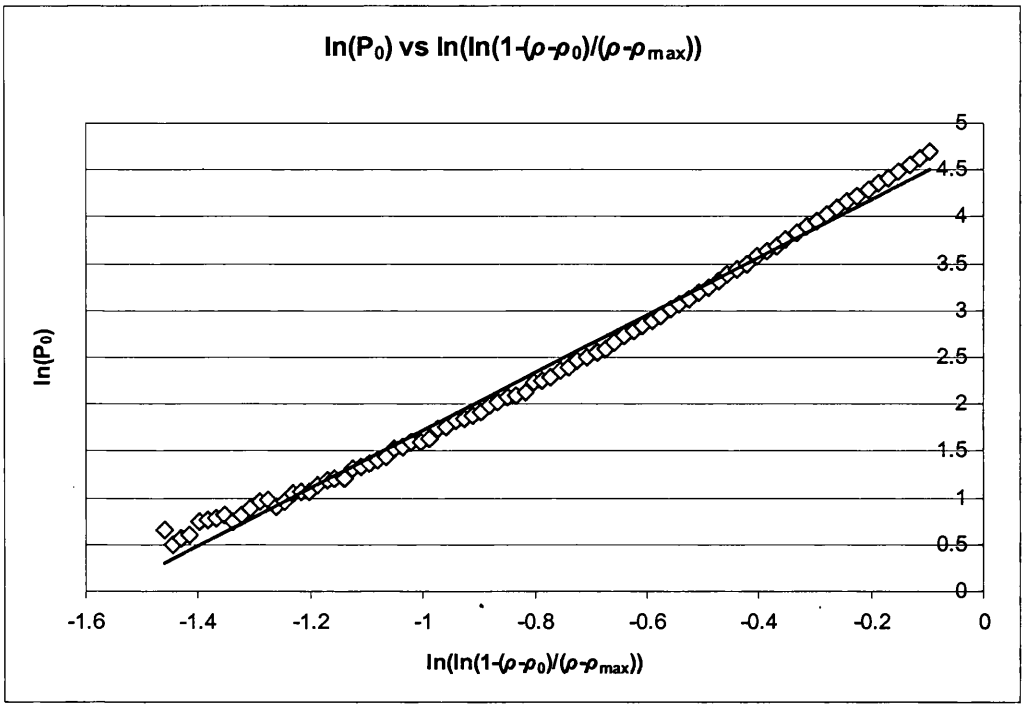

Figure A1.8 Derivation of model parameters

The values of K_3 for each point were obtained from equation 2.2. The final material parameter K_3 was the mean of those values.

Once the initial values for the material parameters were known they were used as a starting point in an optimisation routine using the MS Excel's Solver facility. Values of P_0 and Q_0 were calculated at each time step of the compaction process through formulae 2.1 and 2.2. These results were then compared to the experimentally obtained values. The solver was then used to minimise the error throughout the duration of the experiment by adjusting first K_1 and K_2 and then Q_{max} and K_3. Once these optimal values were obtained they were fed into the numerical model.

The final step of the characterisation process was to simulate the experiment and compare the experimental results with numerical ones. This led to some fine-tuning adjustments to the material parameters. This final step was repeated until satisfactory agreement between the experiment and the simulation was achieved.

For the tungsten carbide powder the material parameters were as shown in Table A1.1:

Table A1.1 Model parameters for tungsten carbide powder

Q_{max}	K_1	K_2	K_3	ρ_0	$\rho^\wedge$	E	ν	μ
625.85	102.72	3.368	1.702	3.2g/cm^3	11.83g/cm^3	8.0E+04	0.3	0.16

The material parameters for Distaloy AE powder are shown in Table A1.2. For this powder a variable friction coefficient that reduces at higher stresses was used, Figure A1.9. From experimental work that will be presented in the chapter on powder friction it was found to be more realistic than a constant friction coefficient. The same can also be observed in published literature on the subject of powder-die friction (Doremus, Toussaint et al. 2001).

Table A1.2 Model parameters for Distaloy AE powder

Q_{max}	K_1	K_2	K_3	ρ_0	$\rho^\wedge$	E	ν	μ
271.05	60.45	1.311	1.8	3.10 g/cm^3	7.4 g/cm^3	8.0E+04	0.3	variable

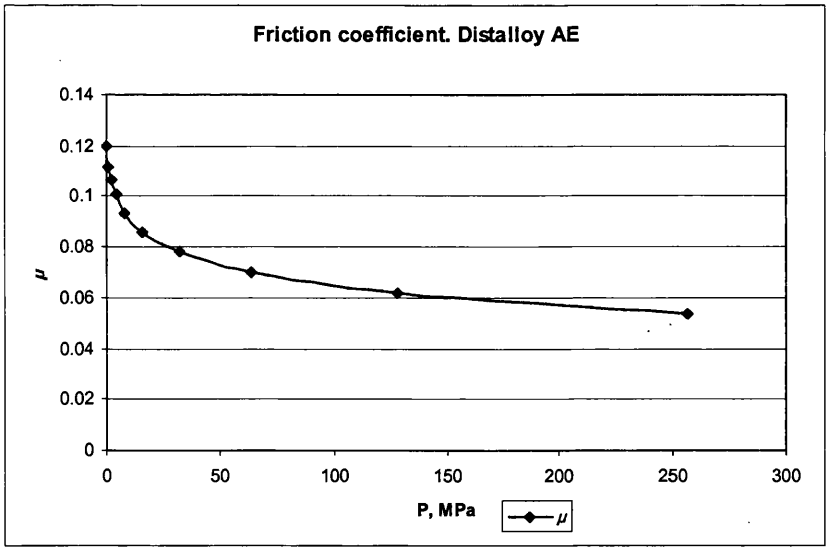

Figure A1.9 ***Evolution of friction coefficient with stress. Distaloy AE***

Finally the material parameters for the Zirconia powder are presented in Table A1.3.

Table A1.3 Model parameters for Zirconia powder

Q_{max}	K_1	K_2	K_3	ρ_0	$\rho^\wedge$	E	ν	μ
18000	150	1.5	3.3719778	1.2g/cm^3	3.6g/cm^3	8.0E+04	0.3	0.2

Appendix 2 Instrumented die – radial pressure measurement

A2.1 Compaction

The readings from the radial pressure strain gauges needed to be calibrated and intterpreted before radial stress data could be obtained. For this, cylindrical samples of rubber elastomer were compressed in the die. The elastomer samples were cast to have slightly smaller diameter than that of the die to facilitate insertion. They were also lubricated with oil to minimise any friction between the elastomer and the die. The elastomer material was used because it was almost incompressible and would fully transmit the axial stress in the radial direction. Thus the radial stress at any point of the calibration procedure would be known from knowing the axial stress.

For accurate measurements, the relationship between the strain gauge readings and the radial pressure is not trivial. It is clear that the height of the compact would determine which sensors are located opposite the compact and which are above it and therefore affect the readings. Additionally due to powder-die friction the radial pressure will not be uniform throughout the height of the compact. The former can be overcome by testing elastomer cylinders having a range of different heights and then interpreting data accordingly. For the latter (Mosbah, Bouvard et al.. 1997) showed that for both uniform and non-uniform distributions of radial stress for compact of the same height the strain of the die at mid compact height remains constant. This permits the use of relationships developed between the radial stress and the radial strain of the die during elastomer compression to measure average radial stress during compaction of powders.

The procedure for interpreting radial strain data into radial stress data involves the compression of elastomer samples of a range of heights. In this case, samples of nominal heights of 20, 30, 40, 50 (20+30) and 60 mm were used. The actual sample heights during the test differed slightly, as although the elastomer is highly

incompressible small height reduction occurs as samples of slightly smaller diameter than that of the die had to be used. The true instantaneous sample heights were used in the actual calculations. The samples were lubricated with a standard machine oil to minimise friction between the elastomer and the die. All samples were compressed to the same pressure of approximately 160 MPa (top punch load of 40 kN).

The radial pressure was then divided by the average of readings from the five sensor bridges. The obtained coefficient was then plotted against compact height to provide a calibration plot, see Figure A2.1. A trend line facility in MS Excel was used to fit an equation that describes the calibration parameter. A third order polynomial was found to provide the best fit. This equation was then applied to the elastomer compression tests for validation – the incompressibility of the elastomer dictates that the radial and the axial stresses in the sample are equal. Figure A2.2 shows the radial and axial stress as the samples are loaded. The radial stress closely follows the axial stress, as expected. The radial stress starts to lag slightly behind the axial stress when the stress reaches 20 MPa – this is likely to represent actual physical phenomena. The likely cause is the entrapment of some of the elastomer material between the punch and the die causing a small amount of frictional losses. Overall, good agreement was observed and the interpretation procedure can be used to convert the radial strain measurements into radial stress.

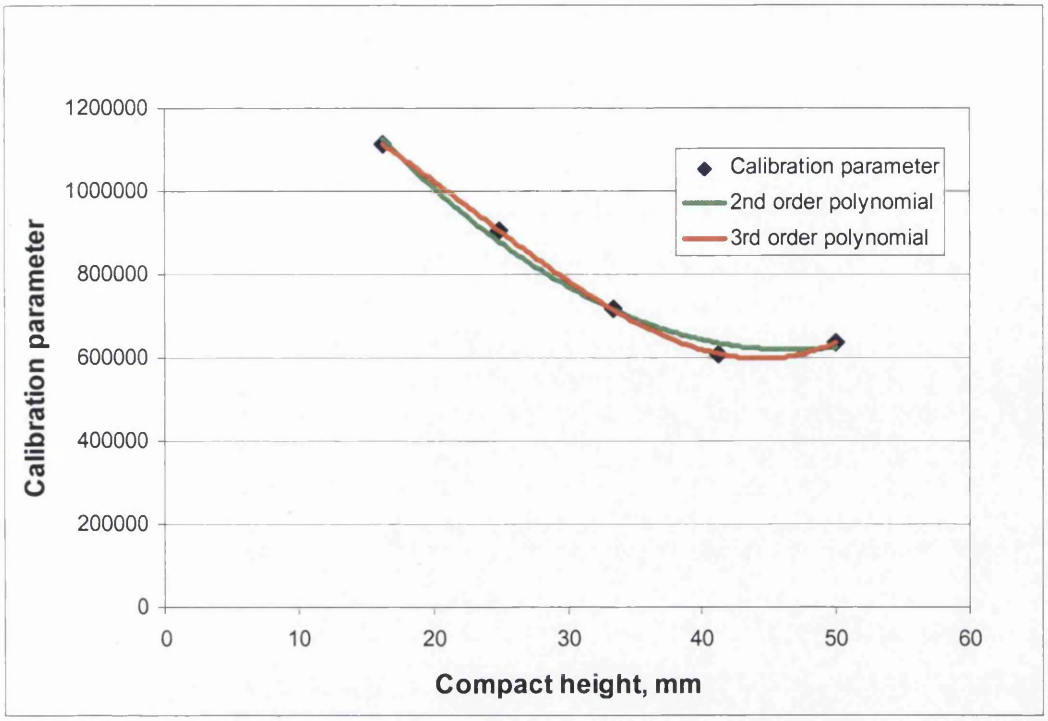

Figure A2.1 Radial stress calibration plot

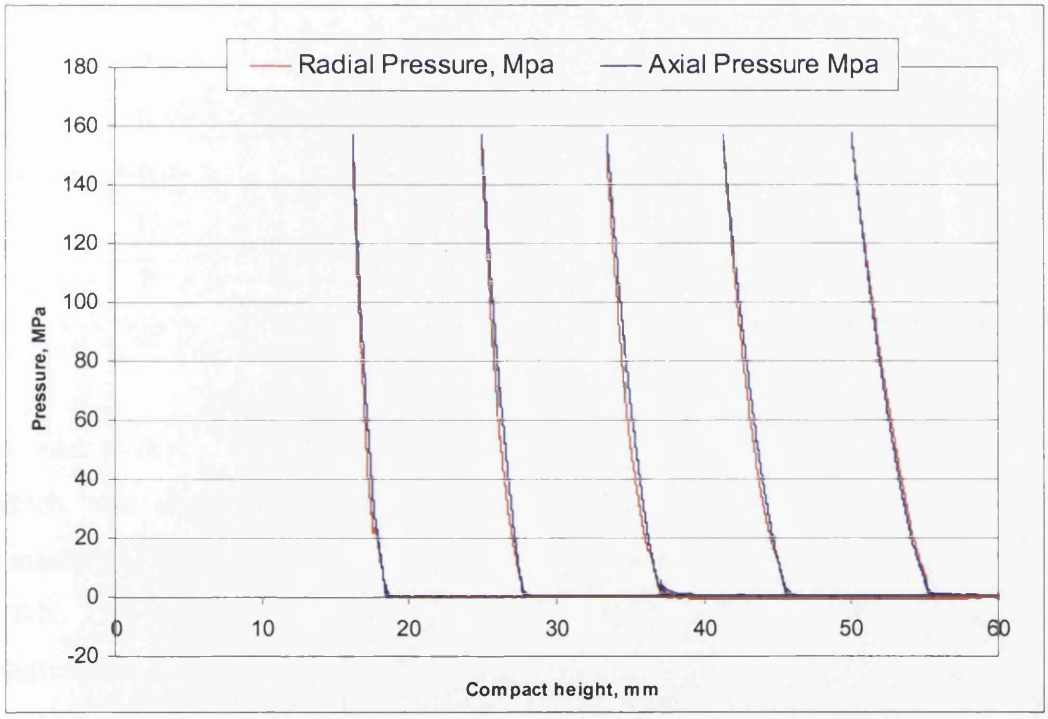

Figure A2.2 Figure Radial stress conversion validation

A2.2 Ejection

The above calibration procedure cannot readily be used during the ejection stage. During the ejection the bottom punch travels upwards and the bottom of the

compact passes over the strain gauge bridges. To account for any inaccuracies thus introduced another calibration function was developed.

First a series of elastomer compression tests was performed with the bottom punch raised. Spacers were used to raise it by 15, 30 and 45mm above its typical position during the compaction stage. Elastomer cylinders of various heights were compressed and the radial stress was calculated by using the calibration function described in Section A2.1. The values of the radial stress obtained were compared with the values of the axial stress recorded during the test. As was explained previously for the elastomer material used these were equal to the true radial stress. The percentage difference in calculated and true radial stress was determined for a range of bottom punch positions and sample heights and tabulated, see Table A2.1.

Table A2.1 Percentage error in radial stress calculation, ejection stage

Bottom punch raised by	**Elastomer sample height**				
	20 mm	**30 mm**	**40 mm**	**50 mm**	**60 mm**
15 mm	***36***	***26***	***8***	***1***	***1***
30 mm	***44***	***28***			
45 mm	***11***	***-5***			

In order to derive the ejection calibration for the 18mm compacts, the ejection of which was considered in Chapter 7, the 20 mm elastomer cylinders were considered. These were actually 16.3mm high when at maximum test load of 40kN. The radial stress calculation error for the 20mm elastomer samples was plotted as a function of bottom punch height. Since no error would be obtained if the bottom punch remained in its original position a point was added to the graph at the origin, see Figure A2.3. The MS Excel trend facility was used to derive a second order polynomial correction function. For bottom punch positions beyond 45mm the error was taken to remain at 0.11.

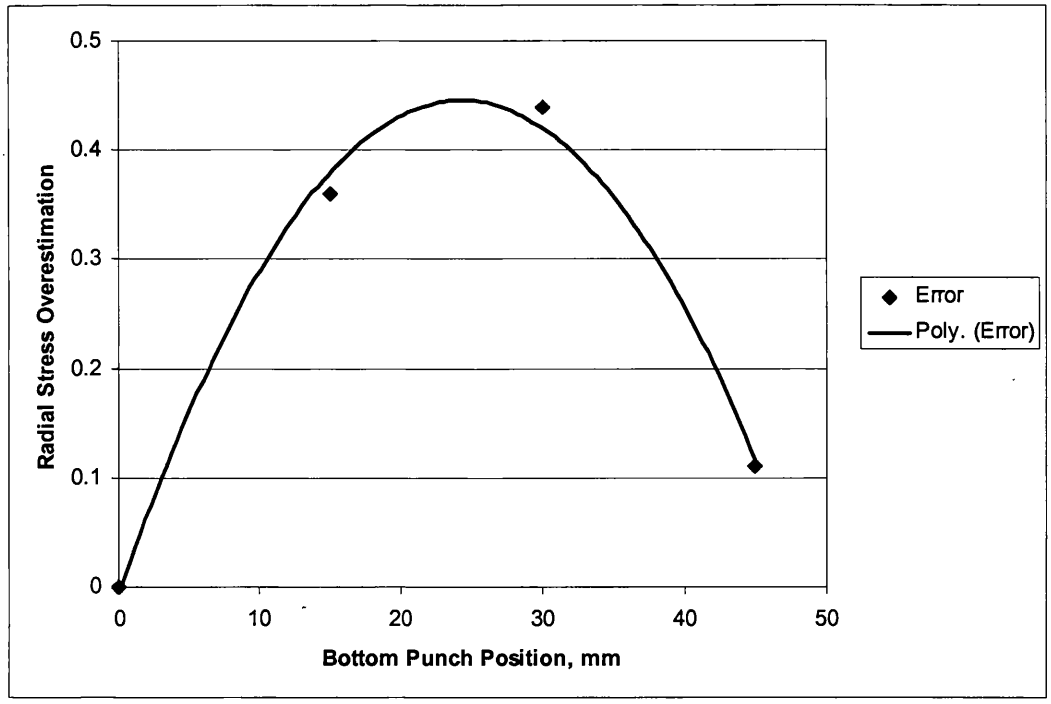

Figure A2.3 Error correction function

The value of the correction function at a given bottom punch position was then used to compensate for the overestimation of the radial stress. E.g. if the bottom punch was raised by 45mm then the corrected value of the radial stress was obtained by dividing the originally calculated value by (1+0.11), where 0.11 is the value of the correction function for this bottom punch position.